The Development of a Tissue Engineered Vascular Graft using a Poly(glycerol sebacate) Methacrylate Scaffold

Thesis submitted to the University of Sheffield for the degree of Doctor of Philosophy

Samand Pashneh-Tala

Department of Materials Science and Engineering

February 2017

Acknowledgments

I would like to thank my primary supervisor Dr Frederik Claeyssens. I would not be here without the guidance and support you provided throughout this project. Your unending optimism, wisdom and belief in me provided light in the darkest of hours. You once said to me “You’re an inventive guy. I know you’ll do something good.” I hope that this work has proved you right and I look forward to our continued collaborations together.

I would like to thank my secondary supervisor Prof Sheila MacNeil. Your years of experience and clarity of thinking were of immeasurable value throughout this work. I hope that I may continue to call upon these in the future.

I would also like to thank my funding body The Engineering and Physical Sciences Research Council. As part of the White Rose Doctoral Training Centre for Tissue Engineering and Regenerative Medicine, you provided the generous funds which allowed me to undertake this ambitions project and to present my research internationally.

I owe a huge thank you to many of the other researchers who I have shared the labs in the Kroto Research Institute with over the last 3 years. Thank you to Dr James Dugan and Dr Anthony Bullock for your knowledge and expertise. Thank you to Dr Ihtesham Rehman, Peyman Zolgharnein and Marcela Garcia for your assistance with ATR-FTIR and Raman spectroscopy. Thank you to Dr Thomas Paterson for your assistance with the DNA quantification assays and thank you to Dr Nicola Green for your technical assistance with the confocal microscope.

To my family and friends, who have been by my side throughout this work, thank you for your love and support. I hope that I have made you proud.

Statement of originality

The work presented in this document is entirely my own.

Abstract

Cardiovascular disease is the number one cause of death worldwide. In the treatment of such disease, vascular surgery commonly utilises grafts to replace or bypass damaged regions of the circulatory system. Currently, autograft vessels represent the gold standard for vascular bypass; however, these are of limited availability and quality. Synthetic conduits are also available, but these are of little use as small diameter vessels (<5 mm) due to high incidence of failure through infection or thrombosis. A need exists for a better vascular graft with tissue engineering offering an attractive solution.

Although the development of tissue engineered vascular grafts (TEVGs) is being explored by a number of research groups using a wide range of methods, to date, a TEVG has not yet been produced that closely matches the mechanical performance of the autograft vessels currently favoured in vascular surgery.

This research aimed to develop a method of manufacturing TEVGs with mechanical properties more similar to the current gold standard vessels. These TEVGs would be biocompatible, non-immunogenic and able to grow and remodel *in vivo*. Additionally, the TEVG manufacturing process would also be readily adaptable to producing more complex geometric shapes than simple tubes. It was hypothesised that this may result in an improvement in the performance of the TEVGs and may also expand the possible clinical applications.

Following a review of the literature, presented in Chapter 1, a synthetic polymer scaffold based tissue engineering approach was selected as the method for producing the TEVGs. This approach has been widely adopted in the field of vascular graft tissue engineering. Synthetic polymer scaffold based methods are compatible with a range of manufacturing processes; have shown success in a variety of *in vivo* studies of TEVGs,

including human trials; and had the potential to be adapted to produce a TEVG in a variety of predefined geometries.

A synthetic polymer scaffold would be developed with properties, such as elasticity, degradation rate and porosity, specifically optimised towards the development of a TEVG with mechanical properties similar to the current gold standard autografts. TEVGs would be produced *in vitro* by seeding cells onto the synthetic polymer scaffold and then culturing them in a bioreactor under physiologically relevant flow to encourage cell proliferation and appropriate ECM deposition.

A novel photocurable form of poly(glycerol sebacate), poly(glycerol sebacate) methacrylate (PGS-M) was proposed as the material for the synthetic polymer scaffold. This material had the potential to provide the mechanical performance and degradation properties identified as requirements for the scaffold, along with being biocompatible and easy to process into various scaffold geometries.

In Chapter 2, different variants of PGS-M were produced which varied in molecular weight and degree of methacrylation (DM). These were characterised using various analytical chemistry techniques. It was determined that both the molecular weight and DM could be controlled by altering the reaction conditions used in the synthesis of the polymer. The degradation of the different variants of PGS-M was examined and this revealed that the polymer was susceptible to enzymatic degradation. Increasing the DM appeared to have an inverse effect on the degradation rate. The mechanical properties of PGS-M were also assessed and found to largely depend on the DM of the polymer and not the molecular weight.

A 30% DM, low molecular weight (30% Low M_w) PGS-M was selected as the most suitable variant of PGS-M for producing a scaffold for use in culturing a TEVG. In Chapter 3, the biocompatibility of 30% Low M_w PGS-M is presented. Flat surfaces of the polymer were able to support the growth and proliferation of human dermal fibroblasts, human adipose derived stem cells and human coronary artery smooth muscle cells (SMCs) for several days in culture. Additionally, growth on the PGS-M

surfaces does not appear to alter the phenotype of the SMCs. It was determined that culture on PGS-M surfaces may have effects on the metabolic activities of the three cell types investigated and that these effects may be subtle and cell specific.

In Chapter 4, porous scaffold structures, suitable for use in tissue engineering, were produced from 30% Low M_w PGS-M using a porogen leaching method with sucrose particles. Combining PGS-M with sucrose particles of different sizes, at different ratios, allowed variation of the scaffolds' handling properties, pore sizes, porosities and wettability. SMCs seeded onto the porous PGS-M scaffolds remained viable for 7 days in static culture and partially infiltrated the scaffold interiors.

A method was then developed to produce the porous scaffolds as tubes of suitable geometry and porosity for use in the generation of TEVGs. Additionally, a method for producing porous PGS-M scaffolds in a variety of geometries was also demonstrated as a proof-of-concept. This method used a novel hybrid additive manufacturing and porogen leaching approach.

A bioreactor was required for the culture of the tubular PGS-M scaffolds, once seeded with cells, to produce TEVGs. In Chapter 5, a design brief was proposed for a bioreactor capable of culturing the TEVGs under dynamic conditions and applying mechanical stimulation. This had been identified as advantageous in previous studies in TEVGs.

A design process was implemented, with a number of initial ideas evaluated to determine an integrated final solution. The final bioreactor design utilised a pulsatile flow to provide mechanical stimulation to the developing TEVGs. The bioreactor was manufactured and assessed for sterility and its ability to provide mechanical stimulation to developing TEVGs. The pulsatile flow could be modulated to produce pressures and flow rates within the range of physiological blood flow which were appropriate for the culture of TEVGs. Modifications to the design were implemented, as required, to improve performance.

The knowledge gained from the previous chapters was combined in Chapter 6. Porous tubular scaffolds, produced from 30% Low M_w PGS-M were seeded with human coronary artery SMCs and cultured in the bioreactor as TEVGs. The TEVGs were cultured for 7 days under dynamic and static conditions. TEVGs cultured under dynamic conditions, with mechanical stimulation produced by the pulsatile flow in the bioreactor, displayed highly variable results, but demonstrated the partial formation of blood vessel-like tissue in a small instance. TEVGs cultured under static conditions produced repeatable results, although with reduced vascular tissue formation compared to the grafts cultured under dynamic conditions. Both culture regimes produced TEVGs containing collagen and elastin and both also appeared to cause a change in the phenotype of the attached SMCs, from contractile to proliferative.

Finally, Chapter 7 suggests the possible further work that may be conducted to explore the PGS-M scaffold based TEVGs, as the original aims of the research were not fully realised. Suggestions of how the bioreactor culture may be modulated and optimised are made along with ideas for generating TEVGs of varied geometries.

Publications

Pashneh-Tala, S., MacNeil, S. & Claeyssens, F. The Tissue-Engineered Vascular Graft—Past, Present, and Future. *Tissue Engineering Part B: Reviews* **22,** 68–100 (2015).

List of Abbreviations

ADSCs	Adipose-derived stem cells
AVFs	Arteriovenous fistulas
α-SMA	Alpha-smooth muscle actin
BM-MNCs	Bone marrow-derived mononuclear cells
BSA	Bovine serum albumin
CABG	Coronary artery bypass grafting
CDl_3	Deuterated chloroform
DA	Degree of acrylation
DM	Degree of methacrylation
DMEM	Dulbecco's modified eagle's medium
ECs	Endothelial cells
ECM	Extracellular matrix
EDTA	Ethylenediaminetetraacetic acid
EPCs	Endothelial progenitor cells
Fem-pop	Femoropopliteal
GFP	Green fluorescent protein
GPC	Gel permeation chromatography
HUVECs	Human umbilical vein endothelial cells
H&E	Haematoxylin and eosin
IMS	Industrial methylated spirit
ITA	Internal thoracic artery
MCP-1	Monocyte chemoattractant protein 1
M_n	Number average molecular weight
MSC	Mesenchymal stem cells
MTT	3-(4,5-dimethylthiazol-2-yl)-2,5-diphenyltetrazolium bromide
M_w	Weight average molecular weight
NMR	Nuclear magnetic resonance
OCT	Optimum cutting temperature
PCL	Poly-ε-caprolactone
PDI	Polydispersity index
PEG	Polyethylene glycol
PEUU	Poly(ester urethane)urea
PGA	Polyglycolide
PGS	Poly(glycerol sebacate)
PGS-A	Poly(glycerol sebacate) acrylate
PGS-M	Poly(glycerol sebacate) methacrylate
PLGA	Poly(lactide-co-glycolide)
PLLA	Poly-L-lactide
PTFE	Polytetrafluoroethylene
PU	Polyurethane
PVA	Polyvinyl alcohol
P4HB	Poly-4-hydroxybutyrate
P(GA/CL)	Poly(glycolide/caprolactone)
P(LA/CL)	Poly(lactide/caprolactone)
P(L/D)LA	Poly(L/D)lactide
RR	Resazurin reduction
SEM	Scanning electron microscopy
SIS	Small intestinal submucosa
SLS	Selective laser sintering
SMCs	Smooth muscle cells
SV	Saphenous vein
TCP	Tissue culture plastic
TESA	Tissue engineering by self-assembly
TEVG	Tissue engineered vascular graft
TGF-β1	Transforming growth factor beta 1
v/v	Volume/volume
w/v	Weight/volume
w/w	Weight/weight

Contents

Chapter 1 - Literature Review, Research Aims and Objectives

1.1 Introduction

Cardiovascular disease is the number one cause of death globally.[1] Disorders are often associated with the narrowing or blockage of blood vessels leading to reduced blood flow and tissue damage due to inadequate nutrient supply. Common presentations are coronary heart disease, cerebrovascular disease, peripheral arterial disease and deep vein thrombosis. It is predicted that the annual incidence of cardiovascular disease related mortalities will rise to 23.3 million worldwide by 2030.[2]

Treatments for cardiovascular disease range from dietary and lifestyle modification to pharmaceutical and surgical intervention.[3] When required, vascular surgery may involve endovascular procedures such as angioplasty, stent insertion or atherectomy to widen a stenosed vessel or remove the obstruction. Alternatively, a vascular graft may be used to replace or bypass a damaged or occluded vessel. Despite the advances in endovascular surgery and its increased popularity over recent decades, vascular bypass grafting remains commonplace and is believed to be the optimal choice for patients requiring long-term revascularisation solutions (life expectancy >2 years).[4–8] Around 400,000 coronary artery bypass grafting (CABG) procedures are performed each year in the USA alone.[9]

Currently, the favoured conduits for vascular grafting are autologous arteries or veins. The structures of these are shown in Figure 1. Although the use of arteries, such as the internal thoracic artery (ITA) or radial artery, is associated with superior patency,[10–13] it is the saphenous vein (SV) that is the most commonly used autograft vessel.[14] This is due to the limited availability of arteries and the more severe complications associated with their removal compared to veins. Despite representing the gold standard, patency rates for SV grafting remain limited with both CABG and femoropopliteal (fem-pop)

bypass grafts showing failure rates of around 50% at 10 years.[14,15] Additionally, autologous vessels have limited availability, may be of poor quality and their extraction causes donor site morbidity.[5,15–17]

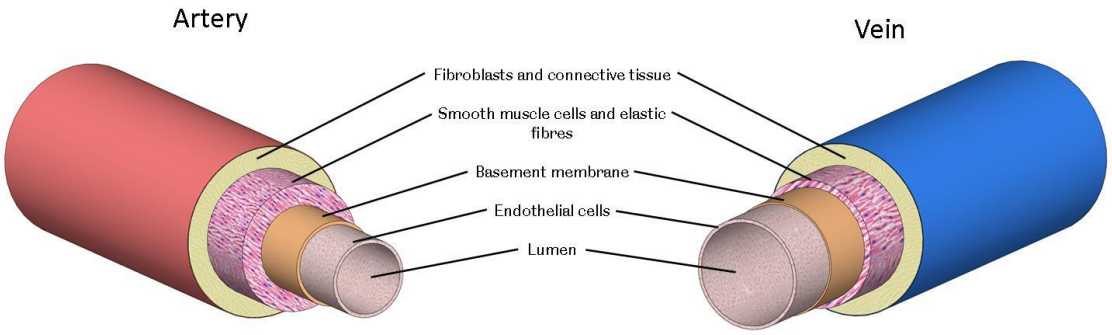

Figure 1. Cellular structure of arteries and veins. Both types of blood vessel are composed of layers of cells. Endothelial cells line the luminal surface. These are supported by a basement membrane which is surrounded by a layer of smooth muscle cells and elastic fibres and then a layer of fibroblasts and connective tissue. The vessel wall is thicker in arteries compared to veins due to the presence of a thicker layer of smooth muscle cells. This is required to resist the high pressure blood flow carried by the arteries.[18]

Synthetic vascular grafts are also available as an alternative to autologous vessels. These grafts have demonstrated satisfactory long-term results when used in large diameter arteries (>8 mm), such as in aorto-iliac substitutes where patency is around 90%,[19] and in medium diameter arteries (6-8 mm), such as carotid or common femoral artery replacements.[20] In small diameter vessels (<6 mm) however, synthetic grafts are of limited use due to poor patency rates. These vessels include the coronary arteries, infrainguinal arteries (below the inguinal ligament) and infrageniculate arteries (below the knee). Autologous vessels have proved superior to synthetic grafts for these installations (Figure 2). In CABG, the use of polytetrafluoroethylene (PTFE) conduits resulted in 1 year patency rates of ~60% compared to over 95% when using the SV. After 2 years, the patency of PTFE conduits declined to just 32% whereas SV grafts remained above 90%.[21–24] In above the knee fem-pop bypass, results have shown PTFE graft patency rates of ~59% at 5 years compared to ~78% when using the SV.[15,25–29] A

synthetic conduit is only suggested as a choice if no other suitable autologous vessel is available.[24] Improvements in patency have been achieved by seeding autologous endothelial cells (ECs) onto the luminal surface of synthetic grafts, however, these grafts have been unable to exceed the performance of autologous vessels.[30]

Vascular graft failures are most commonly associated with thrombosis, intimal hyperplasia, atherosclerosis or infection. Thrombosis occurs as a result of damage to, or the absence of, ECs lining the graft lumen leading to the adherence of blood proteins and the activation of clotting mechanisms.[31,32] Intimal hyperplasia is caused by the migration of vascular smooth muscle cells (SMCs) from the vessel media to the intima and their proliferation and extracellular matrix (ECM) deposition. Intimal hyperplasia may occur in the graft vessel or in the native vessel around the anastomosis. There are multiple causes including (i) compliance mismatch between the graft and native vessel; (ii) vessel diameter mismatch; (iii) damage to, or a lack of, ECs; (iv) suture line stress concentrations; (v) trauma during surgery and (vi) haemodynamic factors causing blood flow disturbances.[33–39] Atherosclerosis appears to be the main cause of graft failure after one year.[40] Atheroma formation is associated with the same factors as in the native arteries and occurs by a similar process. Monocytes invade the vessel neointima forming macrophages and, eventually, foam cells resulting in the development of atherosclerotic plaque.[39,41,42] Graft infection is more common in synthetic conduits due to their susceptibility to bacterial colonisation. Infections cause chronic inflammation and release toxins which complicate graft healing and can lead to sepsis and anastomotic failure or rupture.[43–47]

Given the limitations of current vascular bypass conduits, a tissue engineered vascular graft (TEVG) presents an attractive potential solution for the future of vascular surgery. A tissue engineered vessel with the ability to grow, remodel and repair *in vivo*, but without the need for autograft surgery has clear advantages and would be of great benefit. This chapter will review the current state of the art in vascular graft tissue engineering including an examination of the design requirements for a TEVG, an overview of the methods being used to produce such constructs, discussion of the various animal and limited human trials that have taken place and some considerations

for the future developments of TEVGs. This review will then be used to justify the research conducted and define the aims and objectives.

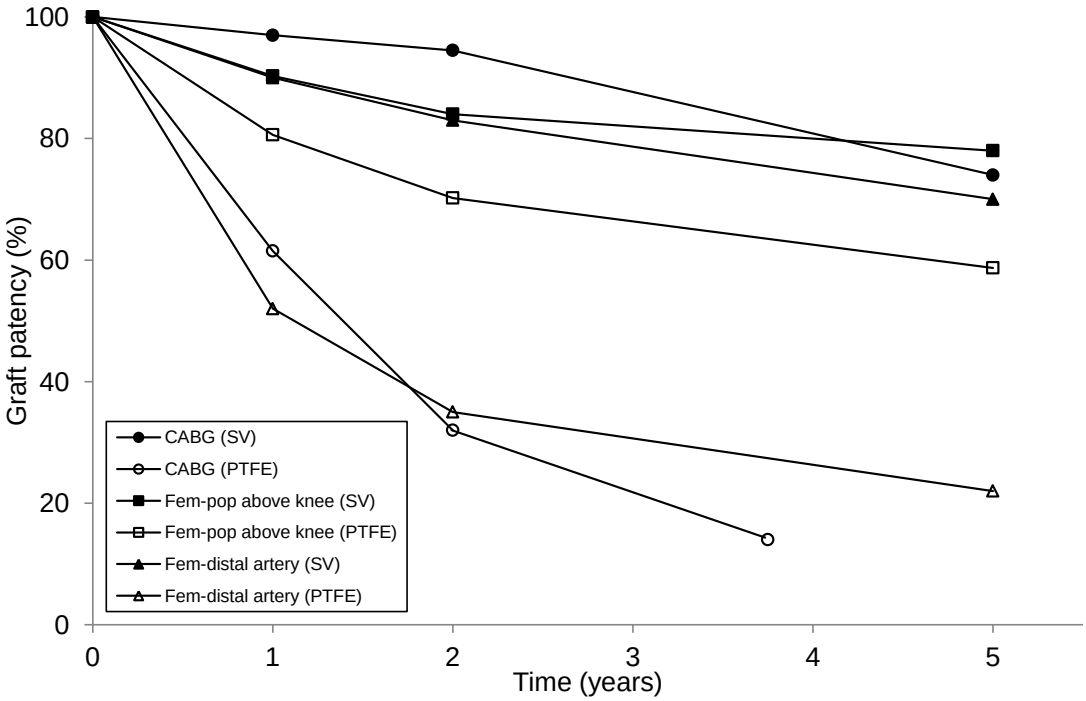

Figure 2. Patency rates for small diameter vascular bypass procedures using the SV and PTFE conduits (data for CABG using PTFE conduits was only available up to 45 months).[14,15,21–29,33,48]

1.2 **Design requirements for a TEVG**

As an integrated part of the vascular network, a TEVG must satisfy a number of design criteria to be fit for purpose.[20,49] Fundamentally, the construct is a conduit for supporting the flow of blood, therefore it must withstand the pressures exerted by this flow without bursting or experiencing permanent deformation through aneurysm. The pressure drop experienced within the flow over the graft length must also be sufficiently small and the luminal surface properties must be such that thrombus formation mechanisms are not triggered. The graft should possess suitable compliance to prevent the formation of high stresses around the anastomosis and be of a

geometry that does not induce certain, undesirable, flow characteristics, as both of these factors have been associated with failures in current bypass solutions.[33,34,38,50–52] The graft should also be non-cytotoxic and should not trigger a negative immunogenic response, such as chronic inflammation, complement cascade initiation or activation of the adaptive immune system. Additionally, from a clinical product perspective, a TEVG should be suitable for implantation; with kink resistance and the ability to be handled, manipulated and sutured; and be able to be mass produced in a range of lengths, quality controlled, stored and shipped at an economically viable cost. Ultimately, the graft should be able to grow, remodel and self-repair *in vivo*.

1.3 **Techniques for manufacturing a TEVG**

The first tissue engineered blood vessel construct was actually produced in the mid-1980s by Weinberg and Bell.[53] Bovine ECs, fibroblasts and SMCs were co-cultured in a collagen matrix and then shaped into tubes. Although tissue architectures analogous to natural blood vessels were achieved, the constructs required the support of a Dacron mesh and their mechanical properties were poor.

Since then, a number of different approaches have been taken to produce a clinically viable TEVG. Although these vary widely in terms of materials, manufacturing methods, cell source and culture protocol, they can be broadly categorised into scaffold based methods, using synthetic or natural materials; decellularised natural matrix techniques and self-assembly processes.

1.3.1 **Scaffold based methods**

Most cell types are unable to organise themselves into complex three-dimensional structures during culture, therefore the use of a scaffold, to provide a template of the required construct, is a popular approach in tissue engineering (Figure 3). Vascular tissue engineering has seen the use of scaffolds made from a range of synthetic and natural materials and manufactured using a number of different techniques.

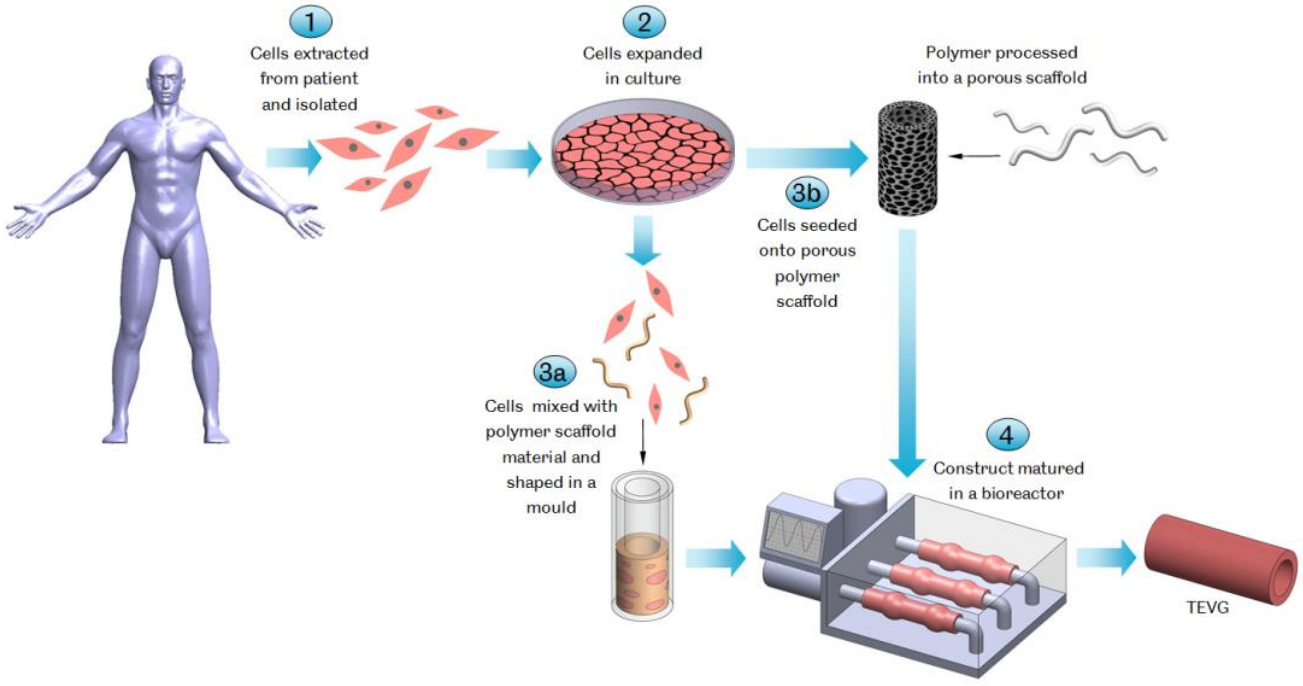

Figure 3. Scaffold based TEVG manufacture. Cells are harvested from the patient and the required types isolated and expanded *in vitro*. The cells are then mixed with a scaffold forming material, such as collagen or fibrin, and shaped in a tubular mould or seeded onto a porous polymer scaffold. The construct is then cultured in a bioreactor and may be conditioned to develop suitable mechanical properties for use as a TEVG.

1.3.1.1 *Synthetic polymers*

To date, the most extensive clinical trial of a TEVG has involved a construct produced using a synthetic polymer scaffold. The group of Shin'oka has developed a vascular graft for use in the treatment of cardiovascular disorders in children. Such disorders are particularly challenging, from a clinical perspective, often requiring multiple interventions as the child matures.[54] A tissue engineered graft solution with the potential to grow, remodel and repair *in vivo* is therefore particularly suited to use in children. Using a porous scaffold produced from a degradable co-polymer mesh of poly-L-lactide (PLLA) and poly-ε-caprolactone (PCL), reinforced with polyglycolide (PGA), vascular grafts for use as extracardiac cavopulmonary conduits to correct single ventricular physiology have been examined in 25 patients for up to 7 years.[55] These grafts were produced by culturing autologous bone marrow-derived mononuclear cells (BM-MNCs), extracted from the anterior superior iliac spine, on the scaffolds *in vitro*, prior to implantation. All grafts remained patent with no rupture, aneurysm formation, infection or ectopic calcification reported, although angioplasty was required in a small number of cases to retain patency.[56] Four patients died from non-graft related issues during the trial. Explant examination showed complete degradation of the scaffold material and the formation of recognisable vascular tissue with a wall of SMCs and a lumenal EC layer. It was noted, at late-term follow-up, that 40% of patients did not require daily medication. This is considerably lower than patients receiving similar procedures using synthetic vascular grafts which often require long-term anticoagulation or anti-platelet therapy.[57,58] Although the success of this trial is encouraging, it must be recognised that the TEVGs constructed were of a large internal diameter (12-24 mm) and were implanted in a high flow, low pressure system. Therefore, the success cannot be expected to easily translate into small-diameter constructs under high pressure, arterial, flow. Shin'oka and colleagues are attempting to adapt their approach to produce a TEVG suitable for such use, although with the focus remaining on potential utilisation in paediatrics.[59]

With the clear aim of developing small-diameter TEVGs for use in arterial flow, Niklason and colleagues have shown considerable success using a synthetic polymer scaffold based approach. This research group pioneered the development of bioreactor systems for generating TEVGs, *in vitro*, using biomimetic mechanical stimulation.[60] It has been well established that mechanical stimulation is important in tissue engineering, having a direct impact on cell function and fate. Niklason's bioreactor design utilises a distensible silicone tube which carries a pulsatile flow of culture medium. When a synthetic polymer scaffold seeded with cells is placed around this tube, it is subjected to physiologically relevant strains. *In vitro* work using PGA or PGA and poly(lactide-co-glycolide) (PLGA) scaffolds seeded with bovine SMCs and ECs showed that ECM formation and vessel strength were increased by the application of mechanical stimulation, compared to statically cultured controls.[60,61] Pulsatile flow was applied for 8 weeks at 2.75 Hz (165 beats per minute), imparting a 5% radial distension, in an effort to mimic foetal development in large animals. Vessel burst pressures of 2150 ± 709 mmHg were achieved, similar to those reported for the human SV (SV average burst pressure is 2134 ± 284 mmHg[62–66]), and vessel architectures and compliance were also comparable to natural vasculature.[67] A subsequent *in vivo* investigation, using autologous SMCs and ECs, showed one of these engineered vessels remained patent for up to 4 weeks when implanted in a Yacatan mini pig as a SV graft with no evidence of stenosis or dilation.

As an interesting progression, Niklason and colleagues then integrated a decellularisation step into their TEVG production process. Using decellularisation allows non-autologous cells to be employed in producing the vessel structure during bioreactor culture on the polymer scaffold. These cells are then removed using a treatment of enzymes and detergents, leaving behind only their ECM onto which autologous ECs can then be seeded, shortly before implantation. This strategy largely decouples the TEVG manufacturing process from the recipient, potentially providing an off-the-shelf graft solution. A number of *in vivo* studies, in small and large animals, have been conducted to explore the efficacy of using an *in vitro*-derived and then decellularised graft. In nude mice, decellularised vessels derived from human SMCs

were implanted as aortic interposition grafts for 6 weeks and showed 83% patency with no deterioration of the ECM as a result of the decellularisation process.[68] In porcine and canine models, decellularised grafts derived from allogeneic SMCs and then seeded with autologous ECs exhibited 100% patency at 30 days and 1 year, respectively, when implanted in carotid artery positions.[69,70] Additional work in canines also showed 100% patency for these grafts as coronary artery bypass conduits for 30 days.[70] In Baboons, similar constructs showed 88% patency over 6 months as arteriovenous fistulas (AVFs).[70] In all cases, grafts showed significant remodelling after implantation and the formation of tissue comparable to the adjacent native vessels. Very little intimal hyperplasia was reported, which was particularly interesting in the porcine carotid artery bypass study, as this animal model is usually considered to demonstrate accelerated intimal hyperplasia formation.[71] These findings resulted in the undertaking of pilot studies in humans with the TEVG employed as an AVF for vascular access in patients with end stage renal disease.[72] TEVGs were implanted into 60 patients with an average follow-up of 16 months. At 12 months, primary and secondary patency rates were 28% and 89%, respectively. The major cause of loss of primary patency was thrombosis. No aneurysms were detected throughout the cohort and this was considered impressive, given the TEVGs were regularly punctured for haemodialysis access. The grafts demonstrated invasion and remodelling by the host, becoming populated with SMCs, and did not appear to generate a significant immune response, suggesting the decellularisation process was sufficient. Notably, the performance of the TEVGs exceeded that of PTFE grafts, in multicentre studies, in terms of patency and infection rate.[73,74] Studies into this type of TEVG are ongoing with a transition towards a commercial product expected.

Results for a number of TEVGs based on synthetic polymer scaffolds have been reported by many other researchers around the world, including successes in animal models. These studies have shown great variation in relation to the polymers employed; scaffold manufacturing methods; seeded cells and culture protocols (Table 1). In Ovine models, non-woven PGA scaffolds seeded with autologous myofibroblasts and ECs have shown long term patency, of up to 100 weeks, as pulmonary artery

replacements.[75,76] These grafts had internal diameters of 10-18 mm and integrated well with the native vasculature, developing comparable tissue structures and showing complete scaffold degradation during the study period. In Lewis Rats, poly(ester urethane)urea (PEUU) scaffolds produced using electrospinning and thermally induced phase separation showed success as aortic interposition grafts for 8 weeks when seeded with rat muscle-derived stem cells or human pericytes.[77,78]

The use of completely acellular synthetic polymer scaffolds as TEVGs is also being explored. Using acellular scaffolds eliminates the need for *in vitro* cell culture and instead focuses on encouraging rapid host cell invasion and scaffold remodelling, after implantation, through scaffold architecture and surface chemistry. In canine models, a scaffold produced from a composite of non-woven PGA, poly(lactide/caprolactone) (P(LA/CL)) and poly(glycolide/caprolactone) (P(GA/CL)) exhibited patency for up to 12 months, as a pulmonary artery replacement.[79] Explants showed scaffold degradation and the formation of SMC and EC layers with ECM contents similar to the native tissue. Similar works showed patency for up to 12 months for non-woven PLLA and PGA scaffolds and 8 weeks for electrospun PCL and polyurethane (PU) scaffolds when implanted as canine carotid artery and femoral artery interposition grafts, respectively.[80,81] Additionally, studies in murine models have shown noteworthy results with grafts produced from electrospun PCL or poly(glycerol sebacate) (PGS) and PCL exhibiting host remodelling, ECM deposition and native tissue structures when implanted in arterial positions.[82,83]

The use of synthetic polymer scaffolds is the most widely investigated method for producing a TEVG and has yielded significant successes. The relatively low expense of producing synthetic polymer scaffolds coupled with the ability to tune various properties associated with them has been key to their extensive use and offers great potential for the future. The mechanical properties of these scaffolds, along with their degradation rate and topography have all been shown to influence the development of TEVGs.[78,82,84–91] Long production times, including extended *in vitro* culture steps,

present a large potential barrier to the clinical application of TEVGs based on synthetic polymer scaffolds. However, the recent use of decellularisation protocols, following *in vitro* culture, to largely move TEVG production offline and the potential of acellular "scaffold only" grafts both offer hope for the future.[70,79–83]

Table 1. Studies towards the development of a synthetic polymer scaffold based TEVG.

Scaffold material and manufacturing method	**Development level**	**Cell source**	**Comments**	**Group**
P(LA/CL) and PGA or PLLA. PGA mesh coated in additional polymers in a mould.	*In vivo* (human trial)	Autologous BM-MNCs	First human trial of a TEVG. Grafts patent for up to 7 years. Explants showed complete degradation of the scaffold. Large diameter vessel in high flow, low pressure system.	Shin'oka *et al.*[55,56]
PGA. Mesh sewn into a tube.	*In vivo* (human trial)	Porcine SMCs and ECs or human SMCs	Early work pioneered pulsatile flow bioreactor culture for TEVGs. Human trials employed TEVGs cultured *in vitro* and then decellularised as AVFs. Across 60 patients, TEVG performance was superior to PTFE grafts.	Niklason *et al.*[61,70,72,92]
PEUU. Thermally induced phase separation and electrospinning.	*In vivo* (murine model)	Murine muscle-derived stem cells or human pericytes	Grafts showed patency for up to 8 weeks. Host cell invasion and good integration observed. Burst pressures estimated at ~4000 mmHg.	Vorp *et al.*[77,78,91]
PGA and poly-4-hydroxybutyrate (P4HB). Non-woven PGA coated in P4HB.	*In vivo* (ovine model)	Autologous ovine ECs and fibroblasts	Graft patent up to 100 weeks as a pulmonary artery replacement (large diameter vessel). Complete scaffold degradation observed. Graft collagen content exceeded the native vessel.	Hoerstrup *et al.*[75,76]
PGS and PCL. Porogen leaching and electrospinning.	*In vivo* (murine model)	acellular	Patent up to 90 days in the rat aorta. Graft stress-strain response similar to the native vessel. Cell infiltration and organised elastin deposition observed.	Wang *et al.*[82,93]
PGA, P(LA/CL) and P(GA/CL). Non-woven PGA coated in P(LA/CL) and reinforced with P(GA/CL)	*In vivo* (canine model)	acellular	Patent for 1 year in the pulmonary artery (large diameter vessel). Scaffold fully degraded by 6 months *in vivo*. SMC and EC layers formed. Elastin and collagen content equalled the native vessel.	Yamazaki *et al.*[79]
PGA and PLLA. Woven PGA and PLLA.	*In vivo* (canine model)	acellular	Graft patent for up to 1 year in the carotid artery. Formation of SMC and EC layers observed. Graft collagen and elastin content increased *in vivo*.	Sawa *et al.*[81]
PU. Porogen leaching.	*In vitro*	Human SMCs	Cyclic strain increased cell proliferation, collagen content, strength and stiffness in cultured grafts.	Santerre *et al.*[94]
PGA and PCL. Polymer sheets seeded with cells concentrically wrapped.	*In vitro*	Bovine fibroblasts, SMCs and ECs	Significant elastin deposition observed. *In vitro*-remodelled graft showed a stress-strain response similar to native bovine arteries.	Vacanti C *et al.*[95]

1.3.1.2 *Natural polymers*

A number of different naturally derived polymers have been employed to generate scaffolds for use in TEVG production (Table 2). Significant successes have been seen using fibrin as a scaffold material. This material can be produced from polymerised fibrinogen isolated from a patient's own blood plasma.[96] The group of Tranquillo used fibrin gel to entrap human dermal fibroblasts and produce tubes using a mould.[97] A TEVG was then assembled by concentrically layering these tubes and allowing them to fuse together, however, after 3 weeks in culture, burst pressure values were just 543 ± 77 mmHg, well below those for natural vessels. Similar to synthetic polymer scaffolds, the application of mechanical stimulation improved the vessels mechanical strength.[98] *In vitro* culture in a perfusion bioreactor; applying cyclic strain and lumenal, ablumenal and transmural flow; generated a TEVG with a burst pressure of 1542 ± 188 mmHg and comparable compliance to natural vasculature. In a similar approach to Niklason's group, Tranquillo and colleagues have also recently reported on the use of decellularisation in their production of TEVGs.[99] Fibrin based grafts were cultured *in vitro* using ovine dermal fibroblasts and then decellularised. These acellular grafts exhibited comparable compliance to human vasculature and burst pressures exceeding those of the human SV. When implanted in the femoral artery of an ovine model these grafts remained patent for up to 24 weeks with no occlusion, dilation or mineralisation reported, representing the first long-term function of a natural polymer scaffold based TEVG in the artery of a large animal model. Explants demonstrated considerable remodelling with complete graft cellularisation and increased collagen and elastin content. These TEVGs also demonstrated somatic growth, over 44 weeks, when implanted into the pulmonary arteries of lambs.[100]

Additionally, Andreadis and colleagues have also examined a fibrin based TEVG in an ovine model. Here, fibrin tubes with entrapped vascular SMCs were implanted as vein interposition grafts in lambs.[101] The lumenal surface of these TEVGs was seeded with ECs prior to implantation and they showed patency for up to 15 weeks. Examination of explants showed that *in vivo* remodelling increased graft mechanical strength;

however, this reached only 25% that of the native aorta. Altering fibrinogen concentrations and using bone marrow-derived smooth muscle progenitor cells was demonstrated to produce stronger vessels, although this design of TEVG still remains to be tested under atrial flow.[102,103] Recently, hypoxia coupled with insulin supplementation was also shown to improve the strength of fibrin based TEVGs by enhancing collagen deposition in the entrapped cells.[104]

Silk-derived fibroin also has potential as a scaffold material for TEVGs. It offers tailorable mechanical properties, slow degradation *in vivo* and is compatible with a number of manufacturing processes.[105] *In vitro* work, using woven and electrospun fibroin scaffolds, has shown acceptable biocompatibility and adherence using a range of vascular cell types.[105–107] In subsequent studies in rats, as abdominal aorta replacements, acellular fibroin scaffolds showed cell invasion by SMCs and ECs and vascular tissue formation. Patency rates of 85% at 12 months were achieved, with no thrombosis or aneurysm observed. It was also suggested that the mechanical properties of these scaffolds could be improved to better emulate those of the native vasculature by using fibre alignment techniques during the manufacturing process.[105] Additionally, Mantovani and colleagues have constructed a scaffold composed of silk fibroin and collagen using electrospinning. Although this was shown to have superior strength compared to fibroin alone, it remained weaker than natural vessels. Viscoelasticity and good cell adherence were also shown, although there are as yet no reports of *in vivo* results.[108]

Building on the early work of Weinberg and Bell,[53] the use of collagen in TEVG scaffolds has continued. The integrity of collagen based scaffolds has been improved by modifying fibre density and orientation, adding crosslinks and using specific shape forming techniques.[109–113] Mechanical stimulation during *in vitro* culture has also been used. Using a bioreactor to apply mechanical conditioning through cyclic strain was shown to improve tissue organisation and significantly increase the strength of collagen gel based TEVGs.[114,115] The addition of elastin fibres to form a hybrid scaffold

was also shown to alter the mechanical properties of engineered vessels to more closely resemble those of natural tissue, with a non-linear, J-shaped, stress-strain response.[116] In all cases however, the ultimate tensile strengths and burst pressures of these constructs remained well below those of native vessels.

The linear polysaccharide chitosan has also been considered for the production of TEVG scaffolds. Chitosan is a derivative of chitin and is similar in structure to glycosaminoglycans which are a common ECM element.[117] Porous structures can easily be fabricated from chitosan using freezing or lyophilisation techniques and, *in vivo*, the material is slowly degraded by lysozyme with little foreign body reaction. Using a mesh of knitted chitosan fibres, coated in a chitosan and gelatine solution and then freeze-dehydrated, a porous scaffold was produced with a burst pressure of 4000 mmHg and a suture retention strength of 4.4 N.[118] Both of these values exceed those of the native vessel they were compared to (ovine carotid artery). The scaffold also showed acceptable cell adhesion and proliferation over 2 days using rabbit vascular SMCs. Although this report is promising in terms of mechanical performance, continued work using this scaffold is lacking. An alternative, constructed from cross-linked and freeze-dried chitosan and collagen, has also been shown to support vascular cell adhesion and proliferation and, additionally, exhibited suitable biocompatibility *in vivo* when implanted in rabbit livers.[119] However, the scaffold mechanical properties reported in this case were inferior to native blood vessels, with an ultimate tensile strength of just 310 ± 16 kPa. A question mark clearly remains over the mechanical properties of a chitosan scaffold and also how these may change over longer periods of *in vitro* cell culture or *in vivo*.

Although advantageous in terms of cell adhesion and biocompatibility, natural polymer based TEVGs have largely remained limited by their poor mechanical strength. Additionally, a high degree of compaction occurs in a number of natural polymer scaffolds, which produces a very dense matrix that vascular cells may have difficulty breaking down to remodel.[120] The use of dynamic bioreactor culture to improve vessel

mechanical properties has now been demonstrated.[98,101,103] Although the use of bioreactors increases production complexity, the recent successes seen in decellularised fibrin based TEVGs show the possibility of an off-the-shelf graft solution even if lengthy *in vitro* culture is required. This graft design has great potential for clinical utility, but is yet to be evaluated in the human circulatory system.

Table 2. Studies towards the development of a natural polymer scaffold based TEVG.

Scaffold material and manufacturing method	**Development level**	**Cell source**	**Comments**	**Group**
Fibrin. Gelled with encapsulated cells.	*In vivo* (ovine model)	Ovine dermal fibroblasts	Fibrin based TEVG cultured *in vitro* then decellularised. Decellularised constructs possessed burst pressures of ~4200 mmHg and compliance similar to natural vessels. Grafts remained patent for up to 24 weeks in the femoral artery and completely recellularised. In lambs, TEVGs demonstrated somatic growth in the pulmonary artery.	Tranquillo *et al*.[97–100]
Fibrin. Gelled with encapsulated cells.	*In vivo* (ovine model)	Ovine vascular SMCs, bone marrow smooth muscle progenitor cells and ECs	Patent for up to 15 weeks in the jugular vein. Grafts integrated well with the native vessel and remodelled to 25% the strength of the ovine aorta. Progenitor cell based TEVGs were stronger than those derived from vascular SMCs and produced greater elastin *in vivo*.	Andreadis *et al*.[101,103]
Silk fibroin. Gel spun into a tube.	*In vivo* (murine model)	Acellular	Patent for up to 4 weeks in the rat aorta. Graft invasion by host SMCs and ECs observed.	Kaplan *et al*.[105]
Silk fibroin. Woven into a tube.	*In vivo* (murine model)	Acellular	Patent for up to 1 year in the rat aorta. SMC and EC invasion observed at 12 weeks. Fibroin content reduced by 48 weeks, while collagen content increased.	Masataka *et al*.[106]
Silk fibroin. Electrospun and then coated with collagen.	*In vitro*	NIH/3T3 fibroblasts	Cells adhered and proliferated on the scaffold. Construct strength was below that of natural vessels (~900 mmHg).	Mantovani *et al*.[108]
Collagen. Gelled with encapsulated cells.	*In vitro*	Porcine SMCs and ECs	Cell proliferation and collagen remodelling observed over 7 days. Very low burst pressures achieved (~18 mmHg).	Mantovani *et al*.[121]
Collagen. Gelled with encapsulated cells.	*In vitro*	Murine aortic SMCs	Construct strength improved by increased collagen deposition as a result of mechanical stimulation. Burst pressures remained well below those of natural blood vessels.	Nerem *et al*.[114]
Collagen and elastin. Freeze dried then crosslinked.	*In vitro*	Human umbilical vein SMCs	Construct strength improved by mechanical stimulation. Stress-strain curve partially matched native vessels.	Feijen *et al*.[116,122]
Chitosan and gelatin. Knitted chitosan tube dipped in gelatine and freeze dried	*In vitro*	Murine vascular SMCs	Burst pressures of 4000 mmHg achieved. Suture retention strengths also exceeded the ovine carotid artery.	Zhang X *et al*.[118]

1.3.1.3 *Hybrid polymer scaffolds – synthetic and natural polymers*

Not all scaffold based approaches to producing a TEVG have been based exclusively on natural or synthetic polymers. A number of researchers have developed scaffold systems that utilise a combination of both (Table 3).

Coating of synthetic polymer scaffolds with natural polymers, in an effort to improve biocompatibility and cell adhesion, has been used extensively with collagen, fibronectin and gelatine all employed.[81,86,123,124] Synthetic polymers have also been used to provide reinforcement to weaker natural polymer scaffolds. Fibrin gels, with encapsulated ovine SMCs and fibroblasts, reinforced with a mesh of poly(L/D)lactide (P(L/D)LA) have been studied in an ovine model.[125] Following 21 day culture in a perfusion bioreactor, these engineered vessels were implanted as carotid artery interposition grafts and showed patency for up to 6 months with dense, although not cohesive, collagen and elastin deposition observed. In other work, a bilayered scaffold with an inner layer of recombinant human tropoelastin and an outer layer of PCL has demonstrated success in a rabbit model.[62] These grafts possessed mechanical properties not significantly different from the human ITA in terms of compliance and burst pressure. The elastin appeared to aid cell attachment and also conferred reduced platelet adhesion. When implanted as acellular grafts in the carotid artery position they showed 100% patency over 1 month with no dilation or thrombosis and little change in mechanical properties. Additionally, good results have been reported for acellular hybrid vessels of PCL, with PU and collagen or spiders silk and chitosan, in arterial positions in canines and rats, respectively.[80,126,127]

These hybrid scaffolds may be considered as new “smart” biomaterials that incorporate the strength, tunability and manufacturing control of synthetic materials with the improved biocompatibility and biochemical cues that come from natural polymer components. Therefore, the use of hybrid scaffolds has the potential to exploit the best of both synthetic and natural polymer scaffold systems to produce TEVGs. However, some of the limitations associated with using polymer scaffolds to

generate a TEVG are likely to remain a factor, particularly the requirement for long periods of *in vitro* culture to generate robust constructs.

Table 3. Studies towards the development of a hybrid polymer scaffold based TEVG.

Scaffold material and manufacturing method	**Development level**	**Cell source**	**Comments**	**Group**
P(L/D)LA and fibrin gel. Extruded polymer surrounded by fibrin gel with encapsulated cells.	*In vivo* (ovine model)	Ovine SMCs, fibroblasts and ECs	Patent up to 6 months in the ovine carotid artery. Graft integrated well with the native vessel. Collagen and elastin deposition observed.	Jockenhoevel *et al.*[125]
PCL and Chitosan. Electrospun.	*In vivo* (ovine model)	Acellular	Patent up to 6 months in the ovine carotid artery. Graft ECM and mechanical properties became similar to the native artery. Only ~9% of the original scaffold material remained after 6 months.	Breuer *et at*.[126]
PCL and collagen. Electrospun.	*In vivo* (lapine model)	Acellular	Patent for up to 1 month as rabbit aortoiliac bypass grafts. Little cell invasion or thrombosis observed.	Atala *et al.*[128]
PCL, spider silk and chitosan. Electrospun.	*In vivo* (murine model)	Acellular	Patent up to 8 weeks in the rat aorta. Host cell invasion shown.	Zhang D *et al.*[127]
PCL and synthetic elastin. Electrospun	*In vivo* (lapine model)	Acellular	Similar mechanical properties to the ITA demonstrated. Grafts remained patent for 1 month in the rabbit carotid artery.	Weiss *et al.*[62]
PCL and PU-collagen composite. Electrospun.	*In vivo* (canine model)	Acellular	Patent for up to 8 weeks in the canine femoral artery. A thin layer of ECs formed *in vivo*.	Zhang J *et al.*[80]
Gelatine-vinyl acetate copolymer. Electrospun.	*In vitro*	Murine SMCs	Dynamic culture conditions increased ECM deposition. Collagen and elastin content reached 70-80% that of the native rat aorta in 5 days.	Nair *et al.*[84]
PU and polyethylene glycol (PEG)-fibrin. Electrospun PU with seeded cells rolled up and coated in PEG-fibrin hydrogel.	*In vitro*	Murine smooth muscle progenitors	Graft stress-strain response after dynamic culture was very similar to the human coronary artery, although with lower ultimate tensile strength.	Hahn *et al.*[87]

1.3.2 **Decellularised natural matrices**

The use of decellularised natural matrices in tissue engineering takes advantage of the structure and mechanical performance of natural tissue ECM while avoiding any adverse immunological reactions due to its origin. The decellularisation process refers to the removal of antigenic cellular material from the tissue (Figure 4). Decellularisation may involve a variety of chemical agents, such as acids and bases, hypo/hypertonic solutions, detergents and solvents; biological agents, such as enzymes and chelating agents; and physical methods, such as agitation, pressure and abrasion.[129] Preservation of the ECM is intended, in order to maintain the tissue's mechanical properties.[130,131] A number of clinical products based on decellularised tissues, both human and animal in origin, are available for a wide range of applications including dermal, soft tissue, cardiac, ophthalmic and dentistry.[129]

Decellularised vascular grafts were first developed in the 1960's using animal tissue.[132] In the years since then, a range of these grafts have been made commercially available. These include Artegraft®, Solcograft® and ProCol® which were based on decellularised bovine blood vessels and SynerGraft® model 100 which was derived from decellularised bovine ureter.[133–140] Although these grafts have been utilised in vascular bypass surgery and as vascular access conduits, largescale adoption of them has not been seen. A number of studies, including prospective, randomised trials, concluded these decellularised xenogeneic grafts offered no clear advantage compared to alternative synthetic conduits.[141–144] Patency rates were comparable, at best, and the probability of graft salvage in the event of complications, such as infection or pseudoaneurysm, was lower. Decellularised xenogeneic grafts also cost considerably more than synthetic grafts.

A product based on decellularised human donor veins has also been developed and commercialised for use as an AVF (SynerGraft® processed human cadaver vein allograft). However, just as with decellularised xenogeneic grafts, this has not been widely adopted. Studies suggested this graft offered no improvement in patency compared to established solutions. The decellularised human vessels appeared more

resistant to infection, compared to synthetic alternatives, but were more susceptible to aneurysm.[145] Additionally, the availability of the human donor vessels required to produce this product is unpredictable and there are complex ethical and regulatory issues associated with the commercialisation of such tissue.

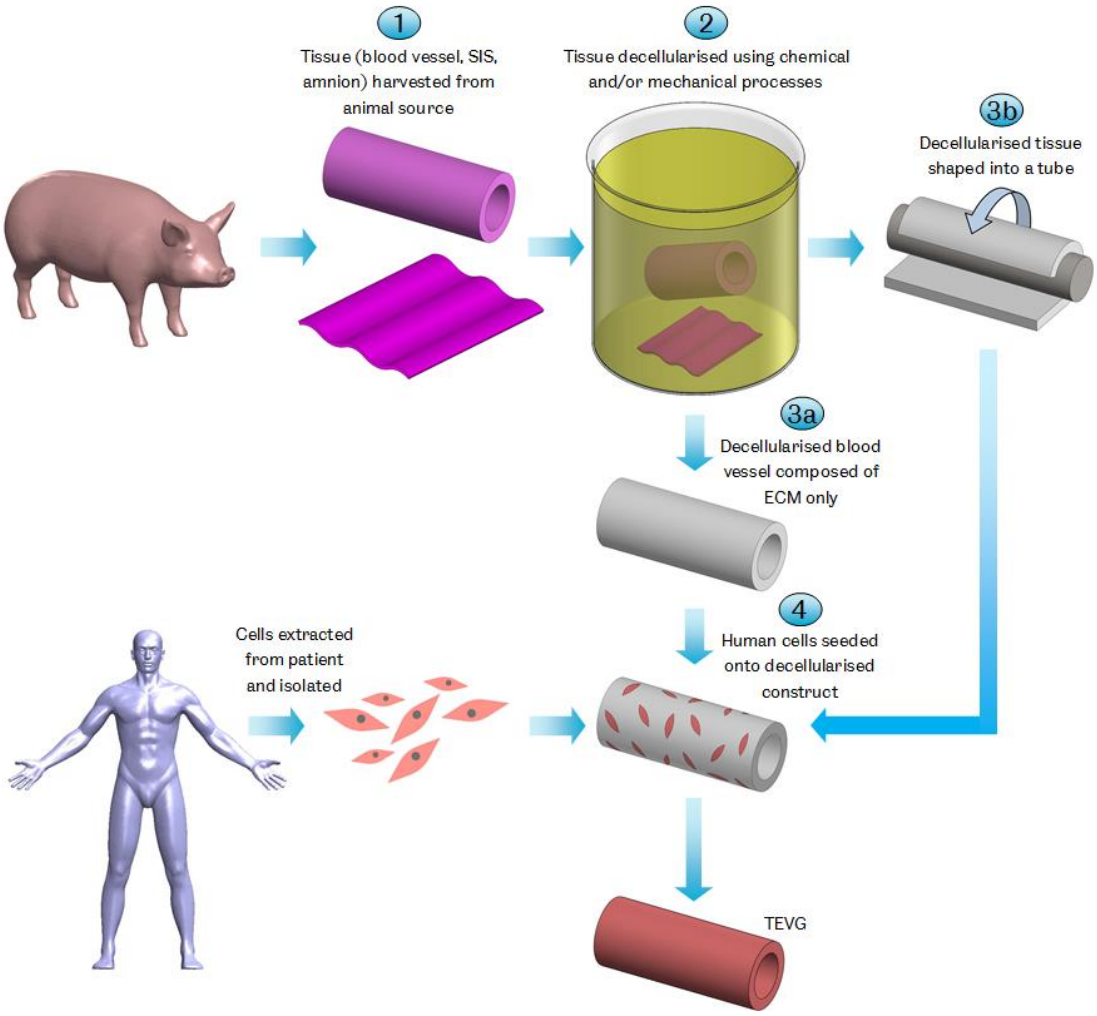

Figure 4. TEVG manufacture using decellularised matrices. Tissue is harvested from an animal source and decellularised using various chemical and/or mechanical processes. Where vascular tissue is decellularised, the result is a tube composed of only ECM. Decellularised non-vascular tissue, such as small intestinal submucosa (SIS) or amniotic membrane, may be shaped into a tubular construct. Cells extracted from the patient are then seeded onto the decellularised scaffold forming a TEVG after maturation.

The limited performance of commercially available decellularised vascular grafts has been suggested to be due to their lack of cellularity on implant.[133,139] The major failure modes observed are graft related thrombosis, infection and aneurysm. These may be combated by adding cells to the grafts, particularly luminal endothelial cells, prior to implantation. TEVG developers have taken to exploring this strategy (Table 4). In a "first in man" study, a decellularised human iliac vein seeded with autologous cells has shown success when used to produce a conduit for extrahepatic portal vein obstruction bypass (meso Rex bypass) in a paediatric case.[146] The vein was decellularised with detergents and enzymes and then seeded with autologous bone marrow-derived ECs and SMCs *in vitro*. After 6 days of bioreactor culture, the vessel was successfully implanted in a 10 year old girl. Patency was reported up to 2 years, although narrowing of the graft, at 9 months, required the insertion of a second section. This procedure offers potential, although only a single human implant has been reported and this was in low pressure flow.

A variety of decellularised vessels seeded with cells have been evaluated in animal studies also. In ovine models, positive results have been reported for decellularised porcine carotid arteries as carotid artery bypass grafts and AVFs. Following seeding with endothelial progenitor cells (EPCs), these grafts showed patency up to 4.3 and 5.6 months, respectively.[147,148] Additionally, in canines, decellularised carotid arteries (porcine and allogeneic) have shown patency up to 2 months in the carotid artery position.[130,131]

Non-vascular tissues, such as the small intestinal submucosa (SIS) and amniotic membrane, have also been decellularised and used to produce TEVGs. The SIS is a natural ECM sheet that has seen clinical application in many areas including skin, bladder, tendon and intestine.[149] Early work used porcine SIS, decellularised by abrasion and sutured into tubes, to produce TEVGs. When implanted in an acellular state, these grafts showed superior patency compared to PTFE conduits over 180 days in the canine carotid artery.[150] Host cell invasion and remodelling altered their compliance and burst pressures to similar to the native vessel.[151] Implantation in the canine aorta also showed good patency and remodelling, although the change in graft

compliance was smaller.[152] Ovine SIS has also been examined *in vitro* for its potential as a TEVG. When cultured as sheets under uniaxial strain, this tissue supported SMCs, differentiated from a hair follicle, which deposited collagen and elastin. The tissue also showed compliance properties similar to the native ovine carotid artery, although with lower tensile strength.[153] Most recently, acellular SIS tubes implanted as carotid artery interposition grafts in an ovine model demonstrated ~92% patency over 3 months.[154] These grafts were quickly populated by host cells, with a confluent endothelium formed after 1 month and significant collagen and elastin deposited. The grafts also demonstrated mechanical properties similar to the native artery.

The amniotic membrane is another natural ECM sheet, forming the inner layer of the placental membrane. It is covered by epithelium and contains collagen, fibronectin and laminins and has been shown to be biocompatible and non-immunogenic in ocular surface transplantation.[155] TEVGs produced *in vitro* using human amniotic membrane supported the growth and proliferation of ECs and SMCs. These constructs utilised decellularised amnion, either shaped around a mandrel and chemically cross-linked with glutaraldehyde or as a base for the culture of a cell sheet before being rolled into a tube.[156,157] In the latter, mechanical testing of the cultured vessels after 40 days under pulsatile flow showed a J-shaped stress-strain response, indicative of soft tissue, and a rupture strength 71% that of the human carotid artery, although the elastic modulus and compliance properties differed somewhat from this vessel. In a further step, TEVGs constructed from human amniotic membrane sutured into tubes were examined in a lamb model as interposition grafts in the jugular vein.[158] These grafts showed 100% patency over 48 weeks with no dilation, thrombosis or stenosis. Despite being implanted with their epithelium intact, little immune response was observed highlighting the low immunogenicity of the amniotic membrane. It remains to be seen how grafts produced using the amniotic membrane perform under arterial flow and pressure.

The natural architecture of decellularised tissues coupled with their diverse structural and functional biomolecular compositions makes them potentially advantageous for use in TEVGs.[159,160] Their inherent mechanical strength reduces the need for *in vitro*

culture or may remove this altogether. Suitably decellularised blood vessels possess mechanical properties ideal for use as vascular grafts and decellularised non-vascular tissue may be conditioned for vascular applications.[153,161] Additionally, as decellularised matrices are remodelled they may release chemoattractants with mitogenic or chemotactic activities that stimulate further host cell invasion and assist TEVG integration and remodelling.[162] However, there are also a number of limitations associated with using decellularised natural matrices. The decellularisation process is a compromise between removing antigenic cellular material and maintaining the ECM. Variation between protocols with respect to this balance is large.[163,164] Inadequate decellularisation has been associated with adverse immune reactions and sudden failures in implants, while aggressive treatments may remove important ECM components, such as elastin, leading to altered mechanical properties that may render the tissue no longer fit for purpose.[165–168] It has also been suggested that *in vivo* recellularisation of decellularised tissues may be inhibited by their dense ECM networks restricting cellular invasion or by chemical alterations to the matrix caused by the cell removal processes.[131,169–171] Indeed, a lack of graft cellularity has been associated with the limited success of the decellularised vascular grafts that have achieved commercial availability. Control over the geometry of decellularised TEVGs is another issue, as the size and shape of the tissue available is restricted. Composite grafts may be constructed, but this adds complexity and expense to the graft manufacturing process and may affect mechanical performance and biocompatibility.[158,159] Additionally, a number of graft properties; including geometry, mechanical properties and chemistry; may vary based on the age and health of the donor, making control of graft quality a challenge.

Table 4. Studies towards the development of a decellularised natural matrix based TEVG.

Scaffold material and manufacturing method	Development level	Cell source	Comments	Group
Bovine carotid artery. Decellularised	*In vivo* (clinical experience)	Acellular	First commercialised decellularised vascular grafts. Comparing performance with PTFE conduits showed no significant improvement in patency as AVFs. Salvage of decellularised grafts was more challenging after complications compared to PTFE grafts.	Sterling *et al.*[138] Johnson *et al.*[172]
Bovine mesenteric vein. Decellularised.	*In vivo* (clinical experience)	Acellular	Poor results when used in peripheral bypass procedures. Failures associated with thrombosis and aneurysm.	Lawson *et al.*[134] Davies *et al.*[136]
Bovine ureter. Decellularised.	*In vivo* (clinical experience)	Acellular	Prospective, randomised trial comparing decellularised bovine ureter with PTFE conduits when used as AVFs. No significant difference found.	Morsy *et al.*[133]
Human vein. Decellularised	*In vivo* (clinical experience)	Acellular	Compared results for decellularised human veins, cryopreserved human veins and PTFE conduits as AVFs. Decellularised grafts showed no improvements in patency.	Kurbanov *et al.*[145]
Human iliac vein. Decellularised.	*In vivo* (human trial)	Autologous SMCs and ECs	First human trial of a decellularised vessel seeded with stem cells. Extrahepatic portal vein bypass. Patent for up to 2 years, although partial narrowing at 9 months required the addition of a second graft section.	Sumitran-Holgersson *et al.*[146]
Porcine artery. Decellularised.	*In vivo* (ovine model)	Autologous ovine ECs	Grafts showed an average patency of 4.4 months as AVFs. ECs covered 50% of the graft lumen after 6 months.	Atala *et al.*[147]
Canine carotid artery. Decellularised.	*In vivo* (canine model)	Canine bone marrow-derived SMCs and ECs	Patent for up to 8 weeks in the carotid artery. Cell seeded grafts performed better than acellular controls. Explants showed a layered vascular wall structure with collagen and elastin deposition.	Kim *et al.*[130]
Human umbilical vein. Frozen, machined to a uniform diameter and then decellularised.	*In vitro*	Human umbilical cord vein ECs or fibroblasts	Bioreactor culture shown to increase vessel burst pressures. Burst pressures remained below that of human arteries at ~1200 mmHg.	McFetridge *et al.*[169]
Human SIS. Decellularised and shaped into a tube.	*In vivo* (ovine model)	Acellular	Patent up to 3 months in the carotid artery. Host cells invaded the graft with a confluent endothelium after 1 month.	Andreadis *et al.*[154]
Porcine SIS. Decellularised and shaped into a tube.	*In vivo* (canine model)	Acellular	Patent for up to 60 days in the carotid artery. Explants showed graft remodelling. Burst pressures exceeded human vessels (~5600 mmHg).	Lantz *et al.*[150,151]
Human amniotic membrane. Membrane seeded with cells and then rolled up.	*In vitro*	Human SMCs and umbilical vein ECs	Graft stress-strain response was similar to human vasculature. Rupture strengths were 71% that of the human carotid artery.	McFetridge *et al.*[156]

1.3.3 **Tissue engineering by self-assembly**

In a departure from the classic paradigm, tissue engineering by self-assembly (TESA) does not utilise a scaffold or supporting matrix in the creation of a TEVG (Figure 5). This approach was pioneered in the form of sheet-based tissue engineering, but now includes other methods, such as microtissue aggregation and cell printing.

L'Heureux and colleagues were the first to use sheet-based tissue engineering to produce a TEVG. The process involves the production of sheets of cells which are then layered and shaped around a mandrel, forming the tubular structure of a vascular graft. Media supplementation is used to encourage the cultured cells to produce large amounts of ECM, thus generating strong and robust sheets for TEVG fabrication.[173]

Early work attempted to produce a TEVG with a structure that mimicked natural arteries.[66] Sheets of human SMCs were wrapped around a mandrel and followed by sheets of fibroblasts. Culture in a flow bioreactor allowed the layers to fuse together before ECs were seeded onto the vessel's lumen. This process produced a vascular graft with a layered structure similar to natural blood vessels. Although 4 weeks were required to produce the cell sheets and an additional 8 weeks to allow the layers to fuse together, this vessel represented the first TEVG that showed physiologically relevant mechanical properties without the presence of a supporting scaffold. The vessels demonstrated burst pressures of 2594 ± 501 mmHg, well above the human SV. They also displayed physiological behaviour including contractile properties, imparted by the medial SMCs.[174] *In vivo* studies in canines as femoral artery interposition grafts showed that these grafts could withstand physiological pressures, demonstrating the feasibility of the sheet-based technique.[66]

Further development saw the removal of the medial SMC layer and an evaluation of graft production using age and risk-matched human cells. Through increased culture times and media optimisation, grafts produced from elderly donors with cardiovascular disease achieved the same mechanical strength as those made from young healthy donor cells.[64] These vessels were evaluated as arterial interposition

grafts in nude rats and in a more biomechanically relevant primate model with patency rates of 85%, after up to 225 days, and 100%, after 8 weeks, respectively. The grafts showed good integration with the surrounding tissue and resistance to aneurysm formation, although the overall production times still remained long at up to 28 weeks. Despite this drawback, the results were encouraging and clinical trials were undertaken with the grafts utilised as AVFs for haemodialysis access.[175] The TEVGs were produced using autologous fibroblasts and ECs taken from patient biopsies. They ranged between 14 cm and 40 cm long, with internal diameters of 4.8 mm and displayed burst pressures of 3512 ± 873 mmHg. Out of an original 10 patients, patency rates were 78% at 1 month (n=9) and 60% at 6 months (n=8) (withdrawal from the study and a non-graft-related death reduced the cohort size). Graft failures were associated with thrombosis or aneurysm formation. Over the 20 month trial, 4 grafts remained patent throughout. The results were in line with the currently set objectives for conventional procedures of 76% patency at 3 months, across all populations. However, the study group represented a particularly challenging patient population where AVF failure was expected to be far higher.[176] With this in mind, and the fact that the AVF may be considered a challenging application for a TEVG given the high puncture frequency it is subjected to, the results were considered to be quite promising. A second study examining leg revascularisation is now being targeted.[175]

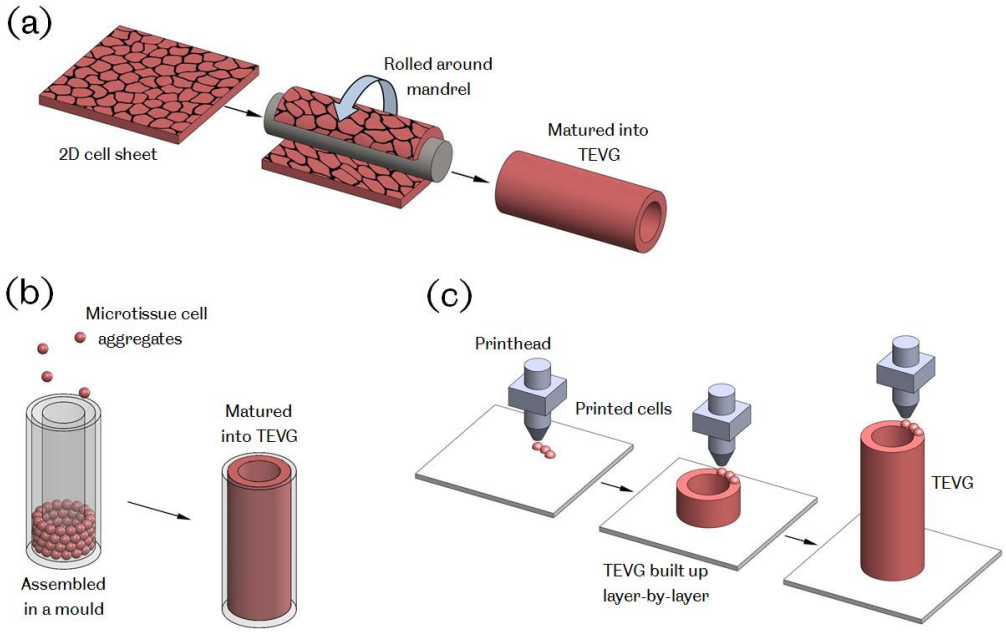

Figure 5. TEVG manufacture by self-assembly. (a) Sheet-based tissue engineering – a 2D cell sheet is cultured and then shaped around a mandrel forming a tube that is matured into a TEVG; (b) Assembly of microtissues - cell aggregates placed in a mould and combined to form a TEVG; (c) Bioprinting – cells and supporting material are deposited in a layer-by-layer manner, building up a 3D construct.

The use of allogeneic cells in sheet-based tissue engineering has subsequently been explored. Grafts produced from allogeneic fibroblasts were devitalised and successfully implanted in three patients to provide haemodialysis access.[177] Although little immune response was evident, in line with other reports which have shown allogeneic fibroblast constructs to be well tolerated, stenosis developed in 2/3 grafts, with intervention required, and failures ultimately occurred due to infection or thrombosis at 7 months. Further work is needed to determine if allogeneic cells can be successfully utilised to produce a TEVG, but this study clearly represents an important first step. Additionally, it has been shown that L'Heureux's sheet-based TEVGs can be manufactured and then stored prior to requirement. A graft was successfully devitalised and stored frozen before being rehydrated, seeded with autologous ECs

and then successfully employed as an AVF in a patient requiring vascular access.[178] This result, coupled with the potential use of allogeneic cells, offers real potential for a truly off-the-shelf TEVG solution.

Finally, the group of L'Heureux has recently described a new TESA method for producing a TEVG: thread-based tissue engineering. Here, cell synthesised threads are produced *in vitro* and assembled into 3D structures using textile techniques such as knitting, braiding or weaving. Grafts produced using this method have been suggested to possess greater strengths, and require shorter production times, than their sheet-based equivalents; although detailed reports are still outstanding.[179,180]

Other researchers have also explored the possibilities of sheet-based tissue engineering (Table 5). Grafts produced from sheets derived from mesenchymal stem cells (MSCs) have shown potential in a rabbit model, where they functioned as interposition grafts in the carotid artery for 4 weeks.[181] The group of Germain used dermal and SV fibroblast cell sheets to generate tubular constructs which were then decellularised, leaving behind only ECM, to act as a TEVG.[182] When implanted as aortic interposition grafts in Sprague-Dawley rats, these decellularised TEVGs remained patent for up to 6 months and became populated, although not completely, by host SMCs and ECs.[183] Additionally, it was shown that decellularised grafts of clinically relevant sizes could be stored for up to 3 months with no detrimental effects. Although only currently at the early stages of *in vivo* examination, this method offers the potential for an off-the-shelf TEVG solution, similar to Niklason's, with the decellularised matrices being produced from allogeneic cells, stored and then seeded with autologous cells just prior to implantation.

Additionally, novel TESA approaches have recently been reported involving the production of TEVGs by self-assembly of microtissue aggregates.[184] Using hanging drop cultures of human artery-derived fibroblasts and human umbilical vein endothelial cells (HUVECs), cell aggregates bound by secreted ECM were generated and then assembled into tubes. After 14 days under pulsatile flow, these aggregates had fused

into confluent structures. In a similar approach, 3D bioprinting was utilised to produce simple and branched blood vessel constructs by precise deposition and fusion of multicellular spheroids and cylinders.[185] After 21 days of culture in a bioreactor, these constructs demonstrated burst pressures of 773 mmHg, although this value appeared to have plateaued.[186] These approaches offer the potential for complex shapes to be produced, such as vascular bifurcations, however, whether they can achieve the required mechanical strength for use in the circulatory system remains to be seen.

TESA side-steps a number of issues associated with TEVG production using scaffold based or decellularised matrix methods. Difficulties associated with the manufacture, mechanical properties or breakdown of these supporting structures are removed. The major limitation of using TESA is the extended *in vitro* culture periods required, with multiple months needed for sheet-based TEVGs to achieve suitable mechanical integrity for vascular applications.[64,175] This drawback may be circumvented in the future by production in anticipation of individual's clinical needs, and then storing the vessels until required, or by employing allogeneic cells to yield an off-the-shelf graft solution. Sheet-based tissue engineering is also potentially limited in terms of the geometries it can produce. Thread-based tissue engineering or cell-aggregate methods, such as 3D bioprinting, may be more suitable for more complex constructs, but have yet to be proven.

Table 5. Studies towards the development of a TEVG using TESA.

TESA manufacturing method	Development level	Cell source	Comments	Group
Sheet-based tissue engineering	*In vivo* (human trial)	Autologous fibroblasts and ECs	First clinical trial of a TEVG under arterial flow as an AVF. 4/10 grafts patent for up to 20 months (in line with current clinical targets).	L'Heureux *et al.*[64,66,175]
Sheet-based tissue engineering followed by decellularisation	*In vivo* (murine model)	Human dermal and vein fibroblasts	Decellularised grafts consisted of ECM components only. Patent for 6 months in the murine aorta. SMCs proliferated successfully on decellularised grafts. Grafts of clinically relevant sizes could be successfully stored for 3 months without detrimental effects.	Germain *et al.*[182,183]
Mircotissue aggregate assembly	*In vitro*	Human artery fibroblasts and umbilical vein ECs	Cell aggregates bound by secreted ECM assembled into tubes. Fused under dynamic culture to form tube structures.	Hoerstrup *et al.*[184]
Bioprinting	*In vitro*	Human umbilical cord SMCs and dermal fibroblasts	Branched vessel produced from the fusion of printed cell cylinders and spheroids. High cell densities achieved with no scaffold. Maximum burst pressure values of 773 mmHg were achieved after 21 days in bioreactor culture.	Forgacs *et al.*[185,186]

1.3.4 **Consideration for the future development of TEVGs**

Despite the large differences between the approaches being pursued to develop a vascular graft using tissue engineering, a number of similar issues are facing all researchers in this field. These include: selecting the most appropriate cell types to use in TEVG production, determining how to achieve and maintain the required graft mechanical properties and understanding the process of TEVG remodelling and integration with the host vasculature.

1.3.5 **Cell source**

A number of different cell types have been used in the *in vitro* preparation of TEVGs (Table 6). The type of cells used may directly affect the structure of the graft and ultimately how it performs *in vivo*, along with impacting the graft manufacturing process.

Autologous adult vascular cells, such as SMCs, ECs and fibroblasts have been employed in many cases in creating TEVGs. These cells may be cultured for extended periods in bioreactors or seeded onto grafts prior to implantation. Despite their popularity, the use of these cells has several drawbacks. Their extraction requires blood vessel biopsies which are invasive, cause donor site morbidity and in some cases may be impossible due to vessel quality or availability.[130] Although some researchers have explored using non-vascular cells in an effort to overcome these issues,[98] adult cells are also limited in terms of replicative and regenerative capacity, due to their age.[187] This limits *in vitro* culture times, may affect graft performance *in vivo* and is particularly pronounced in the elderly, who are involved in the majority of revascularisations. Although improvements have been made to the replicative potential of adult vascular cells, using gene therapy, little effect on their regenerative properties has been achieved.[187,188] It has also been shown that extended culture periods and media optimisation can allow age and risk-matched human fibroblasts to produce TEVGs of

similar quality to those made from young healthy donor cells; yet such methods may ultimately be impractical.[64]

Given the limitations of autologous adult cells, various stem cell sources have been investigated for vascular tissue engineering. These include (i) progenitor cells; (ii) BM-MNCs; (iii) MSCs; (iv) adipose, (v) muscle or (vi) hair follicle-derived stem cells and (vii) induced pluripotent stem cells (iPSCs).

(i) Progenitor cells

Compared to adult cells, progenitor cells may be isolated from bone marrow or blood, using far less invasive procedures, and demonstrate greater proliferative and replicative capacity.[103,147,148] Using these cells may allow for longer *in vitro* culture periods, generating more robust TEVGs.[189] Ovine bone marrow-derived smooth muscle progenitor cells produced stronger and tougher TEVGs, *in vitro*, compared to using adult vascular SMCs directly. Progenitor cell based grafts also produced more organised elastin when implanted *in vivo* as jugular replacements in lambs.[101,103] Additionally, using vascular EPCs may be advantageous, as they induce nitric oxide mediated vascular relaxation. This process is more pronounced in arteries than veins and has been associated with contributing to the superiority of artery bypass conduits compared to veins.[190] Vascular EPCs may be depleted in elderly patients however, thus making them potentially difficult to obtain.[191]

(ii) Bone marrow mononuclear cells

BM-MNCs can be extracted from the bone marrow and include MSCs and hematopoietic stem cells. An extract of BM-MNCs has the potential to generate various cell types including vascular ECs, SMCs and fibroblasts.[192] These cells also lack major histocompatibility complexes, along with other important immuno-stimulatory molecules, offering potential as allogeneic cells for TEVG production.[193] Shin'oka and colleagues employed autologous BM-MNCs, extracted from the superior iliac spine, with great success in their pioneering clinical trial.[55] Additionally, these cells may be utilised to generate SMCs and ECs for seeding onto TEVGs *in vitro*.[130,146]

(iii) Mesenchymal stem cells

MSCs may be separated from BM-MNC extracts or other tissues including blood, adipose tissue, muscle and liver.[194–197] They are able to differentiate into SMCs with *in vitro* studies on TEVGs highlighting the effect that mechanical stimulation and certain growth factors can have on this process.[198] MSCs have demonstrated little potential to generate ECs, but work in animal models has suggested that they may have a role in assisting EC colonisation of TEVGs.[199,200] Additionally, MSCs may possess anti-thrombogenic qualities, potentially allowing for their use in TEVGs, *in vivo*, without the requirement for ECs.[201]

(iv) Adipose-derived stem cells

Adipose tissue also contains its own stem cells which have been shown to differentiate into both SMCs and ECs and have been used as a source of cells for vascular tissue engineering.[202–204] These cells can be extracted in high quantities from adipose tissue aspirate which is often readily available and easy to harvest. Since the majority of revascularisation procedures are conducted on elderly patients, utilising adipose-derived stem cells may have particular advantages. It has been demonstrated that these cells maintain high potency, with their potential to form ECs appearing unaffected by age.[205] Additionally, their numbers do not appear to diminish with advancing age with some evidence suggesting they may actually be more abundant in older subjects.[205,206]

(v) Muscle-derived stem cells

Muscle-derived stem cells have been utilised in successful *in vivo* studies of TEVGs.[77] When seeded onto PEUU scaffolds and implanted in rat aortas, these constructs demonstrated patency for up to 8 weeks; integrated with the surrounding tissue and became populated with ECs and SMCs. Although these results are positive, muscle-derived stem cells can only be obtained from muscle biopsies. These

procedures are invasive and painful, and therefore the clinical use of this particular stem cell source may be limited.

(vi) Hair follicle stem cells

Recently, hair follicle stem cells have been utilised to recellularise SIS and umbilical arteries, following decellularisation, to potentially create vascular grafts.[153,207] Although only early, *in vitro*, work has been reported, the hair follicle represent an abundant and easily harvested potential source of stem cells for use in TEVG production.[208] Hair follicle stem cells have been suggested to be similar to MSCs from bone marrow, although with a greater ability to proliferate in culture.[209] They may also have low immunogenicity, giving them potential as allogeneic cells.[210]

(vii) Induced pluripotent stem cells

The relatively new discovery of induced pluripotency opens up the possibility of obtaining suitable cells for vascular tissue engineering by transforming adult cells.[211] In a recent study, murine iPSCs were differentiated into SMC and EC phenotypes and used to construct a TEVG which remained patent for up to 10 weeks when implanted in the inferior vena cava of a mouse model.[212] Niklason and colleagues generated a TEVG from iPSCs derived from neonatal fibroblasts. These remained patent for 14 days as abdominal aorta interposition grafts in nude rats.[213] Additionally, human iPSCs, established from vascular fibroblasts, were used to generate proliferative SMCs which were combined with a PLLA scaffold to create a TEVG that demonstrated vascular tissue formation when implanted subcutaneously in a mouse model.[214]

Although these studies are promising and iPSCs have exciting potential for the generation of patient specific TEVGs, significant knowledge has still to be gained regarding their use. For example, ECs differentiated from iPSCs derived from adult cells have shown reduced proliferation compared to those from embryonic stem cells, suggesting that the original source for iPSCs may influence the properties of the ultimately derived cells.[215] As with other pluripotent cells, iPSCs also carry a risk of

teratoma formation. Greater understanding of this revolutionary cell type is required and a drive towards achieving this is already clear.[216]

(vii) Non-autologous cells

The possibility also exists to employ non-autologous cells in vascular graft tissue engineering. This could eliminate the problems with cell quality and variation that are associated with patient specific cells and also remove the delay in graft availability that is often caused by their culture requirements, potentially making grafts available off-the-shelf. Allogeneic cells have been employed successfully in treatments for other tissues, particularly the skin, where allogeneic dermal fibroblasts have been used in approved products, such as Apligraft® and Dermagraft®, without immunological issues. Additionally, BM-MNCs and hair follicle stem cells have both been shown to elicit low immune responses in allogeneic applications, thus presenting another possible source of donor cells for TEVGs.[193,210] L'Heureux and colleagues have trialled a sheet-based TEVG produced from allogeneic fibroblasts in the clinic.[177] Although patency was limited, an adverse immune response did not appear to be present, suggesting there is more to be learned about utilising allogeneic cells in vascular graft tissue engineering.

The range of possible cell types that may be utilised in a TEVG has recently been widened by the use of decellularisation protocols for producing engineered vessels *in vitro*, using polymer scaffolds or TESA.[70,182] With the decellularisation process removing the immunogenic cellular material from the grafts, therefore separating the cells used to engineer them from the intended patients, restrictions on cell source become reduced. Allogeneic, or even xenogeneic, banked cells or cell lines could be employed for the *in vitro* culture of the grafts.

Acellular grafts

The possibility of generating a TEVG without the need for *in vitro* cells is also being explored by a number of research groups. The earliest commercially available vascular grafts based on decellularised tissues did not utilise *in vitro* seeded cells; however,

their performance has been limited. No clear advantage of these products over alternative, and less expensive, synthetic conduits has been demonstrated.[141–144] The complications and failures seen when using these grafts were largely associated with thrombosis and aneurysm and, although the specific mechanisms behind these issues are not fully understood, the lack of graft cellularity has been suggested as a contributory factor.[133,139] As such, a number of researchers developing decellularised matrix based TEVGs have now taken to adding *in vitro* cells prior to implantation. Despite this, research into developing a TEVG that may be acellular at implant has continued. A number of acellular grafts based on synthetic or natural polymer scaffolds, along with decellularised matrices, have now been explored, although with varied results. Successful cell invasion, remodelling and integration of acellular polymer grafts has been reported in some *in vivo* studies in rats, canines and sheep.[79,81,82,154] However, other works have reported poor results with similar grafts showing the development of substantial intimal hyperplasia and calcification or a reduction in integrity after remodelling.[85,128] Conflict is seen between studies using similar scaffolds, animal models and timescales, but different implantation sites, suggesting that *in vivo* tissue engineering responses are complex and dependent on as yet unknown factors, such as the haemodynamic environment, inflammation and the immune response.[83,85] Additionally, numerous reports have shown failures in acellular grafts, implanted *in vivo*, directly associated with thrombosis due to the lack of a lumenal EC layer.[69,77,130,148,217] Indeed, platelet adhesion assessments in TEVGs have demonstrated the success of ECs in reducing thrombosis.[128] However, biochemical surface modification, such as heparin coating, has been suggested as a means to counter thrombosis without the addition of ECs.[131]

Removing *in vitro* cells from the "TEVG equation" has substantial practical and economic implications; greatly simplifying the pathway to clinical adoption and reducing potential therapy costs. However, it is unclear if *in vivo* tissue engineering can be relied on alone, especially in elderly or diseased patients, to generate successful vascular grafts.

Table 6. Range of cell types employed in TEVG development.

Cell type	Specific cells	Advantages	Disadvantages	Reference
Autologous somatic adult cells	Vascular SMCs Vascular Fibroblasts Vascular ECs Dermal Fibroblasts	Proven by a number of groups in TEVG manufacture. In the case of vascular cells, TEVGs are composed of the same cells as native blood vessels.	Harvest of vascular cells is invasive and may be limited by vessel quality or availability. Limited replicative and regenerative potential.	[65,70,75,98,102,105,107,118,125,156,175,185]
Progenitor cells	Bone marrow-derived smooth muscle progenitor cells Vascular EPCs	May be isolated from bone marrow or blood. Compared to adult cells, show greater replicative and regenerative capacity and may be cultured for extended periods to generate more robust TEVGs.	Certain progenitor cells may be depleted in elderly patients.	[87,103,147,148,189]
Natural stem cells	BM-MNCs	Isolated from bone marrow and contain various stem cells. Can generate SMCs, fibroblasts and ECs.	Bone marrow harvest is invasive.	[55,130,146,192]
	MSCs	May be extracted from bone marrow, blood, adipose tissue and liver. Able to differentiate into SMCs. Assist EC colonisation of TEVGs. Possess some anti-thrombogenic qualities.	Little ability to differentiate into ECs	[198,200,201,218,219]
	Adipose-derived stem cells	May be isolated from adipose tissue biopsies. Able to differentiate into SMCs and ECs. Patient age appears to have little effect on cell numbers and differentiation potential.	Only early, *in vitro*, work reported.	[202,203,205]
	Muscle-derived stem cells	Some success shown *in vivo* with seeded TEVGs integrating with the native tissue well.	Muscle biopsies are invasive and painful.	[77]
	Hair follicle stem cells	Hair follicles represent an abundant and easily harvested source of stem cells. Can differentiate into SMCs. Greater proliferative potential in culture compared to bone marrow-derived MSCs.	Only early, *in vitro*, work reported.	[153,207]
iPSCs	Various adult and embryonic cell sources	Great potential to generate cells for vascular tissue engineering from various adult or embryonic cells.	Differentiated cells produced from iPSCs show varied proliferative potential depending on the original cells used in iPSC generation, highlighting cell source as an important factor.	[212,214]
Non-autologous cells	Allogeneic fibroblasts (many other possible cells yet to be explored)	Time taken to expand patients own cells in culture avoided. Variation in cell quality between patients avoided. Off-the-shelf grafts possible. A wide variety of cell types, both human and animal, may potentially be used.	Potential immunological issues. Regulatory approval may be challenging.	[180]

1.3.6 **Mechanical properties**

1.3.6.1 *Design targets*

Given the load bearing nature of blood vessels, resulting from the pressurised fluid flow they support, the mechanical properties of a TEVG are important design requirements. Sufficient mechanical strength to retain integrity and resist permanent deformation may be considered one of the most fundamental performance criteria. Graft compliance and the way in which deformation under loading occurs is also important, as adverse biological responses have been associated with compliance mismatch between native vessels and both synthetic and biological vascular grafts.[33,38] Additionally, the ability of the graft to retain sutures must also be considered, given the surgical methods that will be employed during implantation. There is, however, a lack of agreement over the target values for these particular graft properties among researchers developing TEVGs. It has been common to use the current gold standard graft, the SV, as a target to emulate, making TEVGs essentially SV substitutes. Matching the SV may be beneficial for clinical adoption of a TEVG; however, patency may ultimately be limited by the same mechanical inadequacies associated with the SV. Using arterial conduits in bypass grafting, such as the ITA, has been shown to produce superior patency compared to the SV.[10–13] These conduits are not used preferentially due to their limited availability and the more severe implications of artery removal compared to veins. Although the ITA may be more challenging to replicate through tissue engineering, due to its increased strength compared to the SV, a TEVG designed to mimic this vessel may also display its improved performance. Figure 6 shows how the mechanical properties of some reported TEVGs compare to both the ITA and the SV. Based on these reported results, it is clear that no TEVG has yet been produced that matches the ITA or SV in terms of vessel burst pressure, suture retention strength and compliance. Of those groups reporting all of these metrics, the vessels produced by Tranquillo, Niklason, Vorp, Kim, Tan, Chen, McFetridge and L'Heureux may be tentatively considered the most promising. Interestingly, these groups span the whole

range of TEVG manufacturing methods. Clearly, no single method has yet proven its superiority and therefore it is very difficult to suggest the type of TEVG design that may ultimately achieve comparable properties to the ITA or SV.

Another consideration is whether any of the autograft conduits currently used in vascular bypass surgery should be used as a target for the mechanical performance of a TEVG. Since a vascular bypass is a non-natural construct, it is likely that the optimum properties required are different from these vessels. Tissue engineering provides the opportunity to work towards this target, but requires additional research to help define any target values. More advanced simulations of vascular biomechanics may be useful in achieving this in the future. Another issue is the variation in blood vessel mechanical properties displayed between different vessels in the human body and between different individuals.[220] Ultimately, it may be possible to tailor specific graft mechanical properties with the intended implantation site.

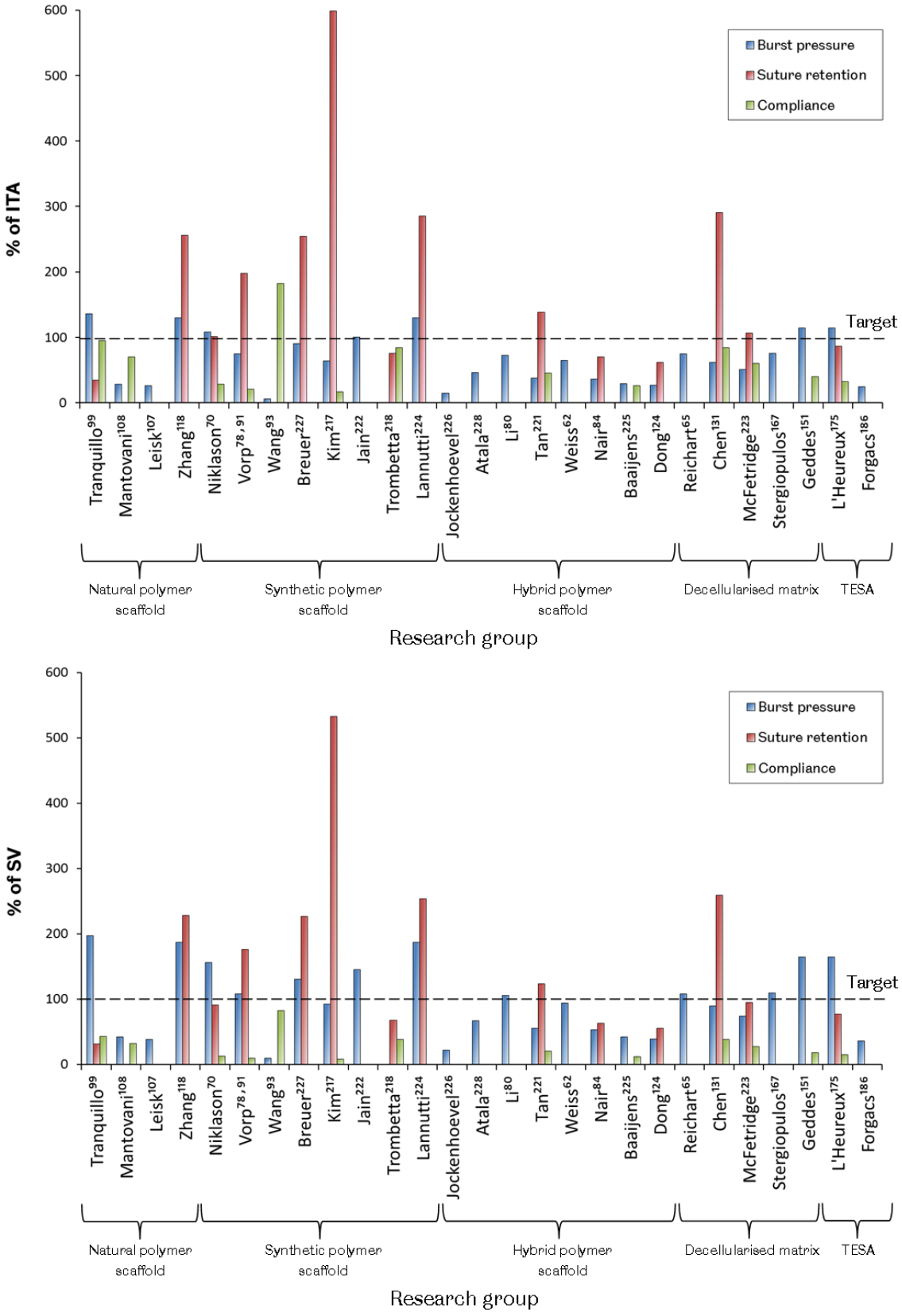

Figure 6. The mechanical properties of reported TEVGs compared to the human ITA and SV. The results are arranged by manufacturing method and represent grafts prior to any implantation.[62,65,70,78,80,84,91,93,99,107,108,118,124,131,151,167,175,186,217,218,221–228] For reference, values for burst pressure, suture retention strength and compliance are 3073 mmHg, 1.72 N and 11.5 %/100 mmHg for the ITA and 2134 mmHg, 1.92 N and 25.6 %/100 mmHg for the SV, respectively.[62–66,218]

1.3.6.2 *The effect of remodelling*

The picture of TEVG mechanics becomes even more complex when considering the remodelling and alteration in mechanical properties that may occur over time, after implantation. It is possible to ask not only what mechanical properties are required, but also when are they required. A number of *in vivo* studies have shown that TEVGs remodel to demonstrate altered mechanical properties after implantation. Some cases have shown a negative result, with conduits becoming weaker or stiffer due to an imbalance of ECM deposition and supporting scaffold degradation or calcification.[85,229] However, positive results with grafts becoming more similar to the native tissue are also reported.[63,70,99,101,151] The question of how different from the target mechanical performance the graft can be, at implant, and how quickly it alters *in vivo* is then raised. Given that failures associated with compliance mismatch, such as intimal hyperplasia, may occur in the first year of graft implantation, understanding the process of graft remodelling and the time taken is crucial and requires further investigation.

1.3.6.3 *Emulating the native stress-strain response*

Emulating the mechanical properties of native blood vessels is a challenge, due to their complex behaviour. Blood vessels display viscoelasticity and a J-shaped stress-strain response. These properties are a result of the different proteins that form the vessel walls. Low strains produce only small changes in stress driven by the compliant and elastic response of elastin fibres. As strains increase, crimped collagen fibres are opened out and engaged in a tensile manner, causing an increase in stress (Figure 7).[230–232]

A number of studies have reported TEVGs with mechanical responses that are similar to natural blood vessels. TEVGs produced from natural SIS sheets were shown to have a similar, J-shaped, stress strain response to the native ovine carotid artery.[153] This finding is understandable given their natural soft-tissue ECM structure. Using synthetic polymer scaffold based methods, a PU and PEG-fibrin hybrid scaffold seeded with

mouse smooth muscle progenitors and cultured under pulsatile flow conditions produced a TEVG with a similar stress-strain response to the human coronary artery.[87] Additionally, a composite vessel produced from layered PCL and PGA sheets seeded with bovine fibroblasts, SMCs and ECs showed a similar stress-strain response to bovine arteries after dynamic culture for 2 weeks.[95] *In vivo*, acellular PGS and PCL grafts implanted in Lewis rat aortas remodelled over 90 days, yielding vessels with closely matching mechanical responses to the native vessel.[82] Mechanical stimulation through pulsatile flow, either *in vitro* or *in vivo*, may have been key in achieving these vessel mechanical behaviours. However, a J-shaped stress-strain response curve similar to the coronary artery was also achieved using an electrospun PEUU scaffold, with integrated rat vascular SMCs, after only 3 days in dynamic culture in a spinner flask.[233] This result suggests that such pulsatile flow stimulation is not a prerequisite for achieving a TEVG with similar mechanical properties to the native vessel, and that scaffold materials may play an important role. Interestingly, an acellular graft produced solely from PGA and PU has also been shown to demonstrate mechanical behaviour similar to the natural porcine carotid artery, presenting the possibility of direct implantation *in vivo*, without the need for any *in vitro* cell culture.[222] It should be noted that it is unclear how the mechanical behaviour of TEVGs produced using scaffold based methods will change over time as the scaffolds degrade. *In vivo* studies of sufficient length and with appropriate time points are required to explore this and capture changes in graft mechanics associated with scaffold breakdown.[81]

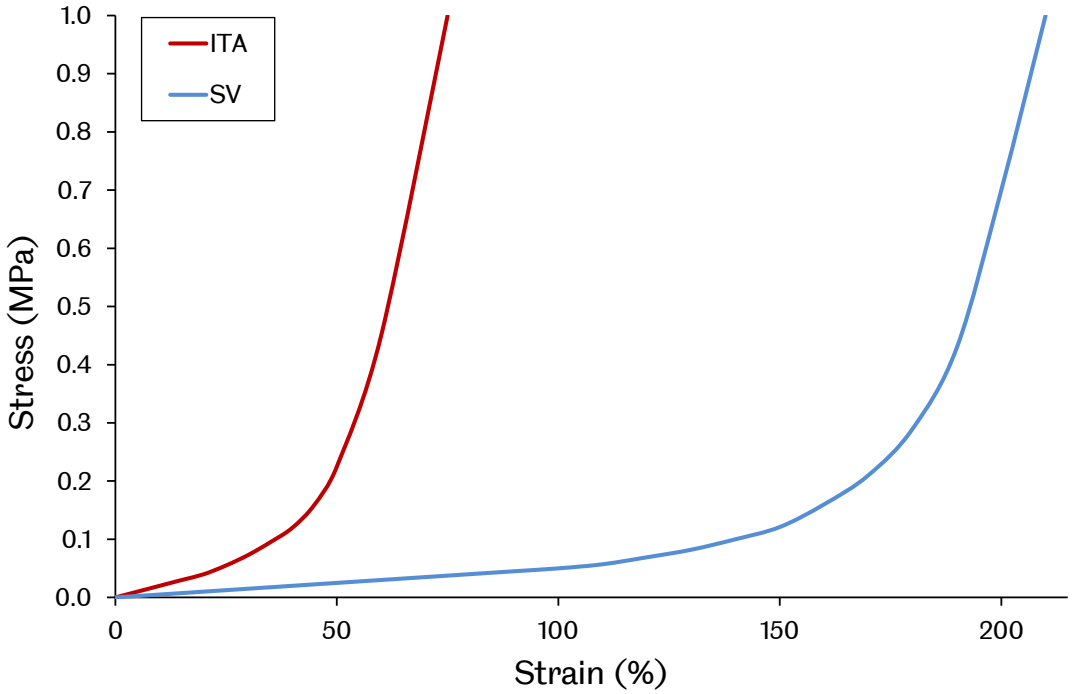

Figure 7. Representative stress-strain responses for the ITA and SV. Both vessels exhibit a J-shaped stress-strain response with a linear toe region.

1.3.6.4 *Elastin*

Another interesting element in the endeavour to engineer the required TEVG mechanical properties is elastin production. Elastin fibres are responsible for the elasticity of blood vessels, preventing dynamic tissue creep by stretching under load and returning to their original shape after the load is removed. This property prevents permanent deformation under pulsatile flow.[230]

Although elastin may not be an issue in TEVGs based on decellularised matrices, as these constructs often already possess this protein, producing it in *in vitro*-derived TEVGs is poorly understood. Although their grafts are undergoing clinical trials, the TEVGs produced by Niklason's group have been shown to possess little elastin. This finding has been suggested to be due to acidic hydrolysis products from the breakdown of their graft's PGA scaffolds reducing elastin synthesis by affecting cell proliferation and function, including ECM deposition.[234] There is some evidence that

scaffold stiffness, degradation rate and topography may influence elastin deposition too.[82,86,88] Comparing identical PGS and PLGA scaffolds showed the more elastic PGS produced a TEVG with organised elastin.[88,93] Further to this, the rapid degradation of a scaffold produced from PGS was also linked to improved elastin deposition in rats.[82] Organised elastin, in fenestrated sheets, has also been demonstrated when aortic SMCs were cultured on hyaluronan gels.[235] Additionally, TGF-β1 was shown to cause increased elastin synthesis in human SMCs only when they were cultured on 3D meshes, not on 2D sheets.[86]

Proteins and various factors have also been linked with affecting elastin deposition in TEVGs. Elastin production may be enhanced by fibrin, as fibrin gels seeded with rat SMCs showed enhanced elastin production compared to collagen gels.[236] Ascorbate has been used in the production of TEVGs due to its positive effect on collagen production.[67,70] However, ascorbate may also inhibit elastin production by destabilising elastin mRNA.[237] Using TGF-β1 and insulin were shown to overcome ascorbate's inhibition of elastin and also further enhance collagenesis.[237] Although, interestingly, Niklason's group used TGF-β1 and ascorbate in the culture of a TEVG and saw little elastin deposition, suggesting that insulin is critical.[198] Adding further to the confusion, the groups of Wang and Jockenhoevel both showed elastin deposition, when using ascorbate supplementation in the production of TEVGs, therefore its level of elastin inhibition remains unclear.[93,125,226] Jockenhoevel and colleagues did use a fibrin containing scaffold however, suggesting a possible balance between any positive effects of fibrin on elastinogenesis and inhibition by ascorbate. Additionally, elastinogenesis has been shown to be accelerated by retinoic acid and calcitriol. These compounds are under further exploration to discern their utility in TEVG production.[229,238]

The influence of mechanical stimulation on elastin production in TEVGs is also unclear. Elastin mRNA expression was shown to be independent of mechanical stimulation in collagen scaffolds.[239] However, in *in vitro* culture in a pulsatile flow bioreactor, a TEVG based on a gelatin–vinyl acetate copolymer scaffold seeded with rat SMCs achieved an elastin content 80% that of the native rat aorta in just 1 week. Although it is unclear

how organised this elastin was, gene expression for elastin was upregulated compared to static culture controls.[84] A synergistic effect between mechanical stimulation and the scaffold material may be in operation. Indeed, it is understandable that the mechanical properties of the scaffold may affect how any mechanical stimulation is transduced onto the cells in a TEVG. Interestingly, in a comparison of PGA and collagen scaffolds cultured under pulsatile flow, elastin expression was only upregulated in the PGA group, compared to static controls, suggesting a combinatorial effect of scaffold and mechanical stimulation.[240,241] Recently, Niklason and colleagues have developed a novel bioreactor able to provide axial and circumferential strain to TEVGs during *in vitro* culture. This biaxial stimulation produced TEVGs with mature elastin fibres, suggesting that axial strain may be another important factor in elastin production.[242,243] Elastin deposition has also been shown on SIS sheets cultured *in vitro* under simple uniaxial tension, not pulsatile flow. Human hair follicle-derived SMCs were utilised, but it remains unclear whether these cells, the mechanical properties of the SIS or its embedded chemical cues may have assisted elastinogenesis.[153]

Evidence for the influence of cell source on elastin production in TEVGs has also been demonstrated. L'Heureux and colleagues were able to achieve elastin deposition *in vitro*, although not quantified, in their sheet-based TEVGs which are based on fibroblasts, not SMCs as are commonly used by others.[66] Additionally, it was shown that using ovine bone marrow-derived smooth muscle progenitor cells, compared to using ovine vascular SMCs directly produced more organised elastin in TEVGs implanted as jugular interposition grafts in lambs.[101,103] Given that elastinogenesis varies throughout the mammalian lifespan, from very high levels during gestation to very low levels in adults, cell age is also likely to be a significant factor in elastin production in a TEVG.[244–247]

TEVGs have also been shown to remodel and gain increased elastin content *in vivo*. A decellularised fibrin scaffold based TEVG implanted in the ovine femoral artery remodelled to contain 8.8% the elastin content of the native vessel over 24 weeks, with these fibres being mature and organised. In a canine model, an acellular TEVG placed in the pulmonary artery obtained equal collagen and elastin contents to the

native vessel in 12 months.[79] Additionally, an acellular graft composed of PGA, PCL, PLLA and collagen implanted as a porcine aorta replacement developed 33% the native elastin content after 4 months, although elastin production then plateaued.[229] Determining the process of elastin deposition in graft remodelling may assist in developing methods to modulate and control this or to improve elastin production in TEVGs *in vitro*.

It has also been shown that elastin expression in cells cultured on TEVGs can be modulated, *in vitro*. It has been demonstrated that inhibition of certain microRNAs resulted in enhanced elastin deposition during the bioreactor culture of TEVGs.[248] This genetic modulation approach may be adapted to TEVGs *in vivo* to direct invading host cells to generate elastin.

It may also be possible to circumvent the need to generate elastin, by adding it to TEVGs directly. Elastin has been successfully added to scaffolds by electrospinning.[228] Indeed, an electrospun PCL and elastin scaffold has demonstrated mechanical properties similar to the ITA and was patent in rabbits for 1 month when implanted in an acellular state.[62] Producing elastin and understanding how to control this is a key challenge in engineering TEVG mechanical properties.

1.3.7 **TEVG haemodynamics**

Vascular bypass haemodynamics have been identified as having an effect on graft patency. In particular, intimal hyperplasia formation around the distal anastomosis has been linked with certain blood flow characteristics, such as flow separation, wall shear stress gradients and flow oscillation or stagnation.[34,249–251] The occurrence of these undesirable haemodynamics has been suggested to be influenced by both anastomosis geometry and graft compliance, although the former appears to have a greater effect.[252,253] To this end, a number of different anastomotic configurations have been explored, using both synthetic and autograft conduits, in an attempt to reduce undesirable haemodynamics and improve long-term graft patency. Interposition vein cuffs, such as the Miller cuff and Taylor Patch, improve graft-host compliance matching

and also alter anastomotic haemodynamics.[254–256] Their effectiveness is questionable, however, with conflicting reports of improved patency restricting their wide scale adoption.[257–260] Additionally, pre-cuffed synthetic grafts are also in production, again with the intention to reduce undesirable haemodynamics; however, their effectiveness is also debated.[261–263]

More complex anastomotic configurations have been designed and explored through simulation work.[264–267] Variation in design parameters such as anastomosis angle, flow area, bypass plane and graft-host ratio have been investigated in an effort to define the ideal geometry in terms of blood flow characteristics.[268–271] It is noted in a number of these works that the designs may be too complex for surgeons to reproduce using current vascular conduits. This difficulty presents a clear opportunity for the TEVG. A tissue engineered vessel may allow for more complex anastomotic configurations to be created and explored. Scaffold or self-assembly based approaches to generating TEVGs could be used to construct more complex vascular grafts with the intention to reduce undesirable haemodynamics and improve overall patency. Computer modelling with computational fluid dynamics and finite element analysis could be utilised to develop optimal graft designs and inform vascular graft tissue engineering.[38,50,272,273] Simulation work is ideal for exploring complex flow parameters, which can be difficult to measure *in vivo*, and also offers high resolution, repeatability and the option to easily change model settings and explore different graft geometry and flow scenarios. It remains for such a strategy to be examined by researchers in the field of vascular graft tissue engineering, but the potential power of this approach should not be overlooked.

It is also important to note that graft haemodynamics may also have an influence on TEVG integration and remodelling. Indeed, the difference between the blood flow in the carotid artery and the aorta was suggested to be the reason for the largely different calcification and graft cellularisation observed between two similar electrospun PCL grafts implanted in an acellular state in a rat model.[83,85] The role that haemodynamics may play in graft integration remains to be determined. In the future, it may advantageous to design TEVGs with consideration of conduit haemodynamics in

relation to both graft integration and remodelling along with the suppression of undesirable flow characteristics associated with causing intimal thickening.

1.3.8 **TEVG remodelling and integration *in vivo***

Although a number of TEVGs have been implanted *in vivo*, in humans and in a number of animal models, the mechanism by which these grafts integrate into the host's circulatory system and remodel into functional blood vessels is largely unclear. Evidence suggests that the host's immune cells, particularly monocytes, macrophages and neutrophils may be the major mediators of graft remodelling and neotissue formation through a modified inflammatory response. Immediately after TEVG implantation, neutrophils and monocytes migrate into the anastomosis and an inflammatory response occurs with the removal of debris, resulting from the surgical trauma, by phagocytosis. This process may last several weeks. Subsequently, signals are produced to direct a shift from inflammation to tissue remodelling and repair. Tissue engineered graft integration appears to consist of an atypical response to vascular injury, including intimal thickening and neointima development, along with biomaterial related effects, in some cases, such as foreign body reaction, fibrosis and the formation of a vascular media.[274]

Monocytes may be particularly important in early graft remodelling. These cells may be attracted to the implantation site due to chemoattractants released by activated neutrophils.[275] In studies using polymer scaffold based TEVGs, it has been shown that monocytes may remain at the implantation site until the scaffold is fully degraded (up to 100 weeks has been observed) with localisation around residual polymer fragments.[76] This finding suggests they may be involved in the complete remodelling process. Monocytes may produce cytokines, growth factors and enzymes important for vascular cell proliferation and tissue remodelling, such as Interleukins 6 and 10 and matrix metalloproteases.[276] Additionally, macrophage invasion has been observed in a number of acellular TEVGs when implanted *in vivo*.[82,85,99,227] These macrophages may

be derived from monocytes attracted to the implant site and have been suggested to be critical for neovessel formation in a mouse model, although the method by which this occurs is unclear.[277] The role of different macrophage phenotypes in biomaterial integration has become clear over recent years and is reviewed more thoroughly elsewhere.[278]

Progenitor cells have also been suggested as having an important role in TEVG integration. There is evidence that circulating progenitor cells from the bone marrow contribute to TEVG colonisation. When acellular silk fibroin scaffolds were implanted as aorta replacements in genetically modified rats, with bone marrow cells modified to express GFP, GFP positive SMCs were found as a major cellular component of the grafts medial layer after 12 weeks.[106] Circulating progenitor cells were also suggested to be the source of the intimal cells that invaded an acellular PGA and PLLA graft implanted in the carotid artery of a canine model.[81] Evidence suggests that invasion of TEVGs by host cells occurs at the anastomosis, and not via the graft lumen.[147] It is possible that the host's immune cells around the anastomosis may modulate this process by recruiting circulating progenitors. Interestingly, there is evidence that monocytes themselves may give rise to endothelial progenitor cells.[279] These cells have been shown to be important in graft endothelialisation and thus may represent an additional method by which monocytes contribute to graft remodelling.

Another important question relating to TEVG remodelling and integration is the role of any seeded cells present on the implanted graft. There is evidence that cells present on TEVGs at implant are quickly lost or replaced by the host's own. GFP labelling of ECs seeded onto a decellularised TEVG showed most were lost and replaced by host cells after 30 days *in vivo* in a porcine model.[69] Another study showed only 10% of seeded endothelial progenitor cells remained present on a decellularised graft after 130 days implanted in the ovine carotid artery.[148] Additionally, studies in rats with PEUU grafts seeded with human pericytes found most were lost from the graft after 8 weeks and replaced by the host ECs and SMCs.[78] It is unclear how cells present on TEVGs at implant may interact with the host and influence graft remodelling, although this process is likely to be dependent on the specific cells involved. Interestingly, human

BM-MNCs seeded onto polymer scaffolds were found to be replaced by monocytes within just a few days of *in vivo* circulation in a mouse model. These monocytes were later replaced by SMCs and ECs. It was noted that the BM-MNCs secreted significant amounts of monocyte chemoattractant protein 1 (MCP-1), as a result of their contact with the polymer scaffold. This may have contributed to monocyte recruitment.[280] It may be possible to exploit this process and encourage monocyte invasion into TEVGs by using MCP-1. Polymer scaffolds have been created with bound MCP-1 releasing microparticles in an effort to achieve this.[280]

The cellular and molecular mechanisms of graft integration and remodelling remain largely unclear. Gaining understanding in this field is vital for the future development of TEVGs and may ultimately allow modulation and engineering of this process.

1.3.9 **Conclusions and research opportunities**

It is clear that a number of different approaches are being explored to produce a TEVG and, with clinical results being reported for a wide range of techniques, the best solution is yet to be determined. Despite the range of technologies all apparently poised for success in this field, similar problems are faced by all developers, particularly in relation to understanding graft integration with the host.

Based on this review of the field of TEVGs, two interesting research opportunities are apparent. These are the production of grafts with suitable mechanical properties and the generation of TEVGs with varied or bespoke geometries.

Although the ideal mechanical properties for a TEVG have yet to be properly defined, and could indeed be variable depending on implantation site and the individual recipients, no TEVG has been produced with mechanical properties that match the current gold standard vessels (autograft veins and arteries). In relation to burst pressure, compliance and suture retention strength, it has not yet been possible for a single TEVG design to equal the performance of the gold standard vessels, in all three

areas. Compliance behaviour appears to demonstrate the greatest shortfall and this has been strongly linked with the elastin content of TEVGs. Elastin plays a major role in dictating the mechanical behaviour of blood vessels; however, producing TEVGs with suitable elastin content and organisation has yet to be achieved.

Additionally, to date, TEVGs have been almost exclusively manufactured as simple tubes. Although tubes may be adequate for a number of applications in vascular surgery, advancing TEVG geometry beyond this simple shape may allow superior modulation of haemodynamics, present additional therapy options and provide the possibility of tailoring TEVG design to specific individuals. It is noteworthy that a number of the manufacturing methods used to produce TEVGs, while able to produce tubes, may be difficult to adapt to producing more complex shapes, such as tapers, bends and bifurcations. Therefore it is important to consider the production of complex vascular graft shapes at the outset of developing a method for producing any TEVG.

1.4 **Research aims**

This research aimed to develop a method of manufacturing TEVGs with mechanical properties more similar to the current gold standard vessels. The mechanical properties of interest were burst pressure, suture retention strength and compliance. The TEVGs would be biocompatible, non-immunogenic and able to grow and remodel *in vivo*. Additionally, the TEVG manufacturing process would also be readily adaptable to producing more complex geometric shapes than simple tubes.

A synthetic polymer scaffold based approach was selected as the method for producing the TEVGs. The use of synthetic polymer scaffolds has been a widely adopted approach in the field of vascular tissue engineering (as discussed previously in 1.3.1.1). This method is also compatible with a range of manufacturing processes, has the potential to be adapted to produce a graft in a variety of predefined geometries and has shown success in a variety of *in vivo* studies, including human trials. A scaffold would be developed with properties, such as elasticity, degradation rate and porosity, specifically optimised towards the development of a TEVG with the aforementioned mechanical performance.

Using a proven approach, TEVGs would be produced *in vitro* in a bioreactor by seeding cells onto the synthetic polymer scaffold and then culturing them under physiologically relevant flow to encourage cell proliferation and appropriate ECM deposition.

1.4.1 **Objectives**

- Select and characterise a suitable synthetic polymer for use as the scaffold material for generating the TEVGs.
- Develop a method for producing tissue engineering scaffolds in a variety of shapes from the selected material.
- Design and manufacture a bespoke bioreactor capable of supporting the culture of TEVGs under dynamic conditions.
- Seed appropriate cells onto the scaffolds and culture in the bioreactor to generate TEVGs

Chapter 2 - Synthesis and Characterisation of Poly(glycerol sebacate)-methacrylate as a scaffold material for TEVGs

2.1 Introduction

In the previous chapter, a review of the literature identified that a TEVG has not yet been produced that has equal or closely matching mechanical properties to the current gold standard autograft vessels used in vascular surgery. Producing a TEVG with these properties was identified as the primary aim of this body of work.

A synthetic polymer scaffold based approach was selected to produce the TEVG. This method was chosen out of the varied manufacturing methods that have been employed to produce TEVGs previously. This was because it was compatible with a range of materials and manufacturing processes; has shown success previously, including in human trials; and has the potential to produce TEVGs of different geometries, which was the secondary aim of this work. The synthetic polymer scaffold would be seeded with cells and cultured in a bioreactor to generate a TEVG.

The material from which the synthetic scaffold was produced was of particular importance. To produce a TEVG with similar mechanical properties to autograft vessels, a number of requirements for the synthetic scaffold material were identified. The scaffold material was required to be biocompatible. This would allow it to support the culture of cells inside the bioreactor in order to generate a TEVG.[281] The elasticity of the scaffold was also identified as an important factor. It has been demonstrated that the compliance of TEVGs was improved by using scaffolds produced from more elastic

materials, with a Young's modulus of ~300 kPa appearing to produce the best results.[93,282] Additionally, the degradation rate of the scaffold has also been shown to influence TEVG development. More rapidly degrading scaffolds appeared to improve TEVG development during *in vitro* culture.[88] Finally, it was determined that the scaffold material should be easy to produce and process into a variety of scaffold shapes.

An examination of the literature revealed that poly(glycerol sebacate) (PGS) appeared to be an attractive potential scaffold material. This material had demonstrated suitable biocompatibility, mechanical properties and degradation rates in previous studies. PGS is a polyester produced from glycerol and sebacic acid monomers. The monomers are combined in a polycondensation reaction to produce a soluble prepolymer which is then thermally crosslinked into an insoluble matrix. The original development of this material was conducted by Wang and Langer.[282] They determined that the thermally crosslinked polymer was highly elastic; exhibiting a Young's modulus of 282 ± 25 kPa which was within the range of various soft tissues, including ligaments, veins and arteries. This was also well below the Young's moduli of various other polyesters commonly used as biomaterials, such as PLA, PLGA and PCL, which have values on the order of MPa. PGS also appeared to degrade rapidly, with subcutaneous implants being completely absorbed after 60 days in rats. The polymer appeared to illicit a similar inflammatory response to that of PLGA, but without the generation of a fibrous capsule. Subsequently, PGS scaffolds appeared to support the growth and proliferation of various cell types including fibroblasts, SMCs, ECs and hepatocytes.[283–285] Wang and colleagues further developed porous PGS scaffolds for use in TEVGs. Indeed, a scaffold produced from PGS was used to produce the most compliant TEVGs yet reported. These TEVGs contained extensive organised elastin fibres and displayed a stress-strain response similar to that of natural blood vessels.[82,88,93,286] This was attributed to the elasticity of the PGS, as a stiffer PLGA scaffold tested in parallel did not show the same elastin content or mechanical properties, and the rapid degradation of the scaffold which encouraged ECM deposition.

Interestingly, the studies by Wang and colleagues on PGS scaffold-based TEVGs were focused on ultimately using the PGS scaffolds in an acellular capacity and directly implanting them as vascular conduits. This approach would then rely on invasion by the host to cellularise the scaffolds. As such, TEVGs produced, *in vitro,* using the PGS scaffolds have only been for developmental purposes and used short bioreactor culture periods (21 days). Producing TEVGs *in vitro* that equalled the mechanical performance of the current vascular graft gold standards was not the goal of the research. The PGS scaffold-based TEVGs possessed inferior burst pressures compared to the gold standard vessels.

It was hypothesised that extending the culture periods for PGS scaffold-based TEVGs may produce mechanical properties similar to the gold standard vessels. Indeed, increasing *in vitro* culture lengths has been shown to increase the burst pressures and suture retention strengths of various TEVG designs to equal those of the gold standard autograft vessels.[61,64,66,67] TEVG compliance still remained limited in these studies, however. Since PGS scaffold-based TEVGs demonstrated excellent compliance, extending their bioreactor culture periods may generate grafts equal to the gold standard autograft vessels in terms of mechanical performance.

It was noted that the processing capabilities of PGS may be limited. PGS is simple to produce as a soluble prepolymer, through the melt-polycondensation reaction of sebacic acid and glycerol. However, to crosslink PGS into an insoluble matrix requires the application of high temperatures for extended periods of time to thermally cure the polymer.[282] These conditions make the creation of accurate shapes difficult and may limit the design of tissue engineering scaffolds produced from PGS.

To counter this limitation, a novel photocurable form of PGS was produced by methacrylating the free hydroxyl groups of the PGS prepolymer. This new polymer, PGS methacrylate (PGS-M), could be rapidly crosslinked (photocured) by exposure to UV light. Photocuring avoided the high temperatures required to thermally cure PGS and offered greater flexibility with regards to the design of the scaffolds for the TEVG.

In this chapter, the synthesis and characterisation of PGS-M is presented including analyses of the polymer's molecular composition, degradation behaviour and mechanical performance.

2.2 Materials and Methods

In the following methods, all chemical reagents were obtained from Sigma Aldrich, UK unless otherwise stated. These reagents were measured and utilised in inert vessels.

2.2.1 Synthesis of PGS prepolymer

PGS prepolymer was formed via the melt-polycondensation reaction of equimolar amounts of sebacic acid and glycerol (Fisher Scientific, UK)(Figure 8). These were combined and stirred in a 1 l, 3-neck, round bottom, flask under nitrogen gas, flowing at 1 l/min, at 120°C for 24 hours. A vacuum was then applied at 9 mbar, to remove water, and the reaction continued for a further 24, 36 or 48 hours to yield prepolymer of varied molecular weights.

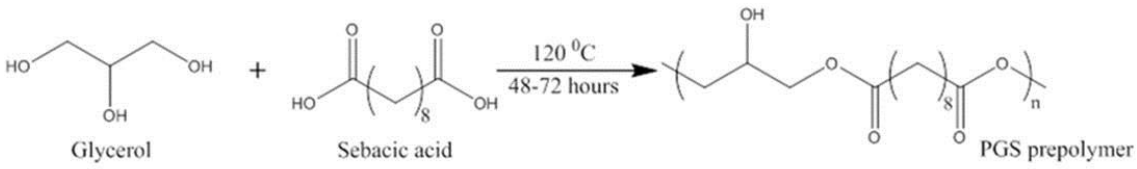

Figure 8. Synthesis of PGS prepolymer by melt-polycondensation.

2.2.2 Characterisation of PGS prepolymer using gel permeation chromatography

The molecular weight of the PGS prepolymer was analysed using gel permeation chromatography (GPC) (Viscotek GPC Max VE 2001). Samples of prepolymer were

taken from three batches after the polycondensation reaction had proceeded for 48, 60 and 72 hours. These samples were dissolved in 1 ml of tetrahydrofuran (Fisher Scientific, UK) at 0.5% (w/v) with 0.35 ml of toluene added as a reference. Samples were analysed at 40 °C using a 650 mm PLgel 5 µm Mixed C column with an injection volume of 100 µl and a flow rate of 1 ml/min, calibrated using a 66,000 Da polystyrene standard. Chromatograph peaks were analysed to deduce the prepolymer molecular weights as number average (M_n) and weight average (M_w) along with the polydispersity index (*PDI*) (M_w/M_n).

2.2.3 **Synthesis of PGS-M prepolymer**

To produce a photocurable polymer, the free hydroxyl groups of the PGS prepolymer were methacrylated. The molar mass of the PGS prepolymer repeat unit (glycerol + sebacic acid) was 258.314 g. It was assumed that two of the three hydroxyl groups present in glycerol reacted with sebacic acid. Therefore, 3.9 mmol of hydroxyl groups per gram of PGS prepolymer were available for methacrylation.[287,288]

Two different molecular weights of PGS prepolymer were methacrylated. Low molecular weight PGS prepolymer (further denoted as Low M_w PGS) was produced by polycondensation of glycerol and sebacic acid for 48 hours, as described previously (2.2.1). High molecular weight PGS prepolymer (further denoted as High M_w PGS) was produced by polycondensation of glycerol and sebacic acid for 72 hours, as described previously (2.2.1).

The PGS prepolymer (either Low M_w or High M_w) was dissolved in dichloromethane (Fisher Scientific, UK) 1:4 (w/v) and methacrylic anhydride, with an equimolar amount of triethylamine, slowly added (Figure 9). Three different concentrations of methacrylic anhydride were used (0.3, 0.5 and 0.8 mol/mol of PGS prepolymer hydroxyl groups) in an effort to vary the degree of methacrylation (DM) of the resulting PGS-M from 30% to 50% to 80%. 4-methoxyphenol was also added at 1 mg/g of PGS prepolymer. The reaction was performed at 0°C and allowed to rise to room temperature over 24 hours.

Additional 4-methoxyphenol was then added at 0.5 mg/g of PGS prepolymer and the solution washed three times with 30 mM hydrochloric acid (Fisher scientific, UK) at 1:1 (v/v). Water was then removed from the solution using granular calcium chloride (Fisher scientific, UK), at 0.4 g/g of PGS prepolymer, and filtration through a 6 µm pore cellulose filter (Whatman - Grade 3, GE Healthcare Life Sciences, UK). Finally, the dichloromethane was removed via rotary evaporation, under a vacuum pressure of 9 mbar, at 8°C to yield PGS-M prepolymer as a viscous liquid. This was stored at -8°C prior to use.

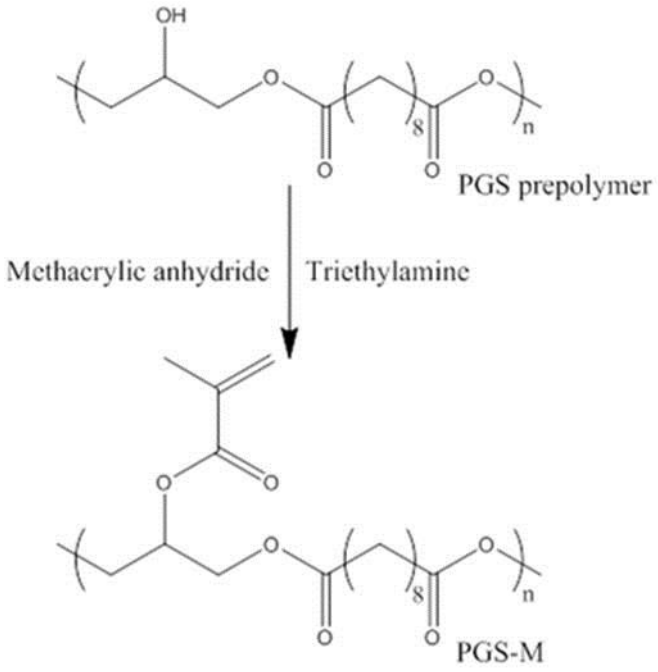

Figure 9. Synthesis of PGS-M prepolymer.

2.2.4 **Characterisation of PGS-M prepolymers by proton nuclear magnetic resonance spectroscopy**

PGS-M prepolymers were characterised using proton nuclear magnetic resonance (NMR) spectroscopy (Burker AVIIIHD 400 NMR spectrometer) at 400 MHz and compared to PGS prepolymer. Prepolymer samples were dissolved in 1 ml of deuterated chloroform ($CDCl_3$) at 1% (w/v). Chemical shifts were referenced to $CDCl_3$ at 7.27 ppm. The chemical composition was determined by calculating signal integrals of -$COCH_2CH_2CH_2$- at 1.2, 1.6 and 2.3 ppm for sebacic acid, -CH_2CH- at 3.7, 4.2 and 5.2 ppm for glycerol and -CH_3,CH_2 at 1.9, 5.6 and 6.2 ppm for the protons on the methacrylate groups. The signal integrals of the sebacic acid methylene groups (1.2 ppm) and the methacrylate groups (1.9, 5.6 and 6.2 ppm) were used to calculate the degree of methacrylation (DM) within each sample.

2.2.5 **Manufacture of flat disks of photocured PGS-M**

PGS-M prepolymers of Low and High M_w and varied degrees of methacrylation, synthesised as described in (2.2.3), were mixed 1% (w/w) with the photoinitiator diphenyl(2,4,6-trimethylbenzoyl)phosphine oxide/2-hydroxy-2-methylpropiophenone (50/50 blend) (further denoted as Photoinitiator) and placed between two sheets of 2 mm thick plate soda-lime glass held 1 mm apart by an aluminium spacer. The PGS-M was then exposed to UV light (100 W, OmniCure Series 1000 curing lamp) in a sealed container lined with reflective foil for 10 minutes, being turned upside-down after 5 minutes. The upper glass plate was then removed and the 1 mm thick cured PGS-M polymer sheet peeled away from the lower glass plate. Using a dissection punch, 7 mm disks were cut from the PGS-M polymer sheet.

2.2.6 **Determination of the soluble fraction of photocured PGS-M**

PGS-M prepolymers of Low and High M_w and varied degrees of methacrylation were photocured and processed into 7 mm diameter, 1 mm thick, flat disks, as described in (2.2.5). These disks were dried at 70°C and weighed until reaching a constant mass. They were then placed in methanol to solubilise any unreacted prepolymer. After 24 hours, the disks were removed and the drying process repeated. Methanol washing and drying was repeated until the disks reached a constant mass again. Controls were subjected to the same drying regime, but without methanol washing.

Experiments were performed three times with triplicate samples. Results were statistically analysed using two-way ANOVA (paired samples) with Tukey multiple comparisons analysis. $P<0.05$ was considered significant.

2.2.7 **Characterisation of PGS-M by attenuated total reflectance Fourier transform infrared spectroscopy**

0.1 ml PGS-M prepolymer samples, synthesised as described in (2.2.3), were examined by attenuated total reflectance Fourier transform infrared spectroscopy (ATR-FTIR) (Thermo Scientific iS50R FT-IR with germanium crystal), between wavenumbers of 4000 and 400 cm^{-1}, and compared to PGS prepolymer, synthesised as described in (2.2.1). ATR-FTIR was conducted in absorbance mode, with spectra obtained at a resolution of 8 cm^{-1}, gain 1 and amplification 6 with 512 scans performed. The data was analysed using OMNIC software.

Additionally, 7 mm diameter disks of photocured PGS-M, manufactured as described in (2.2.5), were washed in methanol for 24 hours, to remove any unreacted prepolymer, dried at 70°C for 1 hour and then also examined by ATR-FTIR.

2.2.8 **Characterisation of PGS-M by Raman spectroscopy**

PGS-M prepolymers and photocured disks were examined by Raman spectroscopy (Thermo Scientific Nicolet DXR with 532 nm laser at 2 cm^{-1} resolution), between Raman shifts of 4000 and 400 cm^{-1}, using a 532 nm laser at 10 mW. The exposure time was 10 seconds, with 20 exposures taken per sample, and the spectrograph aperture set at 50 µm. Fluorescence correction was also applied. The data was analysed using OMNIC software.

PGS-M prepolymer samples (0.1 ml), synthesised as described in (2.2.3), were examined; along with 7 mm diameter disks of photocured PGS-M, manufactured as described in (2.2.5), then washed in methanol for 24 hours, to remove any unreacted prepolymer, and dried at 70°C for 1 hour.

2.2.9 ***In vitro*** **degradation of photocured PGS-M**

PGS-M prepolymers of Low and High M_w and varied degrees of methacrylation were photocured and processed into 7 mm diameter, 1 mm thick, flat disks, as described in (2.2.5). These disks were then placed in methanol, to remove any soluble prepolymer, for 24 hours and subsequently dried to constant mass, at 70°C.

In vitro degradation was assessed using 3 different treatments: cholesterol esterase enzyme (porcine pancreas) (40 units/ml), lipase enzyme (*Thermomyces lanuginosus*) (40 units/ml) and PBS. PGS-M disks were placed in the wells of 12-well plates (Greiner bio-one, Germany), in triplicate, and 1 ml of each treatment solution added. Controls were left in wells untreated. Well plates were placed on an orbital shaker (SeaStar, Heathrow Scientific, USA) operating at 90 rpm in an incubator at 37°C.

The disks were treated for 8 days in total. After every 2 days, they were removed from their wells, rinsed in PBS and then dried to constant mass, at 70°C. They were then placed in new wells with fresh treatment solution added and returned to the orbital shaker.

The results were statistically analysed using one-way ANOVA with Tukey multiple comparisons analysis. $P<0.05$ was considered significant (*), $P<0.01$ was considered very significant (**) and $P<0.001$ was considered extremely significant (***).

2.2.10 Examination of degraded photocured PGS-M using scanning electron microscopy

The PGS-M disks subjected to degradation for 8 days, as described in (2.2.9), were examined using scanning electron microscopy (SEM). At the conclusion of the degradation study, the dry PGS-M disks were affixed to aluminium stubs, using carbon tape, and coated with gold using a sputter coater (Edwards S150B). The gold coated disks were then examined in a scanning electron microscope (Philips XL-20) at 13-15 kV.

2.2.11 Tensile testing of PGS-M

The mechanical properties of PGS-M were assessed by tensile testing (Hounsfield H100KS tensile testing machine). Procedures were performed as specified in BS ISO 37:2011 using Type 2 dumb-bell test pieces.[289] PGS-M prepolymers were mixed 1% (w/w) with photoinitiator and cast into silicon moulds. These were then exposed to UV light (100W, OmniCure Series 1000 curing lamp) in a sealed container lined with reflective foil for 10 minutes, being turned upside-down after 5 minutes. The photopolymerised PGS-M test pieces were then placed in methanol, to remove any soluble prepolymer, for 24 hours and subsequently dried to constant mass, at 70 °C, before use. Tensile testing was performed at a crosshead speed of 500 mm/min with samples elongated to failure. Three experiments were performed with triplicate samples of each PGS-M variant. The results were statistically analysed using one-way ANOVA with Tukey multiple comparisons analysis. $P<0.05$ was considered significant (*), $P<0.01$ was considered very significant (**) and $P<0.001$ was considered extremely significant (***).

Further testing was conducted on 30% Low M_w PGS-M following sterilization by autoclaving and peracetic acid. Methanol washed 30% Low M_w PGS-M test pieces were placed in dH_2O and autoclaved at 121°C for 30 minutes. Additional samples were also subsequently washed in 0.5% peracetic acid for 1 hour and then rinsed in dH_2O. Tensile testing was performed on all samples immediately following their removal from dH_2O. Three experiments were performed with triplicate samples of each PGS-M variant. The results were statistically analysed using one-way ANOVA with Tukey multiple comparisons analysis. $P<0.05$ was considered significant (*), $P<0.01$ was considered very significant (**) and $P<0.001$ was considered extremely significant (***).

2.3 Results

2.3.1 Characterisation of PGS prepolymer using GPC

PGS prepolymer was synthesised by the polycondensation reaction of glycerol with sebacic acid at 120°C. The duration of the reaction was varied from 48 to 72 hours to determine the effect on the resulting PGS prepolymer. GPC analysis demonstrates that the reaction duration has an effect on the molecular weight of the prepolymer. Molecular weight, calculated as both M_n and M_w, increased as the reaction duration was increased from 48 to 72 hours (Figure 10 and Figure 11).

Mean average molecular weights were 2,227, 2,774 and 3,356 Da for M_n and 5,419, 8,957 and 17,339 Da for M_w at reaction lengths of 48, 60 and 72 hours, respectively. Variation was seen between different batches of PGS prepolymer, with standard deviations of 43, 98 and 54 Da for M_n and 435, 844 and 760 Da for M_w at reaction lengths of 48, 60 and 72 hours, respectively.

The polydispersity index (*PDI*) was also calculated (M_w/M_n) and shown to increase with increasing reaction duration (Figure 12). Mean average values were 2.43, 3.22 and 5.17 at reaction lengths of 48, 60 and 72 hours, respectively.

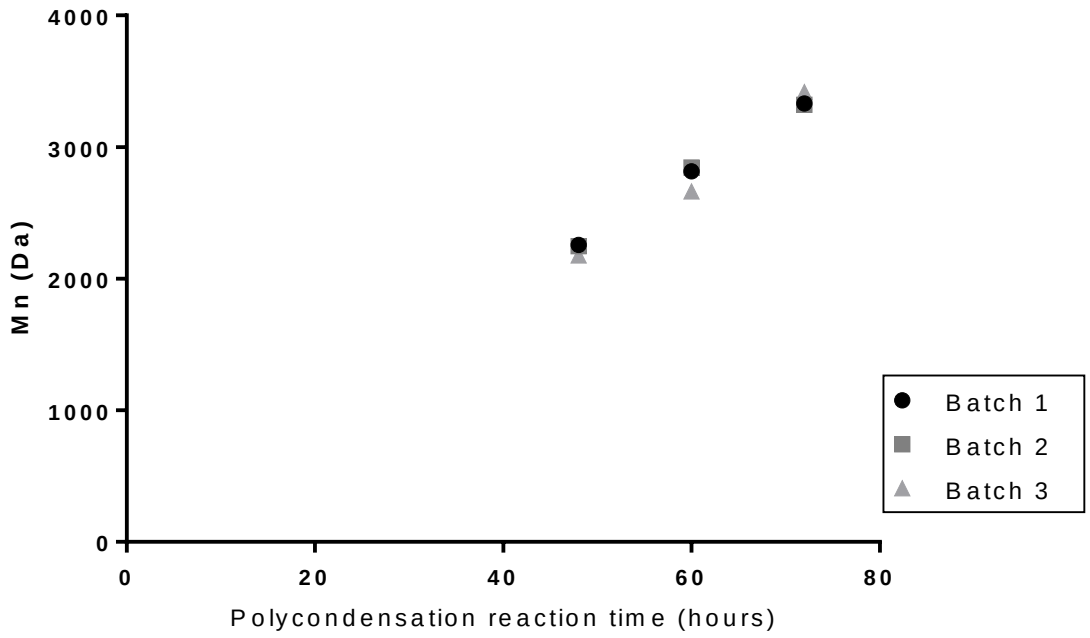

Figure 10. Variation in PGS prepolymer number average molecular weight as a result of increased polycondensation reaction time (*n* = 3).

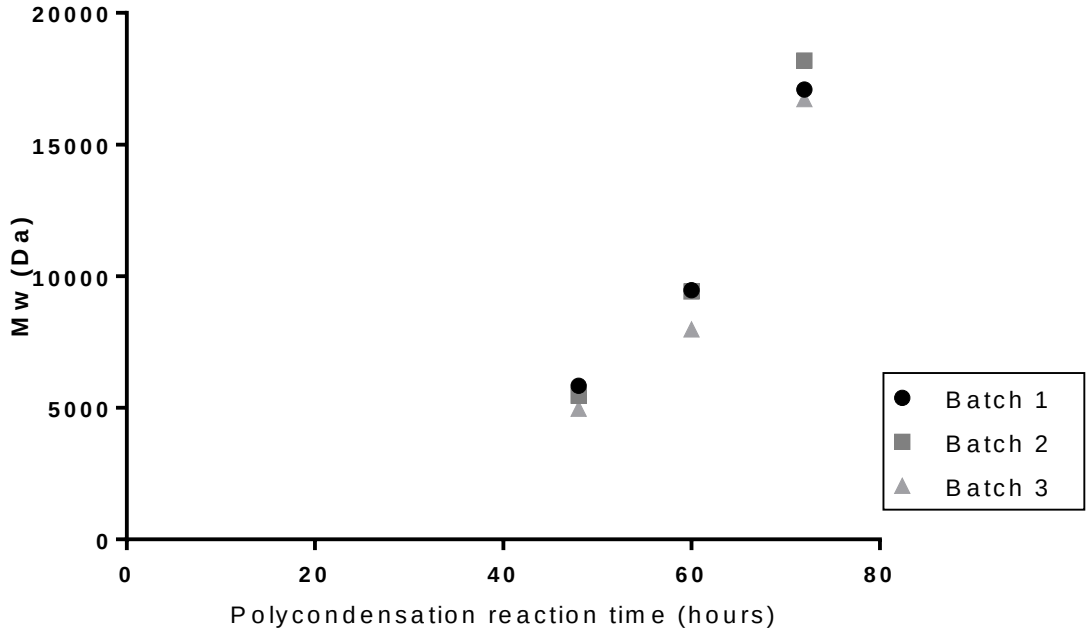

Figure 11. Variation in PGS prepolymer weight average molecular weight as a result of increased polycondensation reaction time (*n* = 3).

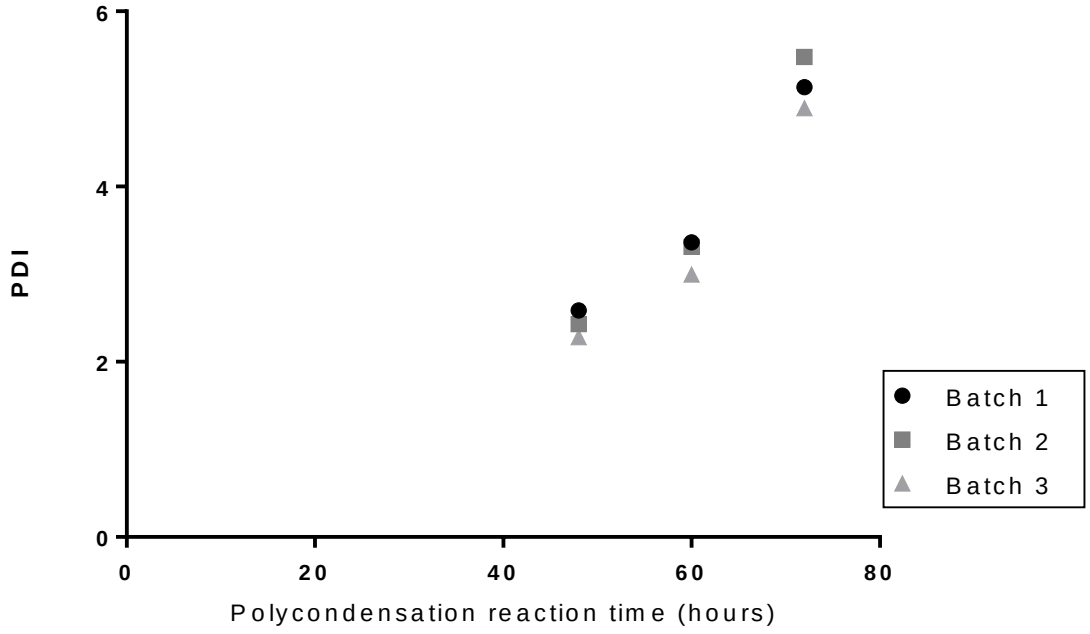

Figure 12. Variation in PGS prepolymer polydispersity index as a result of increased polycondensation reaction time (n = 3).

2.3.2 **Characterisation of PGS-M prepolymers by proton NMR spectroscopy**

Low M_w and High M_w PGS prepolymers were methacrylated to produce photocurable PGS-M prepolymer. Note that it was not possible to produce a High M_w PGS-M with a DM greater than 50%, due to spontaneous polymerisation during synthesis. Following methacrylation, the molecular structure of the PGS-M prepolymers was examined using proton NMR and compared to the PGS prepolymer. The spectra for the PGS prepolymer was comparable with those published in previous studies.[287,288,290] The chemical composition was determined by calculating signal integrals of -CH_2CH- at 3.7, 4.2 and 5.2 ppm for glycerol and –$COCH_2CH_2CH_2$- at 1.2, 1.6 and 2.3 ppm for sebacic acid. The incorporation of methacrylate groups into the PGS-M prepolymers was confirmed by the appearance of peaks at 1.9, 5.6 and 6.2 ppm which are associated with the hydrogen environments of this group (Figure 13). These peaks were absent from the spectra of the PGS prepolymer.

Peaks associated with organic solvents were also present in some spectra. In the Low M_w PGS-M spectra, peaks at 5.3 ppm were associated with dichloromethane. This was likely a residue from the PGS-M synthesis process. Additionally, the spectra for 30% and 80% Low M_w PGS-M and the PGS prepolymer also showed peaks at 2.2 ppm. These correspond to acetone and were likely residues from the cleaning of the sample vessels used in the NMR equipment.

The DM of the PGS-M prepolymer was calculated by comparing the integrals of the peaks for the methylene groups of sebacic acid (1.3 ppm) with those of the methacrylate group hydrogens. DM was found to correlate well with the molar ratio of methacrylic anhydride to PGS prepolymer hydroxyl groups used in the methacrylation process (Figure 14). Strong agreement was shown between the results and a 1:1 relationship between the molar ratio of methacrylic anhydride to PGS prepolymer hydroxyl groups and the resulting DM suggested, with an R^2 value of 0.9485.

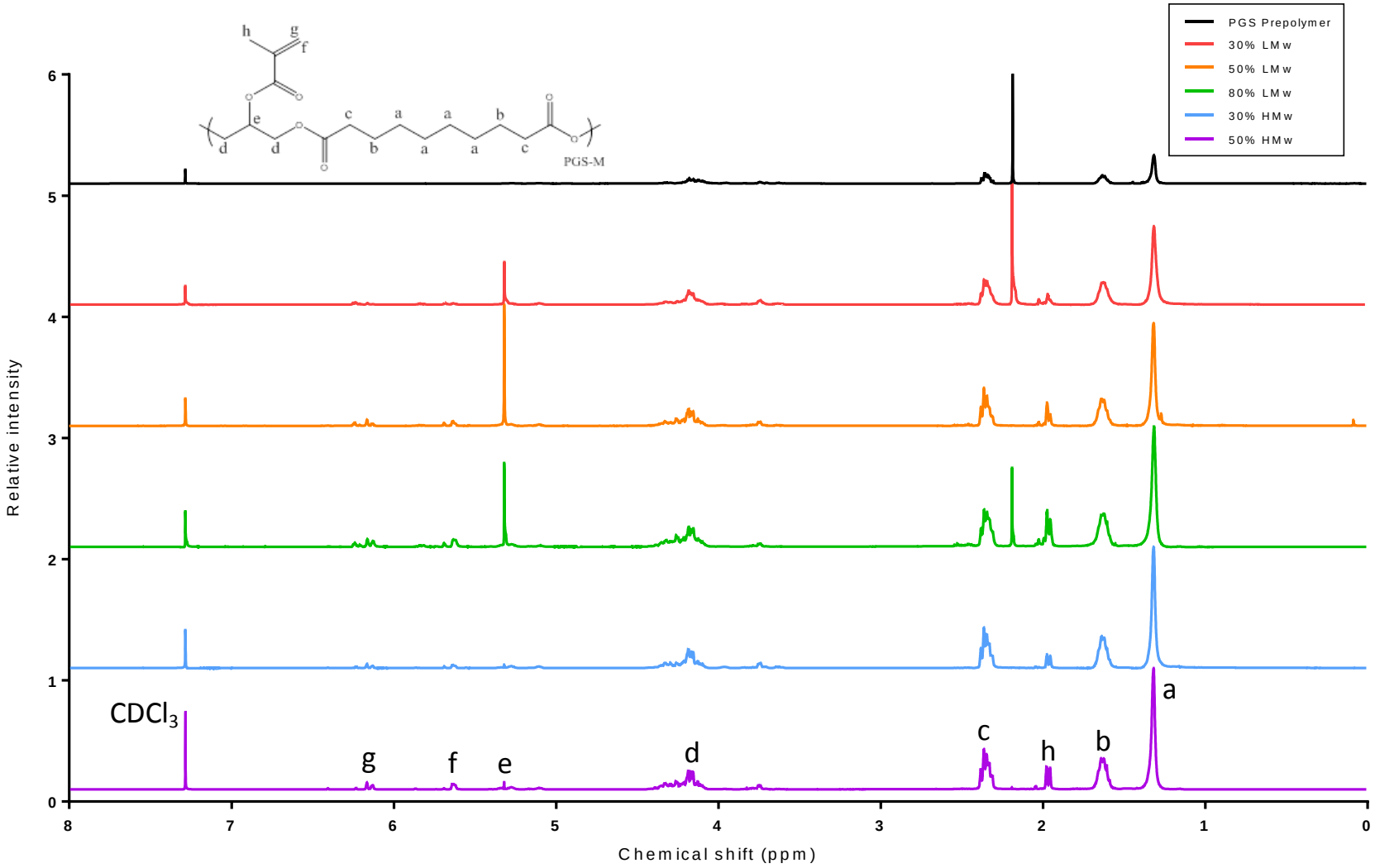

Figure 13. Proton NMR analysis of PGS and PGS-M prepolymers. Spectra of PGS and PGS-M prepolymer at varied DM (30%, 50% and 80%) and Low and High M_w (LMw and HMw). Peaks at 1.9, 5.6 and 6.2 ppm for PGS-M samples are associated with the hydrogen environments of the methacrylate group (hydrogen environments “f”, “g” and “h”). Comparing the integrals of these peaks with those of the methylene groups of sebacic acid (1.3 ppm, hydrogen environment “a”) allowed the DM to be calculated.

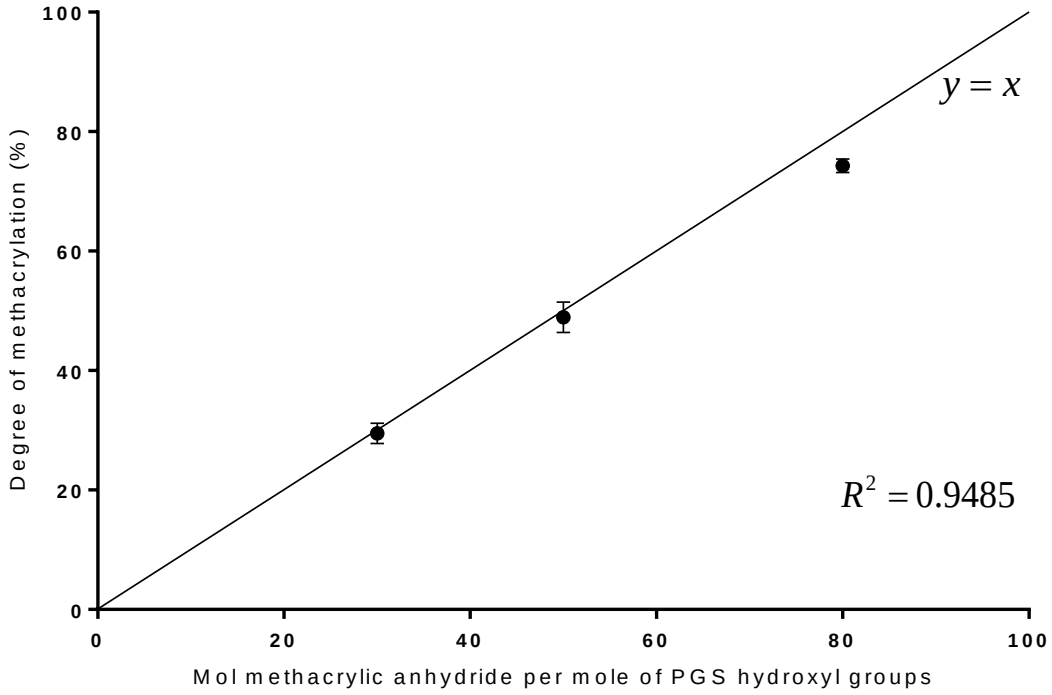

Figure 14. Molar ratio of methacrylic anhydride to PGS prepolymer hydroxyl groups compared to the resulting DM of the PGS-M prepolymers. The data show strong agreement with the line $y = x$ ($R^2 = 0.9485$). Error bars are SEM ($n = 3$).

2.3.3 **Determination of the soluble fraction of photocured PGS-M**

Disks of photopolymerised PGS-M, of varied M_w and DM, were washed in methanol to determine the soluble fraction of polymer they contained. After 24 hours, all test samples showed a statistically significant ($P<0.001$) reduction in mass compared to their corresponding controls (Figure 15). The percentage mass remaining correlated with the DM, and with the M_w of the PGS-M. Within the Low M_w samples, the 30% DM PGS-M showed the least mass remaining (mean = 72.6%) and the 80% DM PGS-M showed the greatest mass remaining (mean = 97.9%). A similar trend was seen within the High M_w PGS-M also. All differences in remaining mass within samples of the same M_w were significant ($P<0.001$). Comparing samples of the same DM showed that Low M_w PGS-M retained less mass than High M_w PGS-M, with these differences also being

significant (P<0.001). There was no significant effect of the interaction between M_w and DM on the remaining mass the PGS-M samples after 24 hours in methanol.

After 48 hours in methanol, no significant reduction in mass was seen in any sample compared to the mass at 24 hours.

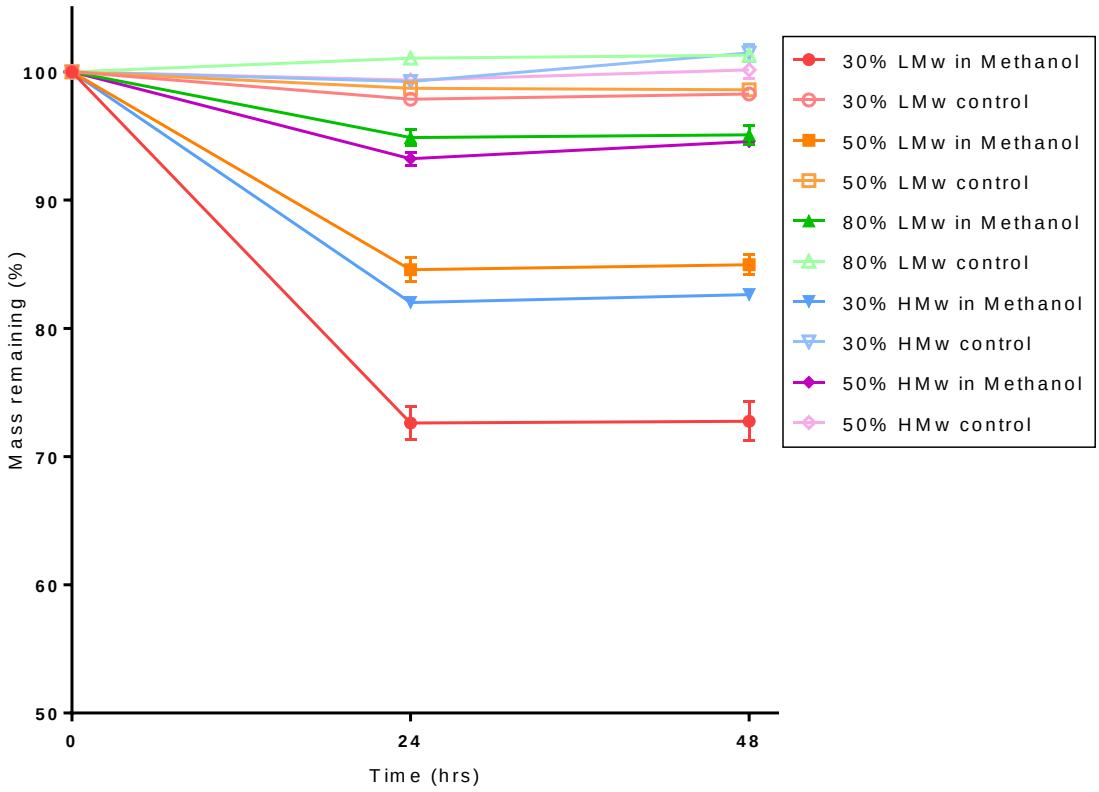

Figure 15. Soluble fraction of photocured PGS-M, of various M_w and DM, in methanol. Significant mass loss was seen after 24 hours in methanol in all samples, compared to unwashed controls (P<0.001). All differences in remaining mass between samples of the same M_w or the same DM were significant (P<0.001). There was no significant effect of the interaction between M_w and DM. No further significant changes in sample mass occurred after a further 24 hours in methanol. Error bars are SEM (n = 3).

2.3.4 **Characterisation of PGS-M by ATR-FTIR**

The molecular structure of the PGS-M prepolymers was further examined using ATR-FTIR. A broad peak associated with the hydroxyl groups was present around 3460 cm^{-1} and sharp peaks associated with the methyl and alkane groups were present at 2924 cm^{-1} and 2851 cm^{-1}.[291,292] A distinct peak at 1735 cm^{-1} was associated with ester bonds, while the peaks around 1291-1050 cm^{-1} where associated with the stretch vibrations of carboxyl bonds.[291–293]

Peaks associated with the methacrylate group were seen in PGS-M prepolymer samples at 940 cm^{-1} (=*C*-*H* bending) and 1640 cm^{-1} (*C*=*C* stretching) (Figure 16).[294] These peaks were absent from the PGS prepolymer. The magnitude of these peaks also correlated well with the DM of the PGS-M prepolymer samples. Comparing PGS-M prepolymer and photocured polymer showed the removal of these peaks after photopolymerisation (Figure 17).

Additionally, some prominent peaks appeared in the Low M_w PGS-M prepolymer spectra, at 700 cm^{-1}, which were not seen in the other spectra. These peaks were associated with *C*-*Cl* bonds, likely present in residual dichloromethane from the PGS-M synthesis process.

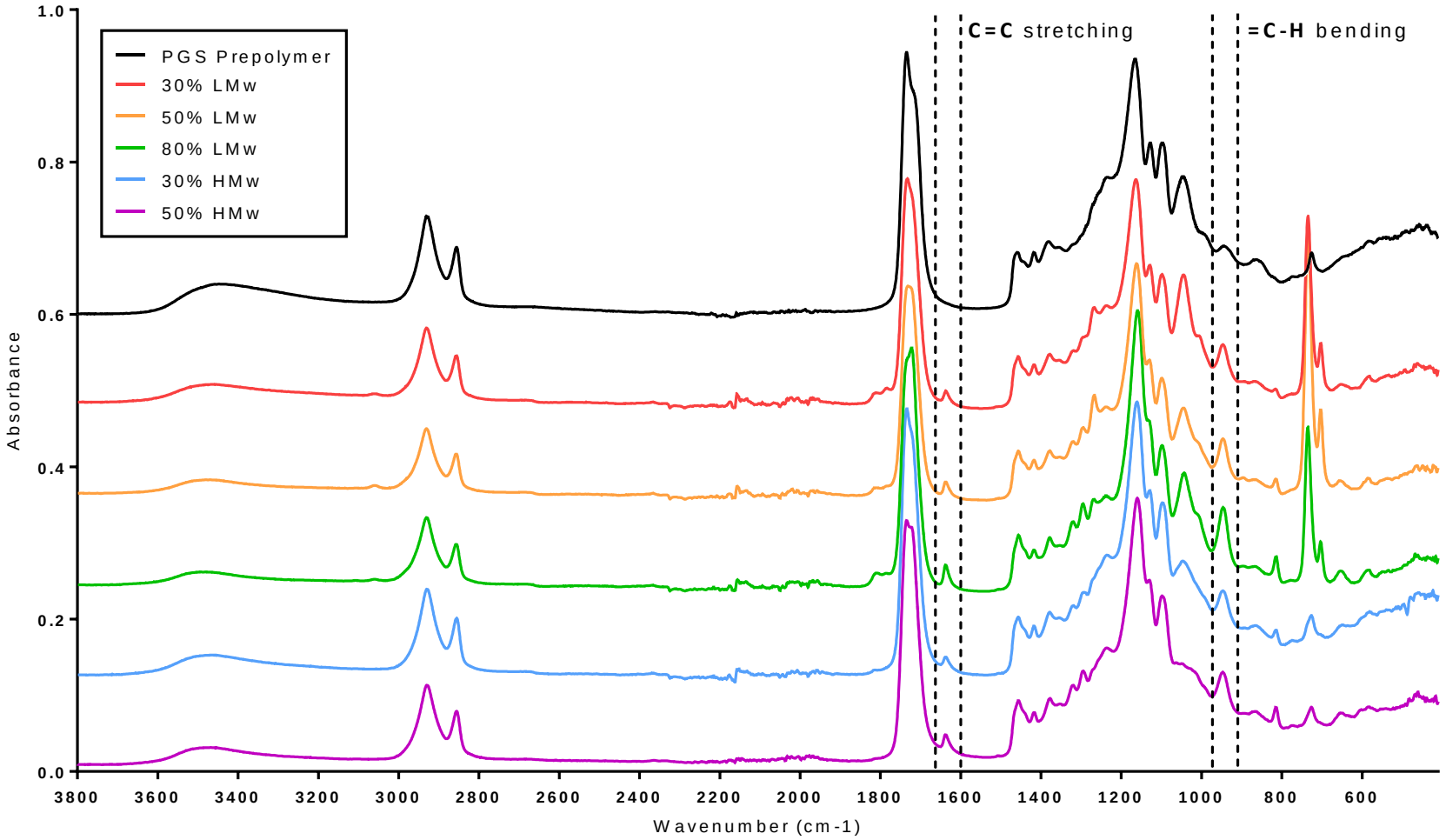

Figure 16. ATR-FTIR spectra for PGS-M and PGS prepolymer at various molecular weights and DM. Highlighted are the regions around 940 and 1639 cm^{-1} showing the absorbance peaks associated with the methacrylate group C=C bond present in the PGS-M prepolymers. The magnitudes of these peaks correlate well with the DM of the associated PGS-M.

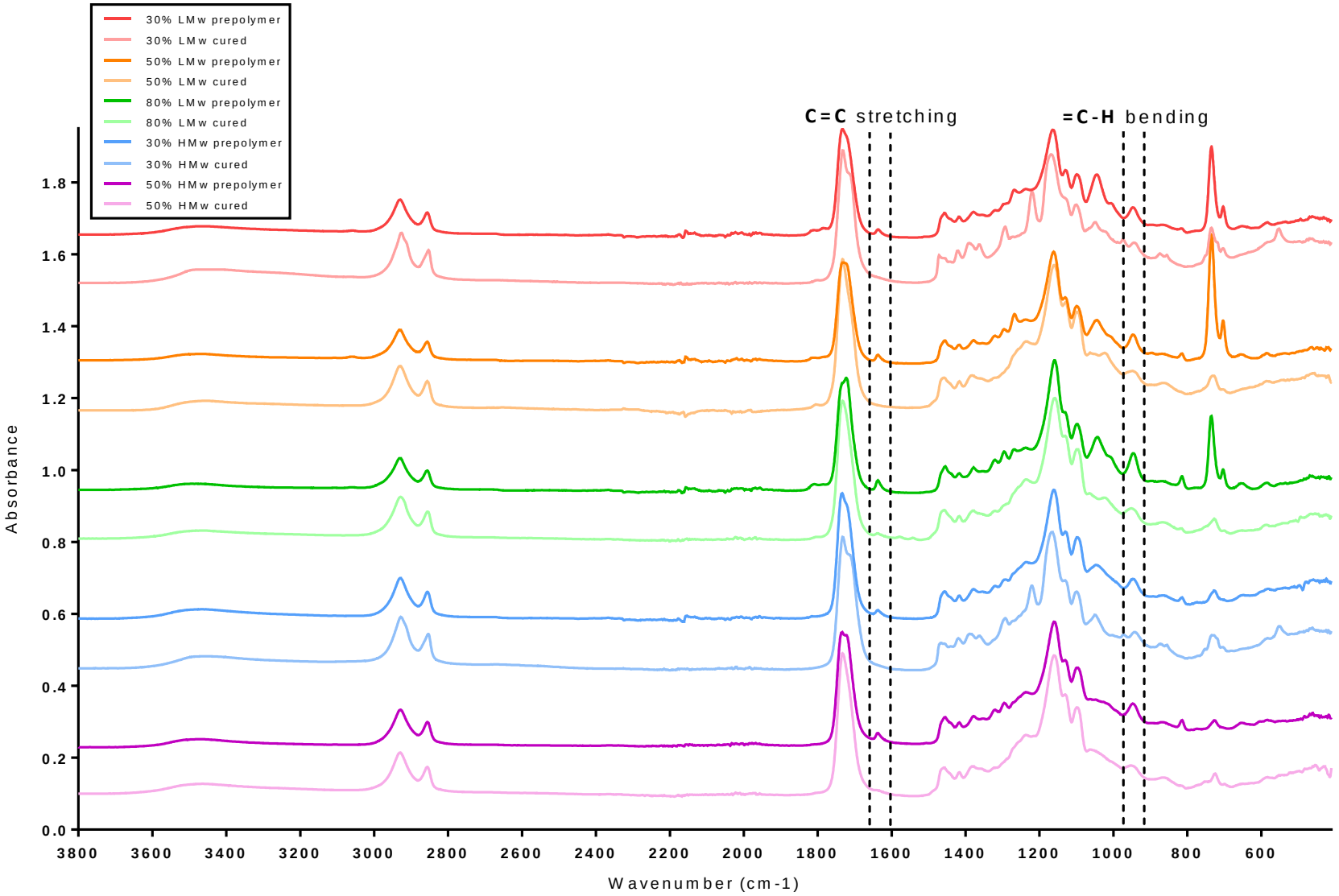

Figure 17. ATR-FTIR spectra for PGS-M prepolymer and photocured polymer. Peaks associated with the methacrylate group, at 940 and 1639 cm^{-1} are not present after photopolymerisation.

2.3.5 **Characterisation of PGS-M by Raman spectroscopy**

The molecular structure of PGS-M was further examined using Raman spectroscopy. Peaks associated with the methacrylate group were seen in all PGS-M prepolymer samples at 1650 cm^{-1} (*C*=*C* stretching).[295] The magnitude of these peaks also correlated well with the DM of the PGS-M prepolymer samples (Figure 18). Additional peaks associated with the methacrylate group were also seen at 3000 cm^{-1}(*C*=*C* stretching), although these were only apparent in the 50% and 80% DM prepolymers. Comparing PGS-M prepolymers and photocured polymers showed the removal of the methacrylate group associated peaks after photopolymerisation.

Additionally, prominent peaks at 700 cm^{-1} appeared in the 80% DM Low M_w prepolymer spectra and both 50% DM PGS-M prepolymer spectra. These signals were largely absent in the other spectra. As in the ATR-FTIR analysis, these peaks were associated with *C-Cl* bonds, likely present in residual dichloromethane from the PGS-M synthesis process.[295]

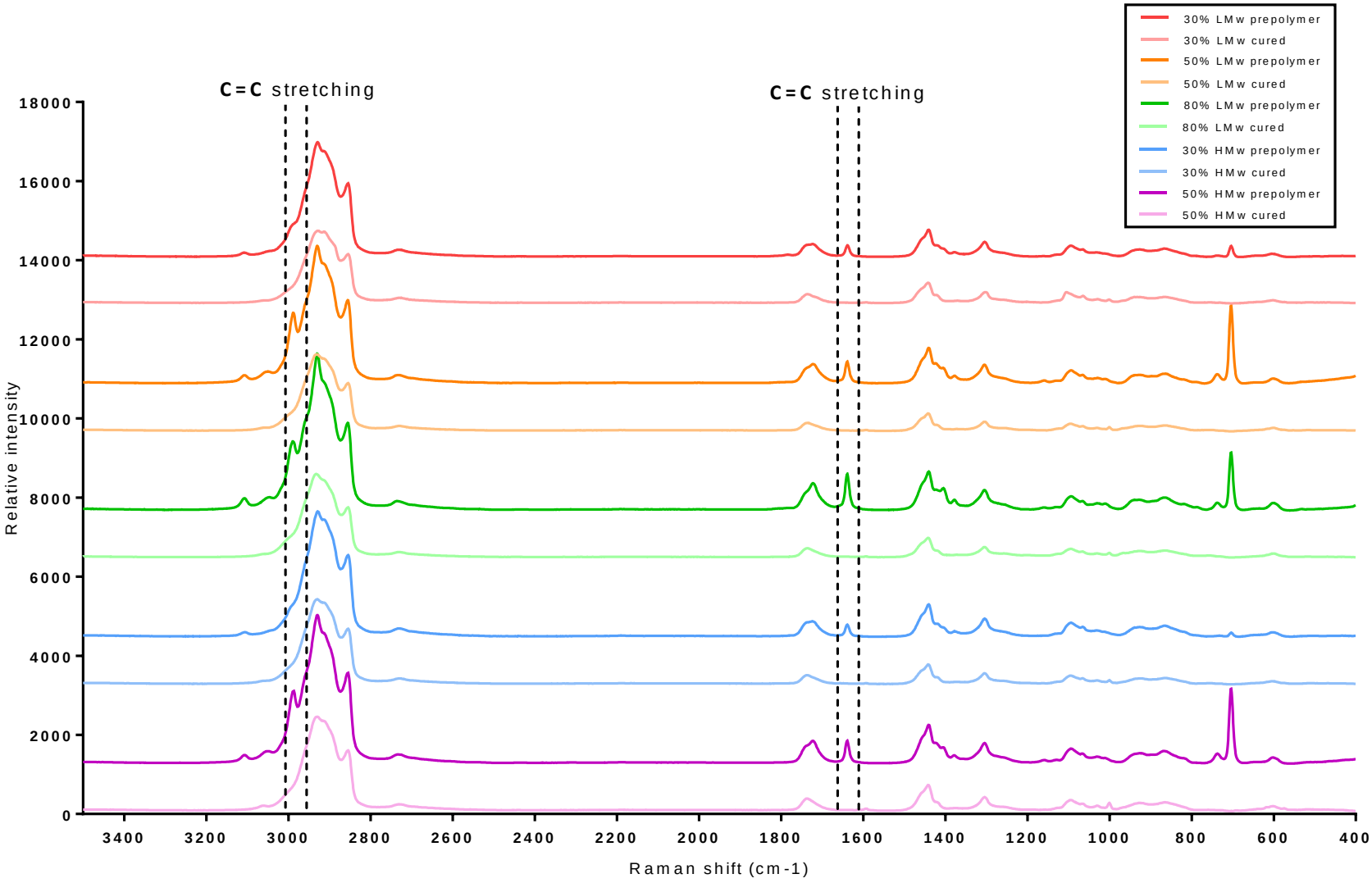

Figure 18. Raman spectra for PGS-M prepolymer and photocured polymer. Peaks associated with the methacrylate group, at 1650 cm-1 and 3000 cm-1 are not present after photopolymerisation.

2.3.6 *In vitro* degradation of photocured PGS-M

The degradation of PGS-M was examined *in vitro* using the enzymes cholesterol esterase and lipase, both of which are known to hydrolyse ester bonds, along with PBS. These are physiologically relevant enzymes, although the concentrations used may have differed from those present *in vivo* due to the complex nature of enzyme expression in different tissues and under different conditions. After 8 days, significant mass loss was seen in 30% Low M_w PGS-M and 30% and 50% High M_w PGS-M treated with cholesterol esterase ($P<0.001$) (Figure 19). The rate of this degradation appeared to be linear when examining the previous time points. Significant mass loss was also seen in 30% Low and High M_w PGS-M treated with lipase ($P<0.01$). PGS-M treated with PBS did not show any significant mass loss compared to untreated controls. Cholesterol esterase treatment appeared to produce greater degradation compared to lipase in all treatments, although this was only significantly different within 30% Low and High M_w PGS-M samples ($P<0.001$, in both cases). The greatest degradation was seen in 30% High M_w PGS-M treated with cholesterol esterase, with 79.1% mass remaining after 8 days. This result was significantly different to all others ($P<0.001$).

The PGS-M samples that had been treated for 8 days were further examined using SEM (Figure 20 and Figure 21). Both the 30% Low and High M_w PGS-M samples treated with cholesterol esterase showed evidence of surface degradation. Compared to the controls, the surfaces of these samples displayed pits and cracks. No evidence of degradation was apparent in any of the other PGS-M samples when treated with lipase or PBS, compared to the controls.

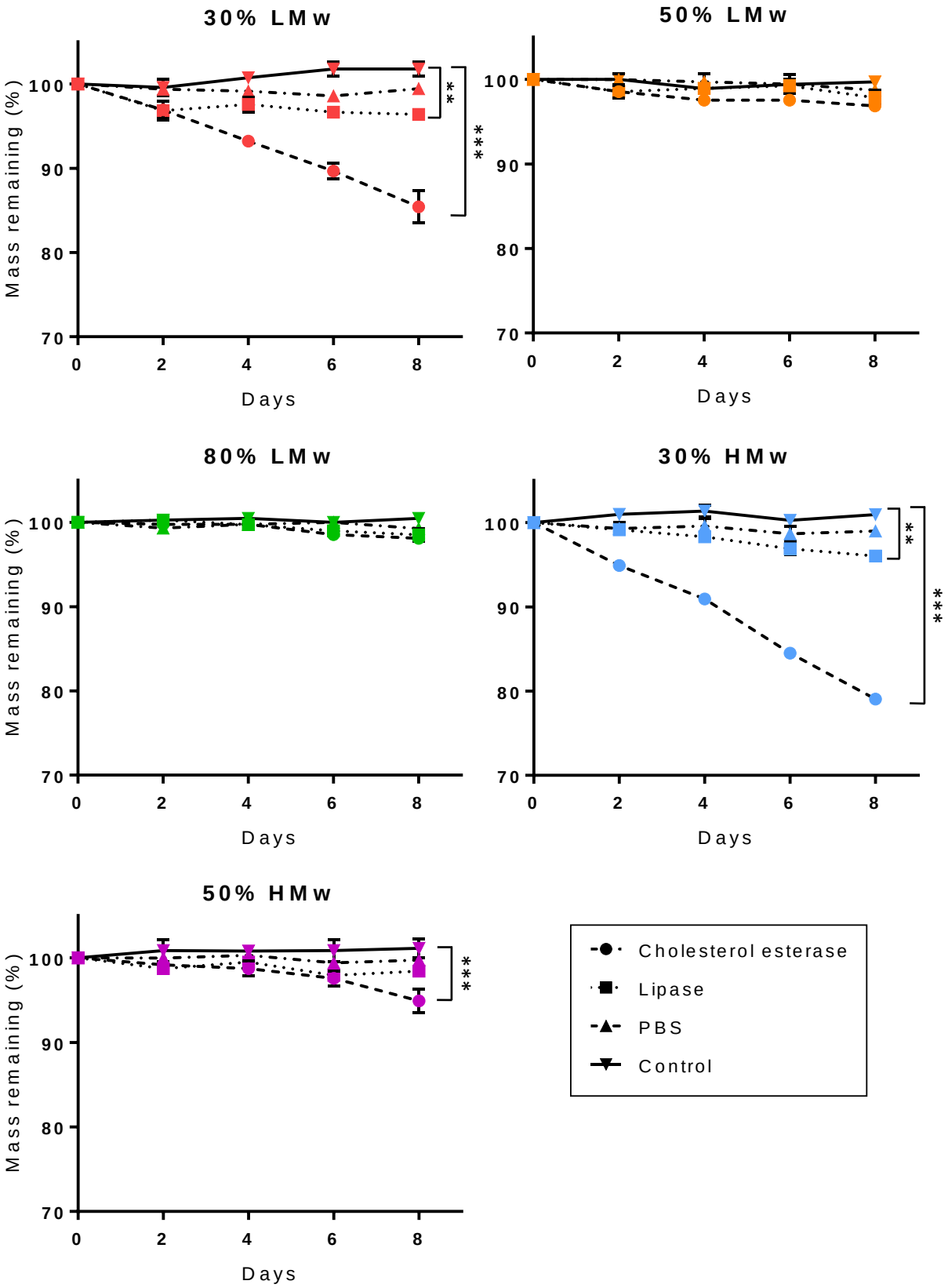

Figure 19. Degradation of PGS-M treated with cholesterol esterase, lipase and PBS. After 8 days, cholesterol esterase produced significant degradation in both 30% DM polymers and the 50% High Mw PGS-M. Lipase only produced significant degradation in the 30% DM polymers. PBS did not produce significant degradation in any sample. Error bars are SEM (n = 3).

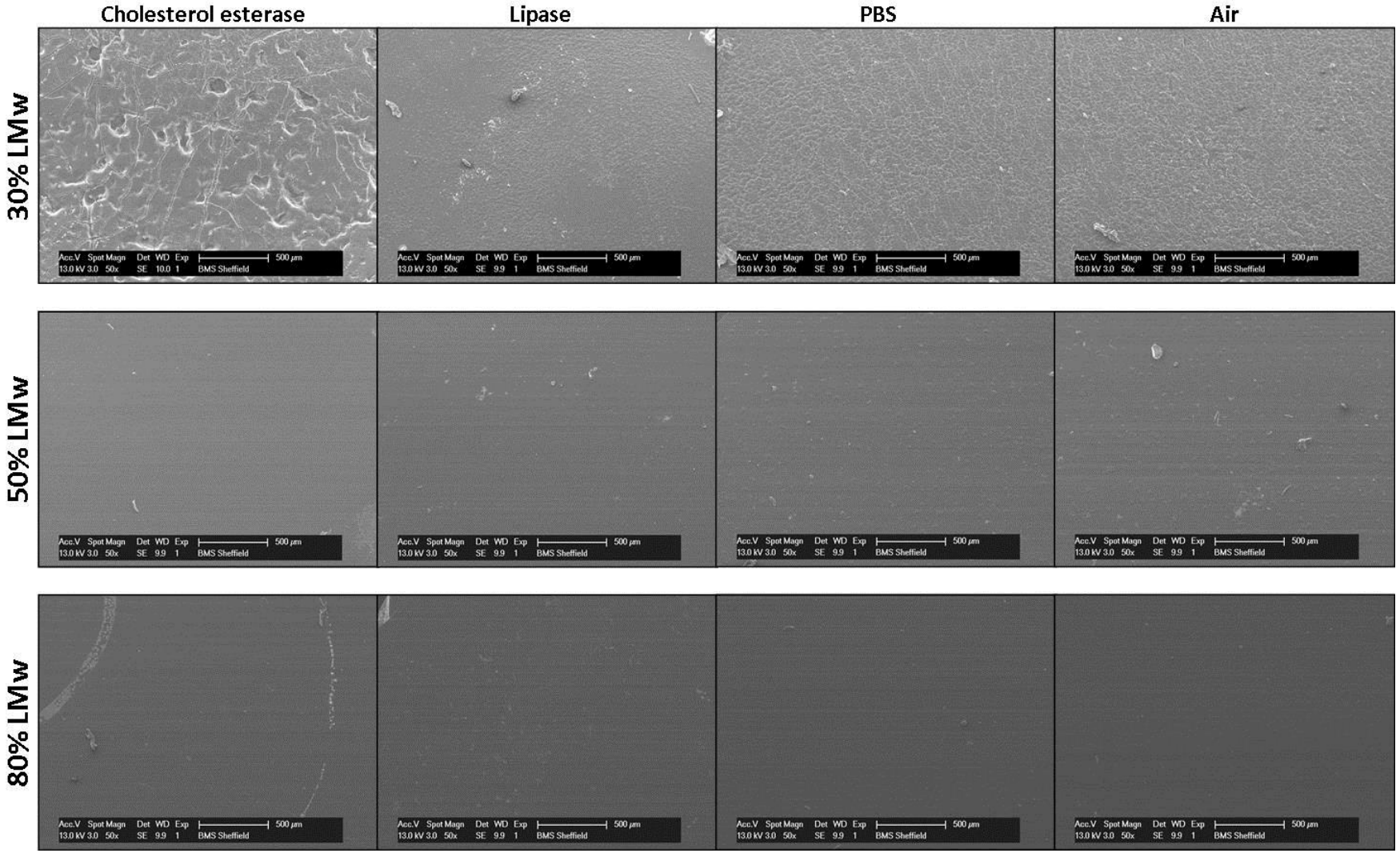

Figure 20. Representative SEM images of Low M_w PGS-M following degradation by cholesterol esterase, lipase and PBS for 8 days. Controls were PGS-M in air.

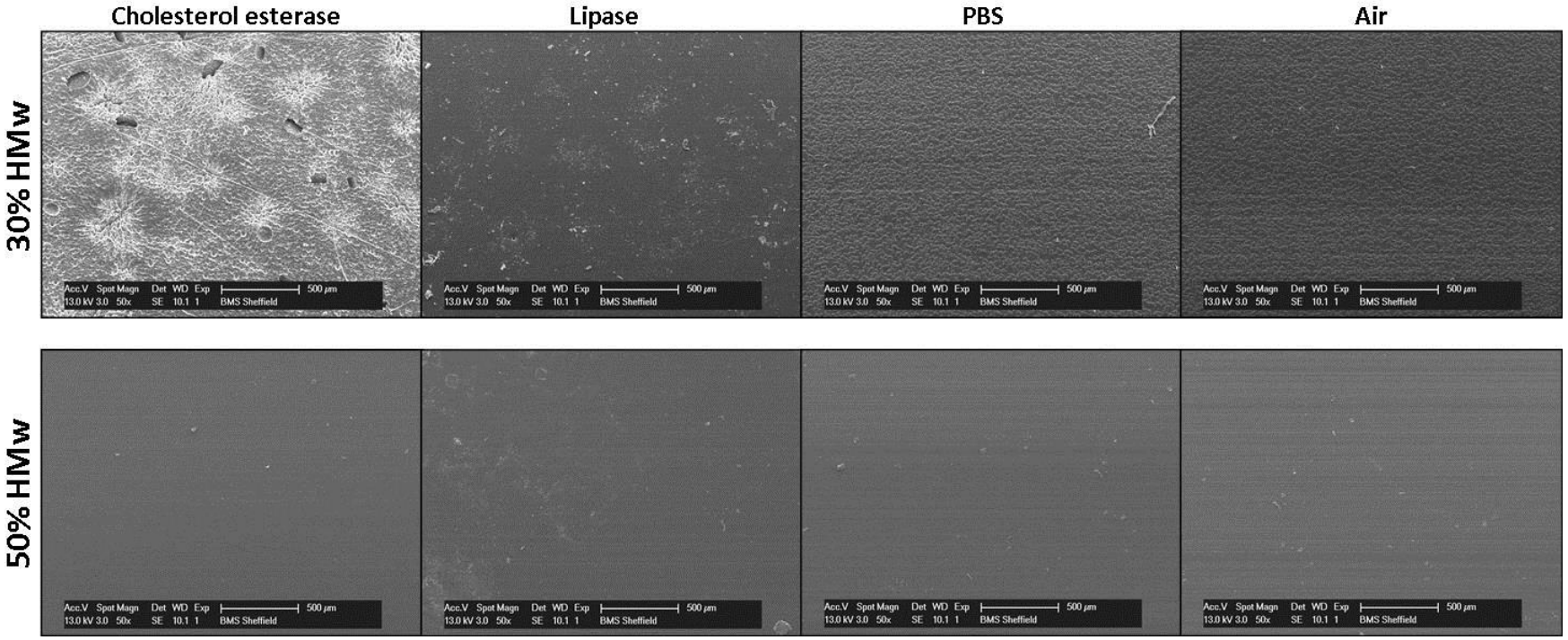

Figure 21. Representative SEM images of High M_w PGS-M following degradation by cholesterol esterase, lipase and PBS for 8 days. Controls were PGS-M in air.

2.3.7 **Tensile testing of PGS-M**

Tensile testing revealed that the mechanical properties of PGS-M varied depending on the polymers composition. Young's modulus was shown to increase significantly with increasing DM, for both Low and High M_w ($P<0.001$ and <0.05, respectively) (Figure 22). The 30% Low M_w PGS-M demonstrated the smallest value, with a mean average of 0.43 MPa. The 80% Low M_w PGS-M demonstrated the largest value with a mean average of 6.74 MPa. A similar trend was also seen in the ultimate tensile strength (UTS) of PGS-M, although in a less pronounced manner (Figure 23). The 80% Low M_w PGS-M demonstrated the greatest strength with a mean average of 3.80 MPa. This was significantly stronger than the 50% and 30% Low M_w PGS-M polymers ($P<0.001$), although these were not significantly different from each other. No significant difference was seen between the UTS of the 30% and 50% High M_w PGS-M polymers either.

Polymer M_w did not appear to have a significant effect on the Young's modulus or UTS of PGS-M. Additionally, the interaction between the DM and M_w had no significant effect on the Young's modulus or UTS of PGS-M.

Sterilisation of 30% Low M_w PGS-M resulted in some modification to its mechanical properties. Following sterilisation by autoclave, the Young's modulus of the polymer was significantly reduced from 0.43 to 0.37 MPa ($P<0.001$) (Figure 24). Further treatment with 0.5% peracetic did not result in any further significant changes in Young's modulus. The UTS of 30% Low M_w PGS-M was not significantly altered by autoclave sterilisation or subsequent peracetic acid treatment (Figure 25).

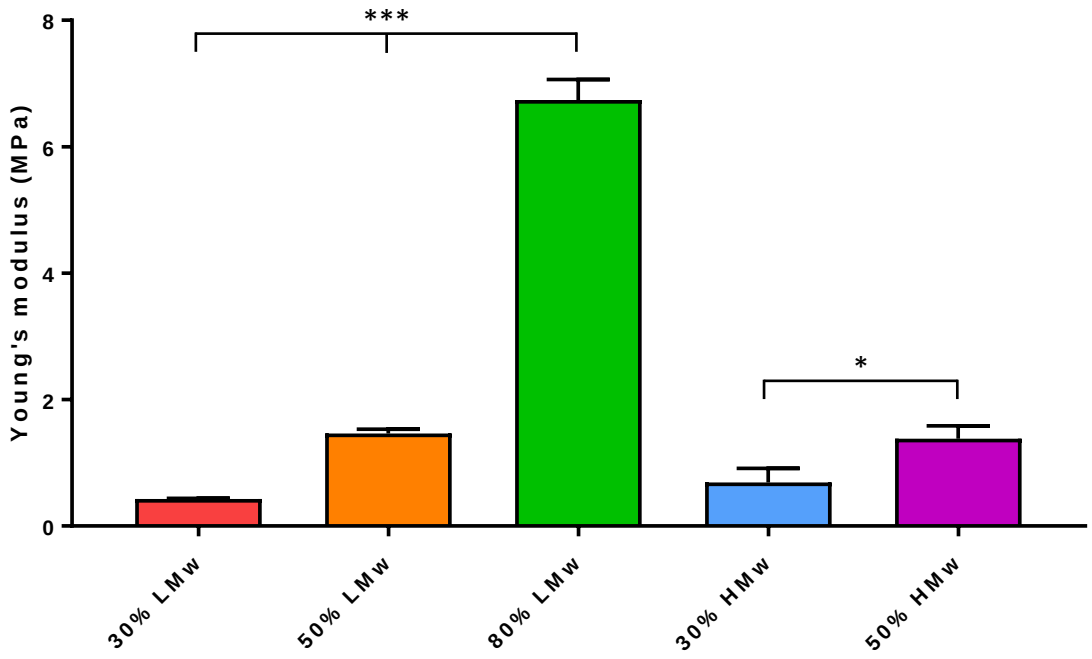

Figure 22. Young's modulus of PGS-M. Error bars are SEM (*n* = 3).

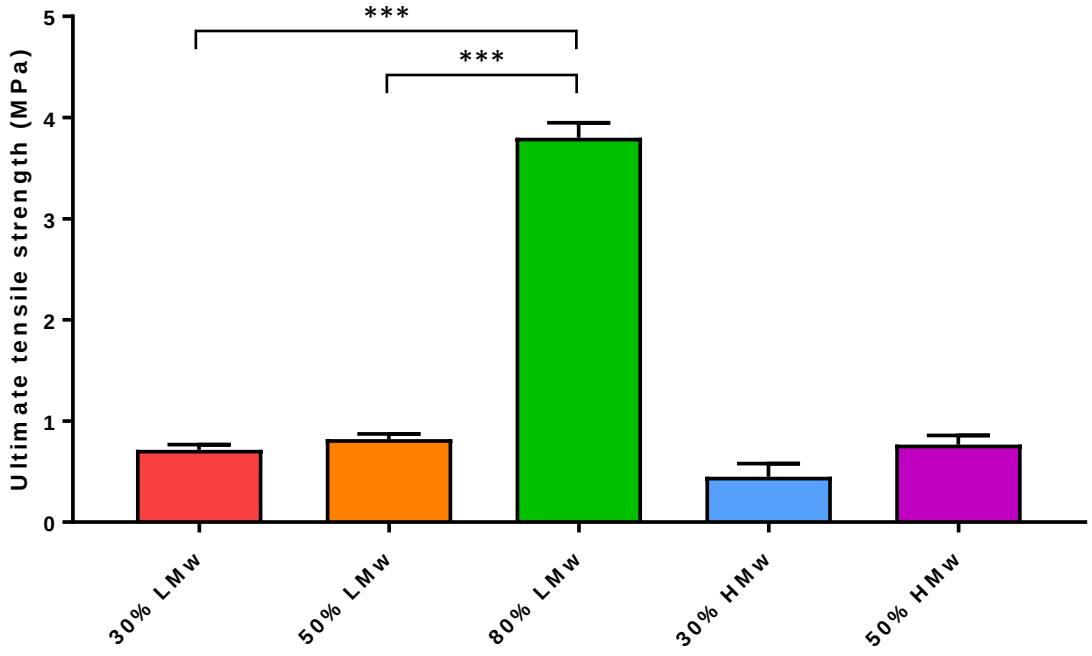

Figure 23. Ultimate tensile strength of PGS-M. Error bars are SEM (*n* = 3).

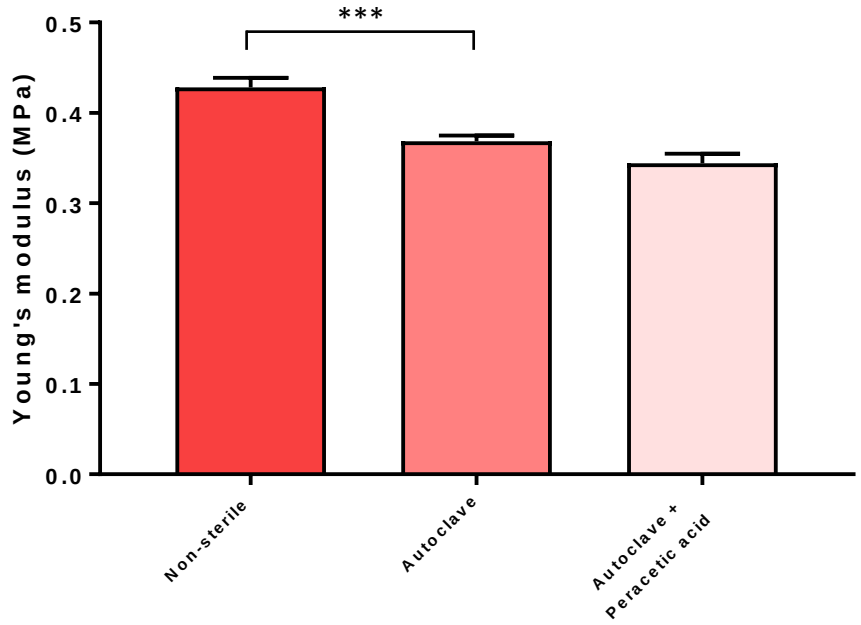

Figure 24. Young's modulus of 30% Low M_w PGS-M after sterilisation by autoclave and peracetic acid. Error bars are SEM (n = 3).

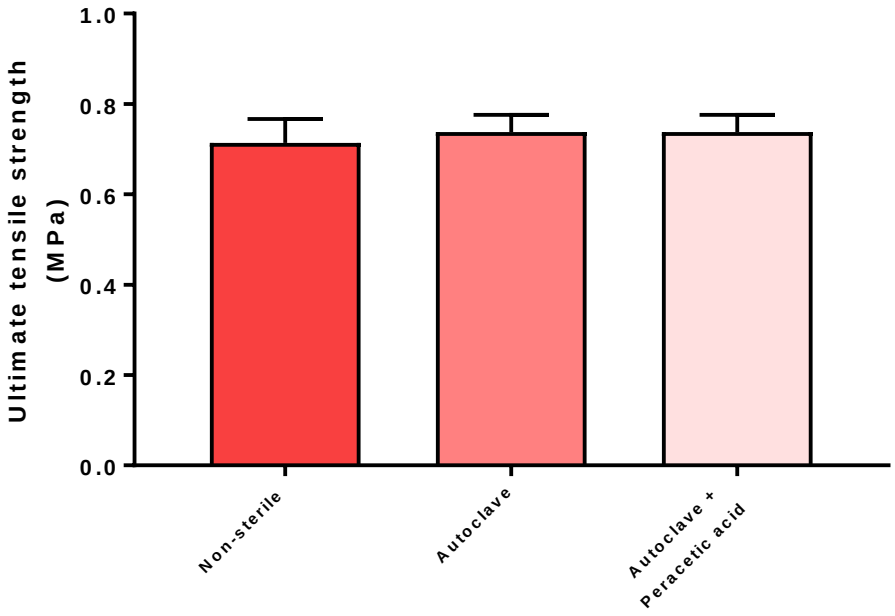

Figure 25. Ultimate tensile strength of 30% Low M_w PGS-M after sterilisation by autoclave and peracetic acid. Error bars are SEM (n = 3).

2.4 **Discussion**

PGS prepolymer was synthesised by the polycondensation reaction of glycerol with sebacic acid (molar ratio 1:1) at 120°C. Analysis using GPC demonstrated that increasing the duration of this reaction resulted in an increase in prepolymer molecular weights, calculated as M_n and M_w. Mean average molecular weights were 2,227, 2,774 and 3,356 Da for M_n and 5,419, 8,957 and 17,339 Da for M_w at reaction lengths of 48, 60 and 72 hours, respectively. Increasing the reaction duration allowed the polymerisation process to continue for longer and more bonds to form between the glycerol and sebacic acid, lengthening the polymer chains and increasing the molecular weight. Comparable results are seen in other studies where PGS prepolymer was synthesised. Ifkovits *et al.* synthesised PGS prepolymer from a 1:1 molar ratio of glycerol and sebacic acid, using similar conditions to those herein, and generated prepolymers with molecular weights (M_w) increasing from 4,060 to 23,460 Da after increasing reaction lengths of between 28 and 65 hours, respectively.[288]

Although the glycerol monomer is trifunctional, due to its three hydroxyl groups, the secondary hydroxyl group is less reactive than the two primary hydroxyl groups. Therefore increased reaction duration favours increased polymer chain extension rather than chain branching.[296] An increase in chain branching can be achieved by modifying the ratio of glycerol to sebacic acid in the polycondensation reaction. A ratio of 2:3 resulted in a totally crosslinked PGS which was insoluble in organic solvents.[297] It was desirable, in the present study, to generate a PGS prepolymer that was soluble in organic solvents, to permit further functionalisation and processing into defined structures. Therefore, a ratio of 1:1 was selected for the polycondensation reaction, as this had been demonstrated to minimize chain branching and produce a soluble prepolymer.[282,287,288]

The melt-polycondensation reaction of glycerol with sebacic acid is an example of step-growth polymerisation.[298] Monomers, small chain fragments (dimers, trimers and

oligomers) and larger chains may all react with each other to produce longer polymer chains. As such, an exponential growth curve for the prepolymer molecular weight with increasing reaction time might be expected. The results suggest exponential growth of the PGS prepolymer when molecular weight is calculated as M_w. However, when the molecular weight is calculated as M_n, a linear relationship between this and increasing reaction duration is apparent. Due to the nature by which M_n and M_w are calculated, $M_w \geq M_n$, therefore, an exponential growth relationship may more easily manifest.[298,299] The reaction may not have progressed for a long enough duration for the exponential growth phase to become apparent when calculating polymer molecular weight as M_n.

Although previous work on the synthesis of PGS prepolymer has shown a trend towards increasing polymer molecular weight with increasing reaction duration, as in this study, there is some variability between the actual polycondensation reaction lengths and resulting prepolymer molecular weights. Although reporting the same reaction conditions as in this study, Nijst *et al.* produced a PGS prepolymer with M_n 6,500 Da and M_w 23,000 Da after a reaction length of just 53 hours.[287] Similarly, the group of Burdick produced a PGS prepolymer with M_n 5,330 Da and M_w 23,460 Da after a reaction length of 65 hours and later a PGS prepolymer with M_n 3,740 Da and M_w 24,240 Da after a reaction length of 72 hours.[288,300] The apparent irreproducibility of PGS prepolymer synthesis was investigated in depth by Li *et al*.[290] They determined that the evaporation of glycerol from the reaction mixture during the polycondensation reaction was a major cause of this. Glycerol evaporation may be affected by the vacuum pressure applied to the reaction flask and the flow rate of any inert gas used at the early stages of the reaction. These factors are often not detailed or quantified in published methods of synthesis, leading to the differing results reported.

The *PDI* values for the PGS prepolymer samples, calculated from the ratio of M_w/M_n, were consistent with those of a polymer produced by step-growth

polymerisation.[288,298] Mean averages were 2.43, 3.22 and 5.17 at reaction lengths of 48, 60 and 72 hours, respectively. Step-growth polymerisation generates a wide distribution of different length polymer chains and thus produces non-uniformity with respect to the polymer molecular weight within a sample.[298] The *PDI* reflects this non-uniformity, with values exceeding 2 considered as representing a broadly distributed polymer sample. Similar polydispersity (ranging from 2-6.6) has been reported in other studies on PGS prepolymer synthesis.[287,288,300,301]

Reasonable consistency was seen between the PGS prepolymer molecular weights and the reaction durations for the different prepolymer batches. Between batches, the standard deviations were 43, 98 and 54 Da for M_n and 435, 844 and 760 Da for M_w at reaction lengths of 48, 60 and 72 hours, respectively. These equate to 1.9, 3.5 and 1.6% for M_w and 8.0, 9.4 and 4.4% at reaction lengths of 48, 60 and 72 hours, respectively. Such variation between batches is not unexpected, given the melt-polycondensation reaction progresses by step-growth. As all of the different length molecules in the reaction, from monomers to polymer chains, are able to react with each other, different polymer chain length profiles can be generated after equal reaction lengths, resulting in variations in the calculated average molecular weight. This is also reflected in the *PDI* results for the PGS prepolymer samples, which suggest high variation between the lengths of the polymer chains within each sample. Additionally, errors associated with the synthesis apparatus may also have contributed to the observed variation between prepolymer batches. Although the different batches were produced using the same apparatus with the same conditions, some equipment error is expected. This may have been particularly prominent in the analogue equipment without feedback systems, such as the vacuum pump and N_2 flow regulator. Small variations (1-2%) in these may have occurred between the different batch reactions and such variations were hypothesised to effect the consistency of PGS prepolymer synthesis by Li *et al*.[290]

Proton NMR spectroscopy demonstrated the successful methacrylation of the PGS prepolymer, forming PGS-M prepolymer. Characteristic peaks associated with the hydrogen environments present in the methacrylate group were present in PGS-M samples and absent from the PGS prepolymer spectra.

Comparable results are seen in the literature where PGS prepolymer was functionalised in a similar way. Nijst *et al.* and Ifkovits *et al.* both produced photocurable PGS by adding acrylate groups to PGS prepolymer, producing PGS acrylate (PGS-A).[287,288] Both studies utilised proton NMR spectroscopy to confirm the successful addition of the acrylate groups. Comparing the spectra for PGS prepolymer with PGS-A showed the clear appearance of peaks associated with the acrylate group hydrogen environments. Comparing spectra for PGS-M with PGS-A shows peaks associated with the hydrogen environments common between acrylate and methacrylate groups appeared in similar locations.

The DM of the PGS-M prepolymer, calculated by comparing the integrals of the peaks for the methylene groups of sebacic acid with those of the methacrylate group hydrogens, showed a strong correlation with the molar ratio of methacrylic anhydride to PGS prepolymer hydroxyl groups used in the methacrylation process. This relationship appeared linear and directly proportional. This suggests that all of the methacrylate groups supplied to the reaction by methacrylic anhydride were incorporated into the PGS-M prepolymer. In the synthesis of PGS-A, a linear relationship between the supplied acrylate groups and the resulting degree of acrylation (DA) of the prepolymer was also seen. However, this was not directly proportional, suggesting that not all of the acrylate groups supplied to the reaction were incorporated into the prepolymer.[287] PGS appears to be more susceptible to methacrylation than to acrylation.

Subsequent analysis of PGS-M using ATR-FTIR also showed peaks associated with the methacrylate group in PGS-M prepolymer spectra. These were not present in the spectra for the PGS prepolymer. The magnitude of these peaks also correlated well

with the DM for the associated PGS-M prepolymer sample, although only a qualitative assessment could be made.

PGS-M samples were also examined using Raman spectroscopy. This is a complementary technique to ATR-FTIR, generating spectra that show less polarisable chemical bonds (symmetric vibrations) more prominently.[295]

Similar to the ATR-FTIR spectra, Raman spectra showed peaks associated with the methacrylate group *C*=*C* bond in the PGS-M prepolymers. The magnitude of these peaks also qualitatively correlated well with the DM of the associated PGS-M prepolymer sample. Interestingly, the spectra for the 30% DM prepolymers lacked a peak at 3000 cm^{-1}, which was present in the samples of higher DM. A peak at 3000 cm^{-1} is indicative of *C*=*C* bond stretching and might have been expected, given the presence of the methacrylate group in the prepolymers and the peak seen at 1650 cm^{-1}, which is also associated with *C*=*C* stretching, in all the PGS-M prepolymer samples. It may be that, due to the reduced quantity of methacrylate groups in the 30% DM prepolymers, the signal at 3000 cm^{-1} was simply too small to deduce from the larger peak adjacent to it, which corresponded to the methylene backbone of the sebacic acid subunit in the PGS-M polymer chains.[295]

Comparing samples of PGS-M before and after photopolymerisation showed the removal of the methacrylate group peaks. Since both peaks were associated with the *C*=*C* bond in this group and this bond is opened during photopolymerisation, allowing crosslinking between polymer chains, the disappearance of these peaks after UV exposure is expected. Similar results were also seen in other methacrylated polymers, where spectral peaks associated with the methacrylate groups disappeared after polymerisation.[302]

Washing photocured PGS-M in methanol revealed the fraction of soluble polymer present. The soluble fraction represents the polymer chains not chemically bound within the crosslinked polymer matrix. These are free to move when solubilised and can be washed out of the sample, thus resulting in a loss of mass. Methanol washing revealed the soluble fraction present within PGS-M samples of varied M_w and DM.

Within polymers of the same M_w, the soluble fraction decreased with increasing DM. This might be expected given the DM represents the number of methacrylate groups present in the polymer sample and that it is through crosslinking of these groups, through photopolymerisation, that an insoluble polymer matrix forms. With increasing DM, more crosslinks can form and the probability of unbound chains being present in the sample decreases, thus decreasing the soluble fraction.

Additionally, within samples of the same DM, the soluble fraction decreased with increasing M_w. Again, this is likely associated with the quantity of chemical bonds present within the polymers. As M_w increases, the quantity of ester bonds within the prepolymer increases, as the polymer chains become longer. As chain lengths increase, there are more possible sites for methacrylate group attachment and therefore a greater possibility of crosslink formation. The number of unbound polymer chains is reduced, resulting in a reduced soluble fraction.

Similar results are seen in PGS-A. Within samples of photocured PGS-A of the same M_w, the soluble fraction decreased with increasing DM.[300] The magnitude of the soluble fractions with relation to the M_w and DM was also comparable with this study. PGS-A of M_w 24,240 Da and a DA of 23.5% demonstrated a soluble fraction of 13.3%. Although the molecular weight was greater than those studied here and acrylation was applied to the prepolymer, the behaviour would fit with that observed for PGS-M.

In PGS, soluble fractions of between 19.8 and 40.7% have been reported, although these are for thermally crosslinked matrices, not photopolymerised matrices as in PGS-M and PGS-A.[300,303,304]

Comparing samples of PGS-M before and after photopolymerisation using ATR-FTIR showed the removal of the methacrylate group peaks. Since both peaks were associated with the *C*=*C* double bond in this group (=*C*-*H* bending at 940 cm^{-1} and *C*=*C* stretching 1640 cm^{-1}) and this bond is opened during photopolymerisation, allowing crosslinking between polymer chains, the disappearance of these peaks after UV exposure is expected. Similar results were also seen in the photopolymerisation of PGS-A, where spectral peaks associated with the acrylate groups disappeared after UV exposure.[287,288]

Photocured PGS-M was susceptible to enzymatic degradation, *in vitro*, over 8 days, although this was dependent on the M_w and DM of the polymer. Cholesterol esterase treatment resulted in the greatest degradation in all variants of PGS-M examined, although this was only significant in the 30% DM samples and the 50% High M_w PGS-M. Examination of the PGS-M samples using SEM only showed surface damage in the 30% DM samples treated with cholesterol esterase.

Increasing the DM of PGS-M appeared to reduce the rate of degradation. This was likely due to the increase in the number of crosslinks present within the polymer which reduced the ability of chain fragments to be cleaved out by the enzymes. A longer study length may be required to show significant degradation in all of the PGS-M variants. Interestingly, it was the 30% high M_w PGS-M which exhibited the greatest degradation, not the 30% Low M_w PGS-M, which contains fewer chemical bonds. It may have been possible that the longer polymer chains present in the high M_w polymer may have allowed larger fragments to be released from the matrix once freed by the enzyme, resulting in an increased loss of mass.

The degradation rates appeared linear in both 30% DM polymers. This suggests only degradation by surface erosion occurred and enzymes were not able to penetrate the surface and cause bulk degradation, which usually results in an exponential loss of mass.[305] Indeed, this is common for enzymatic degradation processes, due to the relatively large size of the enzymes which limits their penetration into polymer matrices.[305] Degradation by surface erosion may be considered more favourable in polymers being utilised as tissue engineering scaffolds, as the mechanical strength of the polymer is reduced over a longer time period, maintaining the structural integrity of the scaffold. This is because only the surface is subjected to weakening by erosion and this produces little reduction in the strength of the complete scaffold structure. Bulk degradation results in more rapid reductions in mechanical strength leading to a loss of scaffold integrity. This is due to the scaffold material being weakened throughout its structure, not just at the surface.[306,307]

Cholesterol esterase has been shown to cause the degradation of various polyesters in previous studies.[287,308–311] This enzyme has been shown to be identical to the esterases produced by macrophages which are known to degrade polyesters *in vivo*.[311] Cholesterol esterase, at the same concentration as in this study, was shown to degrade PGS-A, with the rate of degradation dependant on the DA of the polymer. Similar to the results here, a lower DA resulted in increased enzymatic degradation. The overall rate of degradation appeared more rapid, with 30% DM PGS-A reduced in mass by 40% in just 48 hours, compared to the 5% mass reduction seen in 30% High M_w PGS-M over the same time. These results are not directly comparable, as the PGS-A polymer was of a higher molecular weight than the PGS-M. Additionally, the shape of the PGS-A samples was not reported and since the surface area of the substrate has a great effect on the rate of an enzyme catalysed reaction, it is unknown how this may have affected the degradation rate. The same study also demonstrated that thermally cured PGS polymer degraded more rapidly than PGS-A, reducing in mass by 60% in 48 hours. It was suggested that the acrylate group may restrict the enzymes' access to the ester linkages within the polymer. A similar effect may be seen in PGS-M.

PGS-M also appeared to be degraded by lipase, although the reduction in mass caused by the activity of this enzyme over 8 days was only significant in the 30% DM PGS-M. No difference was seen between the Low and High M_w 30% PGS-M samples, both showing a reduction in mass of ~4% over the study period. Similar to cholesterol esterase, the effect of lipase appeared to reduce with increasing DM and this may have been due to similar reasons, with the increase in the number of crosslinks present within the polymer, as the DM increases, reducing the ability of chain fragments to be released. Lipase may have a lower specificity for PGS-M compared to cholesterol esterase, resulting in its reduced rate of degradation. A longer study length may result in significant degradation by lipase in all PGS-M variants.

Lipase has also been shown to degrade various polyester biomaterials in other studies.[301,305,312,313] In examining thermally cured PGS, lipase treatment produced a reduction in mass of ~12% after 8 days and ~30% after 31 days, *in vitro*.[312] Notably, this

study used a much lower concentration of lipase enzyme (110 units/µl) than herein. This suggests that lipase has a much greater effect on thermally cured PGS compared to PGS-M. Similar to cholesterol esterase, this may be due to the methacrylate groups limiting the enzymes' access to ester bonds.

PBS appeared to have no significant effect on the degradation of any of the PGS-M variants examined in this study. Since degradation in PBS alone would be the result of uncatalysed hydrolysis, it was expected that this treatment would result in the least mass loss from the PGS-M polymers. It is likely that significant degradation in PBS would occur over a long enough study period. In examining PGS-A, a 22% reduction in mass was seen after 18 weeks.[300] The samples were 10 x 2 x 1 mm and had a DA of 23% and a M_w of 24,240 Da. Considering the differences in crosslink density and M_w, 30% High M_w PGS-M may show similar degradation over the same time period. Thermally cured PGS also showed degradation in PBS, reducing in mass by 10% over 31 days.[312] Additionally, a number of different photopolymerisable biomaterials have demonstrated degradation in PBS, with this also being dependent on the degree of crosslinking within their matrices.[314–316]

It must be noted that the rates of degradation observed in this simple study may be different to those produced in more complex *in vitro* environments containing living cells or *in vivo*.[305] The types of enzymes produced by different cells and their concentrations vary greatly and this can have a great effect on the degradation rate of a biomaterial.[305] Environmental factors such as the surrounding pH, presence of enzyme inhibitors and the application of flow, mechanical loading or agitation to the material can also have an impact. Indeed, this has been demonstrated in both PGS-A and PGS, with implanted materials degrading at a faster rate than *in vitro* counterparts.[282,288]

Variation in the DM and M_w of PGS-M had an effect on the mechanical properties of the photocured polymer. Tensile testing demonstrated that the mechanical properties

of PGS-M were more dependent on the DM of the polymer than the M_w. Significant increases in Young's modulus resulted from increasing the DM from 30% to 50% to 80% in Low M_w PGS-M polymers and from 30% to 50% in High M_w PGS-M polymers. Changes in UTS also followed a similar trend, although only resulting in significantly different results for the Low M_w 80% PGS-M compared to the other Low M_w polymers. Interestingly, variation in M_w was not found to have a significant effect on the Young's modulus or UTS of PGS-M.

As the DM is increased, more crosslinks are able to form within the polymer matrices resulting in an increase in crosslink density. Increasing the crosslink density reduces the mobility of the individual polymer chains within the matrix, resulting in an increase in the stiffness of the bulk polymer and an increase its Young's modulus.[306,317] The effect of increased crosslink density on Young's modulus is evident in the behaviour of PGS-M at varied DM. Additionally, due to the crosslinks containing covalent bonds, an increase in crosslink density commonly results in an increase in the UTS of a polymer, as additional chemical bonds must be broken to produce failure.[317] This behaviour manifested to a lesser extent in PGS-M, with no significant difference observed between the UTS of 30% and 50% DM polymers of the same M_w. These findings may have been due to the limited number of test pieces examined, since the mean average values for these polymers did fit with the classical behaviour.

As the M_w of a polymer is increased the average length of its constituent chains increases. This results in an increase in the number of chemical bonds present within the bulk material and an increase in stiffness and strength.[306,317] Additionally, as chain length increases, chain entanglement also increases, further increasing the polymers resistance to deformation. This behaviour was not evident in PGS-M. No significant differences in Young's modulus or UTS were found between Low and High M_w polymers of the same DM. It may be that the difference between the chain lengths of the Low and High M_w polymers was not great enough for any significant change in polymer stiffness or strength to be detected. Additionally, the increasingly disperse nature of the PGS prepolymer as M_w is increased likely resulted in a photopolymerised

PGS-M composed of a large range of different polymer chain lengths. This dispersity may also have affected the mechanical properties of the bulk materials with the combination of various chain lengths not ultimately resulting in an increase in stiffness or strength.

Similar results have been reported in the literature for PGS-A. Varying the DA of PGS-A, between 1% and 88%, while maintaining constant M_w resulted in an increase in Young's modulus and UTS in three different studies.[287,288,300] These reported values were also comparable with those produced by PGS-M (Table 7). Additionally, variation in the M_w of PGS-A did not result in any significant changes in Young's modulus or UTS.[288] Other photopolymerisable biomaterials have also displayed similar behaviour with an increase in crosslinking density resulting in an increase in stiffness and mechanical strength.[316,318,319]

Table 7. Mechanical properties of PGS-M compared to reported values for PGS-A (± denotes standard deviations).

Polymer	DM/DA (%)	M_w (Da)	Young's Modulus (MPa)	UTS (MPa)	Ref
PGS-M (herein)	30	5,419 ± 435	0.43	0.73	
		17,339 ± 760	0.69	0.45	
	50	5,419 ± 435	1.47	0.82	
		17,339 ± 760	1.39	0.77	
	80	5,419 ± 435	6.74	3.80	
PGS-A	21	4,060	0.6	-	288
		7,020	0.6	-	288
	34	23,000	0.568	0.270	287
	54	23,000	1.375	0.498	287
	88	4,060	13.2	-	288

The mechanical properties exhibited by 30% Low M_w PGS-M coupled to its degradation rate and more rapid synthesis compared to the 30% High M_w polymer suggested that it was the most suitable variant of PGS-M for manufacturing a scaffold for producing a TEVG. Therefore, an investigation into the mechanical properties of 30% Low M_w PGS-M following sterilisation was conducted. Autoclave sterilisation resulted in a significant reduction in the Young's modulus of the polymer, from 0.43 to 0.37 MPa. However, no significant change in the UTS was apparent. This suggests that the autoclave treatment did not cause degradation of the polymer matrix and covalent bonds were largely unbroken. The partial solvation of the polymer following removal from dH_2O immediately prior to tensile testing may have resulted in a disruption of the intermolecular forces between the polymer chains. This could have resulted in a reduction in the stiffness of the material.[317] Additionally, the high temperature and aqueous environment of the autoclave may have resulted in the reorientation of the polymer chains within the bulk material. Chain entanglement may have been reduced and this can affect the stiffness of the polymer.[317]

Subsequent treatment with peracetic acid did not cause any significant changes in the mechanical properties of 30% Low M_w PGS-M. Although the hydrolysis of ester bonds is known to increase in acidic environments, it is likely that the exposure time of 1 hour was not sufficient to cause significant degradation of the bulk material and alter the mechanical properties.[307]

2.5 **Conclusions**

A novel photocurable form of PGS, PGS-M was synthesised and characterised for potential application as the material for a scaffold to support the growth of a TEVG *in vitro*.

Different variants of PGS-M were produced, with a range of molecular weights and degrees of methacrylation and their compositions confirmed using various analytical chemistry techniques. It was determined that both the molecular weight and DM could be controlled by altering the reaction conditions used in the synthesis of the polymers. The degradation of the different variants of PGS-M was examined and revealed that the polymers were susceptible to enzymatic degradation with increasing the DM appearing to have an inverse effect on this. Finally, the mechanical properties of PGS-M were assessed and found to largely depend on the DM of the polymer and not the molecular weight.

30% Low M_w PGS-M was selected as the most suitable variant for producing a scaffold for use in culturing a TEVG. This polymer displayed the required properties identified for the scaffold material (Young's modulus of ~300 kPa, rapid degradation rate, and simple processing).

Chapter 3 - 2D Cell Culture on PGS-M Surfaces

3.1 Introduction

In the previous chapter, the novel polymer PGS-M was successfully synthesised and characterised in terms of its structural, mechanical and degradation properties. It was found that the mechanical and degradation properties could be modulated, by altering the structure of the polymer by changing its molecular weight and DM. It was determined that a PGS-M polymer with a 30% DM and a M_w of ~5,400 Da (30% Low M_w PGS-M) was the most suitable for producing a scaffold for use in culturing a TEVG.

In this chapter, the interaction of 30% Low M_w PGS-M with living cells in simple 2D cultures is presented. Three different cell types relative to vascular graft tissue engineering were selected and cultured on PGS-M surfaces. These were fibroblasts, adipose-derived stem cells (ADSCs) and smooth muscle cells. Fibroblasts and smooth muscle cells are both major cellular components of arteries and veins, being found in the tunica adventitia and tunica media, respectively. As such, both cell types have been commonly employed in the production of tissue engineered blood vessels for use as vascular grafts.[61,66,76,92,94,95,97,108,125,146]

In recent years, ADSCs have attracted interest in a number of tissue engineering applications.[320,321] These cells offer similar differentiation potential to bone marrow and mesenchymal stem cells, however, they are more easily harvested. A number of studies have explored using stem cells in producing TEVGs.[55,77,198,202,203,207,212,214] These aimed to take advantage of the multi/pluripotency of these cells and induce differentiation towards vascular cell lineages during culture to generate tissue engineered blood vessels. Studies using ADSCs are limited in the field of TEVGs

however, therefore they were also selected for study when cultured on PGS-M surfaces to determine their potential for use in the future generation of a TEVG using PGS-M as a scaffold material.

The three different cell types were cultured on PGS-M surfaces for several days. Their metabolic activity and proliferation was examined at various time points and used to assess their response to the novel polymer surface. Additionally, the expression of phenotypic cell markers was examined in SMCs to determine the effects of PGS-M on these.

3.2 Materials and Methods

In the following methods, all chemical reagents were obtained from Sigma Aldrich, UK unless otherwise stated. These reagents were measured and utilised in inert vessels.

3.2.1 Surface coating of glass coverslips with PGS-M

Borosilicate glass coverslips (13 mm diameter, No 2 thickness)(Scientific Laboratory Supplies, UK) were cleaned in a 3:1 (v/v) solution of sulphuric acid (95.0-98.0%) and hydrogen peroxide (30 wt% in H_2O) for 1 hour and then rinsed with five washes of dH_2O and three washes of methanol. The coverslips were then immersed in a 10% (w/v) solution of 3-methacryloxypropyltrimethoxysilane in toluene for 24 hrs, in the absence of light, before being rinsed in methanol three times, and dried at room temperature.

50 µl of 30% Low M_w PGS-M prepolymer, synthesised as described in (2.2.3), containing 1% (w/w) photoinitiator, was applied to the centres of individual coverslips by pipetting and then distributed evenly across their surfaces by spin coating (Laurell Technologies WS-400B-6NPP/Lite) at 4,000 rpm for 40 seconds. PGS-M coated coverslips were photocured by exposure to UV light (100W, OmniCure Series 1000 curing lamp) in a sealed container lined with reflective foil for 5 minutes. Following this,

the coated coverslips were washed in methanol for 4 days (changed daily) followed by dH_2O for 4 days (changed daily). Coverslips were then sterilised by autoclave at 121°C for 30 minutes, prior to cell seeding.

3.2.2 **Preparation of fibroblast growth medium**

Dulbecco's modified eagle's medium (DMEM) AQmedia was modified with 10% (v/v) foetal calf serum, 1% (v/v) Penicillin (10,000 units/ml), 1% (v/v) Streptomycin (10 mg/ml) and 0.25% (v/v) Amphotericin B (250 µg/ml).

3.2.3 **Preparation of smooth muscle cell growth medium**

SMC growth medium with supplements was purchased from PromoCell, Germany. Smooth Muscle Cell Growth Medium 2 was combined with a supplement mixture as described by the manufacturer. Final supplement concentrations in the medium were 5% (v/v) foetal calf serum, 0.5 ng/ml epidermal growth factor (recombinant human), 2 ng/ml basic fibroblast growth factor (recombinant human) and 5 µg/ml insulin (recombinant human).
Additionally, 1% (v/v) Penicillin (10,000 units/ml), 1% (v/v) Streptomycin (10 mg/ml) and 0.25% (v/v) Amphotericin B (250 µg/ml) were also added to the growth medium.

3.2.4 **Culture of human dermal fibroblasts and human adipose-derived stem cells on PGS-M surfaces.**

Human dermal fibroblasts and human ADSCs from primary dermal tissue or lipoaspirate, respectively, were obtained with informed consent (ethics reference: 15/YH/0177) and processed and stored in accordance with the Human Tissue Act 2004 (licence number 12179). Isolated cells were cultured on tissue culture

plastic (TCP) in fibroblast growth medium, prepared as described in (3.2.2), at 37 ^{0}C and 5% CO_2 in an incubator.

Cells between passage 4 and 6 were harvested using trypsin (0.025%)/EDTA (0.01%) solution at 0.067 ml/cm^2 of culture area. This was quenched after 5 minutes with an equal volume of fibroblast growth medium and the cell suspension centrifuged at 1,000 rpm for 5 minutes (Hettich Zentrifugen Rotofix 32A with 131 mm rotor radius) before being resuspended in fibroblast growth medium at 50000 cells/ml.

Suspended cells were then seeded onto PGS-M coated coverslips, prepared as described in (3.2.1), in 12-well tissue culture plates (Greiner bio-one, Germany), at 50,000 cells per well. The cells were allowed to attach for 6 hours and then the coverslips were transferred to new wells for further culture, ensuring only cells attached to the coverslips were included in future analyses.

Untreated glass coverslips, sterilised by autoclave at 121°C for 30 minutes, were also seeded with cells, in an equivalent manner to the PGS-M coated coverslips, to act as positive controls. Additionally, unseeded PGS-M coated coverslips were cultured in fibroblast growth medium, in parallel with the seeded coverslips, to act as negative controls. Each culture well contained 1 ml of growth medium and this was changed every second day.

Fibroblast seeded coverslips, and associated control samples, were cultured for 1, 3 or 7 days before being analysed. ADSC seeded coverslips, and associated control samples, were cultured for 1, 7 or 14 days before being analysed.

3.2.5 **Culture of human coronary artery smooth muscle cells on PGS-M surfaces.**

Human coronary artery SMCs were obtained commercially from PromoCell, Germany. The SMCs were cultured on TCP in SMC growth medium, prepared as described in (3.2.3), at 37 ^{0}C and 5% CO_2 in an incubator.

Cells between passage 9 and 11 were harvested using trypsin (0.025%)/EDTA (0.01%) solution at 0.067 ml/cm^2 of culture area. This was quenched after 5 minutes with an equal volume of trypsin inhibitor (PromoCell, Germany) and the cell suspension

centrifuged at 1,200 rpm for 4 minutes (Hettich Zentrifugen Rotofix 32A with 131 mm rotor radius) before being resuspended in SMC growth medium at 50,000 cells/ml.

Suspended cells were then seeded onto PGS-M coated coverslips, prepared as described in (3.2.1), in 12-well tissue culture plates (Greiner bio-one, Germany), at 50,000 cells per well. The cells were allowed to attach for 6 hours and then the coverslips were transferred to new wells for further culture, ensuring only cells attached to the coverslips were included in future analyses.

Untreated glass coverslips, sterilised by autoclave at 121°C for 30 minutes, were also seeded with cells, in an equivalent manner to the PGS-M coated coverslips, to act as positive controls. Additionally, unseeded PGS-M coated coverslips were cultured in fibroblast growth medium, in parallel with the seeded coverslips, to act as negative controls. Each culture well contained 1 ml of growth medium and this was changed every second day.

The seeded coverslips, and associated control samples, were cultured for 1, 3 or 7 days before being analysed.

3.2.6 **Resazurin reduction assay for cell viability on PGS-M surfaces**

The viability of cells cultured on PGS-M surfaces, as described in (3.2.4) and 3.2.5), was assessed using the resazurin reduction (RR) assay. Resazurin sodium salt is the active ingredient in the commercially available cell viability assay reagent alamarBlue®. 0.0251% (w/v) resazurin sodium salt was dissolved in dH_2O. The solution was filter sterilised using a 0.22 µm filter and mixed 10% (v/v) with the appropriate cell growth medium (fibroblast growth medium for use with fibroblasts or ADCSs and SMC growth medium for use with SMCs).

At the time points described in (3.2.4) and (3.2.5), the growth medium was removed from the culture wells containing the cell seeded coverslips, and parallel controls, and replaced with the same volume of resazurin-containing growth medium. Samples were then returned to the incubator. An equivalent sample of the resazurin-containing

growth medium was also incubated, in parallel, for use as a blank. After 4 hours, samples were removed from the incubator and 200 µl of solution was extracted from each well, in triplicate, and placed in the wells of a 96-well plate. This plate was then read using a fluorescence plate reader (Bio-tek instruments FLX800) at 540 nm excitation and 635 nm emission, with the reading from the blank subtracted. Each time point was examined three times, using cells sourced from different donors for the fibroblasts and ADSCs, with triplicate samples for each cell type and control.

The results were statistically analysed using two-way ANOVA with Tukey multiple comparisons analysis. $P<0.05$ was considered significant (*), $P<0.01$ was considered very significant (**) and $P<0.001$ was considered extremely significant (***).

3.2.7 **Production of a standard curve for the PicoGreen® DNA quantification assay**

The Quant-iT^{TM} PicoGreen® dsDNA quantification assay was purchased as a kit (Thermo Fisher Scientific, USA). The assay measures the quantity of double stranded DNA present in a sample by means of fluorescence. In accordance with the manufactures instructions, a standard curve of fluorescence values was produced using dilutions of a 10 µg/ml λDNA standard in a 0.25% (v/v) solution of TE buffer (10 mM Tris-HCl, 1 mM EDTA) in dH_2O. Dilutions were made to produce solutions containing 200, 400, 600, 800 and 1,000 ng/ml DNA. An equivalent sample containing none of the λDNA standard was also produced to act as a blank. 100 µl, in triplicate, of each dilution was then extracted and placed in the wells of a black 96-well plate. This plate was then read using a fluorescence plate reader (Bio-tek instruments FLX800) at 480 nm excitation and 520 nm emission with gain 20. The reading from the blank was then subtracted from the value for each well. A standard curve describing the relationship between the quantity of sample DNA and the fluorescence detected was then produced using the values obtained and nonlinear regression using a second order polynomial.

3.2.8 **PicoGreen® DNA quantification assay for cells cultured on PGS-M surfaces**

The quantity of cells present on PGS-M surfaces cultured, as described in (3.2.4) and (3.2.5), was assessed using the PicoGreen® DNA quantification assay, purchased as a kit (Thermo Fisher Scientific, USA). The assay measures the quantity of double stranded DNA present in a sample by means of fluorescence. This can be used to infer the number of cells present.

At the time points described in (3.2.4) and (3.2.5), the growth medium was removed from the culture wells containing the cell seeded coverslips, and parallel controls. The coverslips were washed with PBS, three times, within their wells and then 500 µl of dH_2O added to each well. Samples were then refrigerated at 4°C for 12 hours before being frozen at -80°C. Frozen samples were then thawed in an incubator at 37°C before being re-frozen at -80°C. Freeze-thawing was conducted three times. After the final thawing, the solution was removed from each sample well and placed in a 1 ml microcentrifuge tube. These tubes were agitated in a vortex mixer for 15 seconds before being centrifuged at 10,000 rpm for 5 minutes (Sanyo MSE Micro Centaur MSB010.CX2.5 with 64 mm rotor). 180 µl was then extracted from each microcentrifuge tube and mixed with 180 µl of a 5% (v/v) TE buffer and 0.5% (v/v) PicoGreen® solution in dH_2O, in accordance with the manufacturer's instructions. 180 µl of dH_2O was also mixed with 180 µl of the 5% (v/v) TE buffer and 0.5% (v/v) PicoGreen® solution in dH_2O to act as a blank. All samples were wrapped in silver foil and agitated in a vortex mixer for 5 seconds before being incubated at room temperature for 10 minutes. 100 µl, in triplicate, was then extracted from each sample and placed in the wells of a black 96-well plate. This plate was then read using a fluorescence plate reader (Bio-tek instruments FLX800) at 480 nm excitation and 520 nm emission with gain 20. The reading from the blank was then subtracted from the value for each well. Each time point was examined three times, using cells sourced from different donors with triplicate samples for each cell type and control. The results were statistically analysed using two-way ANOVA with Tukey multiple comparisons

analysis. P<0.05 was considered significant (*), P<0.01 was considered very significant (**) and P<0.001 was considered extremely significant (***).

3.2.9 **Visualisation of cell proliferation on PGS-M surfaces**

Borosilicate glass coverslips coated in 30% Low M_w PGS-M were prepared and sterilised as described in (3.2.1). The sterile coverslips were placed individually in the wells of a 12-well plate and a stainless steel (316L medical grade) cylinder (4 mm diameter, 4 mm length), sterilised by autoclave at 121°C for 30 minutes, placed in the centre of each. This stainless steel cylinder would act as a mask, preventing cell adhesion to an area at the centre of each coverslip.

Cells (Fibroblasts, ADSCs and SMCs) were cultured on TCP and harvested as described in (3.2.4) and (3.2.5), respectively. Suspended cells were seeded into the wells containing the masked coverslips at 50,000 cells per well. The cells were allowed to attach for 6 hours and then the stainless steel masks were removed and the coverslips were transferred to new wells for further culture, ensuring only cells attached to the coverslips were included in future analyses.

Additionally, masked PGS-M coated coverslips were cultured in parallel with seeded coverslips, in an equivalent manner, to act as negative controls. Each culture well contained 1 ml of the appropriate growth medium for the cell type and this was changed every second day.

The seeded coverslips, and associated unseeded control samples, were cultured for up to 14 days. They were imaged using light microscopy (Olympus IX73) every other day to examine the extent of cell proliferation. The size of the remaining masked area was calculated from the images using software (ImageJ, version 1.45s). The boundary between the proliferating cells and the masked area was determined visually and traced using the Freehand Selection tool. The area of the defined section was then calculated in pixels and converted to mm^2 using the scale bar for calibration.

3.2.10 **Fixation and sectioning of human umbilical cord tissue**

Human umbilical cords, collected with informed consent (ethics number: STH15599), were used to provide positive control samples for various tissue analysis assays. Cords were rinsed with PBS and squeezed longitudinally to remove coagulated blood from the umbilical vein and arteries. Lengths of ~5 mm were then cut and placed in 3.7 % formaldehyde (methanol free) for 24 hours, to fix the tissue. Following fixation, the tissue was rinsed with PBS, three times, and then immersed in optimal cutting temperature (OCT) compound (Tissue-Tek, Sakura, Japan) and frozen at -20 °C. Frozen samples were mounted on stubs and cryosectioned (Lieca CM1860 UV), at -25°C, across their cross-sections, at a thickness of 5 µm. Sections were mounted on glass slides (Superfrost® Plus, Menzel-Gläser, Germany) and, after 24 hours, rinsed in dH_2O to remove the OCT compound.

3.2.11 **Immunofluorescence staining of SMCs for alpha-smooth muscle actin**

SMCs seeded and cultured on glass coverslips coated in 30% Low M_w PGS-M for 7 days, as described in (3.2.5), were examined for the presence of alpha-smooth muscle actin (α-SMA) using immunohistochemistry. The growth medium was removed from each culture well and the coverslips washed with PBS, three times, before being fixed with 1 ml of 3.7% formaldehyde (methanol free). After 1 hour of fixation, the formaldehyde was removed and the samples washed with PBS, three times, before staining commenced. The staining process began by permeablising the samples with 100 µl of a 0.5% (v/v) solution of Triton X 100 (Fisher Scientific, UK) in PBS. After 1 hour of permeablisation, the Triton X 100 solution was removed and the samples washed with PBS, three times, before being blocked with 100 µl of a 5% (w/v) solution of bovine serum albumin (BSA) in PBS. After 1 hour, the BSA solution was removed and 100 µl of a 0.2% (v/v) anti α-SMA mouse monoclonal antibody conjugated with Cy3™ and 5% (w/v) BSA in PBS solution was added to each sample. After incubation at room temperature, in the absence of light for 2 hours, the antibody solution was removed

and each well again washed with PBS, three times. Finally, all samples were rinsed with dH_2O, to remove any remaining salts. The coverslips were then imaged, in their wells, using a fluorescence microscope (Olympus IX73) with 550-570 nm excitation and 600-660 nm emission.

Various controls were also produced and imaged. PGS-M coated coverslips, with attached SMCs, that were fixed, permeablised and blocked, but not treated with antibody, were used to establish the effect of any background fluorescence. Additionally, unseeded PGS-M coated coverslips, cultured in parallel with the SMC seeded coverslips, in an equivalent manner, were fixed and stained to act as negative controls. Finally, sections of human umbilical cord, prepared as described in (3.2.10), were stained to act as a positive control. Experiments were conducted three times with triplicate samples.

3.2.12 **Immunofluorescence staining of SMCs for calponin**

SMCs seeded and cultured on glass coverslips coated in 30% Low M_w PGS-M for 7 days, as described in (3.2.5), were examined for the presence of calponin using immunohistochemistry. The seeded coverslips were prepared, permeablised and blocked as described in (3.2.11). Following the removal of the BSA blocking solution, 100 µl of a 0.4% (v/v) anti calponin 1 rabbit polyclonal antibody conjugated with FITC (Insight Biotechnology, UK) and 5% (w/v) BSA in PBS solution was added to each sample. After incubation at room temperature, in the absence of light, for 2 hours the antibody solution was removed and the sections again washed with PBS, three times, followed by once with dH_2O, to remove any remaining salts. The coverslips were then imaged, using a fluorescence microscope (Olympus IX73) with 480-500 nm excitation and 510-550 nm emission.

Control coverslips and sections of human umbilical cord artery were also produced as described in (3.2.11). Experiments were conducted three times with triplicate samples.

3.3 **Results**

3.3.1 **RR assay for cell viability on PGS-M surfaces**

Human dermal fibroblasts, human ADSCs and human coronary artery SMCs were cultured on glass coverslips coated in 30% Low M_w PGS-M. Cell viability was assessed by reduction of resazurin sodium salt to resorufin, measured using fluorescence detection.

Fibroblasts were cultured on PGS-M surfaces for 1, 3 and 7 days. The results for each time point are shown in Figure 26. The fluorescence detected increased over the duration of the study. The results at day 7 were significantly different to days 1 and 3 ($P<0.001$ and 0.05, respectively), although these were not significantly different to each other. Similar results were seen in the positive controls, where fibroblasts were cultured on borosilicate glass. The fluorescence signal at day 7 was significantly different to days 1 and 3 ($P<0.001$ and 0.05, respectively), and these were not significantly different to each other. Comparing the results for cultures on PGS-M and glass at each time point showed no significant differences between the two surfaces. There was also no significant interaction between the type of surface and the time points assessed. All the results for fibroblasts cultured on PGS-M and glass surfaces were statistically significantly different to the negative controls (unseeded PGS-M coated coverslips) which showed negligible fluorescence.

ADSCs were also cultured on PGS-M surfaces. Due to their slower growth rate, time points at 1, 7 and 14 days were examined. The results for each time point are shown in Figure 27. The fluorescence signal detected over the duration of the study increased, although a significant difference was only seen between days 1 and 14 ($P<0.05$). Similar results were seen in the positive controls (ADSCs cultured on borosilicate glass), although with a slightly greater degree of significant difference between days 1 and 14 ($P<0.01$). As in the culture of fibroblasts, comparing the results for ADSCs cultured on

PGS-M and glass at each time point showed no significant differences between the two surfaces, along with no significant interaction between the type of surface and the time points assessed. All the results for the ADSC cultures were statistically significantly different to the negative controls (unseeded PGS-M coated coverslips) which showed negligible fluorescence.

Finally, SMCs were cultured on PGS-M surfaces for 1, 3 and 7 days. The results for each time point are shown in Figure 28. As in the cultures of fibroblasts and ADSCs, the fluorescence signal detected over the duration of the study increased. The results at days 3 and 7 were significantly different from day 1 ($P<0.001$, in both cases), although these were not significantly different from each other. In the positive controls (SMCs cultured on borosilicate glass) the results at day 7 were significantly different to days 1 and 3 ($P<0.001$, in both cases), although these were not significantly different to each other.

As in the culture of fibroblasts and ADSCs, comparing the results for SMCs cultured on PGS-M and glass at each time point showed no significant differences between the two surfaces. However, unlike in the culture of fibroblasts and ADSCs, a significant interaction was shown between the type of surface and the time points assessed ($P<0.01$). The results across the time points were dependent on the type of surface. All the results for the SMC cultures were statistically significantly different to the negative controls (unseeded PGS-M coated coverslips) which showed negligible fluorescence.

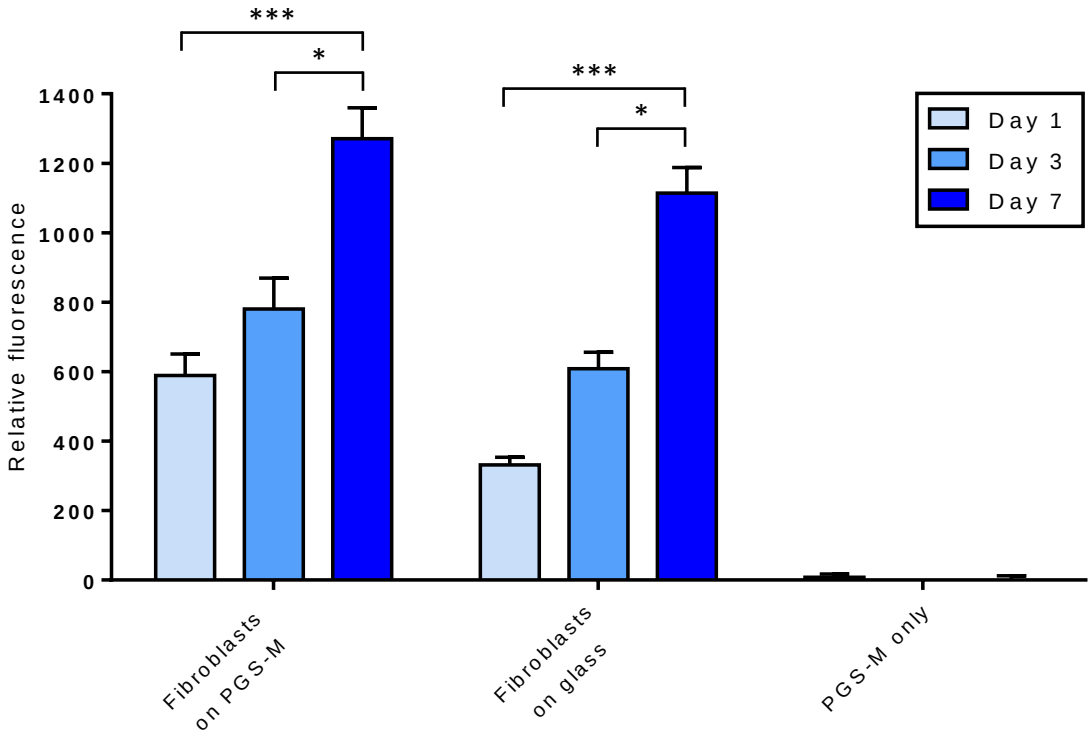

Figure 26. RR assay for fibroblast viability on 30% Low M_w PGS-M surfaces after 1, 3 and 7 days in culture. Positive controls were fibroblasts cultured on borosilicate glass (Fibroblasts on glass). Negative controls were unseeded PGS-M surfaces (PGS-M only). Error bars are SEM (n = 3).

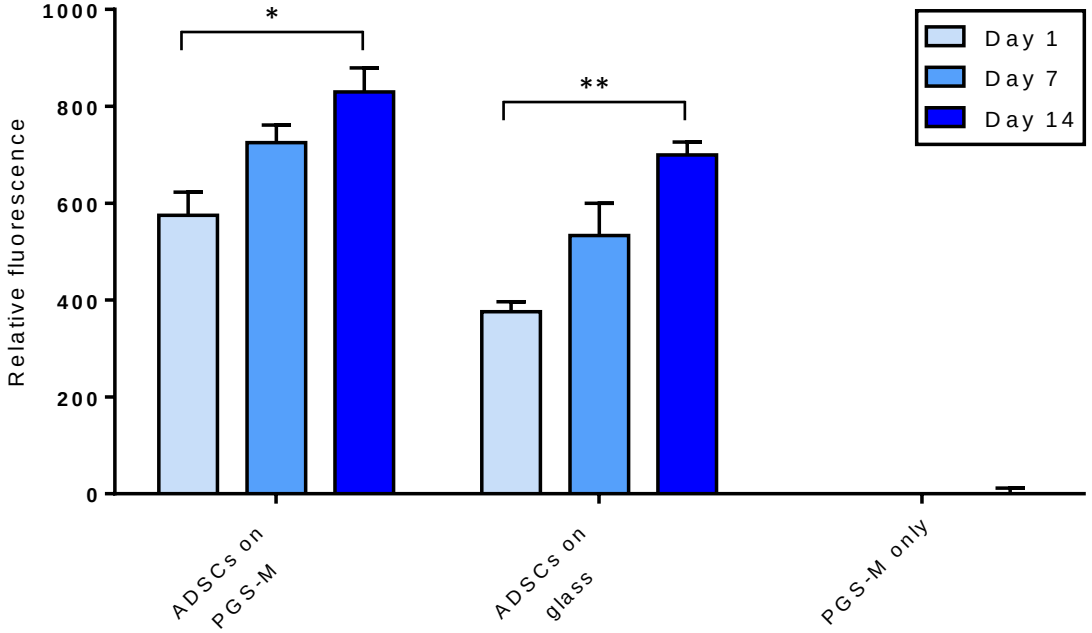

Figure 27. RR assay for ADSC viability on 30% Low M_w PGS-M surfaces after 1, 7 and 14 days in culture. Positive controls were ADSCs cultured on borosilicate glass (ADSCs on glass). Negative controls were unseeded PGS-M surfaces (PGS-M only). Error bars are SEM (n = 3).

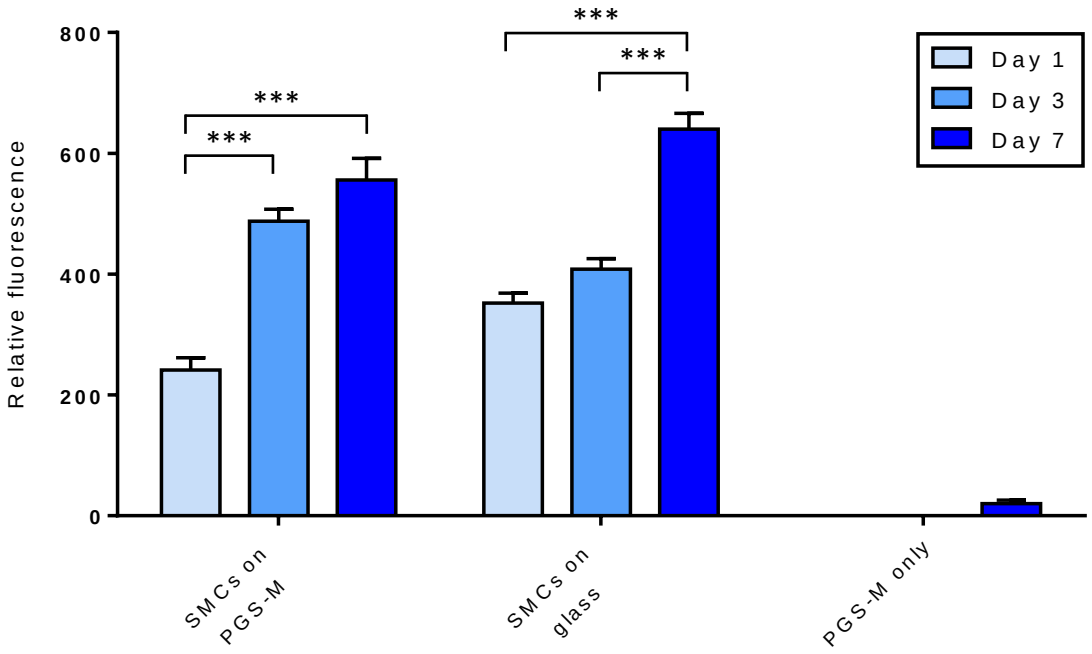

Figure 28. RR assay for SMC viability on 30% Low M_w PGS-M surfaces after 1, 3 and 7 days in culture. Positive controls were SMCs cultured on borosilicate glass (SMCs on glass). Negative controls were unseeded PGS-M surfaces (PGS-M only). Error bars are SEM (n = 3).

3.3.2 **PicoGreen® DNA quantification assay for cells cultured on PGS-M surfaces**

The quantity of fibroblasts, ADSCs and SMCs present on PGS-M surfaces in culture was assessed using the commercially available PicoGreen® DNA quantification assay. The assay measured the quantity of dsDNA present in each sample by means of fluorescence. This was then used to infer the number of cells present using a standard curve (Figure 29). The standard curve was generated through fitting a second order polynomial to the fluorescence values generated from known quantities of λDNA (0-1,000 ng/ml DNA). The fitted curve showed strong agreement with the data (R^2 = 0.99).

Fibroblasts were cultured on PGS-M surfaces for 1, 3 and 7 days. The results for each time point are shown in Figure 30. The fluorescence detected increased over the duration of the study. The results at day 7 were significantly different to days 1 and 3 ($P<0.001$ and 0.01, respectively), although these were not significantly different to each other. In the positive controls, where fibroblasts were cultured on borosilicate

glass, the fluorescence signal also increased across the time points studied. At day 7, the result was significantly different to days 1 and 3 ($P<0.001$, in both cases), and these were also significantly different to each other ($P<0.01$). Comparing the results for cultures on PGS-M and glass at each time point showed no significant differences at day 1, but significant differences at day 3 ($P<0.05$) and day 7 ($P<0.001$), with the positive controls showing the greater values. There was a significant interaction between the type of surface and the time points assessed ($P<0.05$). The results across the time points were dependent on the type of surface.

Using a standard curve, the mass of DNA present on each coverslip surface at each time point was determined. This was then used to infer the number of cells present on each surface, based on a single cell containing 3.5 pg of dsDNA.[322] At day 1, PGS-M surfaces supported 4,500 ± 200 cells, rising to 37,700 ± 3,000 cells, by day 7. Glass surfaces supported 10,000 ± 600 cells at day 1 and 69,900 ± 5,400 cells by day 7.

All of the results for fibroblasts cultured on PGS-M and glass surfaces were statistically significantly different to the negative controls (unseeded PGS-M coated coverslips) which showed negligible fluorescence.

ADSCs were cultured on PGS-M surfaces for 1, 7 and 14 days. The results for each time point are shown in Figure 31. Over the three time points, the fluorescence signal detected increased. A significant difference was only seen between days 1 and 14 ($P<0.01$) and not between days 1 and 7 or days 7 and 14. In the positive controls (ADSCs cultured on borosilicate glass), significant differences were seen between the results at day 1 and days 7 and 14 ($P<0.01$ and 0.001, respectively), but not between day 7 and day 14.

Unlike in the culture of fibroblasts, comparing the results for ADSCs cultured on PGS-M and glass at each time point showed no significant differences between the two surfaces, along with no significant interaction between the type of surface and the time points assessed.

Using a standard curve, the mass of DNA, and subsequently the number of cells present, on each surface was determined. PGS-M surfaces supported 9,200 ± 1,300 ADSCs at day 1 and 27,200 ± 2,800 ADSCs, by day 14. Glass surfaces supported 8,400 ± 400 ADSCs at day 1 and 32,400 ± 1,600 cells by day 14.

All of the results for the ADSC cultures were statistically significantly different to the negative controls (unseeded PGS-M coated coverslips) which showed negligible fluorescence.

Finally SMCs were cultured on PGS-M surfaces for 1, 3 and 7 days. The results for each time point are shown in Figure 32. As seen in the other two cell types examined, the fluorescence signal detected over the duration of the study increased. Similar to the results seen in the culture of fibroblasts, the fluorescence signal at day 7 was significantly different from those measured at days 1 and 3 ($P<0.001$, in both cases). The results at days 1 and 3 were not significantly different from each other. A similar trend was seen in the positive controls (SMCs cultured on borosilicate glass) with the results at day 7 being significantly different to days 1 and 3 ($P<0.001$, in both cases) and these not being significantly different to each other.

Comparing the results for the two different culture surfaces across the time points showed significant differences at day 7 only ($P<0.001$). A significant interaction was shown between the type of surface and the time points assessed ($P<0.001$). The results across the time points were dependent on the type of surface.

Using a standard curve, the mass of DNA, and subsequently the number of cells present, on each coverslip was determined. PGS-M surfaces supported 8,500 ± 1,300 SMCs at day 1 and 43,400 ± 1,600 SMCs, by day 7. Glass surfaces supported 4,700 ± 500 SMCs at day 1 and 65,700 ± 3,000 cells by day 7.

All the results for the SMC cultures were statistically significantly different to the negative controls (unseeded PGS-M coated coverslips) which showed negligible fluorescence.

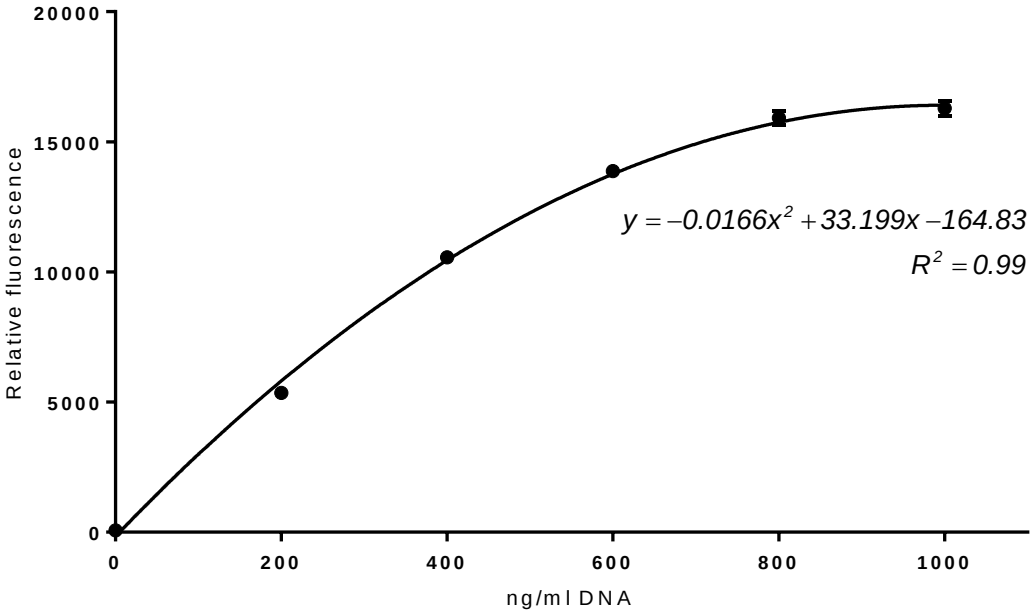

Figure 29. PicoGreen® assay standard curve produced from known concentrations of λDNA standard (*n* = 2).

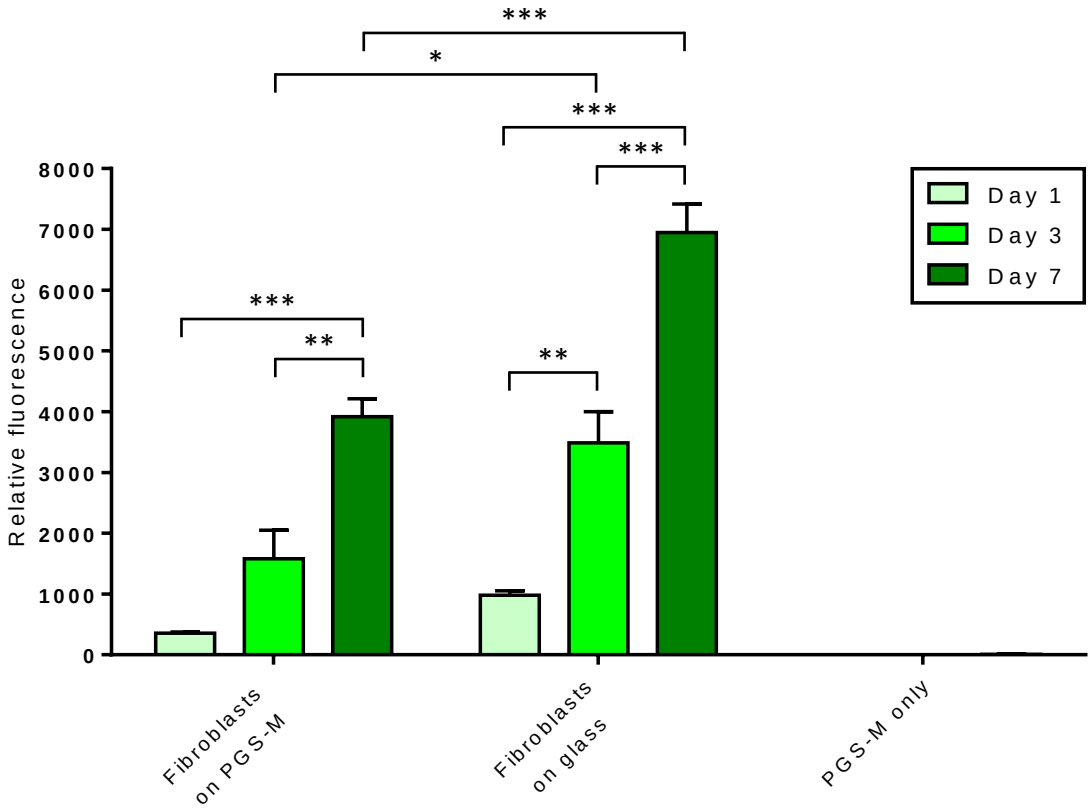

Figure 30. PicoGreen® assay for Fibroblast dsDNA on 30% Low M_w PGS-M surfaces after 1, 3 and 7 days in culture. Positive controls were Fibroblasts cultured on borosilicate glass (Fibroblasts on glass). Negative controls were unseeded PGS-M surfaces (PGS-M only). Error bars are SEM (*n* = 3).

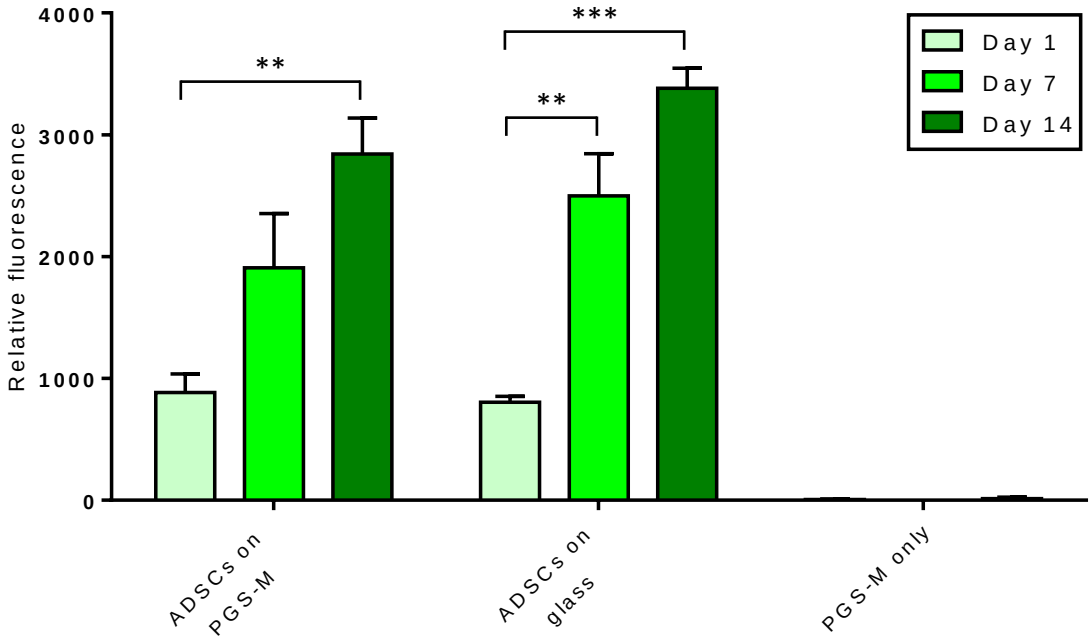

Figure 31. PicoGreen® assay for ADSC dsDNA on 30% Low M_w PGS-M surfaces after 1, 7 and 14 days in culture. Positive controls were ADSCs cultured on borosilicate glass (ADSCs on glass). Negative controls were unseeded PGS-M surfaces (PGS-M only). Error bars are SEM (n = 3).

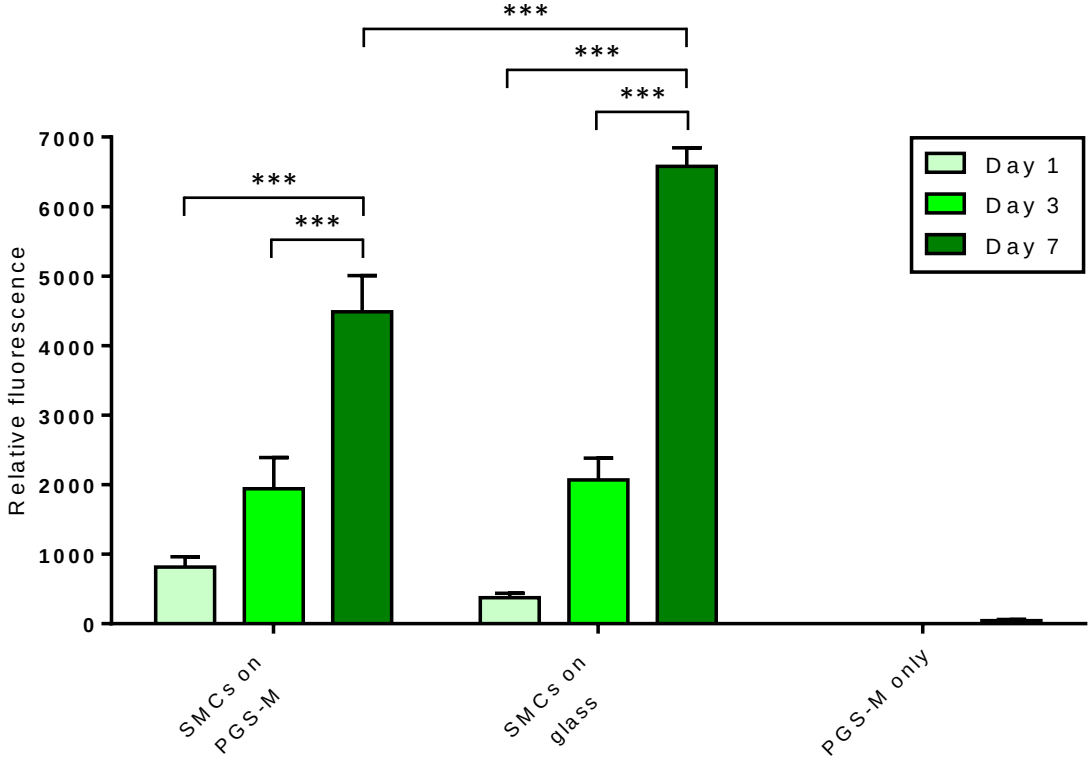

Figure 32. PicoGreen® assay for SMC dsDNA on 30% Low M_w PGS-M surfaces after 1, 3 and 7 days in culture. Positive controls were SMCs cultured on borosilicate glass (SMCs on glass). Negative controls were unseeded PGS-M surfaces (PGS-M only). Error bars are SEM (n = 3).

3.3.3 **Visualisation of cell proliferation on PGS-M surfaces**

To visualise the proliferation of fibroblasts, ADSCs and SMCs on PGS-M surfaces, the cells were cultured on polymer coated coverslips on which a central region was masked during cell seeding. This produced a cell free region which was observed to see how it was invaded by proliferating cells over time.

Figure 33 shows representative images of the proliferation of fibroblasts on PGS-M surfaces at 0, 2, 4 and 6 days after the masked area was uncovered. The masked area is free from cells initially, at day 0. Fibroblasts moved into the masked area from the edges over the time points, reaching its centre by day 6. The fibroblasts appeared to form confluent sheets of evenly distributed cells. They displayed a long thin, spindle-like, morphology. Negative controls (unseeded PGS-M coated coverslips) did not show the presence of fibroblasts at any time point.

Figure 34 shows representative images of the proliferation of ADSCs on PGS-M surfaces at 0, 4, 8 and 13 days after the masked area was uncovered. The masked area is free from cells initially, at day 0. ADSCs moved into the masked area from the edges over the time points. The cells reached the centre of the masked area by day 8 and completely covered it by day 13. The ADSCs presented a non-uniform distribution with areas of higher cell density clearly visible. Their morphology was spindle-like with multiple focal adhesions and long, thin processes. Negative controls (unseeded PGS-M coated coverslips) did not show the presence of ADSCs at any time point.

Figure 35 shows representative images of the proliferation of SMCs on PGS-M surfaces at 0, 2, 4 and 6 days after the masked area was uncovered. The masked area is free from cells initially, at day 0. SMCs moved into the masked area from the edges over the time points, having completely covered it by day 4. The SMCs were uniformly distributed and showed spindle-like morphology with multiple focal adhesions and long, thin processes. Negative controls (unseeded PGS-M coated coverslips) did not show the presence of SMCs at any time point.

The size of the masked area remaining at each time point during the culture of fibroblasts, ADSCs and SMCs on PGS-M surfaces was measured semi-quantitatively. Using software (ImageJ), the boundary between the masked area and the proliferating cells was traced and the area, in mm^2, of the section produced determined. The results for the culture of all three cell types are shown in Figure 36. SMCs appeared to proliferate at the fastest rate, completely covering the masked area after 4 days. The ADSCs demonstrated the slowest rate of proliferation, taking 13 days to cover the masked area.

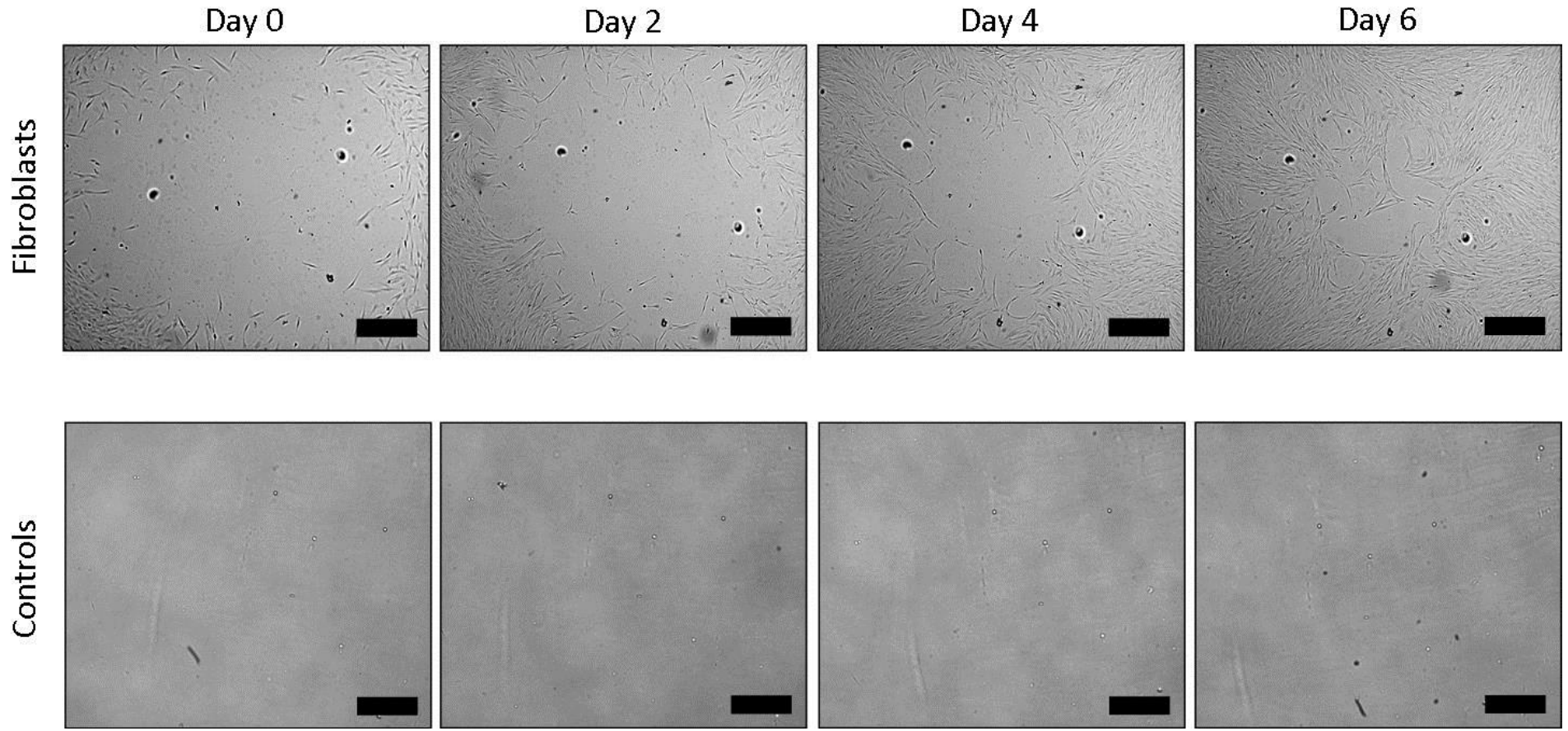

Figure 33. Representative images of the proliferation of fibroblasts on PGS-M surfaces. The cylindrical stainless steel masks were removed at Day 0, 24 hours after cells had been seeded. Fibroblasts proliferated into the masked areas over 6 days. Controls were masked and unseeded PGS-M surfaces. Scale bars are 500 µm.

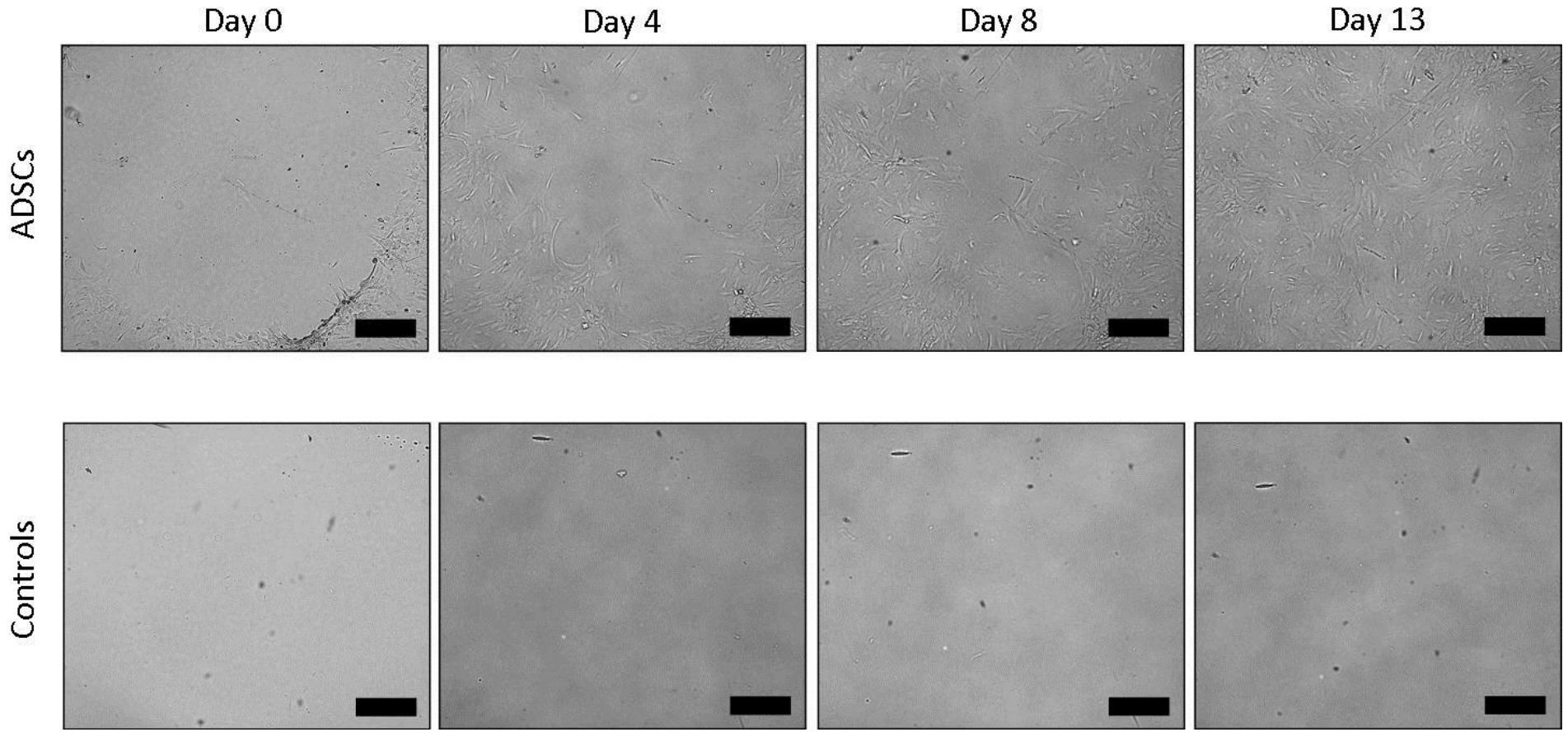

Figure 34. Representative images of the proliferation of ADSCs on PGS-M surfaces. The cylindrical stainless steel masks were removed at Day 0, 24 hours after cells had been seeded. ADSCs proliferated into the masked areas over 13 days. Controls were masked and unseeded PGS-M surfaces. Scale bars are 500 µm.

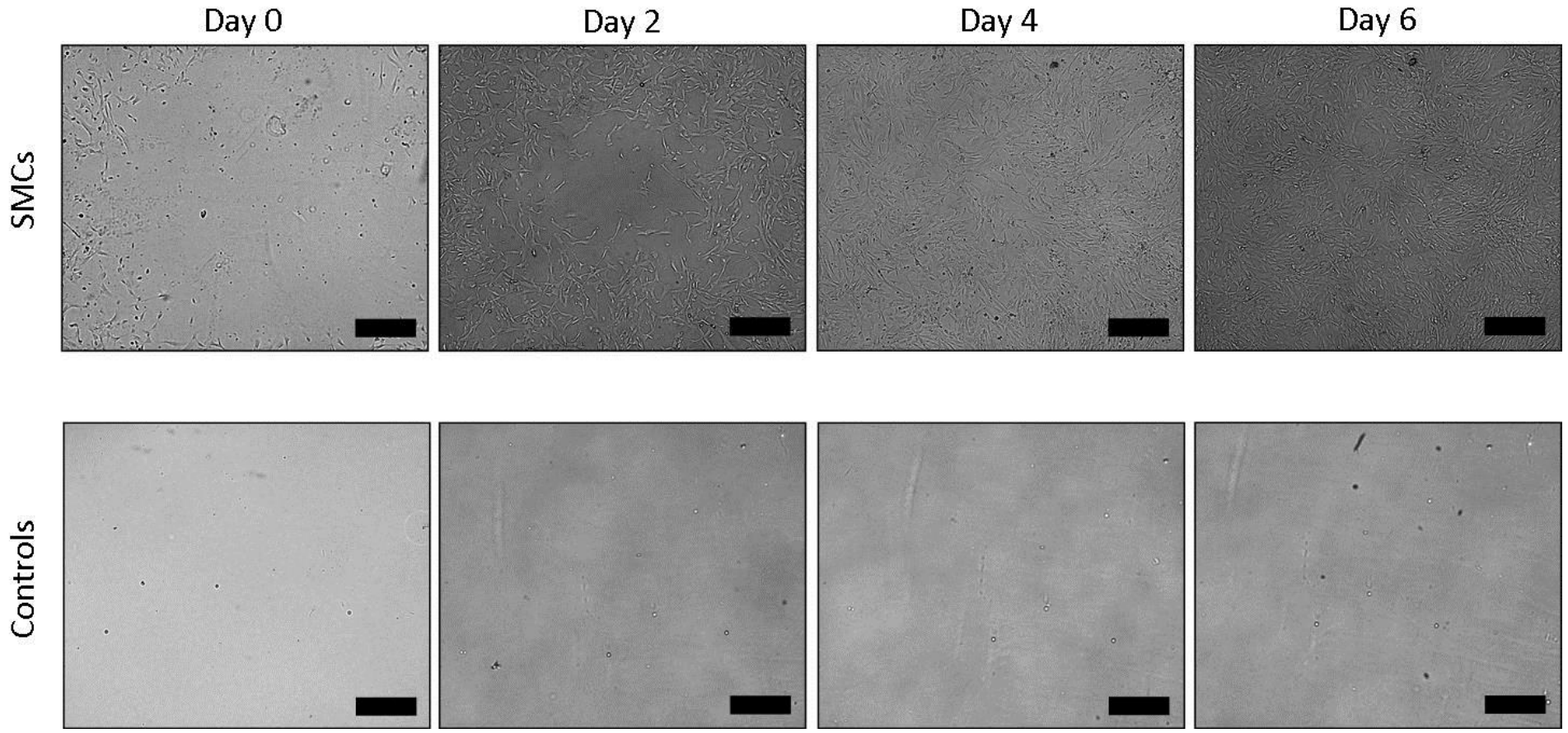

Figure 35. Representative images of the proliferation of SMCs on PGS-M surfaces. The cylindrical stainless steel masks were removed at Day 0, 24 hours after cells had been seeded. SMCs proliferated into the masked areas over 6 days. Controls were masked and unseeded PGS-M surfaces. Scale bars are 500 µm.

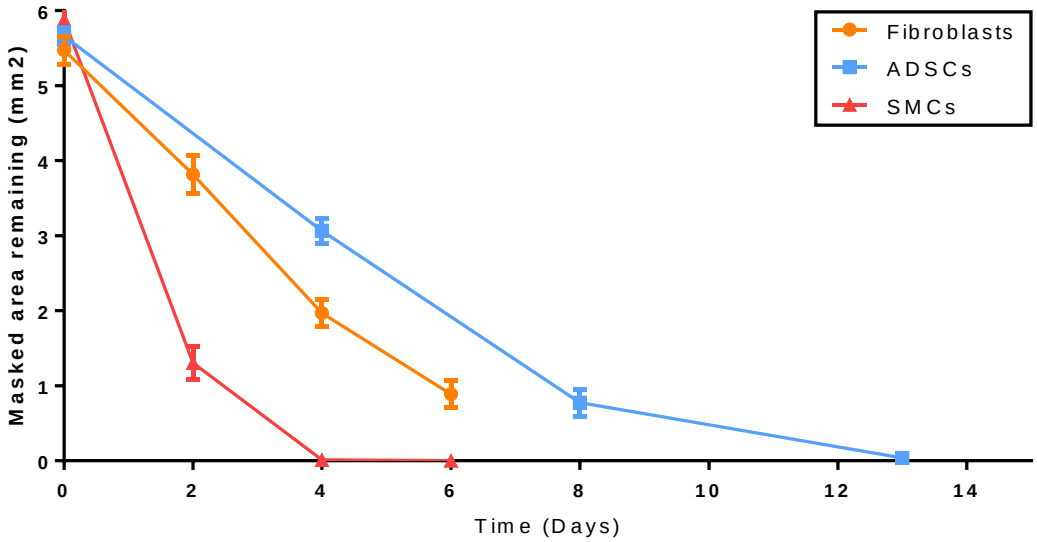

Figure 36. Semi-quantitative analysis of cell proliferation on PGS-M surfaces. In all three cell types, the size of the remaining masked area was determined from optical microscopy images, using software (ImageJ), at each time point. SMCs demonstrated the highest rate of proliferation, having completely covered the masked area by day 4. ADSCs proliferated at the slowest rate, taking 13 days to cover the masked area (n = 3).

3.3.4 **Immunofluorescence staining of SMCs for α-SMA**

Immunohistochemistry was used to assess the expression of α-SMA in SMCs cultured on PGS-M surfaces. α-SMA is a strong marker for contractile phenotype in SMCs. After 7 days in culture on PGS-M, SMCs stained positive for α-SMA (Figure 37). α-SMA was present throughout the cytoplasm. Sections of human umbilical cord artery were used as a positive control. These also stained strongly for α-SMA. Negative controls were blocked, but unstained, SMCs cultured on PGS-M surfaces and unseeded PGS-M surfaces with and without any staining treatment. Some background fluorescence was present in the blocked, but unstained, SMC cultures and the unseeded and stained PGS-M surfaces; however, this did not constitute a strong signal. Unseeded and unstained PGS-M surfaces displayed negligible fluorescence.

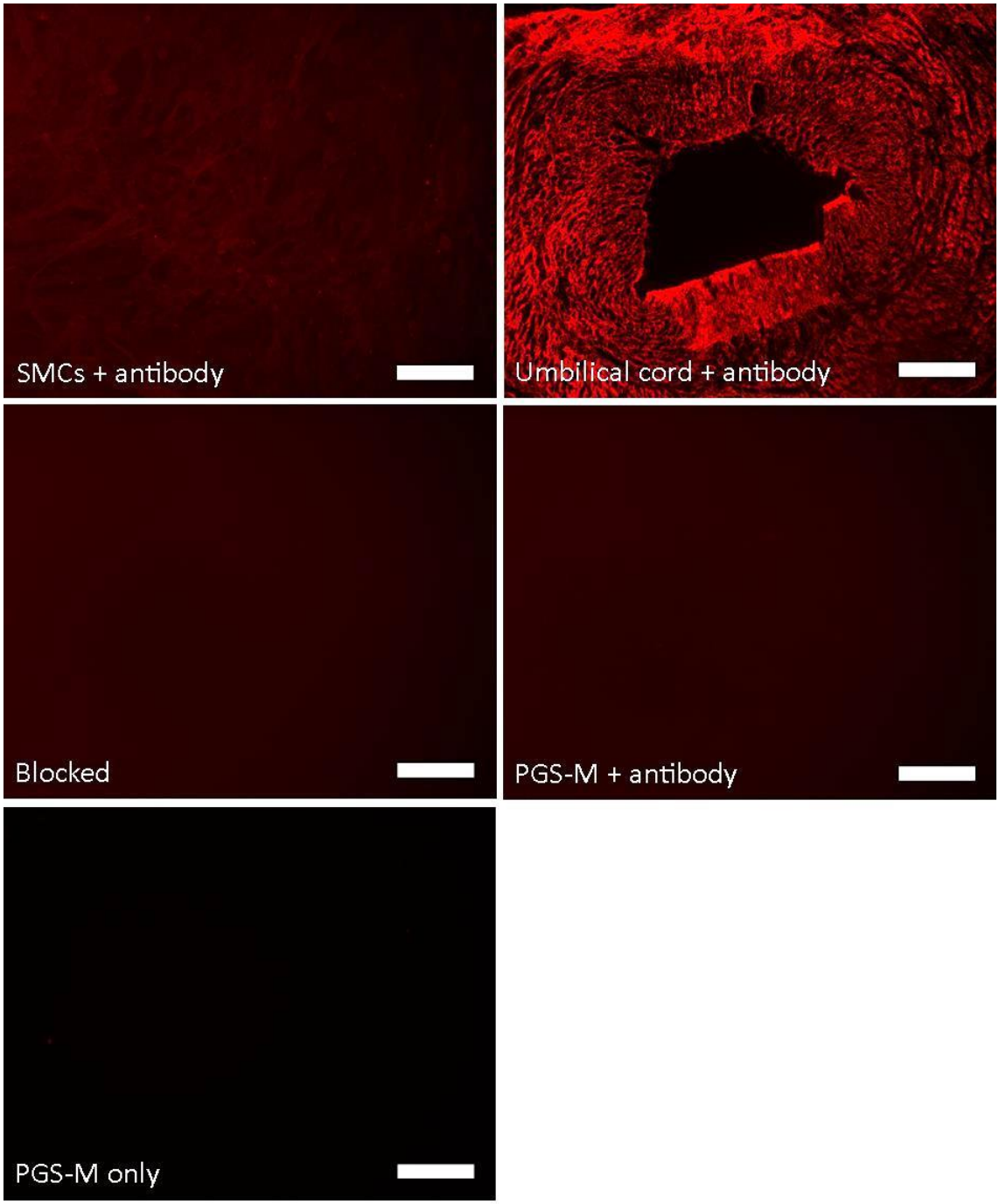

Figure 37. Representative images of SMCs cultured on PGS-M surfaces, for 7 days, stained positive for α-SMA (SMCs + antibody) (*n* = 3). Human umbilical cord arteries were stained as a positive control (Umbilical cord + antibody). Negative controls were blocked, but unstained, SMC cultures on PGS-M surfaces (Blocked) and unseeded PGS-M surfaces with and without any staining treatment (PGS-M + antibody and PGS-M only, respectively). All images were captured and processed using equal exposure and display settings. Scale bars are 200 µm.

3.3.5 **Immunofluorescence staining of SMCs for calponin**

Immunohistochemistry was also used to assess the expression of calponin in SMCs cultured on PGS-M surfaces. Calponin is another strong marker for contractile phenotype in SMCs. After 7 days in culture on PGS-M, SMCs stained positive for calponin (Figure 38). This was present throughout the cytoplasm. Sections of human umbilical cord artery were used as a positive control and also stained strongly for calponin. Negative controls were blocked, but unstained, SMCs cultured on PGS-M surfaces and unseeded PGS-M surfaces with and without any staining treatment. Some background fluorescence was present in the blocked, but unstained, SMC cultures and the unseeded and stained PGS-M surfaces; however, this did not constitute a strong signal. Unseeded and unstained PGS-M surfaces displayed negligible fluorescence.

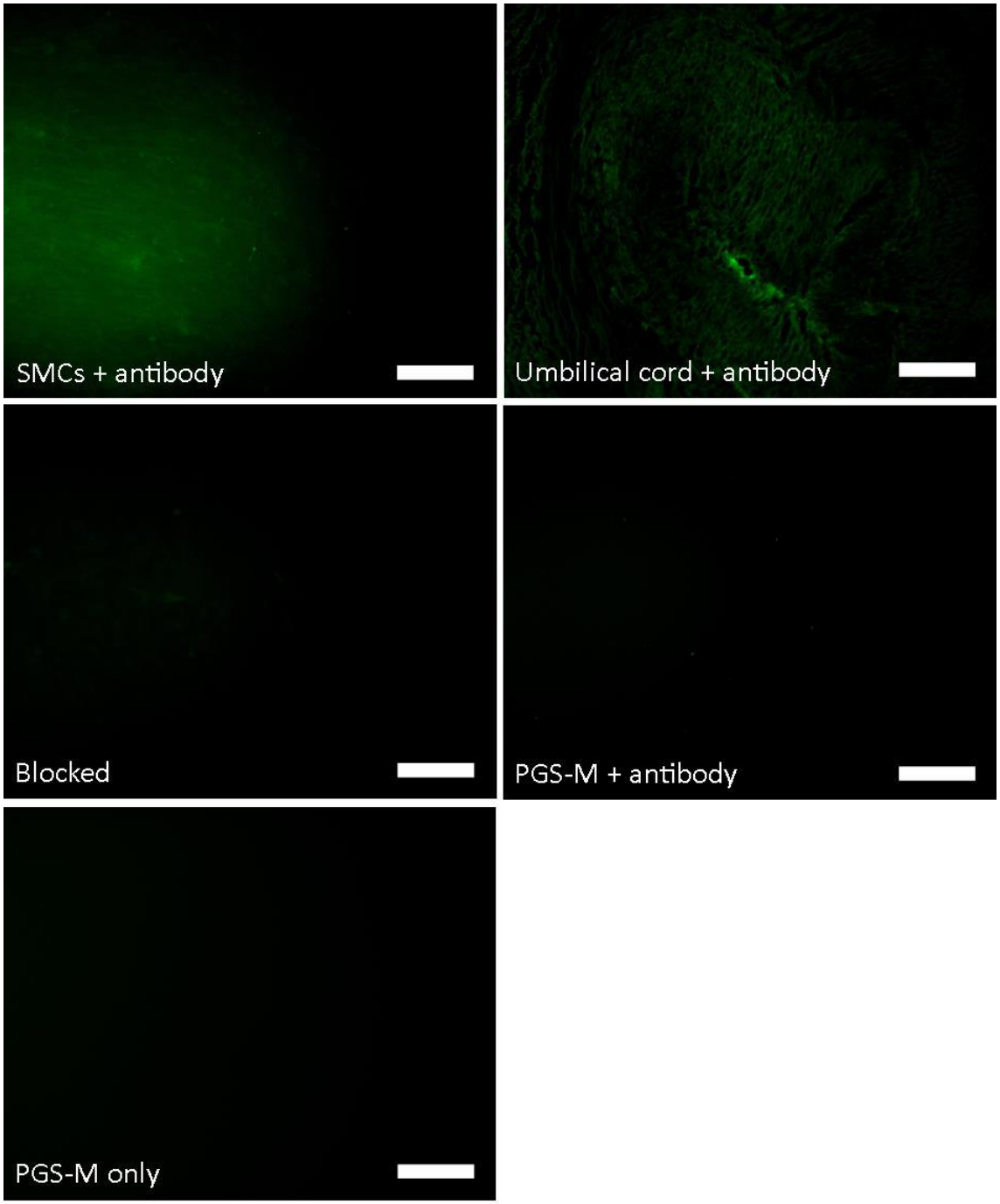

Figure 38. Representative images of SMCs cultured on PGS-M surfaces, for 7 days, stained positive for calponin (SMCs + antibody) (*n* = 3). Human umbilical cord arteries were stained as a positive control (Umbilical cord + antibody). Negative controls were blocked, but unstained, SMC cultures on PGS-M surfaces (Blocked) and unseeded PGS-M surfaces with and without any staining treatment (PGS-M + antibody and PGS-M only, respectively). All images were captured and processed using equal exposure and display settings. Scale bars are 200 µm.

3.4 **Discussion**

Human dermal fibroblasts, human ADSCs and human coronary artery SMCs were all cultured on 30% Low M_w PGS-M coated glass coverslips. The proliferation of these cells was examined by measuring the metabolic activity of the cells on each surface, using the RR assay; the quantity of dsDNA present on each surface, using the PicoGreen® DNA quantification assay, and by a visual examination of each surface, over several days.

The metabolic activity of fibroblast cultures on PGS-M surfaces appeared to increase over time. The RR assay showed a significant increase in the reduction of resazurin to resorufin, detected as a fluorescence signal at 635 nm, over 7 days. Viable cells maintain a reducing environment in their cytosol. Resazurin is able to pass through cell membranes and is reduced to its fluorescent form in the cytosol of viable cells. The increase in the quantity of resazurin reduced by the fibroblasts cultured on PGS-M surfaces demonstrates an increase in the metabolic activity of these cultures. This suggests an increase in the number of cells present; however, it is possible for other factors, such as changes in the growth medium over time and the advancing age of the cells to have an effect on their metabolic rate. To complement the results from the RR assay, the number of fibroblasts attached to the PGS-M coated coverslips was assessed by measuring the quantity of dsDNA present using the PicoGreen® DNA quantification assay. The results showed a significant increase in the quantity of dsDNA present in the fibroblast cultures between 1 and 7 days. Accept during mitosis, the quantity of dsDNA in a human somatic cell remains relatively constant, at ~3.2 x 10^8 base pairs (~3.5 pg).[322] Therefore an increase in dsDNA is associated with cell division and an increase in cell numbers. The PicoGreen® assay results were therefore evidence of the proliferation of fibroblasts on PGS-M surfaces over 7 days. This finding was supported by the results from the RR assay, with the increase in cell numbers producing an increase in the metabolic activity of each culture. The RR assay results also

demonstrated that the fibroblasts remained viable at day 7, which the PicoGreen® assay cannot determine.

The findings of the RR and PicoGreen® assays were further supported by visually examining fibroblast cultures on PGS-M surfaces over time. Observing initially cell-free regions of the PGS-M surfaces, produced by masking during cell seeding, demonstrated how the fibroblasts proliferated over time. The size of the initially masked areas reduced over 6 days, as the surrounding fibroblasts proliferated into them. The fibroblasts demonstrated characteristic morphology throughout the culture period, suggesting that they remained viable.[287,323]

Similar results are reported in the literature. Primary human foreskin fibroblasts demonstrated proliferation on PGS-A surfaces when cultured in a similar growth medium to that employed in the present study.[287] Cell proliferation was measured by counting the cells present in randomly selected areas of the culture surface over 12 days. The number of cells present increased from an initial ~2950 cells/cm^2 to ~15,000 cells/cm^2 over 6 days. This represented ~2.3 population doublings. This is comparable to the present study, where ~3.1 population doublings occurred over the same time period (~4500 cells/coverslip on day 1 rising to ~37,700 cells/coverslip on day 7). The primary foreskin fibroblasts cultured on PGS-A also maintained a fibroblastic morphology and this was similar to that demonstrated in control cultures on TCP.

Additionally, cultures of NIH 3T3 fibroblasts on thermocured PGS surfaces demonstrated an increase in metabolic activity over 6 days, when measured using the 3-(4,5-dimethylthiazol-2-yl)-2,5-diphenyltetrazolium bromide (MTT) assay, and this exceeded the performance of the associated positive controls (fibroblasts cultured on PLGA).[282] No quantification of the actual number of cells present in each culture was presented, however. The morphology of the fibroblasts remained normal throughout the culture period.

Similar to fibroblasts, the metabolic activity of ADSC cultures on PGS-M surfaces also appeared to increase over time. The RR assay showed a significant increase in the

reduction of resazurin over 14 days. The PicoGreen® assay results also showed a significant increase in the quantity of dsDNA present in the cultures over 14 days. These results coupled together demonstrate that ADSCs proliferated on PGS-M surfaces and remained viable for 14 days. Visual examination of initially masked regions of PGS-M surfaces seeded with ADSCs also demonstrated how the cells proliferated. The ADSC clearly colonised the initially cell-free region, completely covering it after 13 days. The cells also maintained a characteristic morphology throughout the culture period, suggesting that they remained stem-like and did not differentiate.[324–326]

In the literature, human stem cells have been shown to proliferate on PGS-A surfaces. Commercially available MSCs were cultured for up to 7 days on PGS-A and their metabolic activity was shown to increase, using the alamarBlue® assay. This coupled to a semi-quantitative assessment of the actin present on each culture surface suggested that the cells had indeed proliferated on the polymer and remained viable.[300]

In the culture of SMCs on PGS-M surfaces the results of the RR assay demonstrated a significant increase in the metabolic activity of the cultures over 7 days. This was consistent with the other two cell types examined. The PicoGreen® assay results also showed a significant increase in the quantity of dsDNA present in the cultures over the same time period. Taken together, these results show that SMCs proliferate when cultured on PGS-M surfaces and remain viable for up to 7 days. This finding is further supported by examining the images taken of the initially masked regions of PGS-M over the 6 day culture period. SMCs can be seen to proliferate and invade the initially masked area, completely covering it after 4 days. The cells maintained a characteristic SMC morphology, suggesting they remained viable.[189,327]

Additionally, staining for α-SMA and calponin showed that this continued to be expressed throughout the cytoskeleton of the SMCs cultured on PGS-M surfaces. Both α-SMA and calponin are considered strong markers for the SMC phenotype and therefore suggests that the phenotype was unchanged by culture on PGS-M.[328,329]

SMCs have also been cultured successfully on thermocured PGS surfaces. Primary baboon carotid artery SMCs were cultured on PGS for 6 days.[189] An assessment of their viability over the culture duration was conducted using the MTT assay. The results showed an increase in the metabolic activity present on each PGS surface culture. Imaging of the SMCs showed they possessed the characteristic spindle-shaped morphology and also stained positive for the SMC phenotypic marker α-SMA.

Examining the PicoGreen® assay results for the three different cell types cultured on PGS-M gives some insight into the different growth rates of the cells on the material. The Fibroblasts demonstrated the fastest growth rate, increasing from a population of 4,500 ± 200 cells on day 1 to 37,700 ± 3,000 cells by day 7. That equated to ~3.1 population doublings over a 6 day period. The SMCs proliferated from 8,500 ± 1,300 cells, on day 1, to 43,400 ± 1,600 cells, by day 7. That equated to ~2.4 population doublings over the 6 days. The ADSCs demonstrated the slowest growth rate. Between days 1 and 7 their population grew from 9,200 ± 1,300 to 18,400 ± 4,100 cells. That equated to only ~1 population doubling. The ADSCs demonstrated an even slower growth rate between days 7 and 14, only experiencing ~0.6 population doublings. This was likely due to their increased confluency by this time point reducing their rate of proliferation. Visually examining the rates at which the three different cell types colonised the initially masked areas of the PGS-M coated coverslips suggested that the SMCs had the fastest growth rate. These cells were able to completely cover the cell free region in just 4 days. However, the semi-quantitative nature of this examination of cell proliferation means that the actual number of cells is not quantified at each time point imaged and no account is made for the difference in size or packing density between the cell types. The fibroblasts appeared to pack more densely together than the SMCs. The size of the fibroblast population can therefore increase without covering the same area as an equivalent number of the SMCs would.

In both the RR and PicoGreen® assays, fibroblasts, ADSCs and SMCs were also cultured on borosilicate glass coverslips. These parallel cultures acted as positive controls.

When comparing the assay results for the three different cell types cultured on PGS-M with their corresponding positive controls, at each time point, interesting behaviours are demonstrated.

In the culture of fibroblasts, no significant differences were seen between the fibroblast cultures on PGS-M and those on glass, at any time point, in the RR assay. However, in the PicoGreen® assay, significant differences were seen between fibroblast cultures on PGS-M and glass at day 3 and day 7, with the glass surfaces supporting greater numbers of cells. There was also significant interaction between the type of culture surface and the time points assessed, suggesting the results across the time points were dependent on whether the fibroblasts were attached to PGS-M or glass. The SMCs showed similar results, with no significant differences between the PGS-M and glass surface cultures, at any time point, in the RR assay, but a significant difference between the two surfaces in the PicoGreen® assay at day 7, again with the glass surface supporting the greater number of cells.

Finally, unlike in the culture of fibroblasts and SMCs, no significant differences were seen between the ADSC cultures on PGS-M and the positive control cultures on glass, at any time point, in the RR assay or the PicoGreen® assay.

It might be expected that differences in the number of cells present on the culture surfaces, as measured by the PicoGreen® assay would equate to similar differences in the metabolic activity of the cultures, as measured by the RR assay. This does not appear to be the case. Regarding the fibroblasts, cultures for 7 days on PGS-M produced similar results to cultures for 3 days on glass, in the PicoGreen® assay, suggesting a similar number of fibroblasts were present on each surface at these time points. However, the RR assay results showed approximately double the metabolic activity in the PGS-M cultures when comparing these same time points. A similar effect is present in the ADSC cultures, with similar results in the PicoGreen® assay linked to far different results in the RR assay. In the SMC cultures, the PGS-M and glass surfaces appeared to support a significantly different number of cells, after 7 days in culture, in the PicoGreen® assay, but did not show significantly different metabolisms in the RR

assay. A comparison of the results from the RR and PicoGreen® assays is shown in Figure 39. Little correlation is visible between the results from the cultures on PGS-M and glass surfaces for the three different cell types.

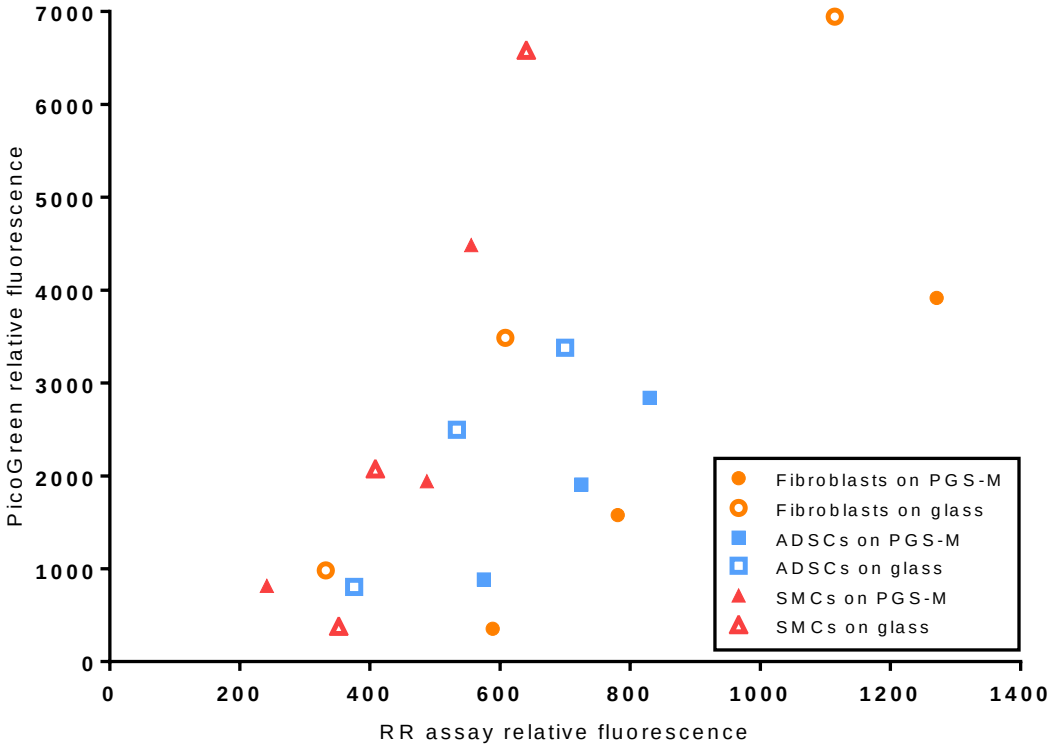

Figure 39. Comparison of the relative fluorescence values for the RR and PicoGreen® DNA quantification assays for Fibroblasts, ADSCs and SMCs cultured on PGS-M and glass surfaces over three time points. Values are mean averages.

Taken together, these results suggest that the metabolic activities of the different cells cultured may be substrate specific. The metabolic activities of fibroblasts and ADSCs may be increased when cultured on PGS-M compared to glass. This would account for the mismatch between the RR and PicoGreen® assay results, with a given number of cells attached to PGS-M able to reduce the same quantity of resazurin as a greater number of equivalent cells attached to glass. The metabolic activity of SMCs may also be different when cultured on PGS-M compared to glass, again accounting for the differences between the results of the RR and PicoGreen® assays across the time

points. Cell confluency may also play a part. As confluency increases, the metabolic activity of the cells may reduce leading to a mismatch between the RR assay and PicoGreen® assay results. This effect may also be cell specific and could be more pronounced in the fibroblasts and ADSCs compared to the SMCs, which would account for the results observed.

It is common in the literature to measure the metabolic activity of cell cultures on biomaterials, and associated positive controls, and to infer that increased activity, over time, is related to comparable increases in cell numbers.[189,282,300] The data presented here suggest that there may be subtle, but significant, differences between the metabolic activities of different cell types on different surfaces and that measuring this alone is not sufficient to draw conclusions about cell proliferation and to make direct comparisons between the performance of novel and known materials. Cell culture surfaces may affect the metabolism of different cells cultured on them due to a number of different factors, such as stiffness, hydrophilicity, topography and surface chemistry.[330–334] The cell surface interface has been identified as having an important influence on cell phenotype. In the present study, it appears that PGS-M has a cell specific effect on the metabolic activities of fibroblasts, ADSCs and SMCs. The reasons for these behaviours are somewhat unclear, however, and would warrant further investigation.

3.5 **Conclusions**

The findings of this chapter have demonstrated that flat surfaces of 30% Low M_w PGS-M are able to support the growth and proliferation of human dermal fibroblasts, human ADSCs and human coronary artery SMCs for several days in culture. Additionally, growth on PGS-M does not appear to alter the SMC phenotype.

Culture on PGS-M surfaces may also have effects on the metabolic activities of the three cell types. These effects may be subtle and cell specific.

Chapter 4 - Manufacture of PGS-M Scaffolds for use in TEVGs

4.1 Introduction

In the previous chapters, PGS-M was identified as a suitable material for producing scaffolds for TEVGs. This material demonstrated suitable mechanical properties, degradation rate and processing capabilities and also supported the *in vitro* culture of vascular cell types.

Porous scaffolds are utilised in tissue engineering to direct the development of tissues into defined 3D architectures. Scaffold porosity is required to support the culture of cells in 3D and allow sufficient diffusion of oxygen and nutrients through the developing tissue constructs. Various methods have been explored in the literature to generate porous scaffolds for use in tissue engineering. These include porogen leaching, freeze drying, emulsion templating, gas foaming and 3D printing.[281,335]

To generate PGS-M scaffolds suitable for use in the production of TEVGs a porogen leaching method was selected. In this method, the scaffold material is mixed with particles (porogens) and shaped into the macroscopic scaffold geometry. The porogens are then dissolved and removed using a solvent in which the scaffold material is insoluble, leaving voids (pores). Porogen leaching is simple, compatible with a variety of scaffold materials, and allows modulation of the sizes of the pores by selection of different sized porogen particles. Porogen leaching is also compatible with a variety of shaping methods which may be used to define the macroscopic shape of the scaffold. Porogen leaching has been employed successfully to produce a number of scaffolds for generating TEVGs.[86,94,286,336]

In this chapter, the development of methods of fabricating porous PGS-M scaffolds suitable for use in generating TEVGs is presented. Scaffolds were initially produced as simple disks to evaluate properties such as pore size, porosity, wettability and biocompatibility, before being produced as uniform tubes for use in TEVGs. Additionally, a proof-of-concept method for producing porous PGS-M scaffolds using a hybrid 3D printing and porogen leaching method is presented.

4.2 Materials and methods

In the following methods, all chemical reagents were obtained from Sigma Aldrich, UK unless otherwise stated. These reagents were measured and utilised in inert vessels.

4.2.1 Mould fabrication using polydimethylsiloxane

Moulds for producing various scaffold structures from PGS-M were fabricated from polydimethylsiloxane (further denoted as Silicone). The silicone was purchased as a kit (Sylgard® 186, Dow Corning, USA) containing an elastomer and curing agent. These were mixed thoroughly at a ratio of 10:1 and then cast into negatives of the required moulds, produced by 3D printing (Shapeways, USA). Air bubbles were removed from the cast silicone by exposing it to cyclic pressure changes, from atmospheric to vacuum at 1 µbar, in a vacuum oven, three times. The silicone was then cured at 60°C for 2 hours, before being removed from the negative moulds, yielding moulds suitable for producing scaffolds.

4.2.2 Fabrication of porous PGS-M disk scaffolds using porogen leaching

A porogen leaching method was used to produce porous PGS-M scaffolds suitable for tissue engineering. To produce disk shaped scaffolds, 30% Low M_w PGS-M prepolymer was prepared with photoinitiator as described in (2.2.5). The PGS-M was then mixed thoroughly with sucrose particles (Tate & Lyle, UK). These sucrose particles were prepared in 4 different size ranges using mechanical sieving (Endecotts Minor 200, UK): 100-200 µm (further denoted as Large), 50-100 µm (further denoted as Medium), a 1:1 blend of 50-100 µm and 38-50 µm (further denoted as Mixed) and 38-50 µm (further denoted as Small). The PGS-M and sucrose particles were mixed at different ratios (w/w) depending on the particle size range used (Table 8). These ratios were selected based on the handling characteristics of the PGS-M and sucrose mixtures and the final scaffolds, in an effort to determine the optimum ratios. Scaffolds produced form each

different mixture ratio were produced in triplicate. The PGS-M and sucrose mixture was packed into 13 mm diameter x 2 mm deep silicone moulds, produced as described in (4.2.1). The mixture was then photocured, to form composite disks, by exposure to UV light (100 W, OmniCure Series 1000 curing lamp) in a sealed container lined with reflective foil for 5 minutes. The partially cured PGS-M and sucrose composite disks were then removed from their moulds and turned upside-down before being photocured again, for a further 5 minutes.

The photocured PGS-M and sucrose composite disks were then washed in dH_2O for 4 days, to dissolve the sucrose particles and produce a porous scaffold structure, then methanol for 4 days, to remove any soluble PGS-M prepolymer and photoinitiator, and finally in dH_2O again, to remove any residual methanol. Washes of dH_2O and methanol were refreshed daily.

Table 8. PGS-M:sucrose particle ratios (w/w) used to produce porous disk scaffolds. Scaffolds produced form each different ratio were produced in triplicate.

Sucrose particle size range	**PGS-M:sucrose particle ratios (w/w) produced**
Large (100-200 µm)	1:1.8, 1:2, 1:2.2, 1:2.4, 1:2.6, 1:2.8, 1:3
Medium (50-100 µm)	1:2, 1:2.2, 1:2.4, 1:2.6, 1:2.8, 1:3, 1:3.2
Mixed (1:1 blend of 50-100 µm and 38-50 µm)	1:2, 1:2.2, 1:2.4, 1:2.6, 1:2.8, 1:3, 1:3.2, 1:3.4, 1:3.6, 1:3.8, 1:4
Small (38-50 µm)	1:2, 1:2.2, 1:2.4, 1:2.6, 1:2.8, 1:3, 1:3.2, 1:3.4, 1:3.6

4.2.3 **Sectioning and examination of porous PGS-M disk scaffolds**

Porous PGS-M disk scaffolds, produced as described in (4.2.2), were removed from dH_2O and then immersed in OCT compound (Tissue-Tek, Sakura, Japan) and frozen at -20°C. Frozen samples were mounted on stubs and cryosectioned (Lieca CM1860 UV), at -25°C, across planes perpendicular to their cross-sections, at a thickness of

5 µm. Sections were mounted on glass slides (Superfrost® Plus, Menzel-Gläser, Germany) and, after 24 hours, rinsed in dH_2O to remove the OCT compound.
The triplicate sections from each scaffold replicate were imaged using light microscopy (Motic B5 professional series).

4.2.4 **Examination of porous PGS-M disk scaffolds using SEM**

The structure of the porous PGS-M disk scaffolds was examined using SEM. Only scaffolds produced from the optimum PGS-M:sucrose particle ratios, determined in (4.2.2), were examined. These selected ratios were 1:2.8, 1:3, 1:3.8 and 1:3.4 for scaffolds produced from large, medium, mixed and small sucrose particles, respectively.
The 13 mm diameter scaffolds were removed from dH_2O and 4 mm diameter disks were cut out of each of them using a dissection punch. These 4 mm diameter disks were then frozen at -80°C for 24 hours before being freeze dried at room temperature and 1 µbar, in a vacuum oven, for 24 hours. The dry scaffolds were then affixed to aluminium stubs, using carbon tape, and coated with gold using a sputter coater (Edwards S150B). The gold coated scaffolds were then examined in a scanning electron microscope (Philips XL-20) at 13-15 kV.

4.2.5 **Determination of porous PGS-M disk scaffold pore sizes**

The sizes of the pores present in the different PGS-M disk scaffolds were semi-quantitatively assessed using SEM images, obtained as described in (4.2.4), and image analysis software (ImageJ, version 1.45s).
Firstly, a grid of 60 equally spaced crosses was overlaid onto each SEM image. Then, using the freehand selection tool, the outline of the pore within which each cross resided was traced to determine the pore area (Figure 40). Where a cross did not appear to reside within a pore, or the complete pore was not visible, the closest pore to the cross was selected. 3 images from triplicate scaffold samples were examined.

For each different scaffold type, the mean average pore area based on the image analysis was determined. This average was then multiplied by a statistical correction factor of 1.333 (pores assumed to be spherical) to adjust for the arbitrary, nonequatorial location of the sections. This generated the average pore area, in the equatorial plane, for each scaffold type examined. Additionally, the average pore diameter was also calculated, after the application of the correction factor.[337]

The results were statistically analysed using one-way ANOVA with Tukey multiple comparison analysis. $P<0.05$ was considered significant (*), $P<0.01$ was considered very significant (**) and $P<0.001$ was considered extremely significant (***).

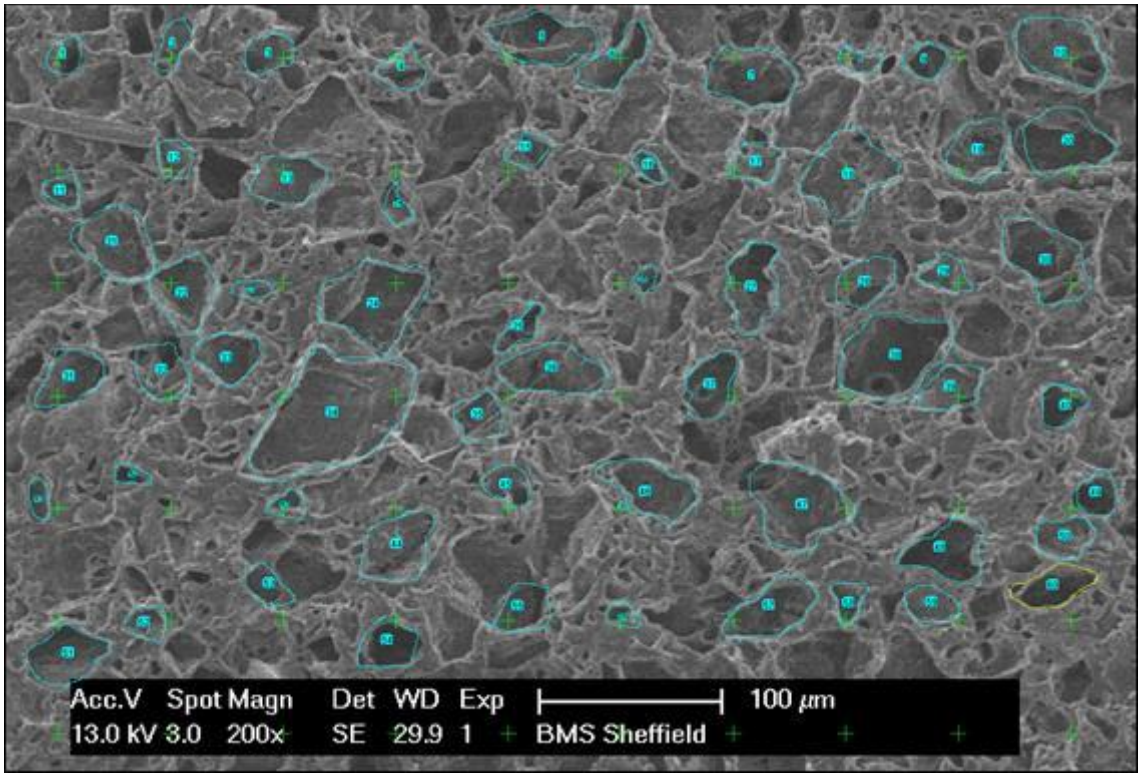

Figure 40. Representative image of the selection of pore outlines for the determination of average pore sizes in PGS-M disk scaffolds. A grid of equally spaced crosses (green) was overplayed onto SEM images of the scaffold surfaces. Pores were then selected (blue) based on their proximity to the crosses.

4.2.6 **Examination of the wettability of porous PGS-M disk scaffolds**

Porous PGS-M disk scaffolds, produced using different PGS-M:sucrose particle ratios, were prepared and freeze dried as described in (4.2.4). The PGS-M:sucrose particle ratios used were 1:2.8, 1:3, 1:3.8 and 1:3.4 for scaffolds produced from large, medium, mixed and small sucrose particles, respectively.

The wettability of the scaffolds was examined by applying 20 µl of PBS containing 0.5% (v/v) blue food dye (Tesco, UK) to the centre of each scaffold and observing the absorption behaviour after 5 minutes, 30 minutes, 1 hour, 1 hour 30 minutes, 2 hours and 2 hours 30 minutes. Scaffold types were examined in triplicate. Additionally, 20 µl of dyed PBS was also applied to 3 glass coverslips and examined in parallel with the PGS-M scaffolds to control for evaporation. The mass of the PBS on the coverslips was measured at the start and end of the experiment.

4.2.7 **Determination of the porosity of PGS-M disk scaffolds using helium pycnometry**

The porosity of the PGS-M disk scaffolds produced from the different size ranges of sucrose particles was determined using a helium pycnometer (AccuPyc 1340, Micromeritics, USA). Scaffolds were produced as described in (4.2.2). For each different sucrose particle size range, scaffolds were produced from two different ratios of PGS-M:sucrose particles. These ratios were 1:2.6 and 1:2.8, 1:2.8 and 1:3, 1:3.6 and 1:3.8, and 1:3.2 and 1:3.4 for scaffolds produced from large, medium, mixed and small sucrose particles, respectively. The 13 mm diameter disk scaffolds were removed from dH_2O and 4 mm diameter disks were cut out of each of them using a dissection punch. These 4 mm diameter disks were then frozen at -80°C for 24 hours before being freeze dried at room temperature and 1 µbar, in a vacuum oven, for 24 hours. The diameters and heights of the dry scaffolds were then measured using digital callipers. These dimensions were used to define the macroscopic volume of the scaffolds, ignoring the porosity. The scaffolds were then placed in the pycnometer using a 0.1 cm^3 chamber

insert. The chamber was pressurised with helium, at 19,500 psi, and the volume occupied by the scaffolds determined. This was the true volume of the scaffolds, including the porosity. Finally, the true volume:macroscopic volume ratio was calculated to determine the scaffold porosity.

Nine scaffolds from each PGS-M:sucrose particle ratio were examined. The results were statistically analysed using one-way ANOVA with Tukey multiple comparison analysis. $P<0.05$ was considered significant (*), $P<0.01$ was considered very significant (**) and $P<0.001$ was considered extremely significant (***).

4.2.8 **Characterisation of porous PGS-M disk scaffolds by Raman spectroscopy**

PGS-M disk scaffolds were examined by Raman spectroscopy (Thermo Scientific Nicolet DXR with 532 nm laser at 2 cm^{-1} resolution) to determine the effectiveness of the sucrose removal process.

PGS-M disk scaffolds were produced using mixed sucrose particles at a PGS-M:sucrose particle ratio of 1:3.8, as described in (4.2.2). These scaffolds were referred to as Washed. Additional scaffolds were also produced, in a similar manner, but without being washed in dH_2O or methanol following photocuring to allow complete retention of the sucrose. These scaffolds were referred to as Unwashed.

The washed and unwashed scaffolds were cut longitudinally and their interiors were analysed by Raman spectroscopy, between Raman shifts of 4000 cm^{-1} and 400 cm^{-1}, using a 532 nm laser at 10 mW. The exposure time was 10 seconds, with 20 exposures taken per sample, and the spectrograph aperture set at 50 µm. Fluorescence correction was also applied.

In addition to the scaffolds, mixed sucrose particles alone were also examined, as a material control.

4.2.9 **Culture of SMCs on porous PGS-M disk scaffolds**

Porous PGS-M disk scaffolds of 13 mm diameter and 2 mm depth were produced as described in (4.2.2), using mixed sucrose particles and a PGS-M:sucrose particle ratio of 1:3.8. These scaffolds were removed from dH_2O and 4 mm diameter disks were cut out of each of them using a dissection punch. These 4 mm diameter disk scaffolds were then placed in autoclave bags and sterilised by autoclave at 121°C for 30 minutes. The sterile scaffolds were placed individually in the wells of 12-well tissue culture plates (Greiner bio-one, Germany) and 2 ml of SMC growth medium added to each well. The scaffolds were placed in an incubator at 37°C and 5% CO_2, for 24 hours, in preparation for cell seeding.

Human coronary artery SMCs (Promocell, Germany) were expanded on TCP in flasks, as described in (3.2.5). SMCs between passage 8 and 10 were harvested using trypsin (0.025%)/EDTA (0.01%) solution at 0.067 ml/cm^2 of culture area. This was quenched after 5 minutes with an equal volume of trypsin inhibitor (PromoCell, Germany) and the cell suspension centrifuged at 1,200 rpm for 4 minutes (Hettich Zentrifugen Rotofix 32A with 131 mm rotor radius) before being resuspended in SMC growth medium at 12.6 x 10^6 cells/ml.

The scaffolds were removed from the incubator and 20 µl of the cell suspension was applied to each. This equated to a cell seeding density of 2 x 10^6 cells/cm^2 of scaffold surface. The cell seeding was performed using modified pipette tips. These tips had their ends removed prior to sterilisation, using scissors, so as to widen the end orifice to ~3 mm. During SMC seeding, the modified pipette tips were pressed down, concentrically, over the PGS-M disk scaffolds while the cell suspension was delivered. This was intended to deliver cells into the scaffold interiors. The seeded scaffolds were returned to the incubator for 6 hours, to allow for cell attachment, and then placed in fresh wells with 2 ml of SMC growth medium. The scaffolds were cultured for a further 18 hours (producing a culture period of 1 day post seeding) or 7 days. Unseeded scaffolds were also incubated, in parallel with the seeded scaffolds, as negative controls. The growth medium was replaced every other day.

4.2.10 **Resazurin reduction assay for SMC viability on porous PGS-M disk scaffolds**

Porous PGS-M disk scaffolds seeded with SMCs, or left unseeded as controls, and cultured as described in (4.2.9) were examined for metabolic activity, and thus cell viability, using the RR assay. 0.0251% (w/v) resazurin sodium salt was dissolved in dH_2O. The solution was filter sterilised using a 0.22 µm filter and mixed 10% (v/v) with the SMC growth medium. At the end of the culture periods, the SMC seeded scaffolds and unseeded control scaffolds were removed from the incubator and the growth medium removed from their wells and replaced with 2 ml of the resazurin-containing growth medium. The scaffolds were then returned to the incubator. An equivalent sample of the resazurin-containing growth medium was also incubated, in parallel, for use as a blank. After 4 hours, the scaffolds were removed from the incubator and 200 µl of solution was extracted from each well, in triplicate, and placed in the wells of a 96-well plate. This plate was then read using a fluorescence plate reader (Bio-tek instruments FLX800) at 540 nm excitation and 635 nm emission, with the reading from the blank subtracted. Each time point was examined twice, with 4 replicate scaffold samples.

The results were statistically analysed using two-way ANOVA with Tukey multiple comparisons analysis. $P<0.05$ was considered significant (*), $P<0.01$ was considered very significant (**) and $P<0.001$ was considered extremely significant (***).

4.2.11 **Haematoxylin and Eosin staining of sections of PGS-M disk scaffolds seeded with SMCs**

Porous PGS-M disk scaffolds seeded with SMCs, or left unseeded as controls, and cultured as described in (4.2.9) were examined using Haematoxylin and Eosin (H&E) staining to examine the distribution of the cells within the scaffolds.

At the end of the culture periods, the seeded scaffolds and unseeded controls were rinsed with PBS, three times, and then fixed with 3.7 % formaldehyde (methanol free) for 24 hours. After this, they were rinsed with PBS, three times, and then immersed in

OCT compound (Tissue-Tek, Sakura, Japan) and frozen at -20°C. Frozen samples were mounted on stubs and sectioned as described in (4.2.3). Following the removal of the OCT compound, the sections were immersed in Modified Harris haematoxylin solution for 90 seconds and then rinsed in H_2O for 4 minutes. They were then immersed in eosin Y solution for 5 minutes before being rinsed with H_2O, twice, followed by 70% industrial methylated spirit (IMS) (Fisher Scientific, UK) solution in H_2O, then IMS and then Xylene. Samples were then coated with DPX mountant, covered with glass coverslips and allowed to dry for 12 hours. The sections were imaged using light microscopy (Motic B5 professional series). Each time point was examined twice, with triplicate scaffold samples. Staining was conducted on 4 sections taken from each scaffold sample.

4.2.12 **Examination of PGS-M disk scaffolds seeded with SMCs using SEM**

Porous PGS-M disk scaffolds seeded with SMCs, or left unseeded as controls, and cultured for 7 days, as described in (4.2.9), were examined using SEM. At the end of the culture periods, the seeded scaffolds and unseeded controls were rinsed with PBS, three times, and then fixed with 3.7 % formaldehyde (methanol free) for 24 hours. After this, they were rinsed with PBS, three times, and then dehydrated by the addition of a series of ethanol solutions (v/v) in dH_2O for 15 minutes. The order of the ethanol solutions was 50%, 70%, 90% and 100%. The dehydrated scaffolds were then air dried for 7 days. Once dry, the scaffolds were affixed to aluminium stubs, using carbon tape, and gold coated and examined by SEM as described in (4.2.4).

4.2.13 **Fabrication of porous tubular PGS-M scaffolds using porogen leaching**

Porous tubular PGS-M scaffolds were produced for use in the culture of TEVGs. 30% Low M_w PGS-M was used in all cases. In total, 6 different methods were examined. In method i, a silicone mould was used to shape the outer surface of the scaffolds. In

methods ii-vi, 1 ml polypropylene syringes (Terumo, USA) with their ends removed were used to shape the outer surface of the scaffolds.

Method i) PGS-M prepolymer was mixed thoroughly with sucrose particles and the mixture packed around a 3 mm diameter x 80 mm length stainless steel (316L medical grade) rod (Figure 41). The mixture and rod were then shaped by insertion into a silicone mould with a semi-cylindrical cavity, produced as described in (4.2.1). The mixture was then photocured, in the mould, by exposure to UV light (100 W, OmniCure Series 1000 curing lamp) in a sealed container lined with reflective foil for 5 minutes. The partially cured PGS-M and sucrose composite was then removed from the mould, rotated 180° about its central axis, and photocured again, for a further 5 minutes.

Method ii) PGS-M prepolymer was mixed thoroughly with sucrose particles and the mixture packed around a 3 mm diameter x 40 mm length polyvinyl acetate (PVA) rod, inside a 1 ml syringe (Figure 41). The PVA rod was maintained concentrically inside the syringe and the syringe plunger retracted incrementally to allow the addition of the PGS-M and sucrose mixture. Once the PVA rod was fully contained within the syringe and surrounded by PGS-M and sucrose mixture, the syringe plunger was depressed and the contents, now referred to as a compact, was extruded out onto a 5 mm deep layer of sucrose particles. The compact, on top of the sucrose particle layer, was then photocured as described in method i, with 180° rotation about its central axis between UV light exposures.

Method iii) PGS-M prepolymer was mixed thoroughly with sucrose particles and the mixture packed into a 1 ml syringe (Figure 42). The syringe plunger was retracted incrementally to allow the addition of the PGS-M and sucrose mixture. Once the syringe was half full, a 3 mm diameter core was cut out from the compact contained within the syringe, using an ultra-thin walled stainless steel tube as a corer. The corer was aligned concentrically with the syringe using a 3D printed guide (Shapeways, USA).

With the core removed, the compact now took the form of tube contained within the syringe. The tubular compact was extruded out of the syringe, by depressing the plunger, onto a 5 mm deep layer of sucrose particles. The compact, on top of the sucrose particle layer, was then photocured as described in method i, with 180° rotation about its central axis between UV light exposures.

Method iv) A tubular compact of PGS-M prepolymer and sucrose particles was prepared within a 1 ml syringe as described in method iii, however, the compact was not extruded out of the syringe and instead was photocured while retained within it (Figure 42). The photocuring process was as described in method i, with 180° rotation of the compact about its axis of rotation between UV light exposures. Once photocuring was complete, the compact was extruded out of the syringe by depressing the plunger.

Method v) A tubular compact of PGS-M prepolymer and sucrose particles was prepared within a 1 ml syringe as described in method iii, however, before being extruded out of the syringe, the cavity left by the removal of the core of the compact was packed with sucrose particles (Figure 43). The tubular compact, with sucrose-packed internal cavity was extrude and photocured as described in method iii)

Method vi) PGS-M prepolymer was mixed thoroughly with sucrose particles and the mixture packed into a 1 ml syringe (Figure 43). The syringe plunger was retracted incrementally to allow the addition of the PGS-M and sucrose mixture. Once the syringe was half full, the cylindrical compact was extruded out, by depressing the plunger, onto a 5 mm deep layer of sucrose particles. The compact, on top of the sucrose particle layer, was then photocured as described in method i, with 180° rotation about its central axis between UV light exposures. Once photocured, the cylindrical compact was reinserted into the syringe and the centre cut out using a pillar drill with a 3 mm twist drill bit. The compact, now in the form of a tube, was then extruded out of the syringe again.

With the exception of method i, all tubular scaffolds were produced using mixed size sucrose particles and a PGS-M:sucrose particle ratio of 1:3.8. In method i, large size sucrose particles were used at a PGS-M:sucrose particle ratio of 1:2.2.

Following fabrication, all photocured scaffold compacts were washed in dH_2O for 4 days, to dissolve the sucrose particles and produce a porous scaffold structure, then methanol for 4 days, to remove any soluble PGS-M prepolymer and photoinitiator, and finally in dH_2O again, to remove any residual methanol. Washes of dH_2O and methanol were refreshed daily. In method i, the stainless steel core was removed from the scaffolds prior to washing in methanol. In method ii, the initial 4 washes in dH_2O were conducted with the dH_2O at 80°C to dissolve the PVA core from the scaffold compact. In each method, scaffolds were produced in triplicate.

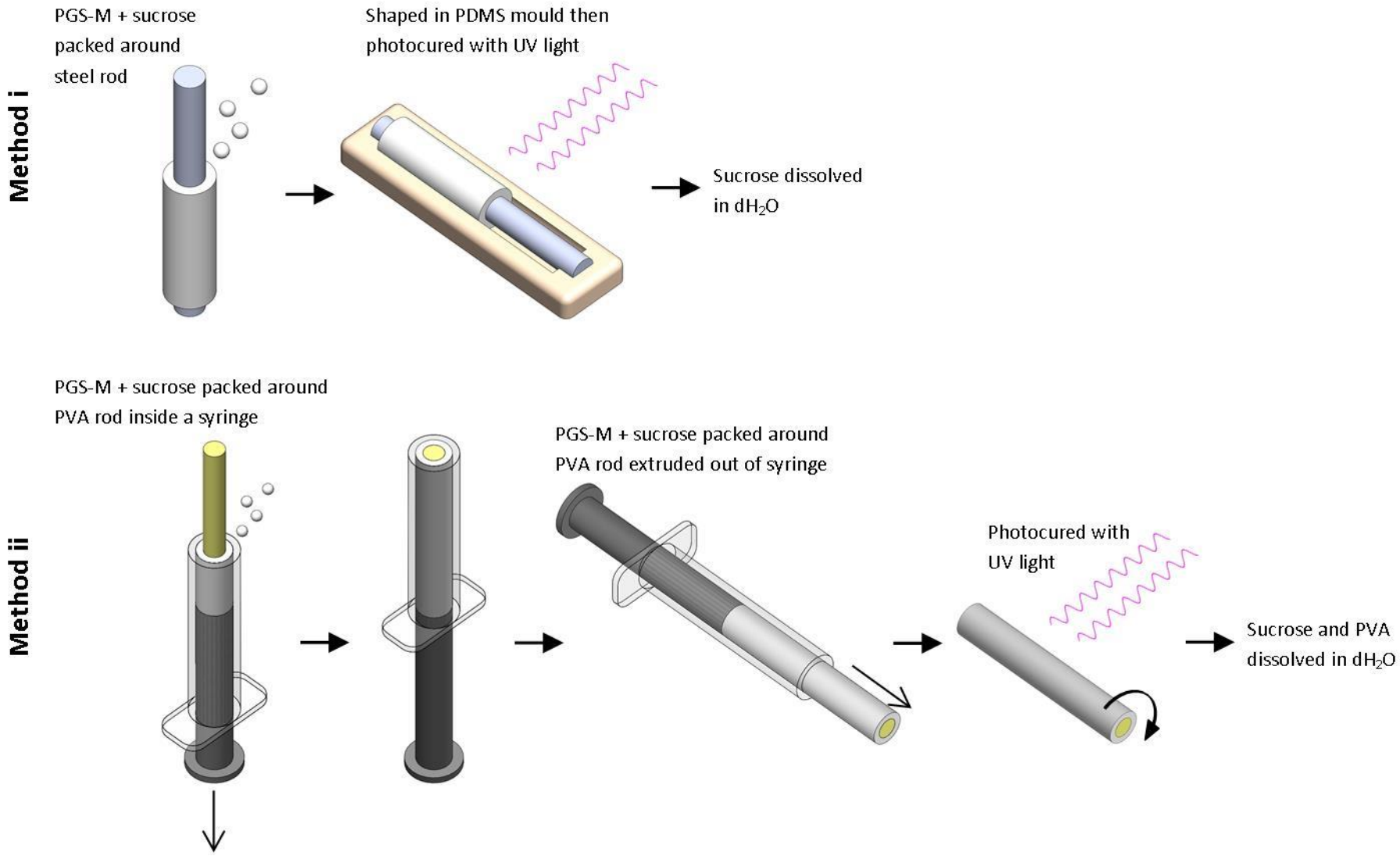

Figure 41. Fabrication of porous tubular PGS-M scaffolds using methods i and ii.

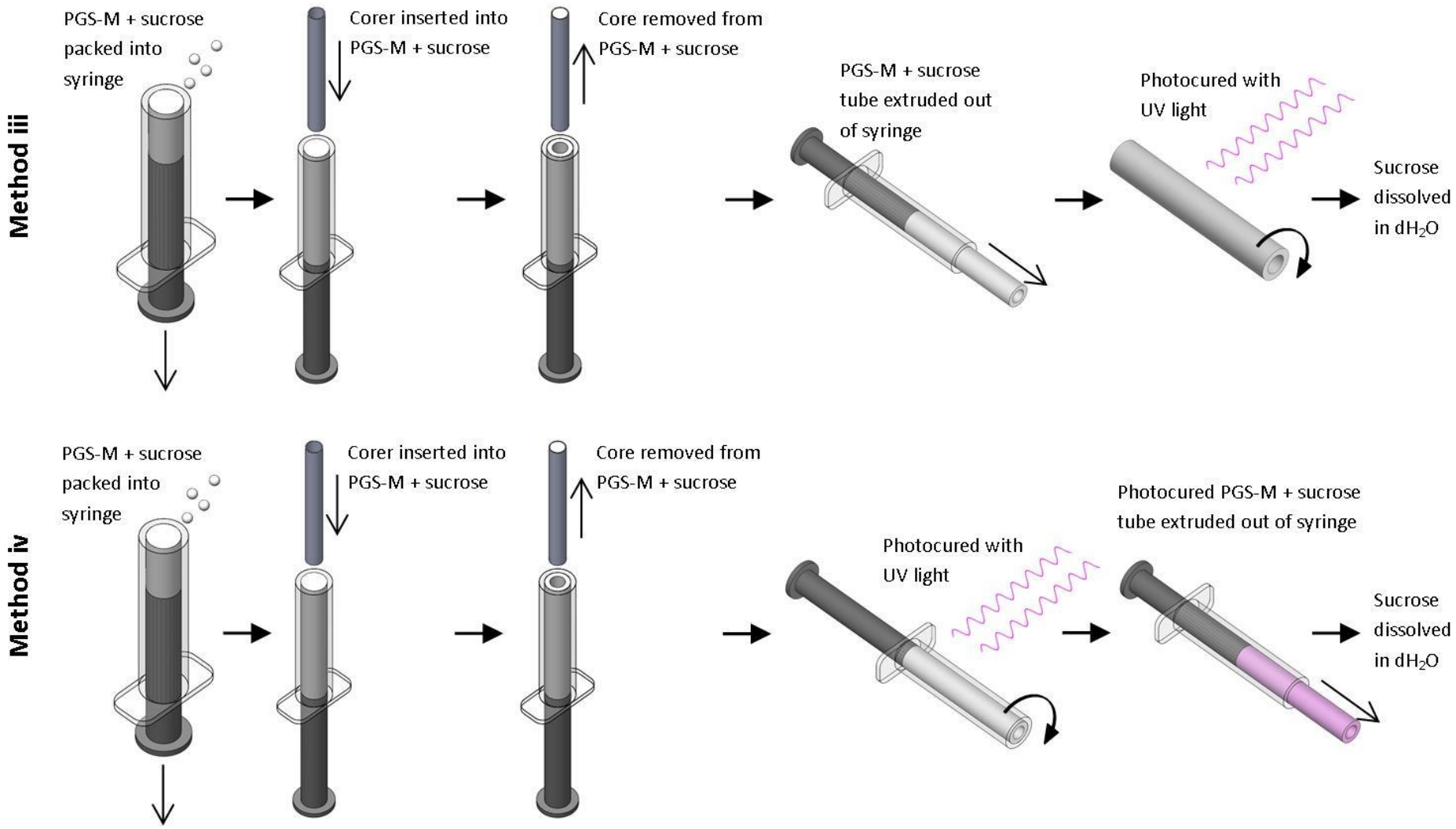

Figure 42. Fabrication of porous tubular PGS-M scaffolds using methods iii and iv.

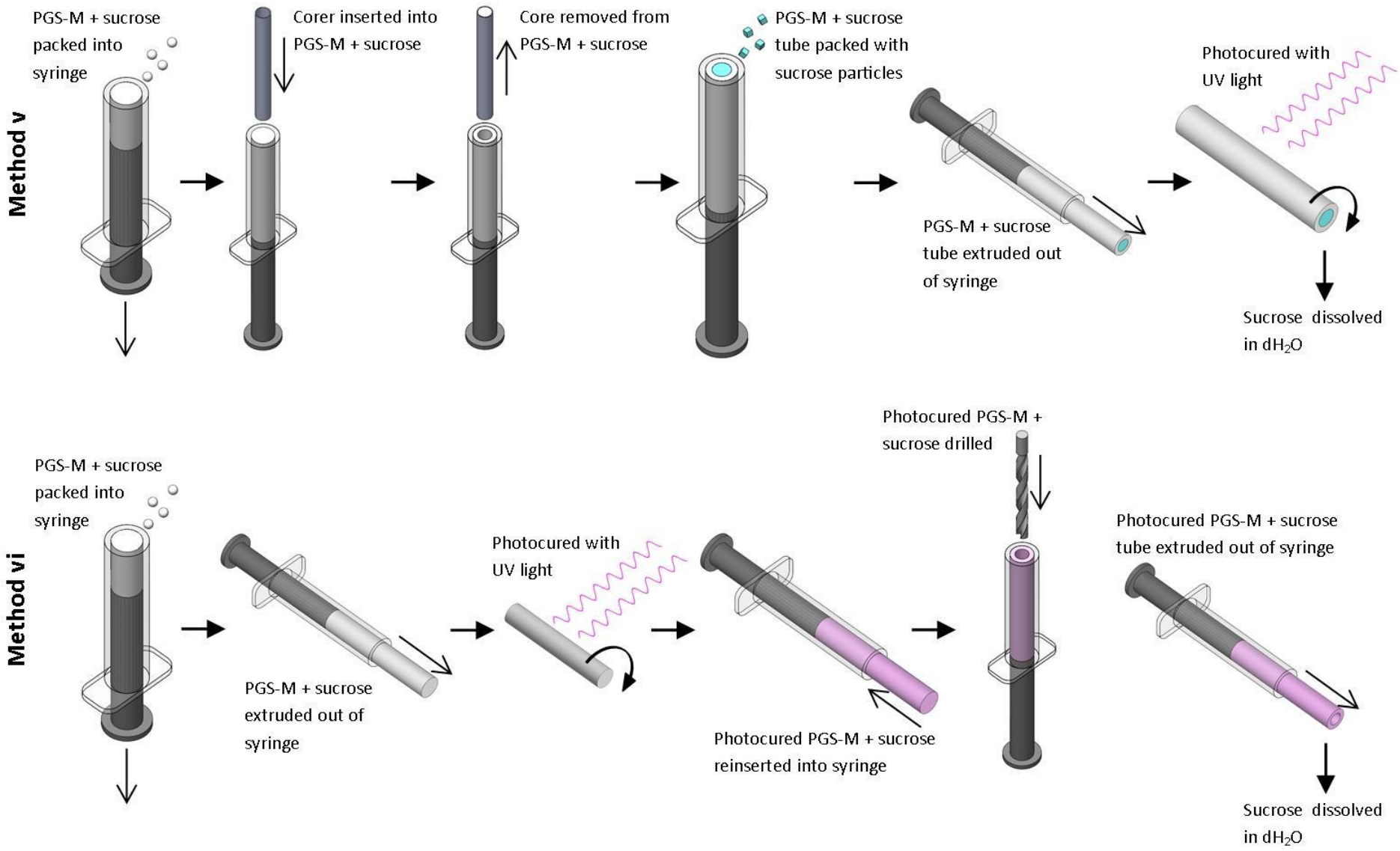

Figure 43. Fabrication of porous tubular PGS-M scaffolds using methods v and vi.

4.2.14 **Examination of porous tubular PGS-M scaffolds using scanning electron microscopy**

Porous tubular PGS-M scaffolds were prepared using the methods described in (4.2.13). The scaffolds were removed from dH_2O and sectioned axially and longitudinally, using a scalpel, before being frozen at -80°C for 24 hours and then freeze dried at room temperature and 1 µbar, in a vacuum oven, for 24 hours. The dry scaffolds were then affixed to aluminium stubs, using carbon tape, and coated with gold using a sputter coater (Edwards S150B). The gold coated scaffolds were then examined in a scanning electron microscope (Philips XL-20) at 15-20 kV.

4.2.15 **Manufacture of porous PGS-M scaffolds using a hybrid additive manufacturing and porogen leaching method**

PGS-M scaffolds were produced using an additive manufacturing approach similar to selective laser sintering (SLS) (Figure 44). A 50 ml polypropylene syringe (Terumo, USA) with the end removed acted as a build chamber for the scaffold. With the plunger positioned 3 mm from the open end, the syringe build chamber was filled with a mixture of PGS-M prepolymer and sucrose particles. The mixture was produced using large size sucrose particles at a PGS-M:sucrose particle ratio of 1:2.8. The PGS-M and sucrose mixture was packed flush with the open end of the syringe build chamber and then a cap placed over this. This cap had an 8 mm diameter hole cut into it, offset 4 mm from the cap's centre. The capped syringe build chamber was then exposed to UV light (100 W, OmniCure Series 1000 curing lamp) in a sealed container lined with reflective foil, for 5 minutes. The light was directed down into the hole in the cap placed over the syringe build chamber. The cap ensured that only the area of the PGS-M and sucrose mixture under the hole was exposed to UV light (selective photocuring). Following UV exposure, the cap was removed from the syringe build chamber and the plunger retracted 1 mm. Additional PGS-M and sucrose mixture was then added to the syringe build chamber until this was flush with the end again. The

cap was then reapplied, but with the hole position rotated 10° clockwise from the previous position. The capped syringe build chamber was then exposed to UV light again, as previously. The process of adding 1 mm layers of PGS-M and sucrose mixture to the build chamber and selectively photocuring part of these by rotating the hole in the syringe build chamber cap was repeated until the cap had completed a full rotation and the hole was returned to the first position. The contents of the syringe build chamber were then extruded into 100 ml of methanol, by depressing the plunger. The methanol dissolved the PGS-M prepolymer that had not been photocured, leaving behind the photocured PGS-M with included sucrose particles as a 3D printed construct. The 3D printed construct (a spiral of disks) was then washed in dH_2O for 4 days, to dissolve the sucrose particles and produce a porous scaffold structure, then methanol for 4 days, to remove any remaining soluble PGS-M prepolymer and photoinitiator, and finally in dH_2O again, to remove any residual methanol. Washes of dH_2O and methanol were refreshed daily.

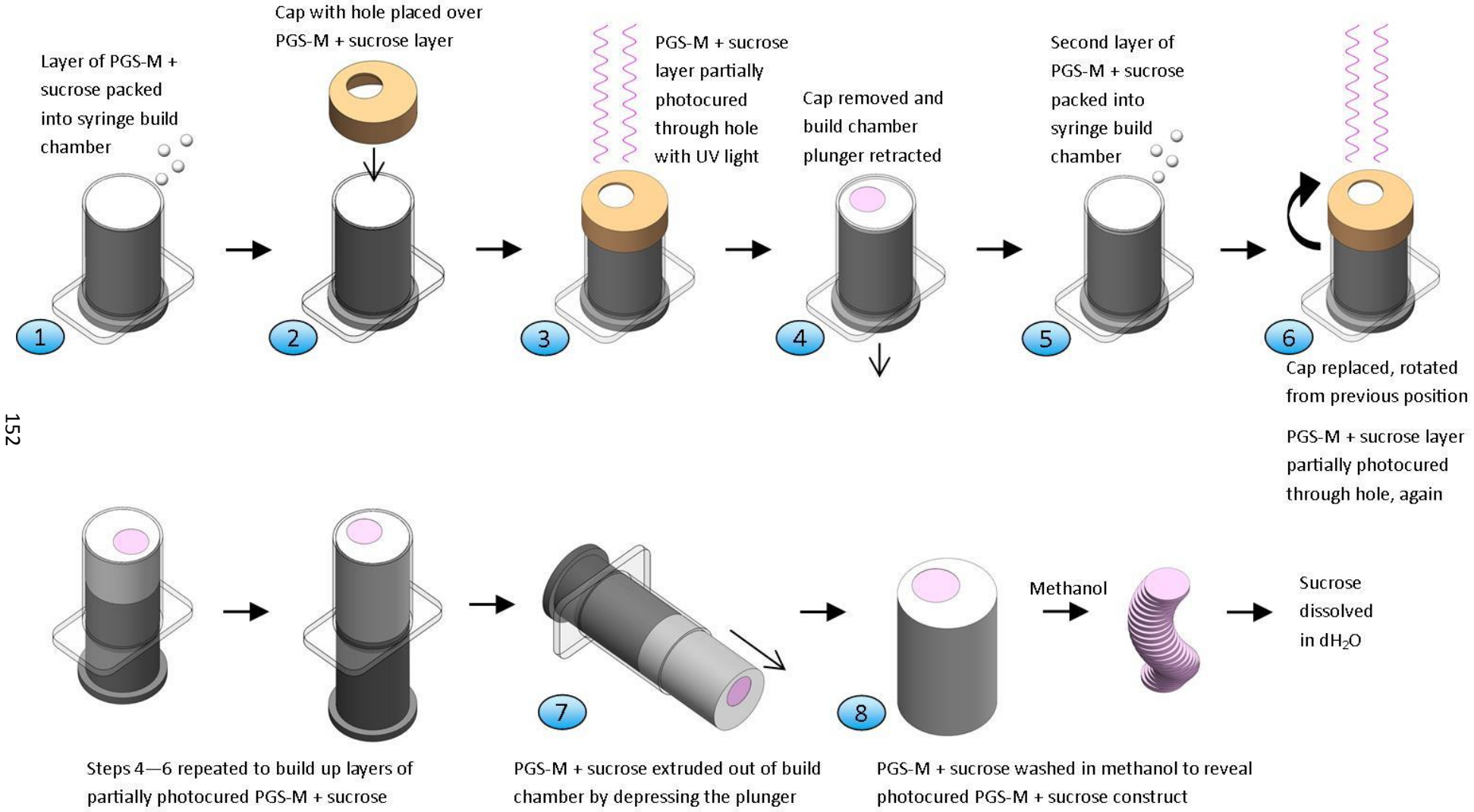

Figure 44. Hybrid additive manufacturing and porogen leaching method for porous PGS-M scaffolds.

4.3 **Results**

4.3.1 **Fabrication of porous PGS-M disk scaffolds using porogen leaching**

Porous scaffolds for tissue engineering were produced from 30% Low M_w PGS-M by porogen leaching. The PGS-M prepolymer was combined with sucrose particles and photocured forming a composite structure. The sucrose was then dissolved to produce a porous structure composed of PGS-M only.

Initially, disk shaped PGS-M scaffolds were produced using the porogen leaching method with 4 different sizes of sucrose particles: large, medium, mixed and small. The PGS-M and sucrose particles of each size range were combined at different ratios to determine the optimum for producing a scaffold. The initial ratios examined were the highest that produced a PGS-M and sucrose particle mixture that could be handled suitably and did not adhere to tools or gloves while manipulated. The PGS-M:sucrose particle ratios were decreased from the initial ratios, incrementally, until the disk scaffolds produced were no longer self-supporting and collapsed under their own weight when wet (Figure 45). The lowest ratio of PGS-M:sucrose particles that produced a self-supporting scaffold was considered the optimum.

Sections from the disk scaffolds produced form the different ratios of PGS-M:sucrose particles were examined by light microscopy. Figure 46 shows a selection of the results for each sucrose particle size range, including the highest ratio examined, the optimum ratio and the ratio at which scaffolds failed to be self-supporting. The sizes of the scaffold pores decreased as the size range of the sucrose particles used to produce them decreased. The interconnectivity between pores also appeared to increase with decreasing ratios of PGS-M:sucrose particles. The optimum ratios of PGS-M:sucrose particles determined were 1:2.8, 1:3, 1:3.8 and 1:3.4 for the scaffolds produced from the large, medium, mixed and small sucrose particle sizes, respectively.

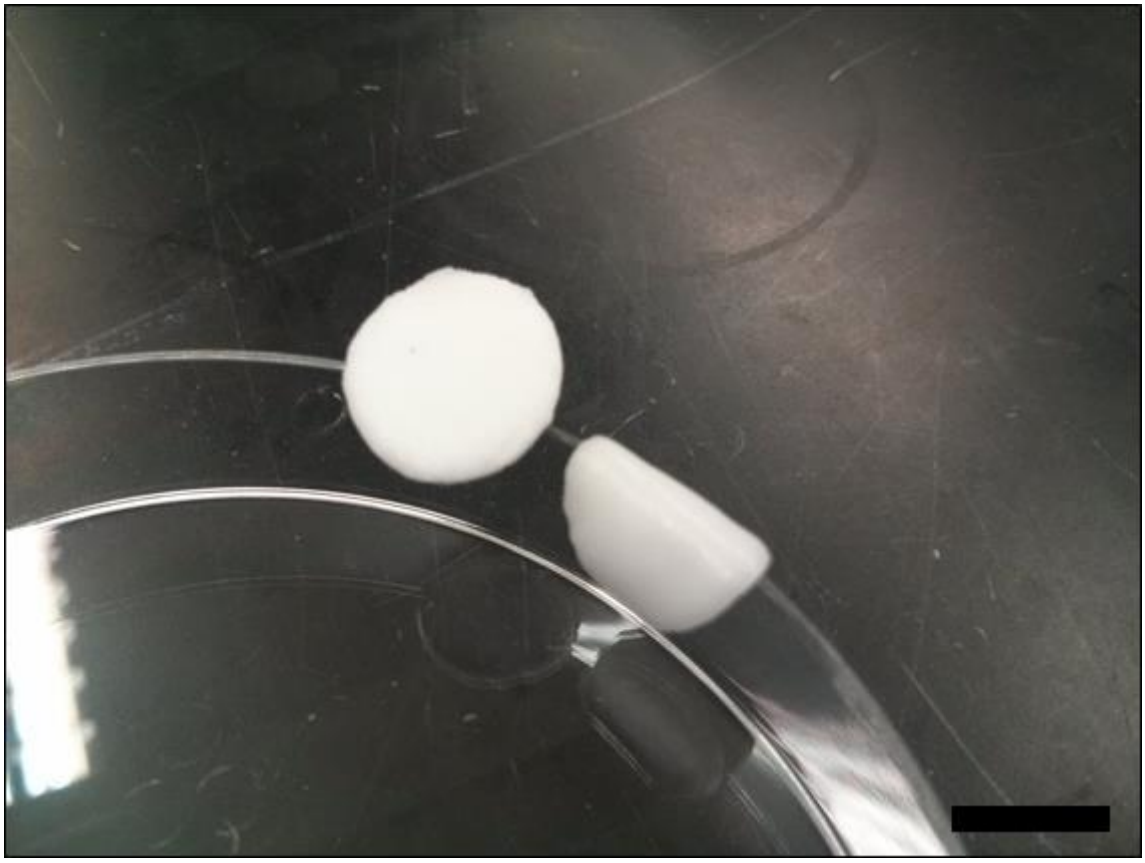

Figure 45. PGS-M disk scaffolds produced from mixed sucrose particles. (Left) self-supporting scaffold produced from the optimum ratio of PGS-M:sucrose particles, 1:3.8. (Right) scaffold produced from a PGS-M:sucrose particle ratio of 1:4 was not self-supporting. Scale bar is 1 cm.

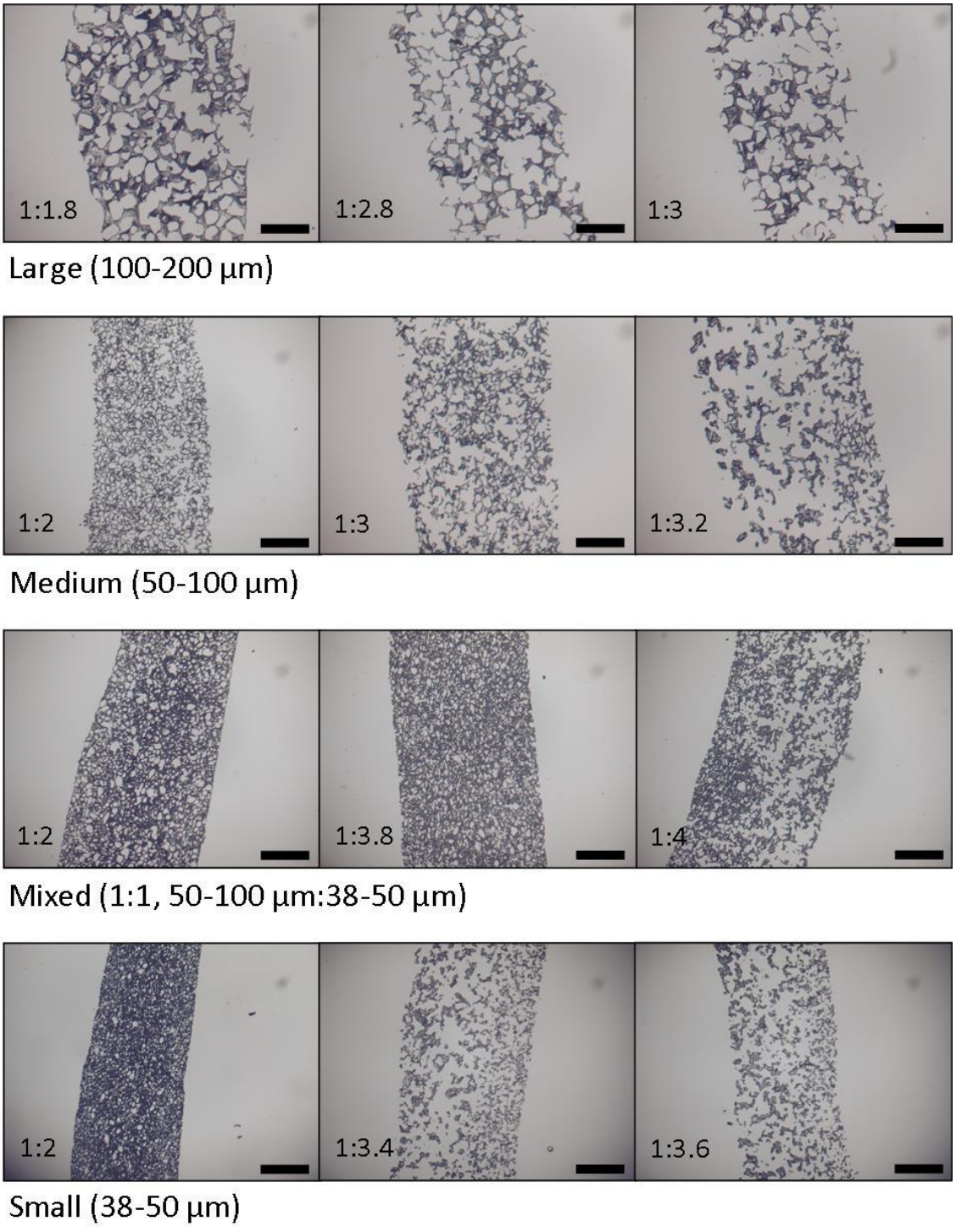

Figure 46. Representative sections of PGS-M disk scaffolds produced with large, medium, mixed and small sucrose particles (*n* = 3). (Left) initial PGS-M:sucrose particle ratios. (Centre) optimum PGS-M:sucrose particle ratios. (Right) PGS-M:sucrose particle ratios that produced scaffolds that were not self-supporting. Scale bars are 500 µm.

4.3.2 Examination of porous PGS-M disk scaffolds using scanning electron microscopy

The structure of the PGS-M disk scaffolds was examined using SEM. The scaffolds were produced using the optimum ratio of PGS-M:sucrose particles determined for each sucrose particle size. The scaffolds appeared to be porous even at low magnification (Figure 47). At increased magnification the porosity was visible in detail and a difference in pore size was seen between scaffolds produced from the different sized sucrose particles (Figure 48). These differences in pore size appeared to correlate well with the different sizes of porogen particles used to produce the scaffolds. Comparing at the same magnification, the scaffolds produced using the large sucrose particles appeared to have the largest pores, whereas scaffolds produced using the small sucrose particles appeared to have the smallest pores. The scaffolds produced using the medium sized sucrose particles appeared to have pore sizes between those of the large and small particle scaffolds. The scaffolds produced using the mixed sucrose particles appeared similar to the medium particle scaffolds with the addition of smaller pores, similar in size to those present in the small particle scaffolds. Interconnectivity between pores was visible in all scaffolds.

The sizes of the pores present in the different PGS-M disk scaffolds was determined from the SEM images. The pore size distributions, measured as both pore area and diameter, within the different scaffolds are shown in Figure 49. The scaffolds produced using the Large sucrose particles demonstrated the largest range of pore sizes while the scaffolds produced using the Small sucrose particles demonstrated the smallest range of pore sizes. The scaffolds produced using the Medium and Mixed sucrose particles appeared to possess a similar range of pore sizes. Average pore size was calculated as both equatorial area and diameter (Figure 50), both of which assumed the pores were spherical. The average pore sizes appeared to correlate well with the size of the sucrose particles used to produce the scaffolds. Large sucrose particles produced the largest pores. Medium sucrose particles produced the second largest pores. Mixed sucrose particles produced the third largest pores and small sucrose particles produced the smallest pores. Pore sizes between the different scaffold types were significantly different to each other ($P<0.05$).

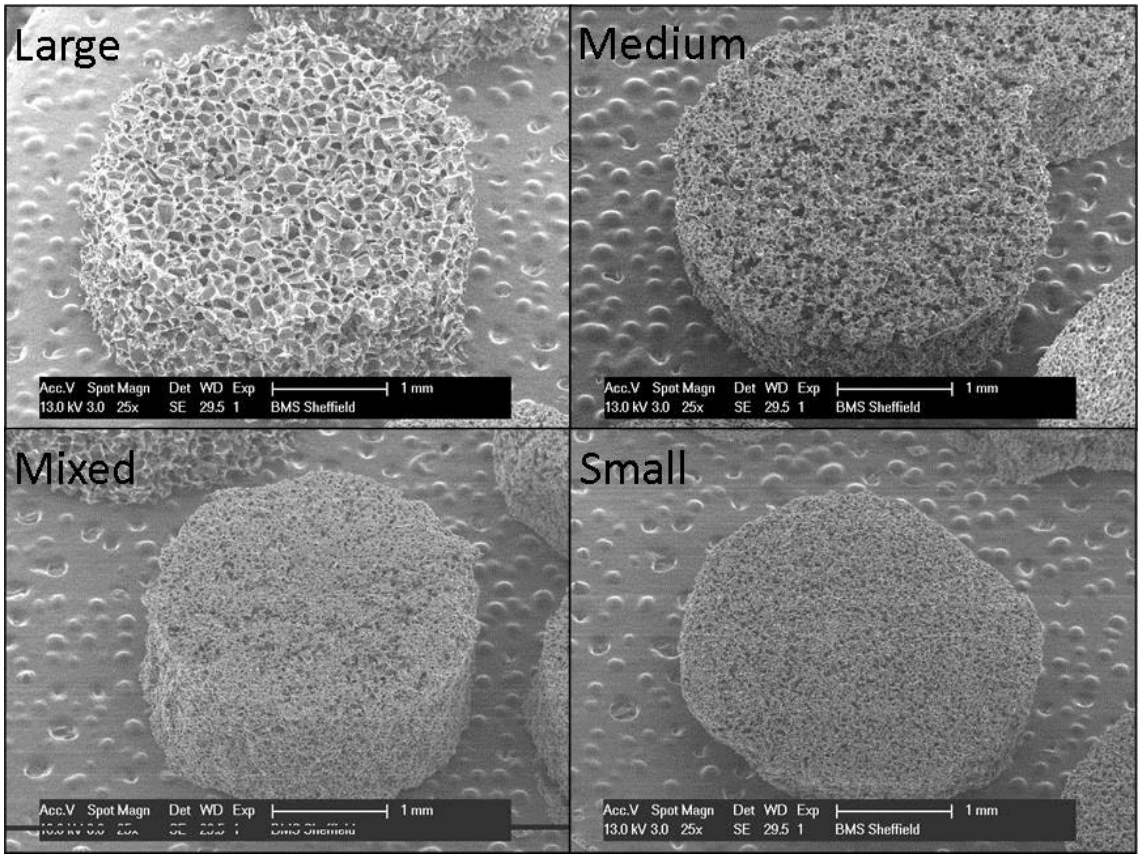

Figure 47. Representative SEM images of porous PGS-M disk scaffolds produced using large, medium, mixed and small sucrose particles at the optimum ratios of PGS-M:sucrose particles determined.

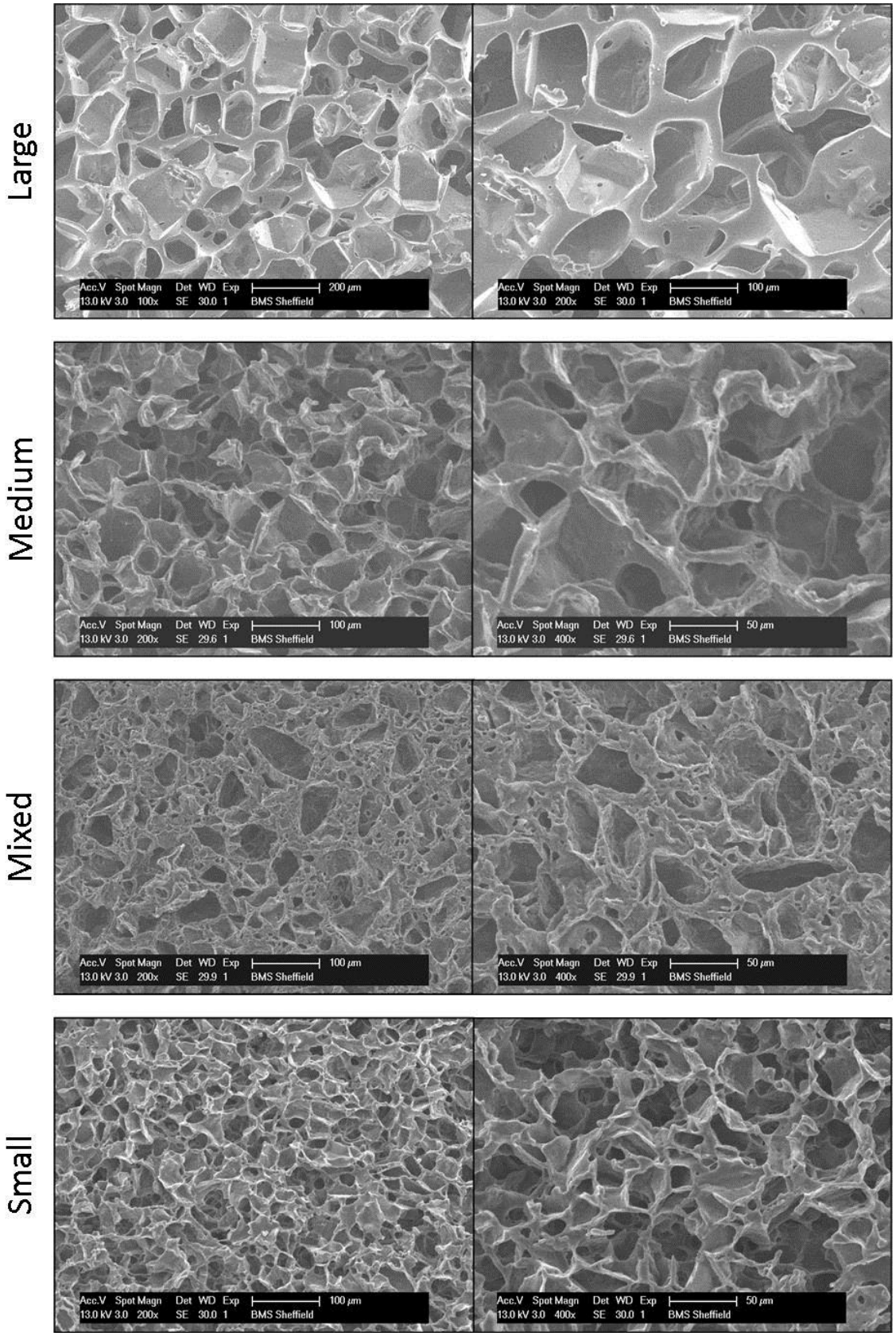

Figure 48. Representative SEM images of the pore structures of porous PGS-M disk scaffolds produced using large, medium, mixed and small sucrose particles at the optimum ratios of PGS-M:sucrose particles determined (*n* = 3).

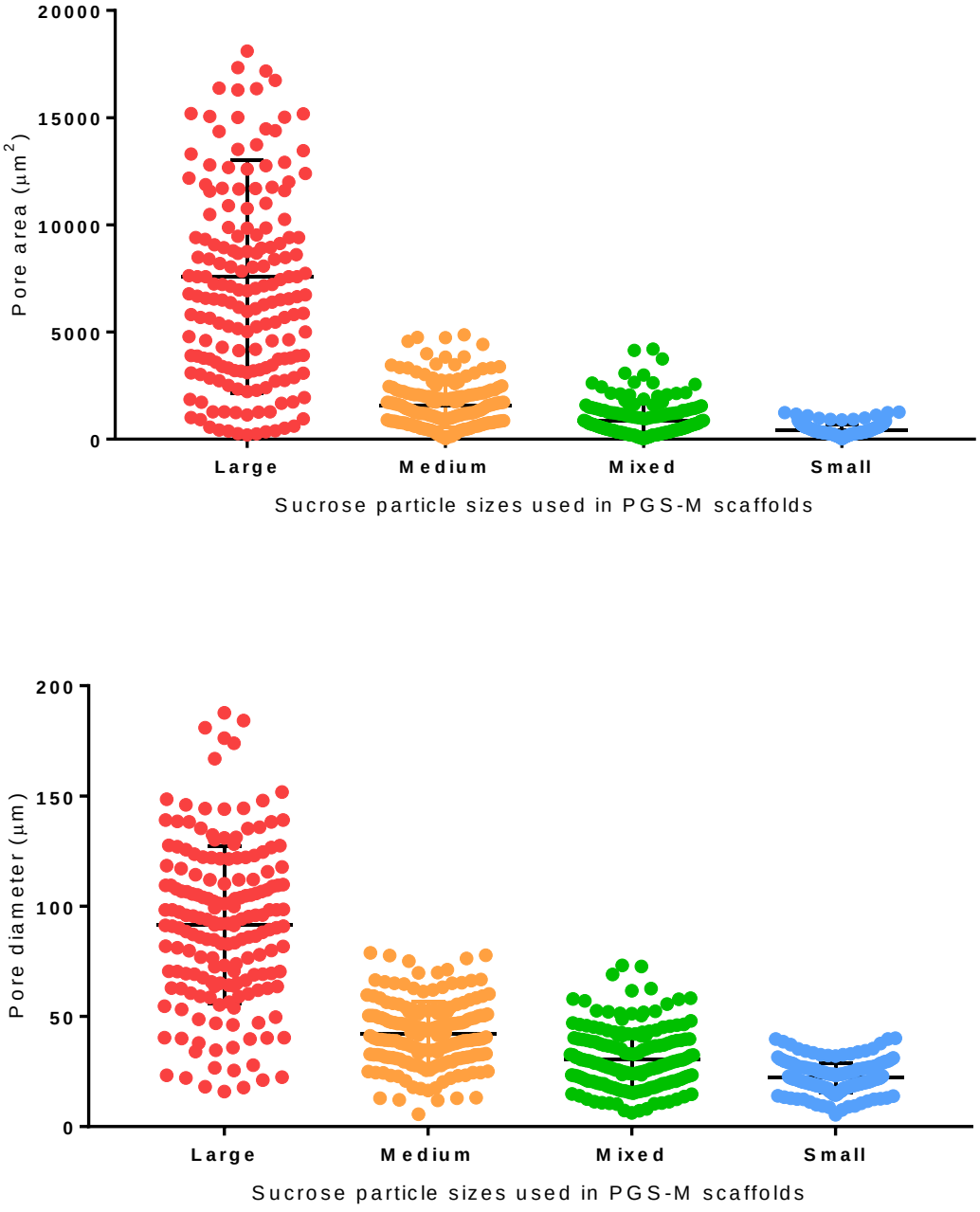

Figure 49. Pore size distributions in PGS-M disk scaffolds produced from large, medium, mixed and small sucrose particles at the optimum ratios of PGS-M:sucrose particles determined. Pore size was calculated as pore area (above) and pore diameter, assuming spherical pores (below). Error bars are standard deviation (*n* = 3).

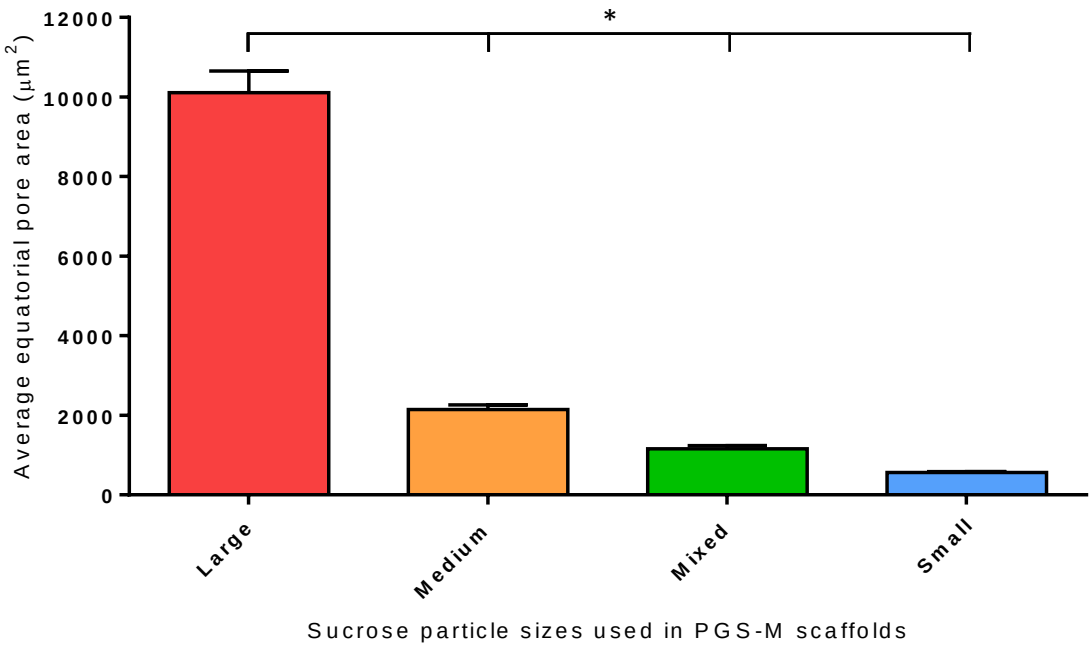

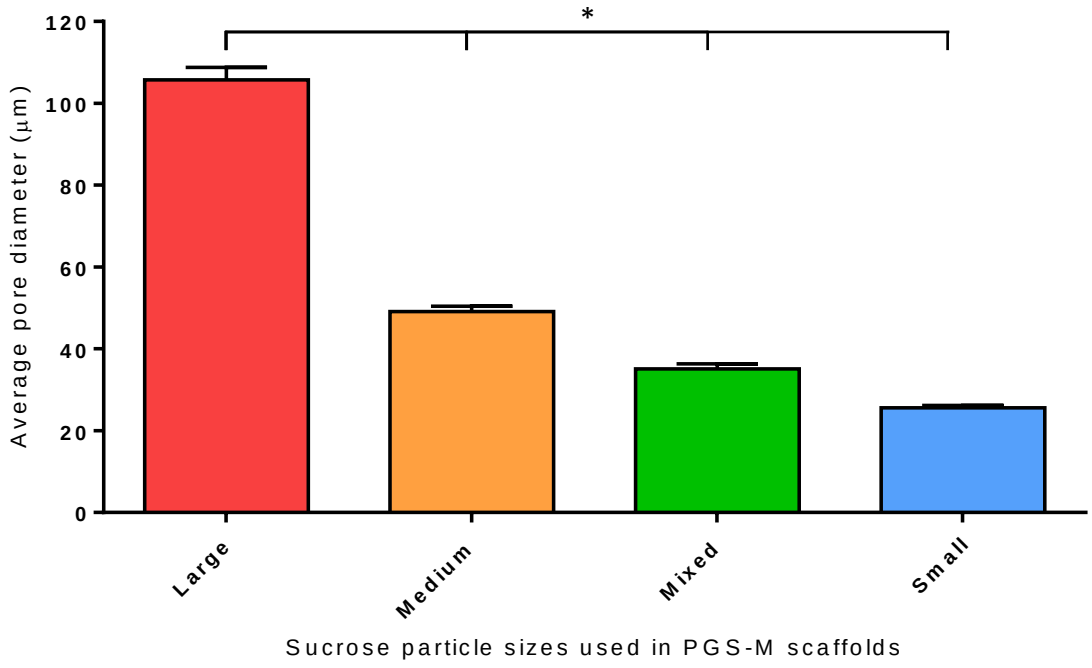

Figure 50. Average pore sizes in PGS-M disk scaffolds produced from large, medium, mixed and small sucrose particles at the optimum ratios of PGS-M:sucrose particles determined. Pore size was calculated as equatorial pore area (above) and pore diameter (below), both assuming spherical pores. Error bars are SEM (*n* = 3).

4.3.3 **Examination of the wettability of porous PGS-M disk scaffolds**

The wettability of the porous PGS-M disk scaffolds produced using the large, medium, mixed and small sucrose particle sizes at their optimum ratio of PGS-M:sucrose particles was examined qualitatively. A 20 µl droplet of blue dyed PBS, placed onto the surface of each scaffold, was observed over 2 hours 30 minutes, as it was absorbed (Figure 51). Initially, the PBS droplets formed tight beads on the surfaces of all of the scaffolds. These beads had contact angles with the surfaces exceeding 90°. Over the time points examined, the PBS appeared to be absorbed into the scaffolds, with the contact angles between it and the scaffold surfaces reducing. The results suggested that the scaffolds produced using the small sucrose particles had the greatest wettability, as the PBS was completely absorbed into these after 2 hours. This was ahead of the other scaffolds, which took a further 30 minutes to fully absorb the PBS. There was a change in the mass of the dyed PBS placed on the glass coverslips and examined in parallel with the scaffolds. This appeared to reduce in mass by ~16%, as a result of evaporation. This suggested that although some evaporation of the dyed PBS may have occurred over the course of the experiment, this was not the overriding effect.

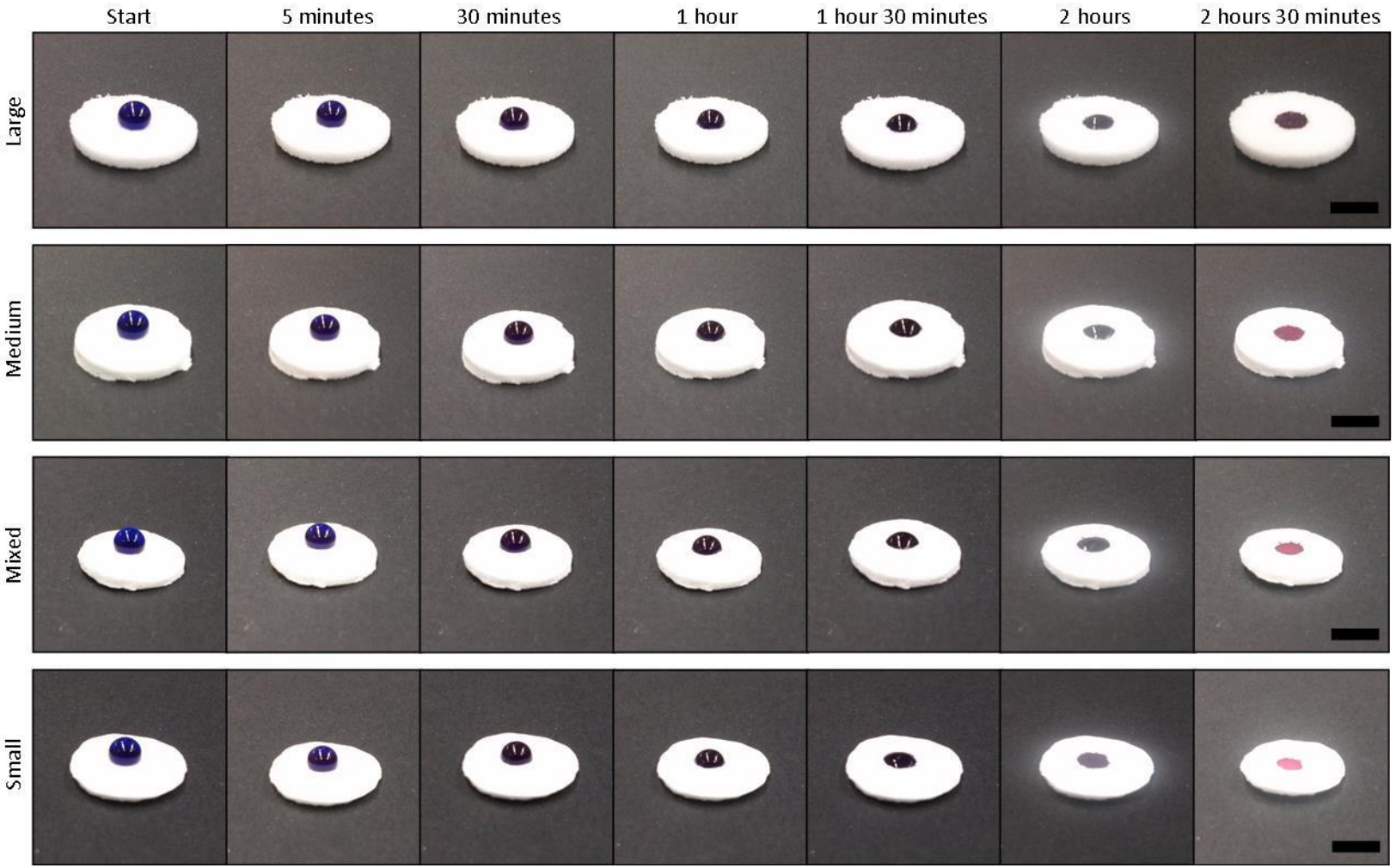

Figure 51. Representative images of the wettability of porous PGS-M disk scaffolds. Scaffolds were produced using large, medium, mixed and small size sucrose particles at the optimum ratios of PGS-M:sucrose particles determined (*n* = 1). Absorption of dyed PBS was observed for 2 hours 30 minutes. Scale bars are 5 mm.

4.3.4 Determination of the porosity of PGS-M disk scaffolds using helium pycnometry

The porosity of the PGS-M disk scaffolds was quantified using helium pycnometry. Scaffolds produced using large, medium, mixed and small sucrose particles were examined. The scaffolds were produced using the optimum ratios of PGS-M:sucrose particles determined for each particle size range, along with the ratios preceding the optimum ratios (sub-optimum) produced in the original scaffold fabrication experiments, described in (4.2.2).

The results demonstrated that the scaffolds produced using the mixed size sucrose particles, at their optimum PGS-M:sucrose particle ratio (1:3.8), possessed the greatest porosity (Figure 52). The porosity of these scaffolds was 81.9% ± 0.7 and this was significantly different to all of the other scaffolds examined ($P<0.01$). Comparing scaffolds produced from optimum and sub-optimum ratios of PGS-M:sucrose particles using the same sucrose particle size showed that the only significant difference was found between the scaffolds produced using the mixed sucrose particles ($P<0.001$).

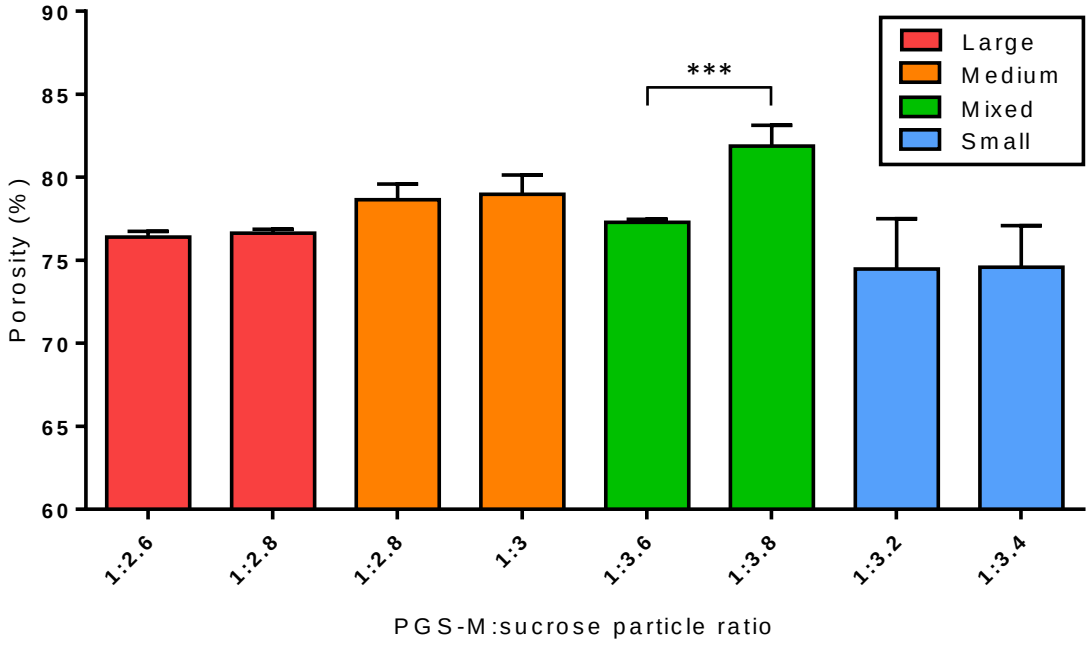

Figure 52. Porosity of PGS-M disk scaffolds produced using large, medium, mixed and small sucrose particles, at optimum and sub-optimum PGS-M:sucrose particle ratios. Error bars are SEM (*n* = 3).

4.3.5 **Characterisation of porous PGS-M disk scaffolds by Raman spectroscopy**

Raman spectroscopy was used to determine if any residual sucrose remained in the porous PGS-M scaffolds following leaching of the sucrose in dH_2O. The spectra from the interiors of fully processed and porous PGS-M disk scaffolds were compared to those of equivalent scaffolds where the sucrose had not yet been washed out, along with the spectra from a sample of pure sucrose and a non-porous disk of pure PGS-M (Figure 53).

The spectra from the pure sucrose and pure PGS-M appeared distinctly different. The spectra from the unwashed PGS-M scaffolds with included sucrose particles appeared to be very similar to the spectra from the pure sucrose. Peaks unique to the spectrum from the pure PGS-M, such as at 1730 cm^{-1}, were absent from the spectrum from the unwashed scaffold, suggesting the sucrose signal dominated. The spectra from the washed PGS-M scaffolds appeared very similar to that of the pure PGS-M, although the peak intensities across the entire spectrum appeared to be reduced. No spectral signals associated with the sucrose could be determined.

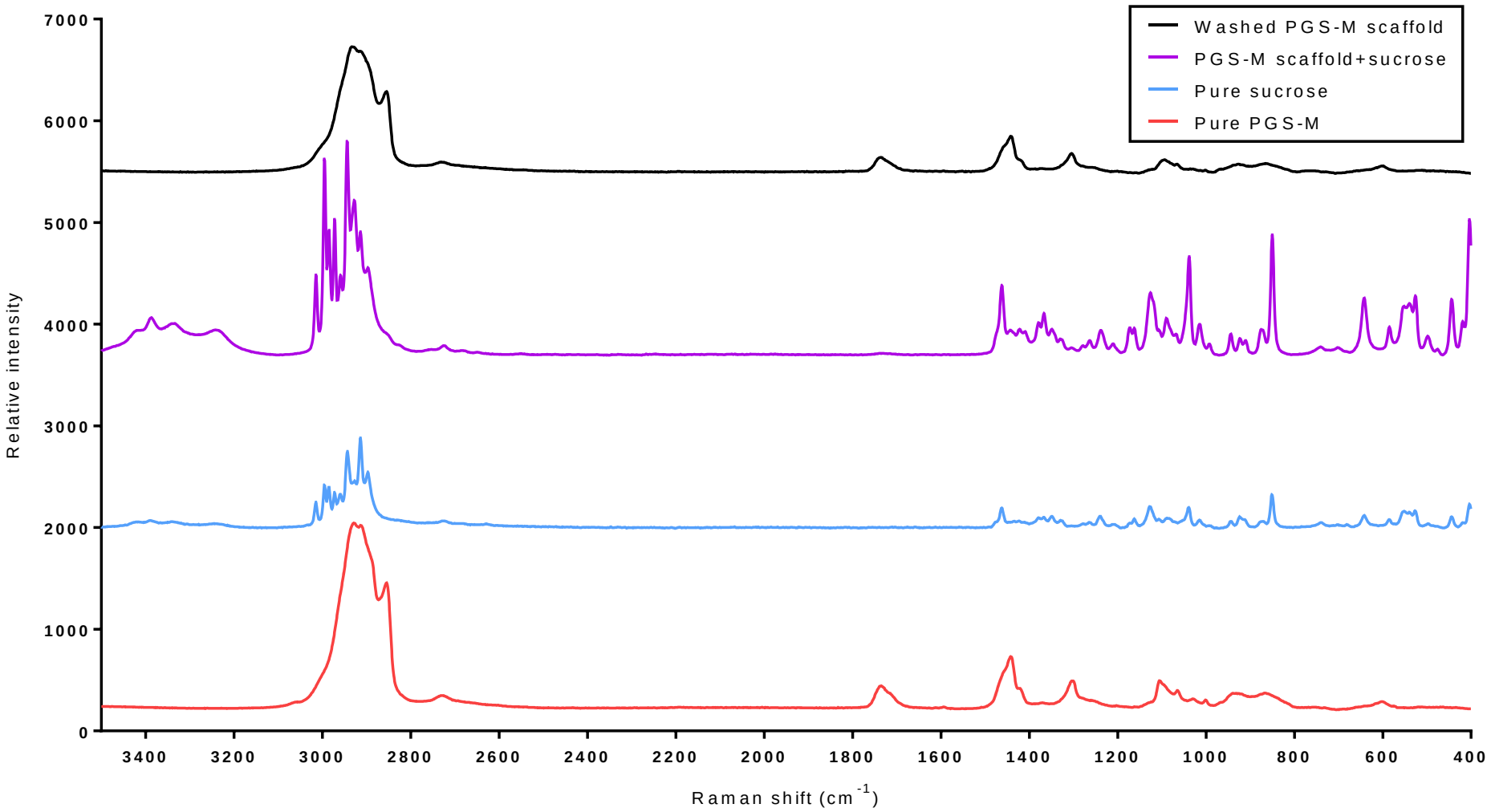

Figure 53. Raman spectra for PGS-M disk scaffolds with sucrose washed out (Washed PGS-M scaffold) or unwashed (PGS-M scaffold+sucrose). Spectra for PGS-M only (Pure PGS-M) and sucrose (Pure sucrose) are included for comparison. The spectrum generated by the washed PGS-M scaffold was similar to that of the pure PGS-M and did not contain recognisable elements from the sucrose spectrum.

4.3.6 **Culture of SMCs on porous PGS-M disk scaffolds**

SMCs were seeded onto porous PGS-M disk scaffolds, produced from mixed sucrose particles at a PGS-M:sucrose particle ratio of 1:3.8, and cultured for 1 and 7 days. At the end of the culture periods, the viability of the cells on the scaffolds was measured using the RR assay. At the end of the assay, the scaffolds seeded with SMCs appeared to be stained strongly purple, whereas the unseeded scaffolds remained white (Figure 54). The results of the assay are shown in Figure 55. Scaffolds seeded with SMCs produced significantly greater fluorescence compared to unseeded PGS-M scaffolds (negative controls) ($P<0.001$). Additionally, the fluorescence produced by the SMCs cultured on the PGS-M scaffolds increased over the duration of the study with the values being significantly different between day 1 and day 7 ($P<0.05$).

The SMC seeded scaffolds were also fixed and stained with H&E for histological examination. The sections from both 1 day and 7 day cultures showed the presence of sporadic SMCs on the surface of the scaffolds and also penetrating into the interiors ~500 µm (Figure 56). No significant differences could be discerned between the seeded scaffolds cultured for 1 day and 7 days, based on the visual examination of the stained sections. Unseeded scaffolds, also stained with H&E, did not show the presence of cells (Figure 57).

Additionally, PGS-M scaffolds seeded with SMCs and cultured for 7 days were also fixed and examined using SEM. The seeded surface of the scaffolds appeared to be almost completely covered by SMCs and ECM (Figure 58).

Figure 54. Porous PGS-M disk scaffolds seeded with SMCs and cultured for 7 days, after RR assay (above). Unseeded scaffolds cultured and assayed in parallel (below). Scale bar is 1 cm.

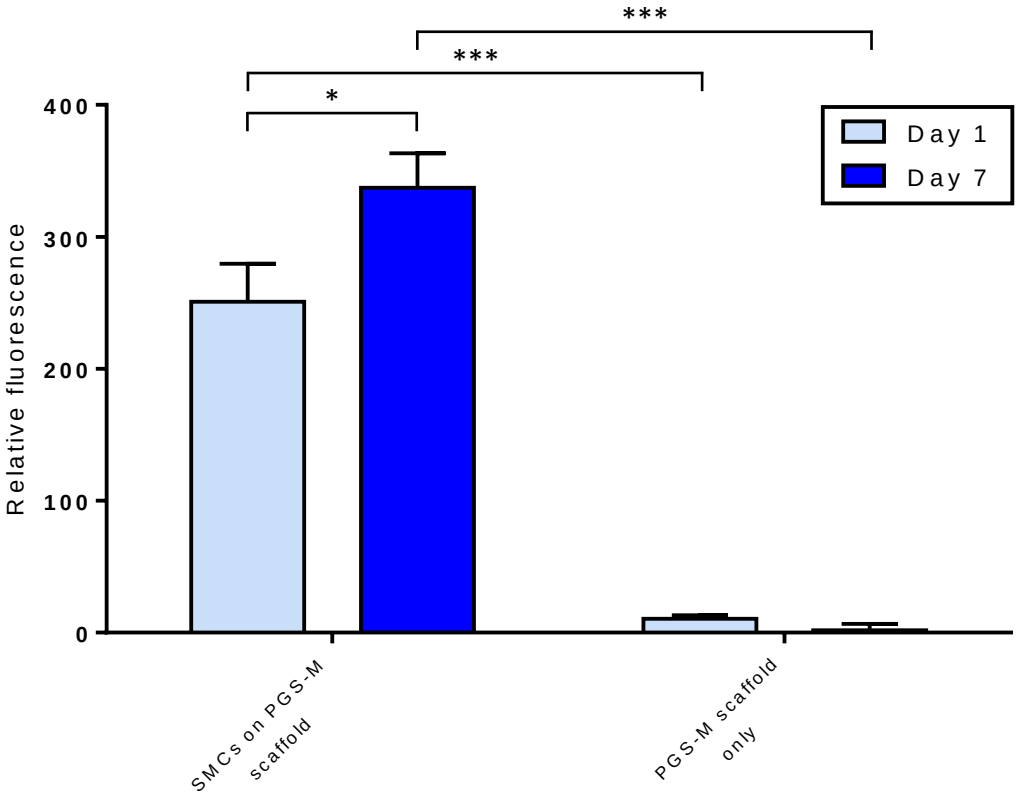

Figure 55. RR assay for SMC viability on porous PGS-M disk scaffolds. Negative controls were unseeded PGS-M scaffolds. Error bars are SEM (*n* = 2).

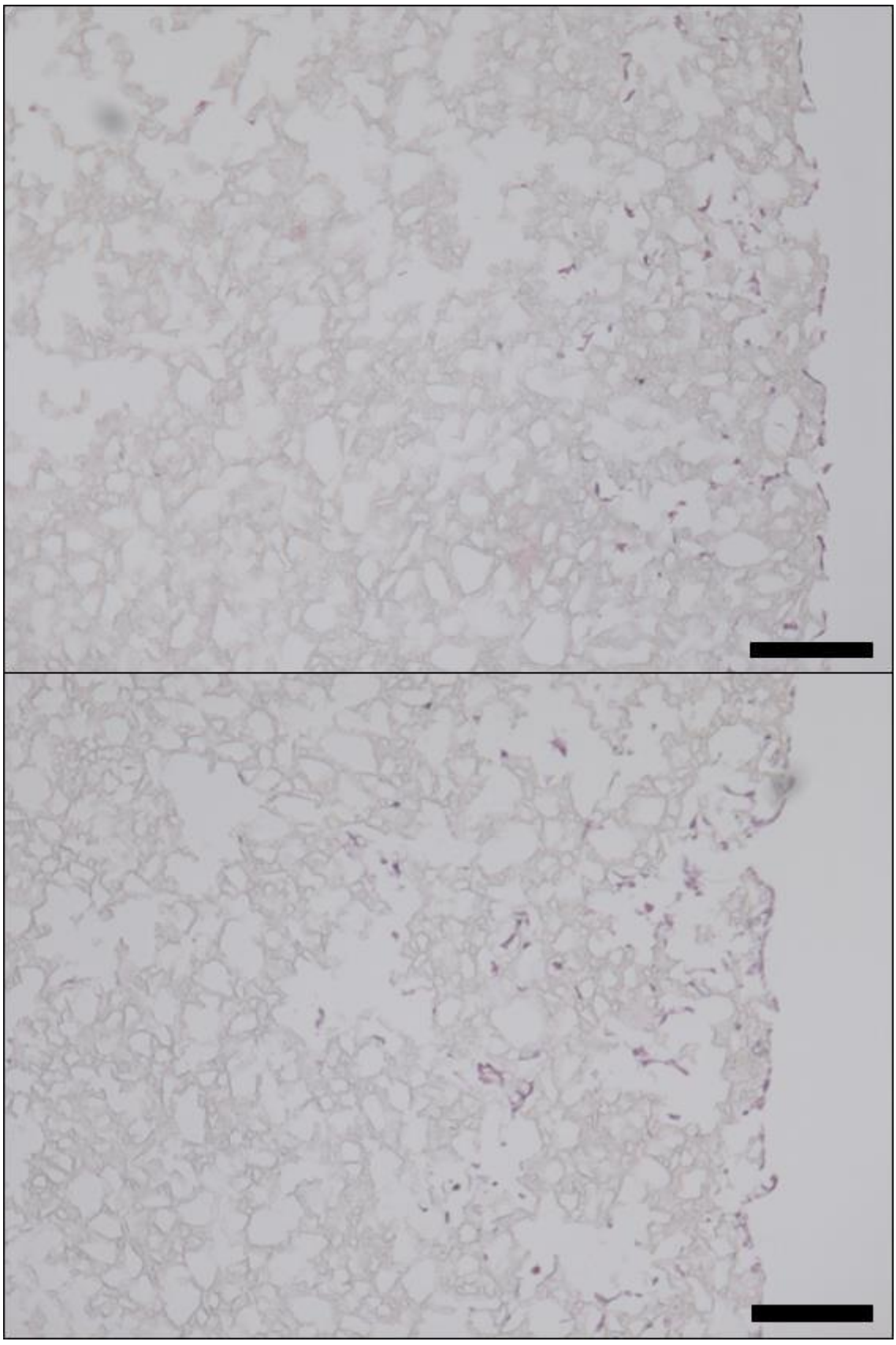

Figure 56. Representative images of H&E stained sections of porous PGS-M disk scaffolds seeded with SMCs and cultured for 1 day (above) and 7 days (below) (*n* = 2). SMCs were present at the surface of the scaffolds and also penetrated into them. Scale bar is 200 µm.

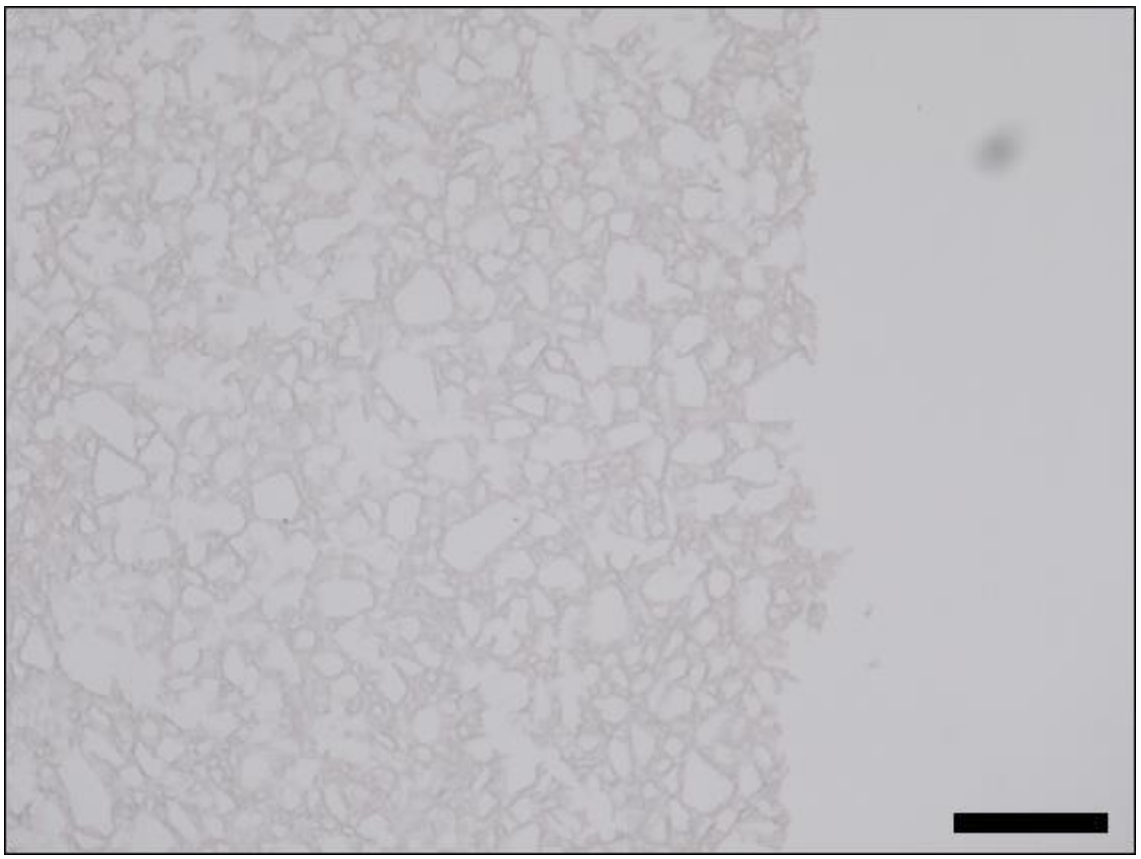

Figure 57. Representative image of H&E stained sections of porous PGS-M disk scaffolds cultured for 1 day and 7 days without seeded SMCs (negative controls) (*n* = 2). No cells appeared to be present within the sections. Scale bar is 200 µm.

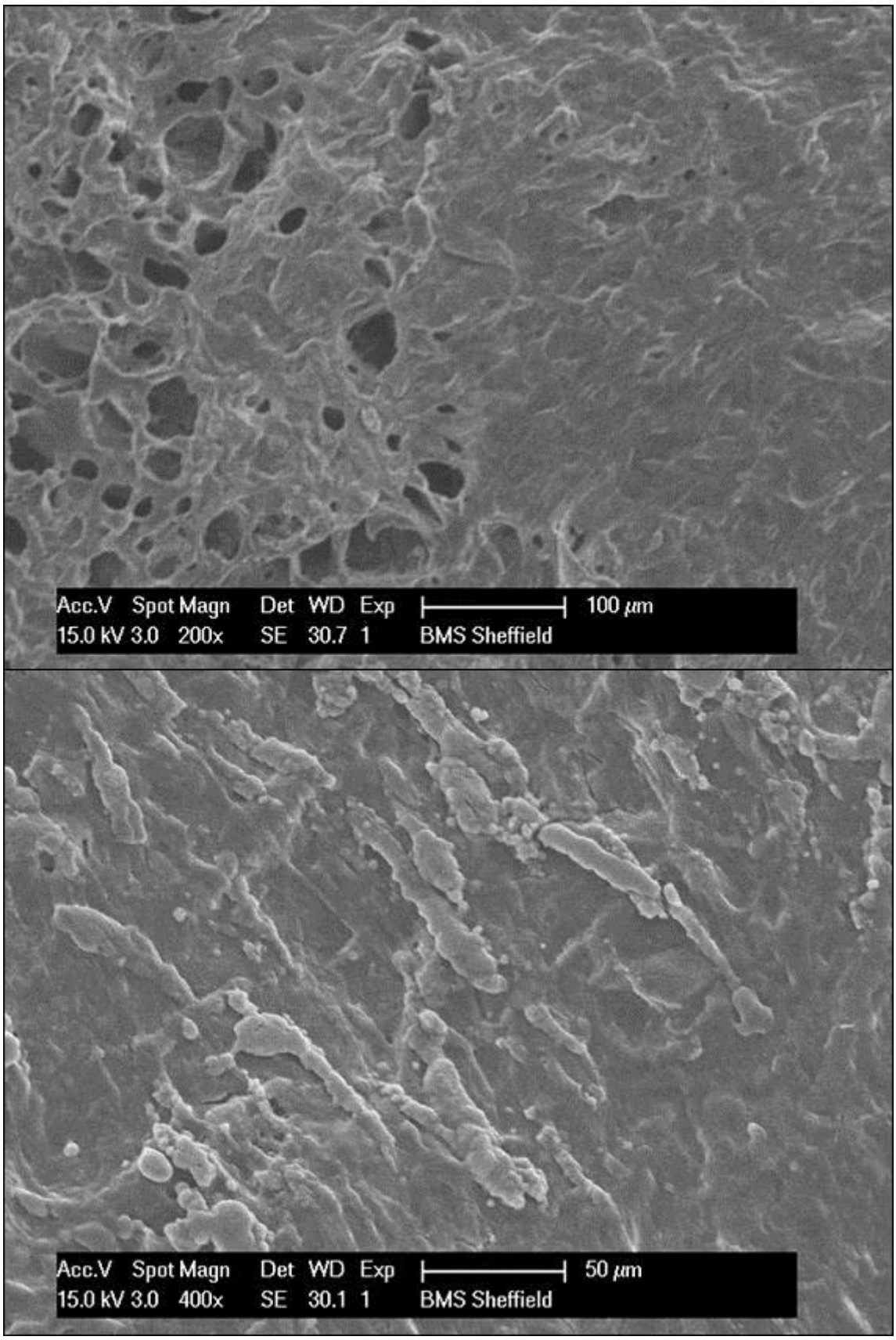

Figure 58. Representative SEM images of porous PGS-M disk scaffolds seeded with SMCs and cultured for 7 days (n = 3). The surface of the scaffolds was almost completely covered (above) by SMCs and ECM (below).

4.3.7 **Fabrication of porous tubular PGS-M scaffolds using porogen leaching**

Several different methods were explored to manufacture porous tubular scaffolds from PGS-M using the porogen leaching technique. These scaffolds were designed with 3 mm internal diameters and thin walls (<1.5 mm) for applications in producing small-diameter TEVGs. The quality of the scaffolds produced by each method was assessed using SEM. The results are summarised in Table 9.

Method i was explored initially and utilised a steel rod and silicone mould to shape the PGS-M and sucrose mixture into a tube. This method was not compatible with the optimum ratios of PGS-M:sucrose particles that were identified in the porous disk scaffolds. PGS-M and sucrose mixtures at these ratios could not be shaped effectively using the steel rod and silicone mould and tended crack and break apart. Examination of the scaffolds that were produced, at sub-optimum PGS-M:sucrose particle ratios, revealed conserved geometries (Figure 59). The tubes were self-supporting and showed uniform wall thicknesses. Additional examination showed that, although the scaffold interiors appeared to be porous, the outer and luminal surfaces were partially covered by a skin of PGS-M, limiting their porosity,

Method ii utilised a syringe and PVA rod to shape the PGS-M and sucrose mixture into a tube. Using mixed sucrose particles, at their optimum ratio of PGS-M:sucrose particles, the scaffolds produced were uniform, self-supporting tubes with consistent wall thicknesses across their length and around their circumference (Figure 59). The scaffolds were porous across their outer surfaces and throughout their interiors. However, their luminal surfaces possessed reduced porosity due to the presence of a skin of PGS-M. This was less pronounced than observed in the scaffolds produced using method i, but still limited the surface porosity compared to the interior and outer surface.

Method iii used a corer to remove the central portion from a compact of PGS-M and sucrose mixture, shaped in a syringe, to produce a tube. This method appeared to produce scaffolds with porous outer and luminal surfaces, as well as interiors (Figure 59). However, the tubular geometry of the scaffolds appeared to be deformed. This

was a result of collapse of the tubular PGS-M and sucrose compacts when they were extruded from the syringes, prior to photocuring.

Method iv was similar to method iii, but the compacts were photocured inside the syringes to avoid collapse on extrusion. The scaffolds produced possessed uniform tubular geometries and retained the porous luminal surfaces seen in method iii (Figure 60). However, their outer surfaces showed large regions of skin formation which appeared to greatly reduce the surface porosity.

Method v was again similar to method iii, except the central cavities of the cored PGS-M and sucrose compacts were filled with sucrose particles to prevent collapse on extrusion out of the syringes. These scaffolds were similar to those produced in method iii, but without the deformation associated with compact collapse (Figure 60). The scaffolds were self-supporting and demonstrated uniform tubular geometry with conserved wall thicknesses throughout. They also appeared to possess porous outer and luminal surfaces, along with porous interiors.

Method vi utilised a drill to cut the central portion from a cylinder of photocured PGS-M and sucrose compact, to produce a tube. This method produced scaffolds with porous outer surfaces; however, the scaffold walls were non-uniform and varied in thickness across the length of the scaffolds (Figure 60). The luminal surfaces, although porous, also appeared disrupted and damaged in some regions.

Table 9. Summary of the structures of the scaffolds produced using methods i to vi.

Tubular scaffold fabrication method	**Outer surface**	**Interior**	**Luminal surface**	**Additional comments**
i	Skin layer present	Porous	Skin layer present	Not compatible with optimum ratios of PGS-M:sucrose particles
ii	Porous	Porous	Skin layer present	
iii	Porous	Porous	Porous	Scaffolds deformed due to collapse of the compact during extrusion from the syringes
iv	Skin layer present	Porous	Porous	
v	Porous	Porous	Porous	
vi	Porous	Porous	Porous	Scaffolds damaged by drill

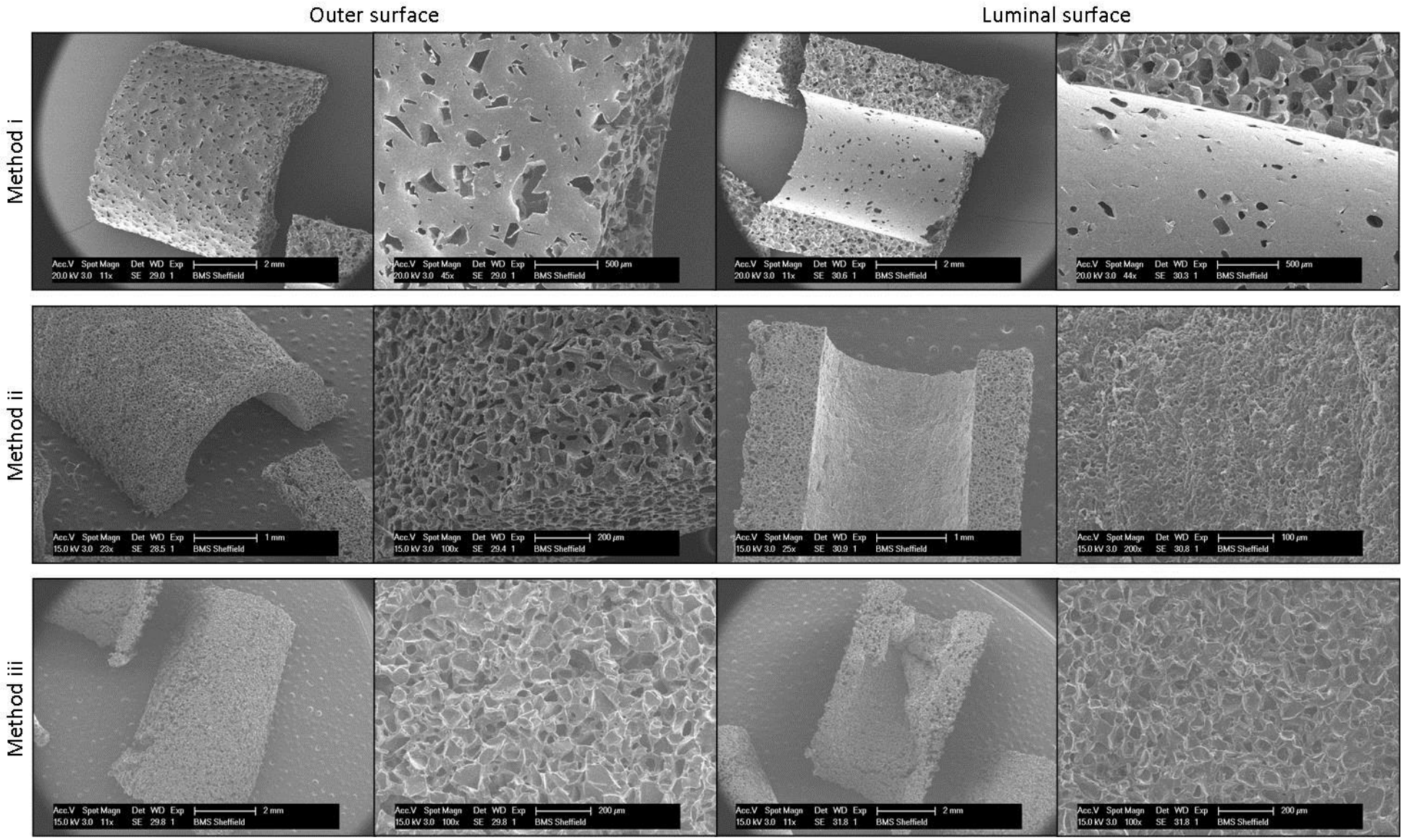

Figure 59. Representative SEM images of tubular PGS-M scaffolds produced using methods i, ii and iii.

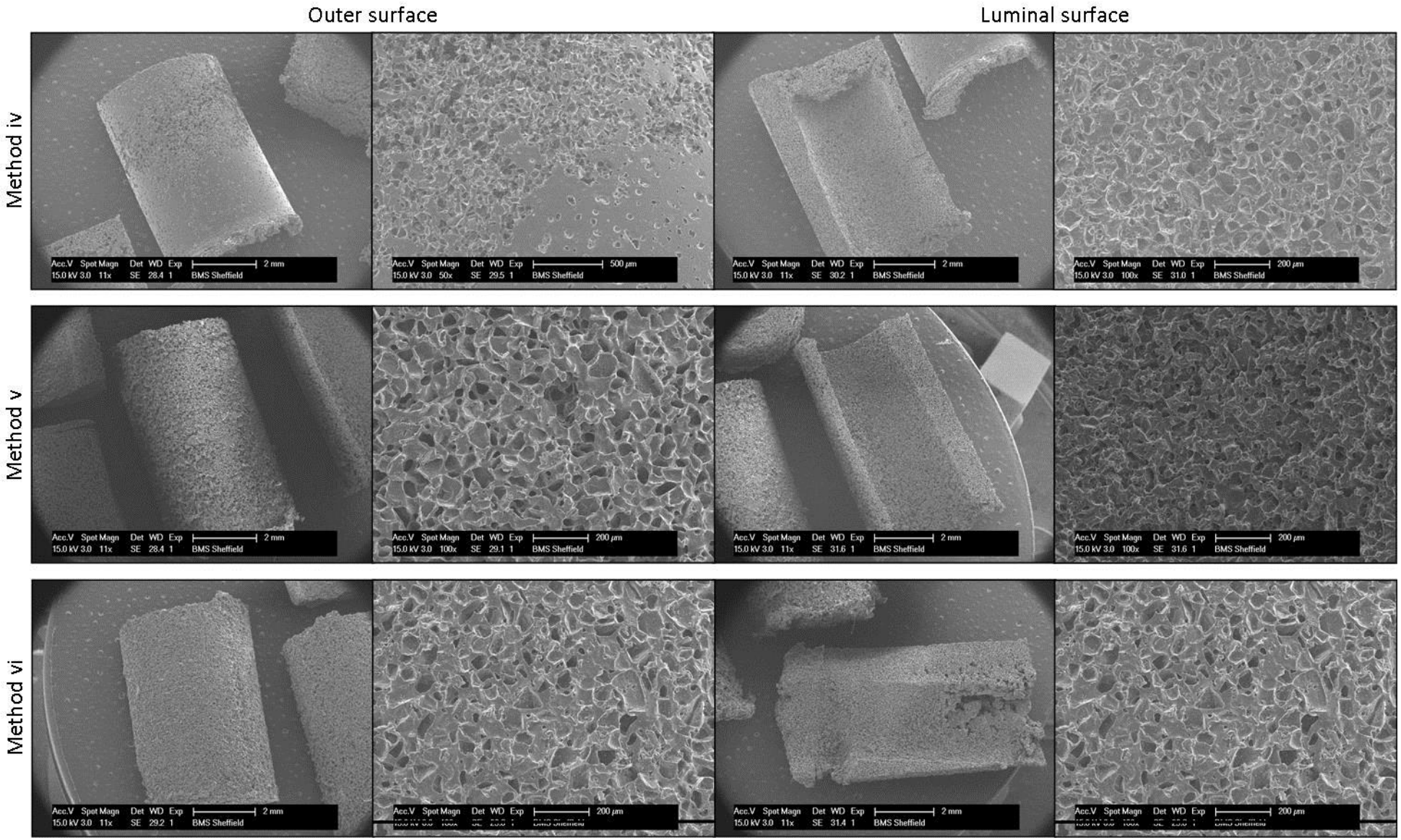

Figure 60. Representative SEM images of tubular PGS-M scaffolds produced using methods iv, v and vi.

With the SEM analysis suggesting that method v produced the best quality tubular PGS-M scaffolds, these scaffolds were further examined for reproducibility. The scaffolds appeared reproducible. The internal and outer diameters displayed some small variation. Average values were 3.245 ± 0.136 mm and 4.346 ± 0.129 mm, respectively (mean average ± standard deviation). Greater variation was seen in the thickness of the scaffold walls, with the average value being 0.555 ± 0.111 mm. All scaffolds produced possessed suitable handling properties for use in the culture of the TEVGs.

4.3.8 **Manufacture of porous PGS-M scaffolds using hybrid additive manufacturing and porogen leaching method**

A hybrid additive manufacturing and porogen leaching method was developed to explore the possibility of producing porous PGS-M scaffolds in more complex and varied geometries then disks or tubes. This method was based on the selective photocuring of thin layers of PGS-M and sucrose compact to build up a 3D structure.

As a proof-of-concept, a scaffold composed of a simple spiral of disks was produced. The manufacturing process appeared to be successful. Methanol washing dissolved the PGS-M which had not been photocured during the manufacturing process and released any surrounding sucrose particles with it. This revealed a construct composed of photocured PGS-M with included sucrose particles. The construct appeared to conform to the intended design and could be seen to consist of many similar sized disks stacked on top of each other and arranged in a spiral (Figure 61). Large regions of connectivity between the disks were visible, although some areas of separation were also present. Interestingly, the diameter of the disks appeared to exceed the diameter of the hole through which they were photocured. Disks appeared to be ~12 mm in diameter whereas the hole was only 8 mm in diameter. Dissolving the included sucrose particles appeared to produce a porous structure with similar handling properties to the disk and tubular scaffolds produced previously.

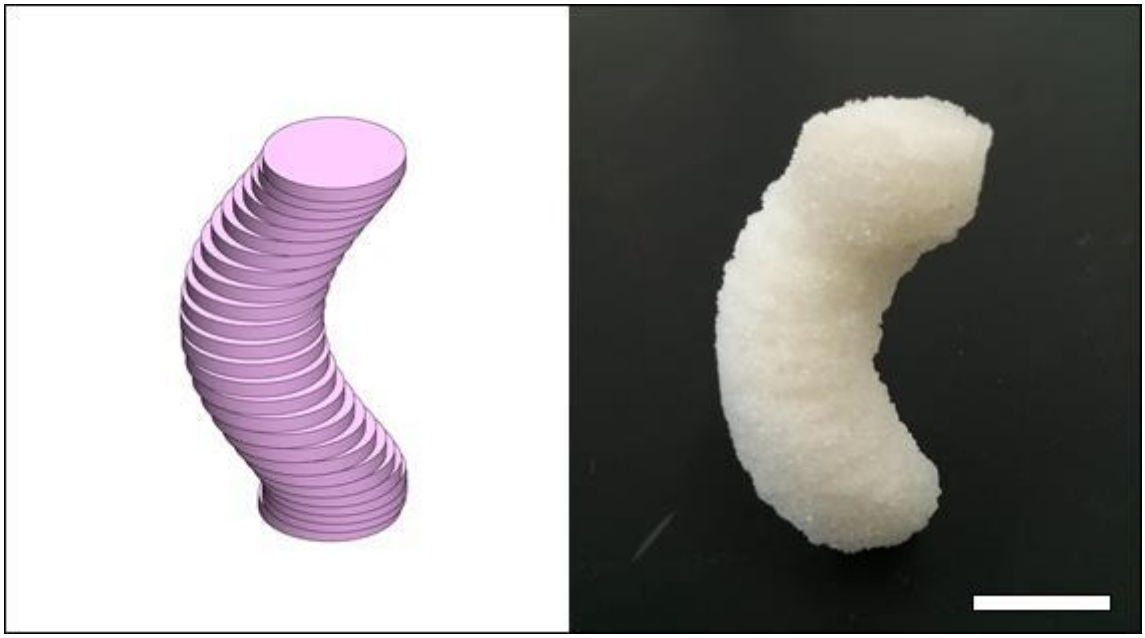

Figure 61. Proof-of-concept PGS-M scaffold produced using hybrid additive manufacturing and porogen leaching method. The scaffold design (left) was well produced using the manufacturing process (right). Scale bar is 1 cm.

4.4 **Discussion**

Porous scaffolds were produced from PGS-M using a porogen leaching method with sucrose particles of different sizes. Initially, disk shaped scaffolds were produced and the optimum ratios of PGS-M:sucrose particles for producing these scaffolds were explored. The optimum ratio of PGS-M:sucrose particles was selected based on a number of factors. The handling characteristics of the PGS-M and sucrose mixtures were important in the production of the scaffolds. Mixtures were required that could be shaped, using moulds, without significant adherence to the tools or gloves used to handle them, but while also maintaining cohesion. Achieving the former required a minimum proportion of sucrose particles in the mixture and defined the upper limit for the ratios of PGS-M:sucrose particles that would be explored within each different sucrose particle size range (large, medium, mixed and small). Maintaining a cohesive mixture of PGS-M and sucrose particles contributed to defining the lower limit for the PGS-M:sucrose particle ratios that were explored. Increasing the fraction of sucrose particles in the PGS-M and sucrose particle mixtures, thereby reducing the ratio of PGS-M:sucrose particles, reduced the adhesiveness of the mixtures. This was because the adhesive quality of the mixture was only provided by the PGS-M prepolymer and not by the sucrose particles. In addition to the handling qualities of the PGS-M and sucrose particle mixtures, the structural properties of the ultimately derived scaffolds were also an important factor. Once the sucrose particles had been washed out, the PGS-M scaffolds were required to be self-supporting and not collapse under their own weight, when wet. This property would contribute to maintaining open pore structures within the scaffolds and also aid in manipulating them. The structural properties of the scaffolds contributed to defining the lower limits for the PGS-M:sucrose particle ratios that were explored. As the ratios reduced, the proportion of PGS-M in the mixtures, and therefore in the ultimately derived scaffolds, reduced. This reduction of material resulted in reduced structural integrity and eventually resulted in scaffold collapse.

To determine the optimum ratio of PGS-M:sucrose particles for each sucrose particle size the upper limit ratio was first determined, based on the handling qualities and

adhesiveness of the PGS-M and sucrose mixtures. The ratio of PGS-M:sucrose particles was then reduced incrementally, until the lower limit ratio was reached, and the scaffolds generated were no longer self-supporting. The optimum ratios were defined as the lowest that produced a self-supporting scaffold. This definition maximised the sucrose content of the mixtures and, subsequently, the porosity of the scaffolds. Maximising scaffold porosity is well established as advantageous for tissue engineering, as this helps facilitate cell in growth, mass transport and nutrient exchange and, in the case of degradable scaffold materials, facilitates increased degradation rates due to greater surface area to volume ratios.[338–341]

Comparing porous scaffolds produced using the different sizes of PGS-M particles showed that the lowest optimum ratio of PGS-M:sucrose particles was achieved using the mixed particles. These could be combined with PGS-M at a PGS-M:sucrose particle ratio of 1:3.8. When considering the large and medium sucrose particles, the optimum PGS-M:sucrose particle ratios determined appeared to correlate with particle size. Large sucrose particles produced the highest optimum ratio of PGS-M:sucrose particles, at 1:2.8, and the medium sucrose particles produced the second highest ratio, at 1:3. Although the optimum ratio of PGS-M:sucrose particles determined for the small sucrose particles was lower than those determined for both the large and medium sucrose particles, it was not lower than the optimum ratio for the mixed particles. The mixed sucrose particles were composed of medium and small particles. It appeared that this combination allowed the PGS-M and sucrose particle mixtures to retain acceptable handling properties, and the derived scaffolds to remain self-supporting, at lower PGS-M:sucrose particle ratios than when using either of the particle sizes alone. A partial explanation for this may come from the observation that the scaffolds produced using the small sucrose particles appeared to retain some residual adhesiveness, even after being washed in dH_2O and methanol. This may have resulted in scaffolds that appeared to not be self-supporting, because of pores collapsing due to adhesion between their surfaces, not because of insufficient strength. It may be possible to produce porous PGS-M scaffolds using the small sucrose particles at a

lower ratio than the optimum that was determined if the residual adhesiveness of the scaffolds could be removed.

PGS-M disk scaffolds, were examined using sectioning and SEM. This revealed the structures of the pores. The sizes of the pores present in the scaffolds appeared to correlate well with the sizes of the sucrose particles used to produce them. Average scaffold pore sizes reduced with decreasing sucrose particle size. In the scaffolds produced using the mixed sucrose particles, a range of pore sizes appeared to be present, reflecting the particle size range. The pore size distribution suggested that pores generated by both the medium and small sucrose particles appeared to be present in these scaffolds, although it is difficult to assess the influence of the small sucrose particles due to the random location of the cutting plane through each pore in the SEM images. The effect of porogen size on pore size has been well established in the literature when using porogen leaching to produce porous structures.[93,94,336,340] Indeed, allowing pore size modulation by selection of different sized porogen particles is a key advantage to the porogen leaching process, as pore size can affect cell phenotype and proliferation.[340,342] The porous structures of the PGS-M disk scaffolds appeared comparable to those demonstrated in published works. Porous scaffolds for use in TEVGs were produced from thermally cured PGS using three different size ranges of NaCl: 75-90 µm, 45-53 µm, and 25-32 µm. These porous PGS scaffolds showed clear differences in pore size, in line with the sizes of the NaCl porogens used, and appeared similar to the scaffolds produced herein, with interconnected clearly defined pores.[93] Porous disk scaffolds produced from PLLA using NaCl particles of between 38 µm and 150 µm also demonstrated similar pore structures.[340]

The pore structures observed within the PGS-M disk scaffolds, using sectioning and SEM, also suggested additional evidence to explain the differences in the optimum PGS-M:sucrose particle ratios that were determined for the scaffolds produced using the different size sucrose particles. The optimum ratios of PGS-M:sucrose particles were higher when using large particle sizes. These ratios were determined based on the scaffolds being self-supporting and not collapsing when wet. Reducing the sizes of

the pores within the scaffolds, as a result of using smaller sucrose particles, may have resulted in an increase in triangulation within the scaffold structures. This increased the stiffness of the scaffolds and their abilities to spread and support mechanical loads without deformation, allowing them to remain self-supporting at lower ratios of PGS-M:sucrose particles.

The ideal pore size required in a scaffold used for the production of a TEVG may depend on the scaffold material and the cell types involved. In the static culture of SMCs, pore sizes of between 38 µm and 200 µm have proven to produce similar results in PLLA and PLGA scaffolds.[338,340] In the culture of TEVGs, under dynamic conditions, pore sizes of between 25 µm and 90 µm all produced favourable results, although there was some preference towards smaller pore sizes.[93] The sizes of the pores present in the different PGS-M scaffolds, determined using the SEM images, were within these ranges and were therefore considered suitable for use in scaffolds intended for producing TEVGs.

It was interesting to compare the sizes of the pores within the PGS-M scaffolds with the sizes of the sucrose particles used to produce them. The sucrose particles were divided into different size ranges using size exclusion. This was performed using sieves which were composed of regularly arranged wire grids with different sized square holes through which selected particles could pass based on their size. If the particles were assumed to be spherical then the sieves essentially selected particles based on their diameters. This allows a comparison to be made with average pore diameters that were determined from the SEM images of the porous PGS-M scaffolds. Making this comparison for the scaffolds produced using the different sizes (diameters) of sucrose particles shows that the pore diameters appeared to be below, or at the lower region of, the diameter range of the sucrose particles within each different size range (Table 10).

Table 10. Sucrose particle sizes (as diameters) compared to the average pore diameters generated in the PGS-M disk scaffolds.

Sucrose particles	**Particle size (diameter) range (μm)**	**Average scaffold pore diameter (μm)**
Large	100-200	106 ± 3
Medium	50-100	49 ± 18
Mixed	1:1 blend of 50-100 and 38-50	35 ± 16
Small	38-50	26 ± 8

This suggests that each of the sucrose particle size ranges produced by the sieving process may actually have contained a significant fraction of particles below the lower limit of the range. Alternatively, the scaffold pores may have experienced some shrinkage during the washes with dH_2O and methanol, following photocuring, or in the freeze drying process prior to SEM examination. Similar effects have been reported in the literature, but these are not universal. The average pore sizes in thermally cured PGS scaffolds produced using NaCl porogens of three different size ranges appeared to be below the lower limits of the porogen size ranges in each case.[93] Here, the average sizes of the pores in the scaffolds were measured using microcomputed tomography (micro-CT) which was likely more robust and accurate than the method employed in the present study. Conversely, when using similar sizes of NaCl porogens to produce porous PLLA scaffolds, the average pore sizes appeared to be larger than the NaCl porogens used to generate them.[340] This study also assessed the scaffold pore sizes using micro-CT. It was suggested that the way in which the micro-CT data was processed may have accounted for the apparently enlarged pore sizes. Smaller interconnected pores, produced by the individual porogens, may have been measured as singular large pores. It is unclear how the processing of this micro-CT data compared to that performed in the study on the porous thermally cured PGS scaffolds, so only limited comparisons can be made. However, it is possible to conceive that the lower stiffness of PGS-M and thermally cured PGS compared to PLLA may have resulted in

increased pore deformation and shrinkage after the removal of the porogen particles from the scaffolds, thus accounting for the differences between porogen sizes and scaffold pore sizes observed in the these studies. Additionally, the shrinkage of photocurable polymers, functionalised by methacrylation, has been observed in other biomaterial applications, such as dental resins.[343] Here, shrinkage of the photocured polymers was attributed to the reduction in the size of the methacrylate groups, as a result of the formation of crosslinks. A similar mechanism may also have affected the pores present in the porous PGS-M scaffolds.

It is important to also acknowledge the limitations of the method used to assess the sizes of the pores present in the PGS-M scaffolds. This utilised measurements of a selection of pores from the SEM images coupled to a correction factor to account for the nonequatorial location of the cutting plane through each pore. Most notably, this method was dependent on the assumption that the pores were spherical. Examination of the SEM images shows that this assumption may only be partially valid. The pores present across the different PGS-M scaffolds show a variety of shapes and were largely not spherical. This reflects the variety in the sucrose porogens used to produce the pores, which were likely not spherical and instead possessed more angular morphologies as a result of the crystalline nature of the sucrose. It may therefore be more prudent to not rely on the specific values for the average pore sizes determined for the scaffolds, using the SEM images, and only to rely on the trends demonstrated between the different sizes of the porogen particles and the sizes of the resulting pores in the scaffolds.

A semi-quantitative analysis of the wettability of the porous PGS-M disk scaffolds suggested that the scaffolds produced using the small sucrose particles were the most wettable. This may have been due to the smaller pores present in these scaffolds producing a larger surface area for contact with the PBS droplet, facilitating more rapid absorbance. It must be noted that there appeared to be little difference between the wettability of the different scaffold types with all appearing to be relatively hydrophobic. The PBS droplets formed tight beads, with surface contact angles

exceeding 90°, when initially placed on the surfaces of all of the scaffolds. Similar results have been observed in porous scaffolds produced from PLLA. These scaffolds showed large surface contact angles and little absorption over 1 hour.[301] Interestingly, the addition of PGS to these PLLA scaffolds produced a large improvement in the wettability of the scaffolds, with absorption times reducing from >1 hour to <30 seconds. The hydrophilic nature of PGS has been well established and is attributed to the non-bonded hydroxyl groups on the PGS polymer backbone.[301,344,345] It was therefore interesting that similar hydrophilicity was not seen in the PGS-M scaffolds, which possess the same polymer backbones with non-bonded hydroxyl groups. It may be that the addition of the methacrylate groups in the PGS-M is responsible for the hydrophobic nature of the material.

The hydrophobic nature of the PGS-M scaffolds was countered during their use in cell culture by pre-treating the scaffolds in appropriate growth medium. This allowed the embedding and attachment of proteins to the scaffold surfaces which then aid cell attachment by providing binding sites for integrins.[346]

The wetting behaviour of the different PGS-M scaffolds may also be a function of their permeability and the pore interconnectivity. However, it is difficult to distinguish the effects of these two factors. Both increased scaffold permeability and increased pore interconnectivity may facilitate the increased absorbance of the PBS droplets into the scaffolds.

The porosity of the PGS-M disk scaffolds was quantified using helium pycnometry. The results showed that the lowest ratio of PGS-M:sucrose particles that was used to produce a scaffold (1:3.8 for mixed sucrose particles) produced the greatest scaffold porosity, at 82.9 ± 0.7%. This was significantly different from the porosities of all of the other scaffolds examined. Since the porosity of the scaffolds was a result of the removal of the sucrose porogen particles, it would be expected to be directly related to the proportion of porogen particles used to produce the scaffolds. Therefore, it is understandable that the scaffolds produced with the greatest proportion of sucrose particles (lowest PGS-M:sucrose particle ratio) contained the greatest porosity.

Interestingly, the porosity of the scaffolds produced using the different sucrose particle sizes did not appear to correlate with the ratios of PGS-M:sucrose particles. At their optimum PGS-M:sucrose particle ratios, the scaffolds produced using the medium sucrose particles demonstrated significantly greater porosity than the scaffolds produced using the small sucrose particles. This may have been a result of the residual adhesiveness that was observed in the scaffolds produced using the small sucrose particles. This may have caused the closure of some of the pores which manifested as a reduced measurement of the scaffold porosity.

Also of note was that the only significant difference in porosity between the scaffolds produced using the same sucrose particle sizes at optimum and sub-optimum PGS-M:sucrose particle ratios was seen when using the mixed sucrose particles. Since the mixed sucrose particles were a mixture of medium and small particles, it may be possible that the small particles facilitated the formation of small pores which acted to connect the pores created by the medium particles. Indeed, examination of the SEM images of the different PGS-M scaffolds suggested this. Scaffolds produced using the mixed sucrose particles appeared to show small interconnecting pores that were not present in the scaffolds produced using the medium sucrose particles. Therefore, in the scaffolds produced using the mixed sucrose particles, the additional small particles present at the optimum ratio of PGS-M:sucrose particles compared to the sub-optimum ratio may have resulted in the formation of more small pore interconnections. This may have then resulted in a significant increase in scaffold porosity due to a reduction in non-connected pores.

The porosities of all of the PGS-M scaffolds produced were within the ranges of those shown to be successful for tissue engineering applications in previous publications where a porogen leaching method was employed. These appeared to range from 60% - 97%.[93,338–340]

Raman spectroscopy was used to determine if any residual sucrose remained in the porous PGS-M scaffolds after repeated washing in dH_2O. The spectra produced from the scaffolds that had been washed in dH_2O appeared to be similar to the spectra

produced by a sample of pure PGS-M. No peaks associated with the sucrose appeared to be present in the spectra from the washed scaffolds. As it was the interiors of the porous scaffolds that were examined, the results suggested that the washing process had been sufficient to remove the sucrose.

Although the peak positions in the spectra were comparable between the washed PGS-M scaffolds and the pure PGS-M sample, they showed different intensities, with those of the latter being higher. This was likely due to the difference between the surface geometries of the two samples. The pure PGS-M samples were disks and presented a flat surface as the target for the laser used during the Raman spectroscopy process. However, the porous nature of the PGS-M scaffolds, coupled to the laser spot size being within the size range of the pores (~50 μm), would have resulted in an uneven surface being presented as the target for the laser. The variation in the height of the surface examined in the porous scaffolds may have resulted in a spectrum with reduced intensity signals compared to that of a flat sample.

It is interesting to note that, although porogen leaching has been a widely utilised method for producing porous structures for tissue engineering in the literature, examinations of the success of the porogen removal processes is usually omitted or neglected. Here it has been demonstrated that Raman spectroscopy offers a simple and non-destructive method for determining the complete removal of the porogen particles from scaffold structures.

Cell viability and proliferation on the porous PGS-M scaffolds was examined using SMCs seeded onto the scaffolds and cultured for up to 7 days. Based on the examinations of the scaffolds produced using the different sizes of sucrose porogens, the scaffolds used for cell culture were produced using the mixed sucrose particles, at their optimum PGS-M:sucrose particle ratio. This particle size was selected because it resulted in the greatest scaffold porosity and this has been identified as advantageous in scaffolds for tissue engineering.[338–341] SMCs appeared to remain viable when cultured on the porous PGS-M scaffolds for 7 days. Comparing the results of the RR assays performed on cultures after 1 day and 7 days showed a significant increase in

metabolism present on the scaffolds. However, this increase cannot be interpreted as evidence of an increased number of SMCs present on the scaffolds after 7 days, as a result of cell proliferation, as discussed previously (3.4). It should also be noted that the PGS-M scaffolds appeared to be stained strongly by the purple resorufin that was produced during the RR assay. This suggested that some of this compound may have been retained by the scaffolds. In the RR assay, resazurin sodium salt is reduced to resorufin when exposed to the reducing environment present in viable cells. The resorufin content is then assessed, using fluorescence detection, to provide a relative measurement of the metabolic activity present in a sample. Any retention of resorufin by the PGS-M scaffolds may therefore have resulted in an inaccurate assessment of the metabolic activity present in the scaffolds.

Histological examination provided some insight into the level of cell proliferation on the SMC seeded scaffolds. Sections stained with H&E showed the presence of cells across the surfaces of the SMC seeded scaffolds and additional cells penetrating into the scaffold interiors. The cells did appear to be limited in numbers and no significant difference could be seen between the cultures after 1 day and 7 days. Given the growth rate the SMCs had demonstrated during 2D culture on TCP (population doubling time ~35 hours) it was expected that significant cell numbers would have been present after 7 days in culture on the PGS-M scaffolds.

Similar results, in terms of both the RR assay and the histological examination of the scaffolds, have been observed in the literature. Canine vascular SMCs cultured on PLLA scaffolds showed little change in metabolism or evidence of cell proliferation over 4 weeks.[340] The distribution of the SMCs within the PLLA scaffolds was similar to that observed in the PGS-M scaffolds. SMCs were present at the surfaces of the scaffolds and also sporadically in the interiors. This study used a similar cell seeding density and scaffolds with similar porosities to those employed herein. Alternatively, the proliferation of SMCs has been observed in static cultures on porous scaffolds produced by porogen leaching. This was attributed to mass transport effects within the scaffolds. Using sucrose particles as porogens, porous scaffolds were produce from PLGA and seeded with SMCs.[338] These scaffolds possessed mm scale villi structures

produced by shaping them in moulds. These villi were designed to increase the boundary surface area of the scaffolds and facilitate greater diffusion of oxygen and nutrients into the scaffolds. The results demonstrated proliferation of the SMCs seeded onto the scaffolds over 2 weeks with increased proliferation observed in the scaffolds with the smallest villi, and therefore the greatest boundary surface area. Limitations on mass transport into the scaffolds may have been responsible for the lack of SMC proliferation on the porous PGS-M scaffolds observed in the present study. To utilise the PGS-M scaffolds for producing TEVGs this limitation may be overcome by perfusion of the scaffolds in a dynamic culture system.

Examination of the SMC seeded PGS-M scaffolds using SEM showed the presence of sheets of ECM covering the scaffolds' porous surfaces. This was similar to the results observed in a previous study. Baboon SMCs were cultured on porous PGS scaffolds for 15 days.[189] At the end of the culture period the surfaces of the scaffolds appeared almost completely covered by a sheet of confluent cells and associated ECM. Trichrome staining suggested that this matrix was largely composed of collagen. It is possible that the matrix observed covering the PGS-M scaffolds seeded with SMCs also had a similar composition.

Following the confirmation of cell viability on the porous PGS-M disk scaffolds, methods for producing porous tubular scaffolds were investigated. These scaffolds were intended for applications in TEVGs.

The first method investigated, method i, appeared to be incompatible with the optimum ratios of PGS-M:sucrose particles that were identified for use in producing the porous scaffolds. This method shaped the PGS-M and sucrose mixture around a stainless steel rod and in a mould. This required the mixture to maintain a certain degree of cohesion and this could only be achieved at sub-optimum ratios of PGS-M:sucrose particles, due to the adhesive effect of the greater proportion of PGS-M present in the mixture. Examination of the scaffolds that were produced, using sub-optimum ratios of PGS-M:sucrose particles, suggested acceptable interior

porosities, but limited outer and luminal surface porosities due to the formation of skins of PGS-M polymer.

To counter the reduced cohesion demonstrated by the PGS-M and sucrose mixtures at the optimum ratio of PGS-M:sucrose particles, the mixtures were constrained inside syringes forming compacts. This technique was employed in the subsequent tubular scaffold fabrication methods that were explored. Method ii coupled the use of the syringes with a PVA rod to produce the middle of the tubular scaffolds. The PGS-M and sucrose compact, packed around the PVA rod, was extruded out of the syringes for photocuring. This produced suitable outer surface and interior porosity, but the luminal porosity continued to be limited be skin formation. Method iii attempted to remove the PVA rod; however, the lack of this constraint resulted in partial scaffold collapse during the extrusion of the PGS-M and sucrose compact out of the syringes. A porous luminal surface was produced, so to avoid the compacts collapsing, in method iv the PGS-M and sucrose compacts were shaped as in method iii, but were photocured while still inside the syringes and then extruded out. This resulted in scaffolds with suitable internal and luminal surface porosity; however, the outer surface now appeared to show the formation of polymer skin.

The results observed from using methods i-iv to produce porous tubular PGS-M scaffolds suggested that contact between the PGS-M and sucrose compact and a smooth surface during the photocuring process resulted in the formation of polymer skin layers that limited the porosity of the derived scaffolds. Contact between the stainless steel/PVA rods and the PGS-M and sucrose compact during photocuring resulted in polymer skin formation on the luminal surfaces of the scaffolds in methods i and ii. Contact between the syringe wall and the PGS-M and sucrose compact during photocuring resulted in polymer skin formation on the outer surface of the scaffolds in method iv. When the PGS-M and sucrose compacts were photocured without contact with a smooth surface, as in method iii, porous outer and luminal surfaces were produced. These results may have been due to some interaction between the PGS-M polymer and the smooth surfaces during the photocuring process. Alternatively, the extrusion of the PGS-M and sucrose compacts out of the syringes, prior to photocuring,

may have acted to remove PGS-M from the outer surface of the shaped compacts through shear. The formation of polymer skins during the production of porous scaffolds has been reported in the literature, but is usually attributed to solvation of the polymer materials used.[340] No solvent was used in the production of the tubular PGS-M scaffolds so the cause of the skin layers remains unclear.

Methods for fabricating the tubular PGS-M scaffolds were subsequently developed which avoided contact between the PGS-M and sucrose compacts and smooth surfaces during the photocuring process. Method v used sucrose particles packed into the middle of the PGS-M and sucrose compact tubes formed inside the syringes. This was intended to prevent the partial collapse of the compacts when they were extruded out of the syringes prior to photocuring, as was observed in method iii. The packed sucrose particles did not present a flat surface in contact with the PGS-M and sucrose compacts. The scaffolds produced using method v appeared to possess interior porosity and both outer and luminal surface porosity. Additionally, method vi explored photocuring the PGS-M and sucrose compacts as cylinders, and then removing the central cavities using a drill to produce tubes. The cylinders were formed inside syringes and extruded out for photocuring, as had proven successful in methods ii, iii and v. Although the drill appeared to produce porous luminal surfaces it caused damage to the scaffolds. This was likely a result of the interaction between the relatively soft photocured PGS-M and sucrose composite and the high rotation speed of the drill. It is possible that a lower cutting speed may produce improved results.

Method v was therefore selected for the production of the tubular PGS-M scaffolds that were used to generate the TEVGs. This method produced suitable scaffold structures with porous surfaces and interiors. Further analysis of these scaffolds demonstrated they possessed relatively conserved internal and outer diameters, although with some variation in their wall thicknesses. This was likely a result of variation in the alignment of the corer relative to the syringe barrel used in the scaffold manufacturing process. Since the corer and syringe barrel dimensions were conserved, these resulted in the relatively conserved values for the scaffolds' internal and outer diameters. Misalignment of the corer and syringe barrel resulted in differences in the

scaffold wall thicknesses. The dimensions of the scaffolds were within the range specified for use in the culture of the TEVGs (internal diameter ~3 mm, wall thickness <1.5 mm).

In addition to the methods for fabricating tubular PGS-M scaffolds, a method was also developed to produce scaffolds of varied and complex shapes, using a combination of additive manufacturing and porogen leaching. This process built up the scaffold structure by selectively photocuring layers of PGS-M and sucrose mixture. The sucrose was then removed from the photocured composite to produce porosity. A single scaffold structure was produced as a proof-of-concept. This appeared to conform to the intended design, a spiral of stacked disks. The disks appeared to be slightly larger than the hole through which they were selectively photocured using UV light. This was likely a result of scattering of the incident light by the white PGS-M and sucrose mixture. The layers of photocured PGS-M were able to fuse together, although not completely with some gaps observed, and the scaffolds demonstrated similar handling properties to the previously produced disk and tubular scaffolds, after the removal of the sucrose.

This method of scaffold fabrication requires further development. Investigations into using different sizes of the sucrose particles are required along with further characterisation of the scaffolds, particularly in relation to the interconnections created between the separately photocured PGS-M layers. It would also be desirable to enhance the selective photocuring mechanism by using image projection to define the geometry of each PGS-M layer. This, coupled to an automated method of delivering each additional layer of PGS-M and sucrose mixture into the build chamber, may produce a system capable of generating a wide range of predefined scaffold geometries.

4.5 **Conclusions**

Porous scaffold structures, suitable for use in tissue engineering, were produced from PGS-M using a porogen leaching method with sucrose particles. Combining PGS-M with sucrose particles of different sizes, at different ratios, allowed variation of the scaffolds' handling properties, pore sizes, porosities and wettability. SMCs seeded onto porous PGS-M scaffolds remained viable for 7 days in static culture and partially infiltrated the scaffold interiors.

A method was developed to produce the porous scaffolds as tubes of suitable geometry and porosity for use in the generation of TEVGs. Additionally, a method for producing porous PGS-M scaffolds in a variety of geometries, using additive manufacturing, was also demonstrated as a proof-of-concept. This process requires further development.

Chapter 5 - Design of a dynamic culture bioreactor for TEVGs

5.1 Introduction

The production of TEVGs requires specialised equipment and protocols. Producing a complex 3D structure cannot be achieved using standard cell culture equipment based on *in vitro* cell culture on 2D surfaces under static conditions.

Aside from a supporting scaffold, or some other means of directing the macroscopic shape of the vessel, a dynamic culture environment is also required to culture TEVGs. This usually takes the form of a bioreactor system. The use of bioreactors has been well established in the literature. In a number of studies, dynamic culture methods yielded superior results to static cultures when generating TEVGs and appear to be a prerequisite to generate TEVGs with sufficient mechanical strength to be employed *in vivo*.[61,66,75,84,87,93,98,122,169,233,336,347,348] Indeed, the research groups at the forefront of producing TEVGs, *in vitro*, utilise dynamic culture bioreactors.

Within the dynamic culture environment, the need to provide mechanical stimulation to developing TEVGs has also been well established. Niklason and Langer demonstrated this in their seminal work on producing TEVGs *in vitro* under pulsatile flow.[61] It was shown that TEVGs based on PGA scaffolds seeded with SMCs developed increased ECM contents and subsequent increased strengths as a result of the mechanical stimulation applied by the pulsatile flow. These findings have been replicated in a number of studies, using a variety of TEVG designs.[61,66,75,84,93,98,122,336]

In this chapter, the design of a dynamic culture bioreactor capable of supporting the culture of TEVGs *in vitro* is presented.

5.1.1 **Design brief**

Produce a bioreactor cable of supporting the growth and development of a TEVG *in vitro*. The TEVG will be composed of a PGS-M porous scaffold seeded with cells. The bioreactor culture environment will be regulated by an incubator. The bioreactor must culture the TEVG under dynamic conditions and apply mechanical stimulation.

5.2 **Materials and Methods**

In the following methods, all chemical reagents were obtained from Sigma Aldrich, UK unless otherwise stated. These reagents were measured and utilised in inert vessels.

5.2.1 **Identification of design objectives**

A list of design of objectives which the bioreactor design had to satisfy was identified. These were then expanded and arranged into an objectives tree to visualise their relationships to each other.[349–351]

5.2.2 **Functional analysis**

Based on the design brief for the bioreactor, a functional analysis was performed to define the scope of the design process and the relevant inputs, sub-functions and outputs.[349,351] The overall function of the bioreactor design was expressed as a simple conversion of inputs to outputs. The overall function was then broken down into sub-functions. These sub-functions would then be targeted during the process of generating initial ideas for design solutions.

5.2.3 **Performance specification**

A performance specification for the bioreactor design was produced. This defined the precise limits within which the design solution would operate.[349,351] Performance attributes were identified and targets and constraints quantified where possible.

5.2.4 **Design solution generation and evaluation**

Based on the functional analysis, described in (5.2.2), the bioreactor design was separated into sub-functions and solutions to these explored. A number of different initial design idea were proposed to achieve these sub-functions.

The initial ideas were then evaluated using a weighted objective evaluation matrix. This process quantified the success of each design in accomplishing the design requirements.[349,351] For each sub-function, several assessment criteria were proposed, guided by the design objectives and performance specification, described in (5.2.1) and (5.2.3). The assessment criteria were then ranked, using pairwise comparisons, and then weight factors assigned to them based on their relative importance towards achieving the overall design brief. The weight factors were assigned based on the distribution of a total score of 100 among the assessment criteria.

The success of each initial design in relation to the assessment criteria was then evaluated and given a score out of 5. These scores were then multiplied by their associated weight factors and the total score for each design, across all the assessment criteria, calculated and compared. A final design was then proposed based on the combined results.

5.2.5 **Manufacture of the bioreactor final design**

The proposed final design for the bioreactor, designated Bioreactor design 1.1, was constructed from a combination of bespoke and pre-manufactured components. These

were sourced from reputable vendors. Where possible, certified or guaranteed components were selected.

5.2.6 **Bioreactor leak testing**

The bioreactor was fully assembled with analogues for the TEVGs, produced from Tygon tubing, inserted into the flow circuit. The culture chamber was then filled with 600 ml of H_2O using the growth medium exchange tank. This was 100 ml greater than the normal working volume to ensure the joint between the culture chamber and its lid was in contact with the fluid. The flow circuit outlet line was positioned in the peristaltic pump (Masterflex L/S variable-speed drive with Easy-Load PPS, SS rotor pump head) and, after priming, the pump applied at 60 rpm. The pressure regulator valve was set to produce a relative pressure of 200 mmHg in the flow circuit, measured using the pressure transducer (MTL844, ADInstruments, UK). To simulate the culture of TEVGs, while the pump was active, the culture chamber was periodically handled (raised, lowered and tilted) and the attached tubing flexed. After 24 hrs, the pump was deactivated and the H_2O was removed from the culture chamber using the growth medium exchange tank. Throughout the testing period, the bioreactor was examined for leaks. Leak testing was conducted 3 times.

5.2.7 **Bioreactor design 1.1 sterilisation by autoclave**

The bioreactor was assembled with the lines which attached to the 0.22 µm air filters, fitted to the culture chamber lid and growth medium exchange tank, capped. The pressure transducer port was also removed and its inlet and outlet lines connected. The bioreactor was then sterilised by autoclave, at 121°C, for 30 minutes and then placed in a biological safety cabinet. Sterile air filters (Minisart®, Sartorius stedim biotech, Germany) were attached to the previously capped lines, and a sterile pressure transducer port attached to the corresponding inlet and outlet lines.

5.2.8 **Bioreactor design 1.1 sterility testing**

The bioreactor was sterilised as described in (5.2.7). 500 ml of fibroblast growth medium, prepared as described in (3.2.3), was then added to the bioreactor culture chamber using the growth medium exchange tank, inside the biological safety cabinet. The bioreactor was placed inside an incubator (Sanyo MCO 175 CO2) with the flow circuit outlet line running through an access port and fitted to the peristaltic pump outside. The pump was applied at 60 rpm. Additionally, 20 ml of fibroblast growth medium was placed in a polypropylene container, sterilised by gamma irradiation (Fisher Scientific, UK), and incubated in parallel with the bioreactor, to act as a positive control. The medium was inspected daily for signs of infection. After 7 days, the medium was withdrawn, via the growth medium exchange bottle, and an RR assay performed on triplicate 1 ml samples. 0.0251 (w/v) resazurin sodium salt was dissolved in dH_2O and the solution filter sterilised using a 0.22 µm filter. The resazurin solution was mixed 10% (v/v) with the samples of medium from the bioreactor, along with equivalent samples of positive control medium. These samples were then placed in the incubator. Additionally, equivalent samples of resazurin-containing fresh fibroblast growth medium were also incubated, in parallel, for use as a blank. After 4 hours, all samples were removed from the incubator and 200 µl of solution was extracted from each, in triplicate, and placed in the wells of a 96-well plate. This plate was then read using a fluorescence plate reader (Bio-tek instruments FLX800) at 540 nm excitation and 635 nm emission, with the reading from the blank subtracted.

The process of inserting a seeded PGS-M scaffold into the bioreactor was then simulated. Inside a biological safety cabinet, the lid was removed from the bioreactor culture chamber and three PGS-M scaffold analogues (Tygon tubes sterilised by autoclave at 121°C for 30 minutes) inserted into the flow circuit using sterile forceps. The lid was then reattached to the culture chamber and the bioreactor filled with 500 ml of fresh fibroblast growth medium. The bioreactor was returned to the incubator with the flow circuit outlet line running through an access port and fitted to the peristaltic pump, as previously. The pump was applied at 60 rpm and the pressure

regulator valve set to deliver a maximum relative intraluminal pressure of 200 mmHg (determined using the pressure transducer). As previously, 20 ml of fibroblast growth medium placed in a polypropylene container sterilised by gamma irradiation was also incubated in parallel with the bioreactor, to act as a positive control. The medium was inspected daily for signs of infection. After 7 days, the medium was withdrawn and an RR assay performed, as described previously, including the positive controls and blanks. The results were analysed using one-way ANOVA with Tukey multiple comparisons analysis. $P<0.05$ was considered significant (*), $P<0.01$ was considered very significant (**) and $P<0.001$ was considered extremely significant (***).

5.2.9 **Bioreactor design 1.2 sterilisation by peracetic acid**

The bioreactor was assembled with three PGS-M scaffolds, manufactured as described in (4.2.13) using method v, or scaffold analogues produced from Tygon tubing, connected to the TEVG channels of the flow circuit, inside the culture chamber. The cell seeding ports and the lines which attached to the 0.22 µm air filters, fitted to the culture chamber lid and growth medium exchange bottle, were capped. The bioreactor was sterilised in two steps: firstly the growth medium exchange bottle was sterilised followed by the bioreactor culture chamber and flow circuit. Working inside a biological safety cabinet, the growth medium exchange bottle was isolated from the rest of the bioreactor using the gate valve. 500 ml of a 0.5% peracetic acid solution in dH_2O was then added to the bottle and the lid closed. After 1 hour, the bottle was placed horizontally to sterilize the lid and associated air filter line. A sterile syringe was used to draw the acid solution up the air filter line fitted to the growth medium exchange bottle. After 1 hour, the bottle was righted and a sterile air filter (Minisart®, Sartorius stedim biotech, Germany) attached to the air filter line.

The gate valve was then opened and the bioreactor culture chamber filled with peracetic acid solution. An additional 100 ml of acid solution was added, making the total volume 600 ml (100 ml greater than the normal working volume). The peracetic acid was circulated through the bioreactor flow circuit using the peristaltic pump at

20 rpm. Sterile syringes (Terumo medical, USA) were used to draw the solution into the cell seeding ports and up the air filter lines in the culture chamber lid. After 1 hour, the acid was removed, through the growth medium exchange bottle, and the inside of the bioreactor rinsed with triplicate washes of 600 ml of sterile PBS.

5.2.10 **Bioreactor design 1.2 sterility testing**

The bioreactor was assembled with PGS-M scaffold analogues, produced from Tygon tubing, inserted into the flow circuit and was sterilised as described in (5.2.9). 500 ml of fibroblast growth medium, prepared as described in (3.2.3), was then added to the bioreactor culture chamber using the growth medium exchange bottle, inside the biological safety cabinet. The bioreactor was placed inside an incubator (Sanyo MCO 175 CO2) with the flow circuit outlet line running through an access port and fitted to the peristaltic pump outside. The pump was applied at 60 rpm. Additionally, 20 ml of fibroblast growth medium was placed in a polypropylene container, sterilised by gamma irradiation (Fisher Scientific, UK), and incubated in parallel with the bioreactor, to act as a positive control. The medium was inspected daily for signs of infection. After 7 days, the medium was withdrawn, via the growth medium exchange bottle, and an RR assay performed on triplicate 1 ml samples. 0.0251 (w/v) resazurin sodium salt was dissolved in dH_2O and the solution filter sterilised using a 0.22 µm filter. The resazurin solution was mixed 10% (v/v) with the samples of medium from the bioreactor, along with equivalent samples of positive control medium. Additionally, equivalent samples of resazurin-containing fresh fibroblast growth medium were also incubated, in parallel, for use as a blank. After 4 hours, all samples were removed from the incubator and 200 µl of solution was extracted from each, in triplicate, and placed in the wells of a 96-well plate. This plate was then read using a fluorescence plate reader (Bio-tek instruments FLX800) at 540 nm excitation and 635 nm emission, with the reading from the blank subtracted.

The process of seeding cells onto the PGS-M scaffolds inside the bioreactor was then simulated. Inside a biological safety cabinet, the TEVG channels were isolated from the

flow circuit, using the three-way stopcocks, and the cell seeding ports opened. 100 µl of fresh fibroblast growth medium was then injected into each port, using a pipette. A sterile syringe was then attached to each port and depressed to move the 100 µl volume of growth medium down the TEVG channels and into the scaffold analogues. The seeding ports were then closed and the TEVG channels reconnected to the flow circuit. The bioreactor was then filled with 500 ml of fresh fibroblast growth medium and returned to the incubator with the flow circuit outlet line running through an access port and fitted to the peristaltic pump, as previously. The pump was applied at 60 rpm and the pressure regulator valve set to deliver a maximum relative pressure of 200 mmHg (determined using the pressure transducer). As previously, 20 ml of equivalent fibroblast growth medium, placed in a polypropylene container sterilised by gamma irradiation, was also incubated in parallel with the bioreactor, to act as a positive control. The medium was inspected daily for signs of infection. After 7 days, the medium was withdrawn and an RR assay performed, as described previously, including the positive controls and blanks. The results were analysed using one-way ANOVA with Tukey multiple comparisons analysis. $P<0.05$ was considered significant (*), $P<0.01$ was considered very significant (**) and $P<0.001$ was considered extremely significant (***).

5.2.11 **Bioreactor design 1.2 flow rate measurement**

To determine the flow rate within the different channels of the flow circuit the bioreactor was prepared as described in (5.2.6), accept with just 500 ml of H_2O (normal working volume) added to the culture chamber. The pump was applied at 60 rpm for 5 minutes to remove any air from the system and then the three TEVG channels and the pressure transducer channel disconnected, downstream of the culture chamber, before they converged into the return line. The pump was then reapplied at 6, 20 and 60 rpm, for 1 minute, and the volume of dH_2O produced from each channel measured, in triplicate.

The results were statistically analysed using two-way ANOVA with Tukey multiple comparisons analysis. $P<0.05$ was considered significant (*), $P<0.01$ was considered very significant (**) and $P<0.001$ was considered extremely significant (***).

5.2.12 **Mechanical stimulation testing**

A pulsatile flow, generated by the peristaltic pump, would be used to apply mechanical stimulation to the TEVGs during culture. The flow was examined using an in-line pressure transducer, calibrated using a pressure gauge, in accordance with the manufacturer's instructions.

The bioreactor culture chamber was filled with 500 ml of dH_2O, as described (5.2.11). The pump was applied at 5, 20 and 60 rpm, with the pressure regulator valve fully open and then closed to produce a maximum relative pressure of 50 mmHg and 200 mmHg.

5.3 Results and Discussion

5.3.1 Identification of design objectives

A list of design objectives which the bioreactor design had to satisfy was identified. These were broadly defined as:

- Simple to manufacture
- Reliable operation
- High safety
- Good operating characteristics

These objectives were further expanded into more specific objectives and arranged into an objectives tree (Figure 62). This showed the relationships between the different objectives and demonstrated how achieving the specific objectives contributed to achieving the broader objectives. The identified design objectives were considered throughout the design process to inform decisions and evaluate competing solutions.

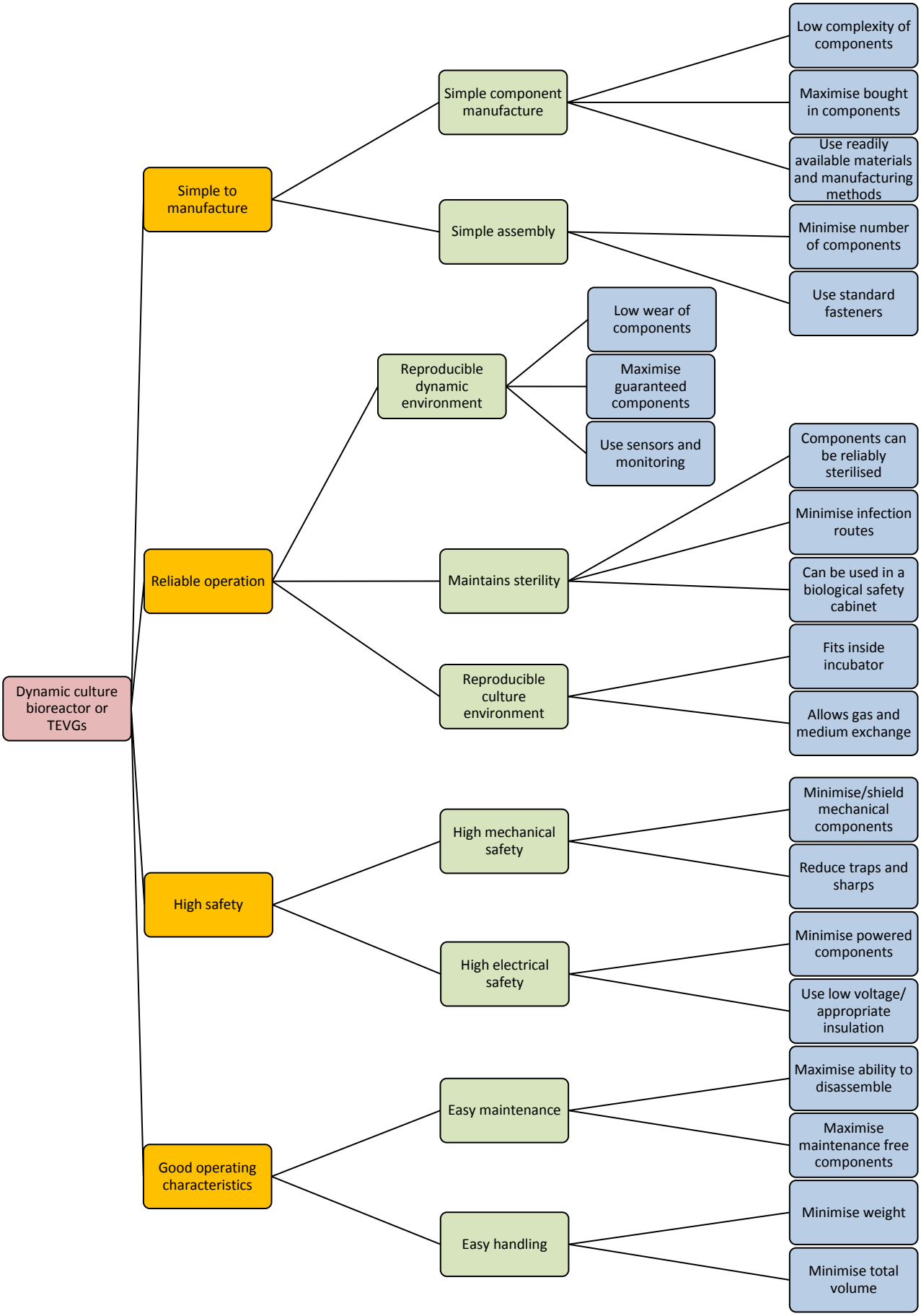

Figure 62. Design objectives tree for the design of the dynamic culture bioreactor for TEVGs.

5.3.2 **Functional analysis**

Based on the design brief, a functional analysis was performed to define the scope of the design process and the relevant inputs, sub-functions and outputs. Firstly, the overall function of the bioreactor design was expressed as a simple conversion of inputs (PGS-M scaffold + Cells) to outputs (TEVG). The overall function was then broken down into sub-functions. These included: sterilisation of the bioreactor before beginning the TEVG culture process, seeding the cells onto the PGS-M scaffold, culturing the seeded scaffold and applying mechanical stimulation (Figure 63). The design process now concentrated on generating solutions to these sub-functions.

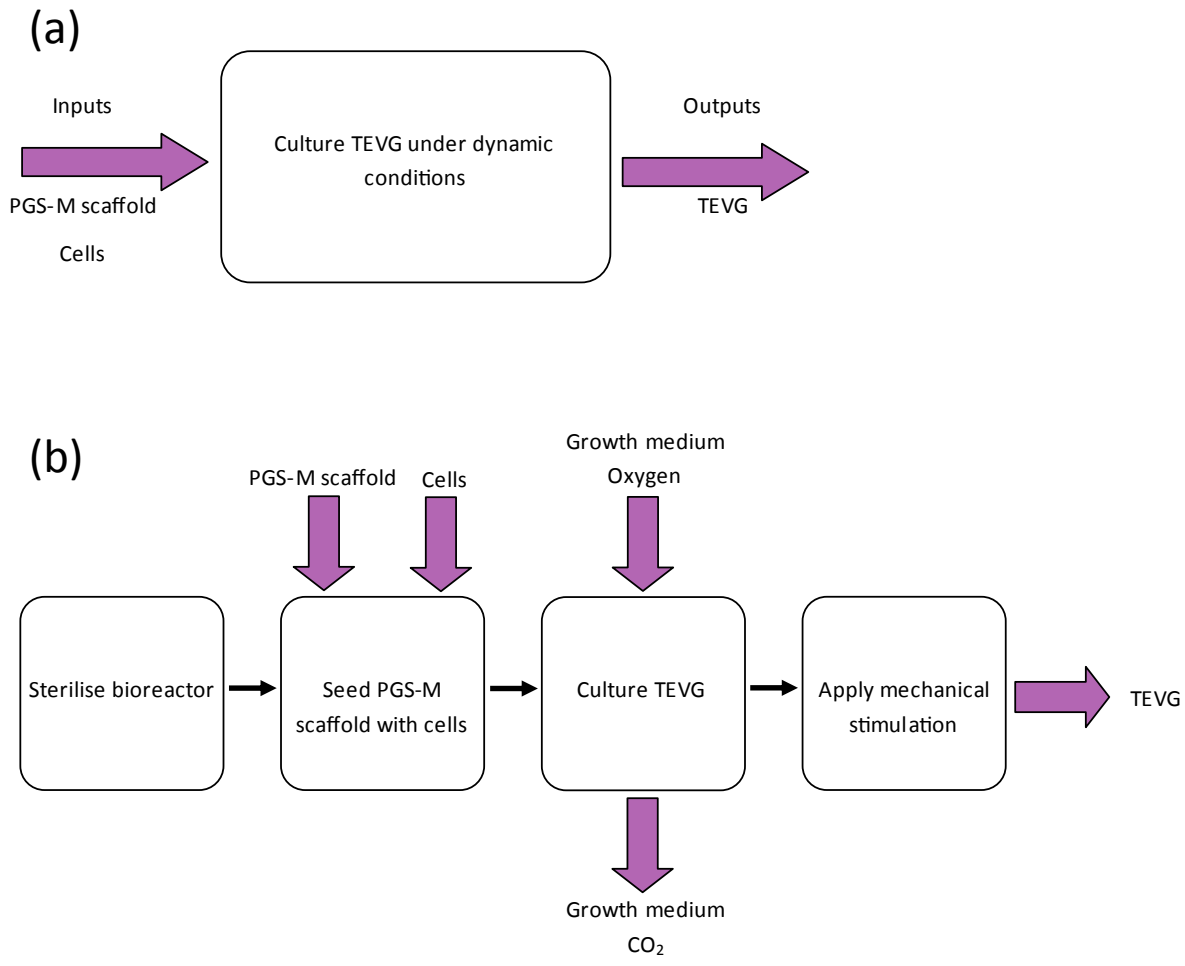

Figure 63. Functional analysis of the dynamic culture bioreactor for TEVGs.

5.3.3 **Performance specification**

A performance specification for the bioreactor design was produced (Table 11). This defined the precise limits within which the design solution would operate.

Some design constraints were implicit at the outset of the design process. These included the cost of the final design and the maximum overall dimensions which were a function of the incubator (Sanyo MCO 175 CO2) and biological safety cabinet (Herasafe™, Heraeus, USA) the bioreactor would be operated in. The maximum mass of the final design was based on a single operator handling the bioreactor with one hand.

It was decided that the bioreactor should be able to culture up to 3 TEVGs simultaneously. This would provide a suitable number of experimental replicates per bioreactor culture cycle, while minimizing the requirements for cells, growth medium and PGS-M scaffolds. The bioreactor should also be able to accommodate TEVGs of a maximum length of 80 mm and outer diameter of 5 mm. Grafts of this size would ultimately be suitable for a variety of characterisation procedures, such as burst pressure and compliance testing, along with implantation in a small animal model.[352]

Modes of sterilisation were selected based on those available. A variety of methods were proposed, including liquid based disinfection and steam sterilisation by autoclave.

A number of performance requirements were defined through the reviewing the literature. The minimum volume of growth medium the bioreactor could accommodate was selected based on the size of the culture chambers used in previously published bioreactors for TEVGs.[95,98,122,226,336,353,354] These were considered to present better guidance than scaling up the medium requirements from *in vitro* cell culture methods on flat surfaces based on the number of cells estimated to populate the TEVGs.

A number of studies on successfully generating TEVGs described using a cell seeding density of between 1 and 2 million cells per cm^2 of scaffold surface. The bioreactor must therefore be able to accept this number of cells, for three scaffolds, in a single cycle of use.[61,70,88,93] Additionally, in terms of mechanical stimulation, a cyclic radial

strain of 5-10% at a maximum of 180 Hz, applied to the TEVG was specified. This had proven to be a successful stimulation regime in a number of studies on TEVGs.[61,70,84] Performance attributes based on infection resistance, biocompatibility, material stability and safety were also defined.

Table 11. Performance specification for the dynamic culture bioreactor for TEVGs.

Attribute	**Specification**
Dimensions	TEVG culture chamber <400 x 400 x 250 mm, to fit inside incubator and biological safety cabinet (reduced size preferred). Ancillaries <500 x 500 x 500 mm These may remain outside the incubator, connected to the TEVG culture chamber through its access ports.
Mass	Total system <8 kg (reduced weight preferred).
Cost	≤£2,000 (reduced cost preferred). Disposable materials ≤ £30 per bioreactor culture.
TEVG size	Must be able to accommodate TEVGs of maximum 80 mm length and 5 mm diameter.
Yield	Must be able to culture up to 3 TEVGs per use cycle.
Volume	Must hold >300 ml of growth medium.
Sterility	Materials are resistant to 70% (v/v) ethanol in H_2O, 0.5% (v/v) peracetic acid in H_2O or autoclave at 121°C for 30 minutes for 1,000 sterilisation cycles. Disposable components must be purchased sterile and fitted in a biological safety cabinet.
Cell seeding	Seeding of cells permitted under sterile conditions or in a biological safety cabinet. Cell suspensions of 2 x 10^6 cells/cm^2 of scaffold permitted. Seeding method distributes cells throughout the PGS-M scaffold.
Mechanical stimulation	Up to 5-10% cyclic radial strain applied to TEVG. Maximum frequency 180 Hz. Monitoring and measurement of stimulation regime permitted.
Infection resistant	Growth medium contacting surfaces impermeable to water at 1 atm. Filters for gas exchange ≤ 0.22 μm pore size. Growth medium exchange permitted under sterile conditions or in a biological safety cabinet.
Biocompatible	Growth medium contacting surfaces are non-toxic.
Stable/reusable	Materials are corrosion resistant and non-reactive with the growth medium. Materials will not alter significantly in terms of chemistry or mechanical strength at between 0 and 121°C. Disposable materials minimised.
Safe	No sharp edges. Electrical components fully insulated. Mechanical components shielded to prevent injury.

5.3.4 **Design solution generation and evaluation**

Based on the functional analysis, the bioreactor design was separated into three sub-functions: cell seeding, TEVG culture and mechanical stimulation. While considering the design objectives and the performance specification, a number of initial design ideas were proposed to accomplish each sub-function (See Appendix).

The success with which each of the initial designs would achieve the design requirements for the bioreactor was then quantified using a weighted objective evaluation matrix. The assessment criteria used for evaluating the initial designs for each sub-function of the bioreactor are shown in Table 12, Table 13 and Table 14.

Weight factors for the assessment criteria and the scores for the initial design ideas are shown in Table 15,Table 16 and Table 17.

Table 12. Assessment criteria for the initial design ideas for the bioreactor cell seeding sub-function.

Assessment criteria	**Description**
Sterility	Assessment of how successfully the design would maintain sterility during cell seeding.
Cell viability	Assessment of how successfully the design would maintain cell viability.
Distribution on scaffold	Assessment of how well the design would distribute cells on the PGS-M scaffold.
Scaffold integrity	Assessment of the potential for the scaffold to retain integrity during cell seeding.
Operation	Assessment of how easily the design may be used.
Manufacture	Assessment of how easily the design could be manufactured.

Table 13. Assessment criteria for the initial design ideas for the bioreactor TEVG culture sub-function.

Assessment criteria	**Description**
Sterilisation	Assessment of how easily the design could be successfully sterilised prior to beginning TEVG culture.
Medium exchange	Assessment of how easily growth medium could be removed and replaced without damaging the developing TEVGs and while maintaining sterility.
Gas exchange	Assessment of the potential for sufficient gaseous exchange during TEVG culture.
TEVG harvest	Assessment of how the design allows for the successful removal of the culture TEVG while retaining their viability and sterility.
Handling and operation	Assessment of how easily the design may be manipulated during use.
Manufacture	Assessment of how easily the design could be manufactured.

Table 14. Assessment criteria for the initial design ideas for the bioreactor mechanical stimulation sub-function.

Assessment criteria	**Description**
Accuracy	Assessment of how accurately the mechanical stimulation could be applied.
Repeatability	Assessment of how successfully the mechanical stimulation regime could be repeated.
Cell viability	Assessment of how successfully the design would maintain cell viability.
Scaffold integrity	Assessment of the potential for the scaffold to retain integrity during stimulation.
Operation	Assessment of how easily the mechanical stimulation could be applied.
Manufacture	Assessment of how easily the design could be manufactured.

Table 15. Weighted objective evaluation matrix for the initial designs of the bioreactor cell seeding sub-function.

Assessment criteria	**Initial designs**					
	1	**2**	**3**	**4**	**5**	**Weight factor**
Sterility	3	3	5	4	4	20
Cell viability	5	5	3	5	4	20
Distribution on scaffold	1	4	2	5	4	14
Scaffold integrity	4	3	1	5	2	16
Operation	4	4	5	4	3	12
Manufacture	5	5	5	1	3	18
Final score (weight factors applied)	376	402	354	396	338	
Rank	**3rd**	**1st**	**4th**	**2nd**	**5th**	

The results of the weighted objective evaluation matrix for the initial designs for the cell seeding sub-function showed that design 2 appeared to be the most suitable solution. This design scored well due to its ease of manufacture and operation and its potential success in retaining cell viability and distributing cells evenly throughout the scaffold. The key aspect of this design was that cell seeding was proposed to be conducted outside of the bioreactor. This reduced the complexity of the seeding system by allowing standard cell culture equipment to be employed. Scaffolds would be seeded with cells intraluminally, using a pipette and forceps, in petri dishes. An even distribution of cells throughout the scaffold would be achieved simply by rotating the scaffolds manually during seeding. The seeded scaffolds would then be inserted into the bioreactor for further culture. This method of cell seeding did present the greatest potential for infection however, as any manipulation of the seeded scaffolds, even inside a biological safety cabinet, would increase the risk of acquiring infection. This risk was determined to be acceptable given the benefits in simplicity and operation that the design offered.

Table 16. Weighted objective evaluation matrix for the initial designs of the bioreactor TEVG culture sub-function.

Assessment criteria	**Initial designs**				
	1	**2**	**3**	**4**	**Weight factor**
Sterilisation	5	4	3	5	22
Medium exchange	3	3	5	1	20
Gas exchange	4	5	5	4	14
TEVG harvest	4	2	4	4	16
Handling and operation	4	2	1	5	10
Manufacture	4	1	2	5	18
Final score (weight factors applied)	346	274	318	320	
Rank	**1st**	**4th**	**3rd**	**2nd**	

The results of the weighted objective evaluation matrix for the initial designs of the bioreactor TEVG culture sub-function revealed that design 1 appeared to be the most suitable solution. This design was considered easy to successfully sterilise, with the potential to use ethanol, peracetic acid or autoclaving, and allowed for the TEVGs to be easily harvested at the completion of the culture period. Additionally, the design would be simple to manufacture and operate. Exchange of growth medium was permitted via an exchange bottle linked to the culture chamber. This represented the weakest area of the design. Although the bottle could be placed inside a biological safety cabinet for medium exchanges, this would increase the risk of infective agents entering the system. This risk was outweighed by the advantages in manufacturing and sterilisation that the design offered.

Table 17. Weighted objective evaluation matrix for the initial design ideas for the bioreactor mechanical stimulation sub-function.

Assessment criteria	**Initial designs**					
	1	**2**	**3**	**4**	**5**	**Weight factor**
Accuracy	3	5	3	5	4	16
Repeatability	3	5	3	5	4	16
Cell viability	5	1	5	1	4	22
Scaffold integrity	5	1	4	1	3	20
Operation	5	3	5	2	1	12
Manufacture	4	2	5	2	1	14
Final score (weight factors applied)	422	302	404	290	294	
Rank	**1st**	**3rd**	**2nd**	**5th**	**4th**	

The results of the weighted objective evaluation matrix for the initial designs of the bioreactor mechanical stimulation sub-function suggested that design 1 would be the most suitable solution. This design would be easy to operate and had the greatest potential for maintaining cell viability and scaffold integrity. The design applied a pulsatile flow of growth medium through each TEVG, producing cyclic radial strain and providing mechanical stimulation to the developing grafts. This was a proven method in the culture of TEVGs and represented a biomimetic solution where the natural environment of blood vessels was simulated.[61,75,88,95,98,116,125,175] This would allow suitable parameters for flow rates and pressures to be suggested from the literature. The design would also be simple to manufacture, as the mechanical components to provide the pulsatile flow could be purchased as a single peristaltic pump unit designed for this purpose. An inline pressure transducer would allow the fluid pressure inside each TEVG to be measured without disrupting the culture. However, regular monitoring would be needed to ensure adjustments to the pressure could be made in order to maintain a constant level of mechanical stimulation.

5.3.5 **Final design – Bioreactor design 1.1**

The most suitable initial designs for the bioreactor sub-functions, identified using the weighted objective evaluation matrices, were integrated together into a final design for the bioreactor, Bioreactor design 1.1. A schematic drawing is shown in Figure 64.

The design featured a single culture chamber capable of supporting up to 3 TEVGs at once, submerged in growth medium. PGS-M scaffolds would be seeded with cells and then connected to the bioreactor through on opening at the top of the culture chamber, covered by a lid. This would be performed in a biological safety cabinet to reduce the risk of infection. The reverse process would be used to harvest the TEVGs at the completion of the culture.

The growth medium in the culture chamber would be exchanged through a bottle connected via a feed line. To fill the chamber, the medium exchange bottle would be placed inside a biological safety cabinet and filled with growth medium under sterile conditions. The medium would then be gravity fed into the culture chamber. The reverse of this process would be used to remove growth medium for exchange.

Gaseous exchange between the bioreactor and the incubator would be achieved through sterile 0.22 µm filters attached to the culture chamber lid. These filters could be purchased sterile and attached to the bioreactor inside a biological safety cabinet. A filter was also fitted to the medium exchange tank to prevent air locks during the filling process.

The culture chamber acted as the reservoir for the flow circuit that would provide mechanical stimulation to the TEVGs. The flow circuit ran from the chamber and passed through a peristaltic pump before branching into channels which connected to the TEVGs. Growth medium would be drawn from the culture chamber and pumped, as a pulsatile flow, through the lumens of the TEVGs before converging and returning to the culture chamber. A channel of the flow circuit also ran outside of the culture chamber, in parallel with the TEVGs, to allow the pressure transducer to be connected. A pressure control valve positioned downstream of the TEVGs would allow the intraluminal pressure to be modulated.

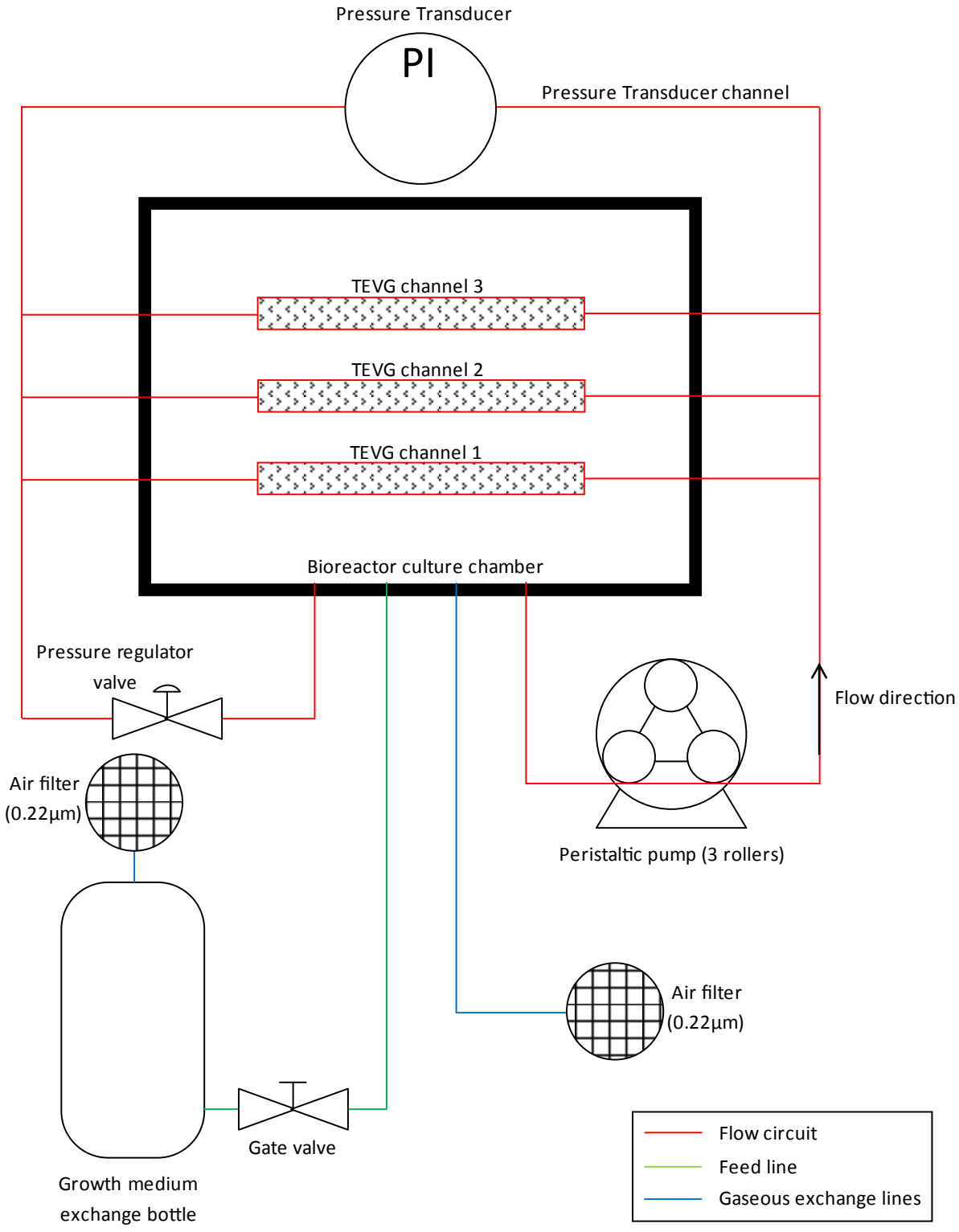

Figure 64. Schematic drawing of bioreactor design 1.1.

The performance requirements for the flow circuit in terms of pressure and flow rate were determined from the literature. A maximum pressure of 200 mmHg, a maximum flow rate of 15 ml/min and a maximum frequency of 3 Hz (180 beats per minute) were suggested.[61,93,122] These values were within the physiological range of human blood flow.[355] The assembled bioreactor could be sterilised by autoclave or by filling it with ethanol or peracetic acid and circulating these through the flow circuit.

The bioreactor was assembled from a range of bespoke and pre-manufactured parts (Table 18). The use of pre-manufactured parts was maximised to reduce costs. In addition to this, certified or guaranteed components were selected, where possible, to improve the reliability of the bioreactor.

The complete assembly of bioreactor design 1.1 is shown in Figure 65.

Table 18. Parts list for bioreactor design 1.1.

Component	Material/Product	Manufactured/Purchased	Comments
Culture chamber + lid	Polycarbonate	Manufactured	Excellent strength, autoclavable, resistant to relevant chemicals (ethanol, peracetic acid, growth medium, H_2O, PBS), easily machined, biocompatible, transparent.
Tubing	Pharmed BPT (flow circuit) Tygon ND 100-65 (TEVG channels and gaseous exchange lines) C-flex (flow circuit and feed line)	Purchased (Cole-Parmer, UK)	Autoclavable, chemically resistant to relevant chemicals (ethanol, peracetic acid, growth medium, H_2O, PBS), biocompatible. Pharmed BPT – 10000 hour peristaltic pump life. Tygon ND 100-65 – highly flexible to aid seeded scaffold installation, transparent. C-Flex – highly flexible to aid pressure regulator valve action and medium exchange tank handling.
Tubing fittings	Nylon/Polypropylene	Purchased (Cole-Parmer, UK)	Autoclavable, available in a range of sizes.
Growth medium exchange tank	Borosilicate glass	Manufactured	Autoclavable, transparent.
Pressure regulator valve	Polypropylene pinch valve	Purchased (Cole-Parmer, UK)	Autoclavable, screw action for precise control.
Gate valve	Polypropylene pinch valve	Purchased (Cole-Parmer, UK)	Autoclavable.
Sterile filters	Minisart®, Cellulose acetate filter	Purchased (Sartorius stedim biotech, Germany)	Pre-sterilised by gamma irradiation.
Pump	Masterflex L/S variable-speed drive with Easy-Load PPS, SS rotor pump head.	Purchased (Cole-Parmer, UK)	Variable speed control, compatible with various tubing sizes, 3-roller pump head utilised in published TEVG culture.[61]
Pressure transducer	MLT844 physiological pressure transducer	Purchased (ADInstruments, UK)	Pressure monitoring between -20 and 300 mmHg. Measures pressure without contact with the flow (reduced infection risk).

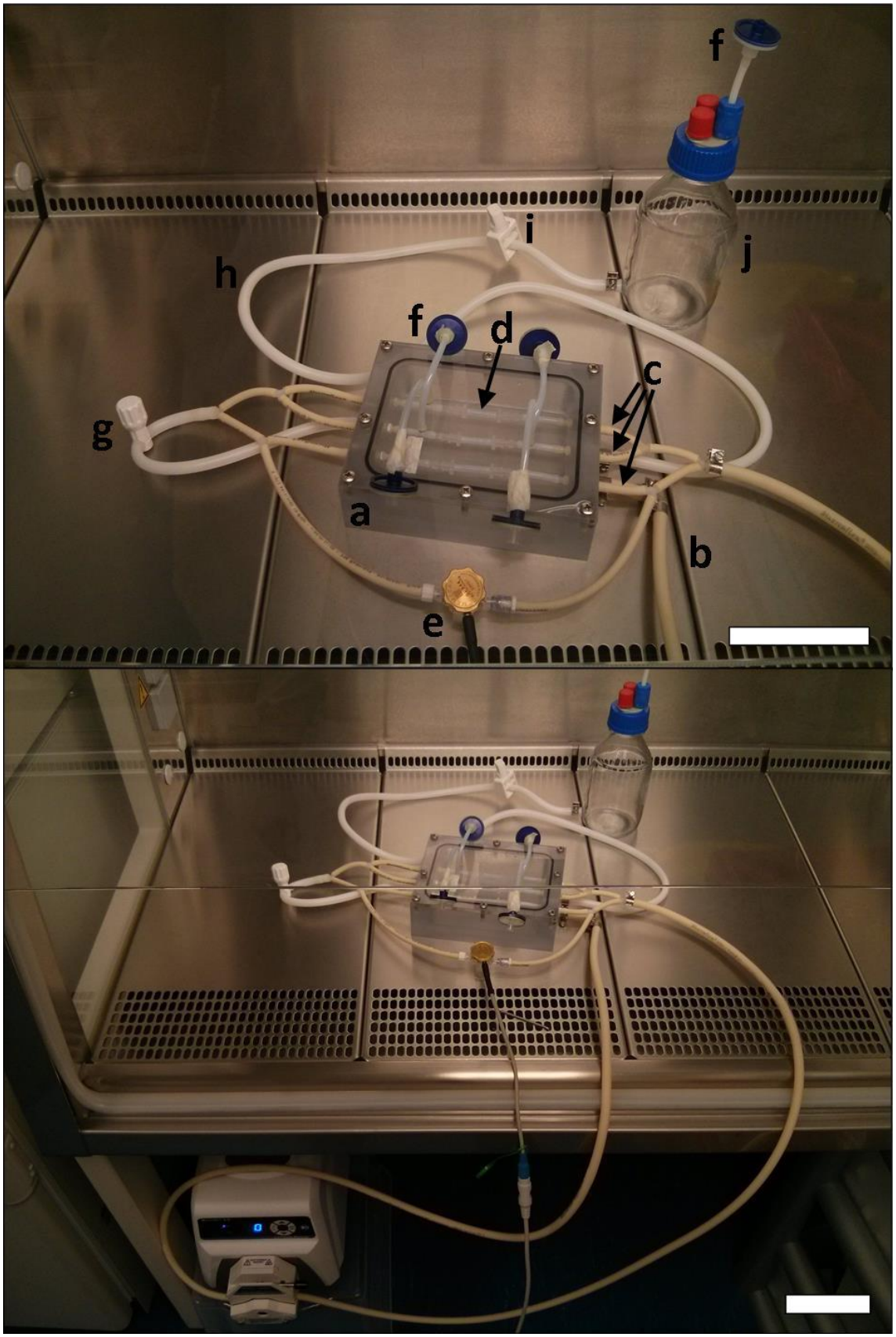

Figure 65. Bioreactor design 1.1. (Above) components are labelled: TEVG culture chamber (a), flow circuit (b), TEVG channels (c), TEVGs (d), pressure transducer (e), air filters (f), pressure regulator valve (g), feed line (h), gate valve (i), growth medium exchange bottle (j). (Below) Bioreactor attached to the peristaltic pump. Scale bars are 10 cm.

5.3.6 **Bioreactor leak testing**

The fully assembled bioreactor was filled with H_2O to examine it for leaks. Analogues for the PGS-M scaffolds, made from Tygon tubing, were inserted into the flow circuit and the peristaltic pump applied at 60 rpm, with the regulator valve set to produce a relative pressure of 200 mmHg within the flow circuit.

In three consecutive tests over 24 hours, no leakage was detected between the bioreactor culture chamber and its lid or around the fittings which connected tubing within the flow circuit. On the initial test, some leakage was detected around the threaded fittings which were used to connect the various lines of tubing to the culture chamber. These fittings were subsequently reinforced using PTFE tape wrapped around their screw threads. No leakage was detected at these points in the following tests.

The results demonstrated that the bioreactor was capable of functioning at the maximum operating pressure and flow pulse frequency designed for without leaking. The system was also robust and able to be manipulated and handled, in a similar fashion to during TEVG culture, without failure.

5.3.7 **Bioreactor design sterility testing**

The culture of TEVGs was simulated in the bioreactor to determine if a sterile environment could be maintained. The bioreactor was sterilised by autoclaving and then filled with fibroblast growth medium and incubated for 7 days. During this time no changes in the colour or clarity of the medium were observed. After 7 days, a sample of the medium was removed and a RR assay performed to determine if any metabolic activity was present. The results demonstrated no significant difference between the fluorescence produced by the samples of bioreactor medium and samples of medium cultured in parallel in a sterile container (positive control). This suggested that there was no metabolic activity present in the medium sample and that the bioreactor had remained sterile. The insertion of three PGS-M scaffolds was then

simulated, using analogues produced from sterile Tygon tubes (Figure 66). During the first repeat, after 3 days, the bioreactor appeared visibly infected with the growth medium pale and cloudy. An RR assay was not performed, in accordance with laboratory protocol. An RR assay was performed on the positive control sample, after 7 days, and this had remained sterile (Figure 67). The experiment was repeated, this time with more stringent sterile conditions employed by using a surgical grade sterile gown and forceps. After 7 days of incubation, following the insertion of the scaffold analogues, the growth medium in the bioreactor appeared unchanged. However, the results of the RR assay suggested that an infection was present, with a significantly greater fluorescence value generated by the medium sample, compared to the controls (Figure 67). These results suggested that it was the insertion of the scaffold analogues that had compromised the sterility of the bioreactor. This process involved the culture chamber being opened for several minutes while the analogues were manipulated inside it. Although this was conducted in a biological safety cabinet, it was clear that infective agents were able to enter the bioreactor.

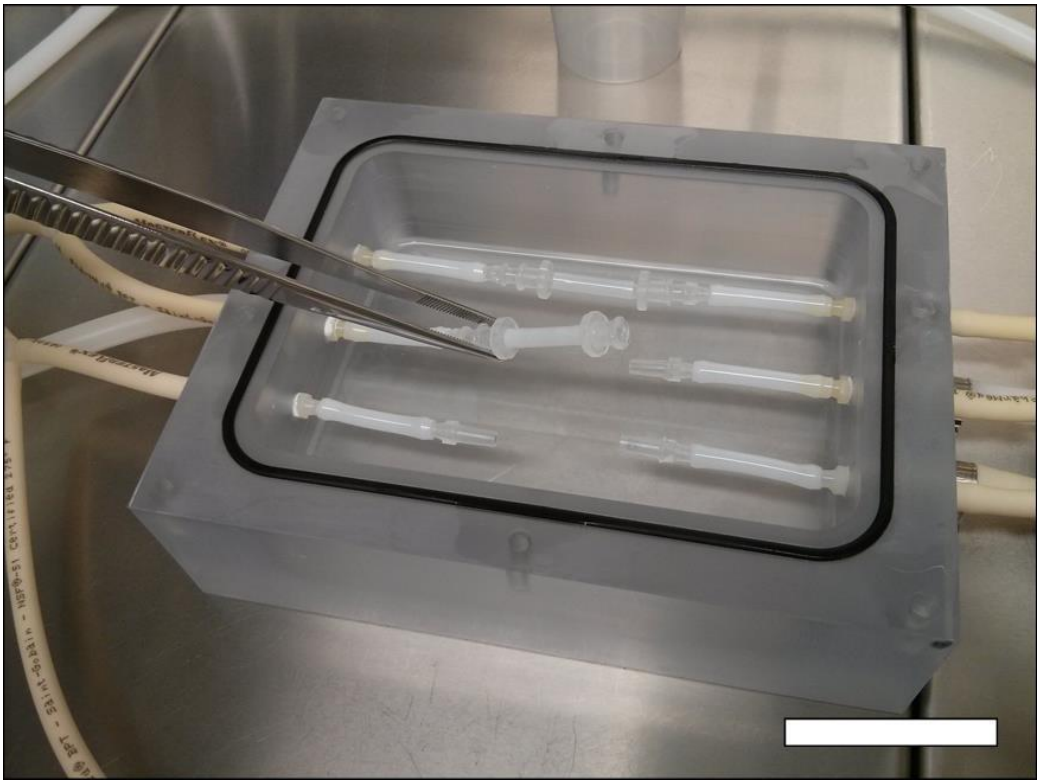

Figure 66. Simulated insertion of PGS-M scaffolds into bioreactor design 1.1. Scale bar is 5 cm.

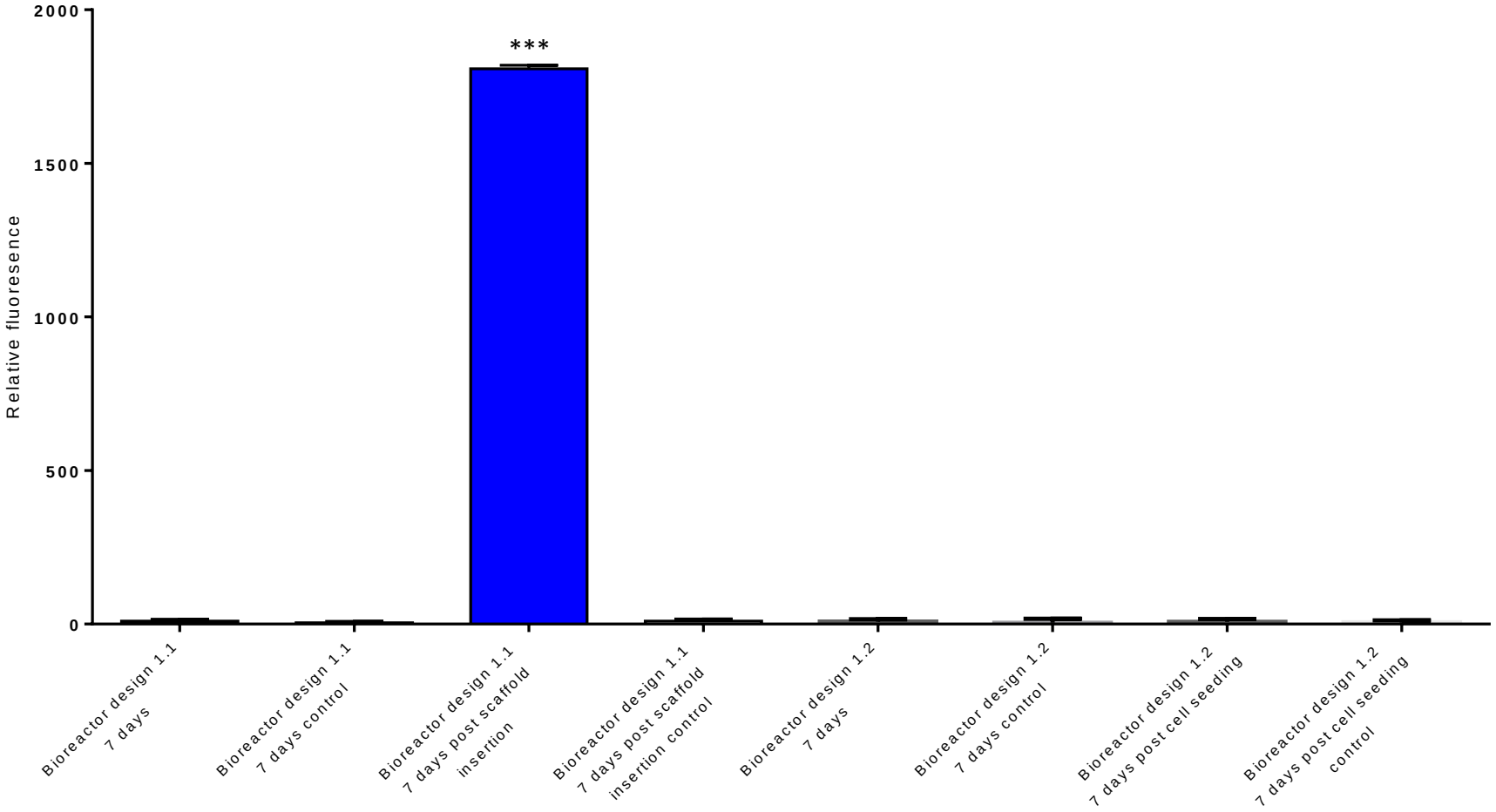

Figure 67. RR assay for testing the sterility of bioreactor designs 1.1 and 1.2. In design 1.1, growth medium was incubated in the bioreactor for 7 days (*n*=2) or for 7 days following the simulated insertion of TEVGs (*n*=1). Controls were equivalent growth medium incubated in parallel in sterile conditions (*n*=2). In design 1.2, growth medium was incubated in the bioreactor for 7 days (*n*=3) or for 7 days following simulated cell seeding (*n*=3). Controls were equivalent growth medium incubated in parallel in sterile conditions (*n*=3). Error bars are SEM.

In light of these results, the bioreactor design was modified to remove the need for PGS-M scaffolds seeded with cells to be inserted. This design had been selected because of the advantages that seeding the scaffolds outside of the bioreactor offered, allowing them to be manipulated more easily during seeding and also to be rotated easily to produce even cell coverage across their lumens. Based on a review of the initial designs for the cell seeding sub-function of the bioreactor and considering the current design, it was decided to add cell seeding ports to the TEVG flow channels. These ports could be opened to allow cell seeding onto PGS-M scaffolds already inside the sterile bioreactor. The bioreactor could also be placed on either side, following cell seeding, to encourage the attachment of cells to either side of the scaffold lumen to produce greater coverage. A schematic of the modified bioreactor, designated Bioreactor design 1.2, is shown in Figure 68. The cell seeding ports could be isolated from the flow circuit using 3-way stopcocks. This would ensure that during cell seeding, all of the suspended cells were directed towards the PGS-M scaffolds in the culture chamber.

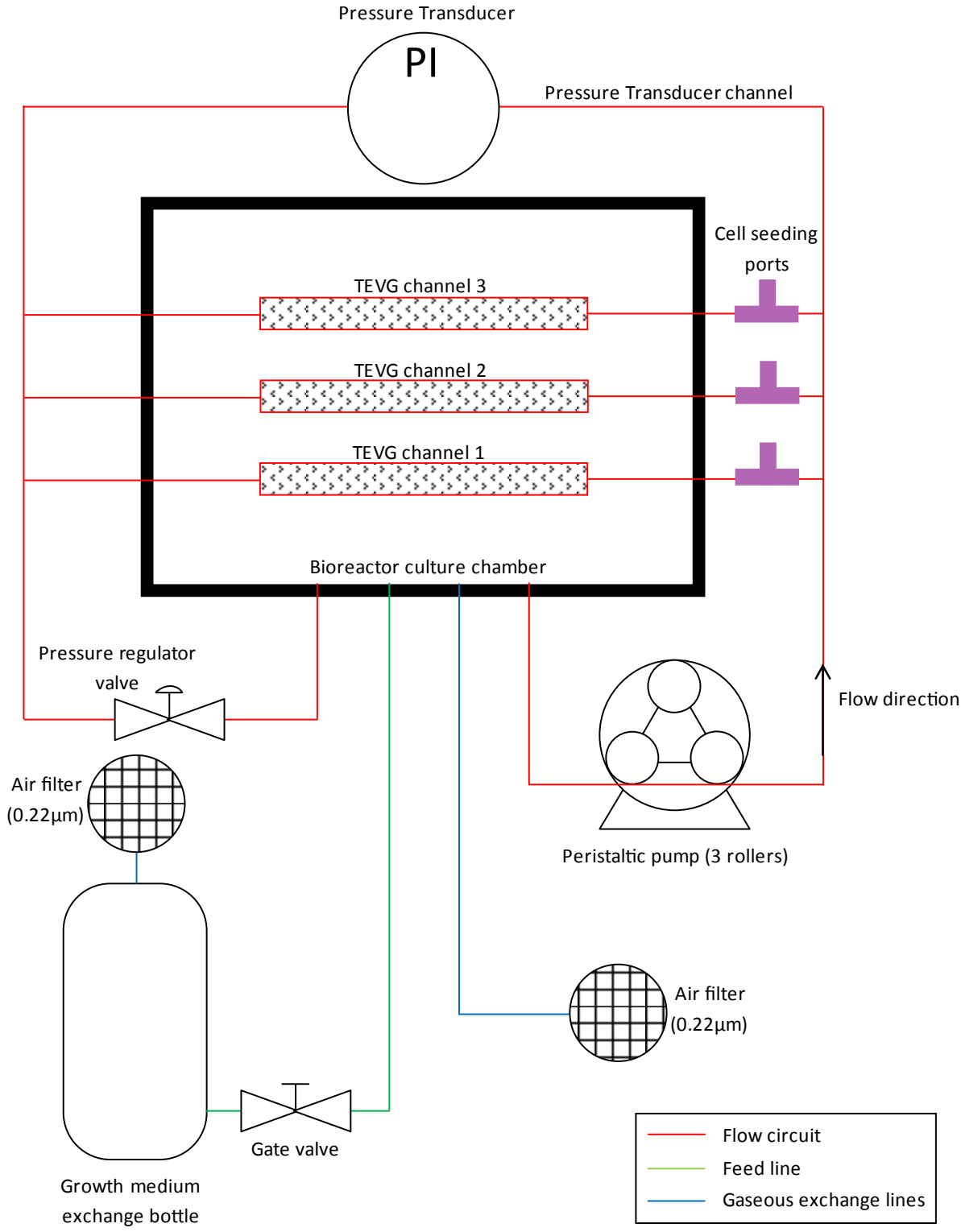

Figure 68. Schematic drawing of bioreactor design 1.2. Cell seeding ports are in purple.

Additionally, it was noticed during the assembly of bioreactor design 1.2 that the polycarbonate culture chamber was displaying signs of stress cracking. These appeared to be focused around stress concentrations, such as the threaded holes which accepted fittings for the various tubing lines attaching to the culture chamber. It was determined that the most likely cause of these stress cracks was the autoclave sterilisation process which exerted high temperatures and pressures on the bioreactor. Although polycarbonate had been selected as the material for the culture chamber based on its ability to be autoclaved, it appeared that the design of the bioreactor had compromised this. As a result, an alternative sterilisation method using 0.5% peracetic acid was employed. This treatment had been shown to be biocidal, fungicidal and sporicidal and used successfully in a number of tissue engineering and biomaterial sterilisation processes.[356–361] It had also been demonstrated that peracetic acid could be used to sterilise PGS-M structures without a significant effect on their mechanical properties. Therefore, using peracetic acid allowed the PGS-M scaffolds to be installed in the bioreactor culture chamber during the sterilisation process.

The complete assembly of bioreactor design 1.2 is shown in Figure 69.

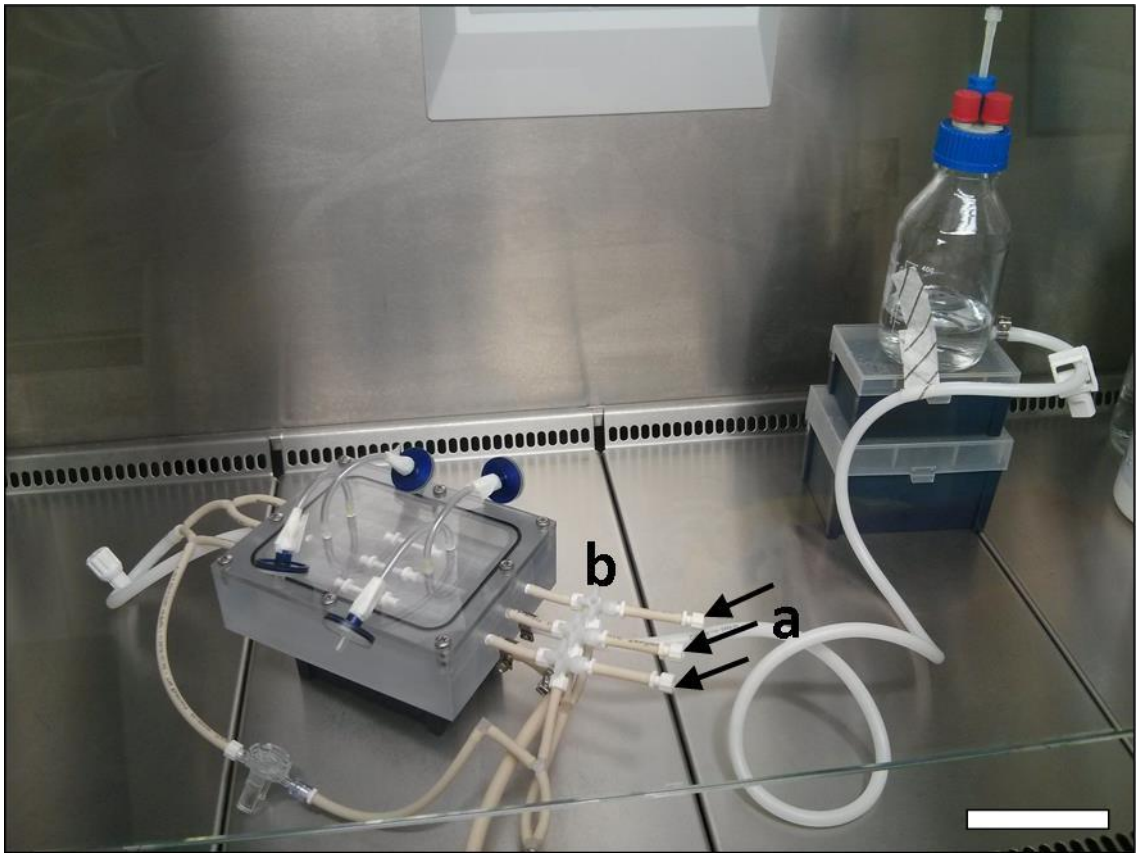

Figure 69. Bioreactor design 1.2. The modifications from the previous design are labelled: cell seeding ports (a) and 3-way stopcocks (b). Scale bar is 10 cm.

Following successful leak testing of bioreactor design 1.2, sterility testing was performed. Tygon PGS-M scaffold analogues were inserted into the culture chamber and the bioreactor was sterilised using peracetic acid, before being filled with fibroblast growth medium and incubated for 7 days. As observed in bioreactor design 1.1, no signs of infection were observed over this time period. Additionally, a RR assay performed on a sample of growth medium extracted from the bioreactor did not show any significant difference compared to the sterile control medium, cultured in parallel, both producing negligible fluorescence values (Figure 67). The process of seeding cells onto the PGS-M scaffolds, through the cell seeding ports, was then simulated. Following this the bioreactor was again filled with growth medium and incubated for 7 days. Again, no signs of infection were observed over the incubation period. Additionally, unlike in the previous bioreactor design, the results of the RR assay also

suggested that the bioreactor had remained sterile, with only negligible fluorescence values generated, with no significant difference from the positive controls. The sterility tests were performed three times, with equivalent results. The modified design of the bioreactor, bioreactor design 1.2, could be successfully sterilised using, peracetic acid, and maintain sterility during simulated operation.

5.3.8 **Bioreactor design 1.2 flow rate measurement**

The flow rates in the different bioreactor channels were measured at 6, 20 and 60 rpm. The results are shown in Figure 70. The flow rates appeared to increase linearly with increasing pump rpm. No significant differences were seen between the flow rates in any of the channels at 6 and 20 rpm. At 60 rpm, the flow rates in all three TEVG channels were statistically significantly different from the pressure transducer channel ($P<0.001$, in all comparisons), but not significantly different from each other. The flow rate in the pressure transducer channel appeared to be significantly greater than in any of the TEVG channels.

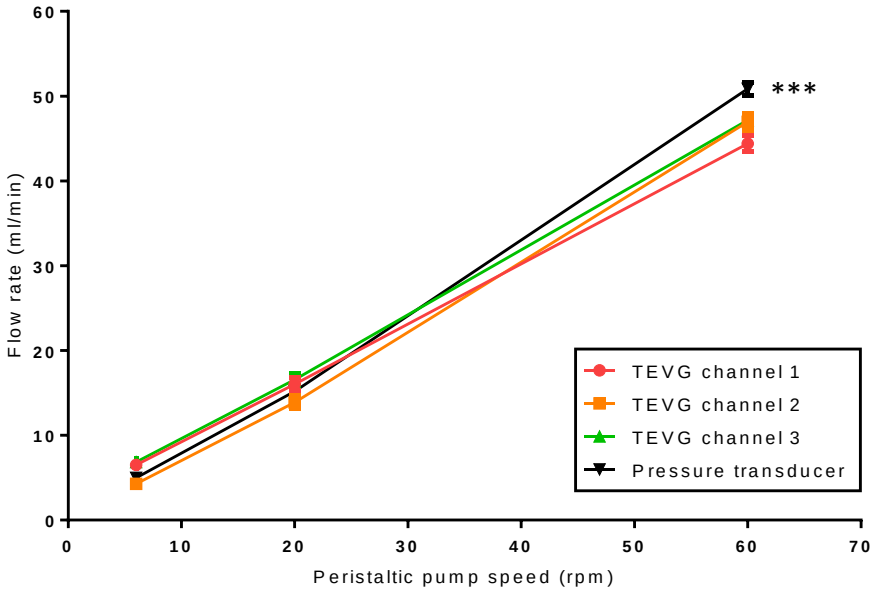

Figure 70. Bioreactor channel flow rates at 6, 20 and 60 rpm. Error bars are SEM (*n* = 3).

The maximum flow rate required in each channel was specified as 15 ml/min. This was achieved at ~20 rpm in all of the channels.

The difference in flow rates may have been due to the differences between the designs of the channels. The three TEVG channels were all of equal length and composition (tubing material, fittings and TEVG analogue). The pressure transducer channel was different to the TEVG channels. It did not feature the same fittings, as it did not have cell seeding ports, it was not required to pass through the bioreactor culture chamber, and had a port for the attachment of the pressure transducer, instead of a TEVG analogue. The differences between the designs of the pressure transducer channel and the TEVG channels may have had an effect on the pressure losses experienced within the flow passing through them. The greater number of fittings may have caused greater pressure losses in the TEVG channels compared to the pressure transducer channel. All of the fittings had a smaller internal diameter than the tubing attached to them. This change in diameter, and thus flow cross-section, would have likely resulted in some disturbance of the flow, in the form of turbulence, and therefore resulted in pressure losses across the TEVG channels. With fewer fittings, the pressure transducer channel experienced a lower pressure drop. The effect of pressure losses on flow rate is demonstrated by considering Bernoulli's principle (Equation 1).

$$\frac{1}{2}\rho(C_2^2 - C_1^2) + \rho g(z_2 - z_1) + P_2 - P_1 + P_{Loss} = 0$$

Equation 1. Bernoulli's principle for steady flow with losses. Fluid density (ρ), fluid pressure (P), fluid velocity (C), elevation (z), acceleration due to gravity (g).

All of the bioreactor channels were supplied by the same peristaltic pump and during the measurement of their flow rates they exhausted into the atmosphere, therefore the difference in pressure between the flow inlet and outlet ($P_2 - P_1$) was the same for all of the channels. Additionally, all of the channels were horizontal and at equal

heights during the flow rate measurements, therefore any difference in elevation could be discounted. Subsequently, any change in fluid velocity (flow rate) is a result of pressure losses only, with increased pressure losses resulting in a reduced fluid velocity. The equation assumes that the fluid is incompressible, which is a robust assumption for dH_2O at atmospheric pressure and temperature. The equation also assumes that the flow is steady. The peristaltic pump did not produce a completely steady flow. Instead, a pulsatile flow was generated due to the action of the rollers which moved the fluid. However, it was assumed that the flow within each fluid pulse was steady and therefore the assumption was valid.

The difference between the flow rates observed in the TEVG channels and the pressure transducer channel were acceptable within the parameters of the bioreactor design. Critically, the flow rates within the TEVG channels were not significantly different. This would insure that during culture of TEVGs each graft would be subjected to comparable flows and therefore would be comparable to each other when analysed. The pressure transducer channel was designed to allow the pressure inside the TEVG channels, and therefore inside the TEVGs, to be measured. The reduced pressure losses generated by this channel may result in an overestimate of the pressure in the TEVG channels. This could be accounted for during the bioreactor culture and could also be considered to provide a degree of safety against over-pressurising the TEVGs during culture.

The design of the bioreactor could have been improved by adding in-line flow rate and pressure monitoring (non-invasive) to each individual TEVG channel. This could be accompanied by valves to allow adjustments to be made to the flow in each channel. This would have added complexity to the design, but would likely result in a more uniform flow regime within the TEVGs.

5.3.9 **Mechanical stimulation**

Modulation of the pulsatile flow, generated by the peristaltic pump, was examined to determine if the system was suitable for applying mechanical stimulation to the TEVGs

during culture. Using the pressure transducer, the pulsatile flow was measured at 6, 20 and 60 rpm with the relative intraluminal pressure set at 0, 50 and 200 mmHg using the pressure regulator valve.

It was shown that the pressure pulse could be modulated between the rpm and pressure range examined (Figure 71). At a given rpm, the intraluminal pressure could be accurately altered using the pressure regulator valve. With the regulator valve fully open, only a small fluctuation in pressure was observed in the flow at 6 and 20 rpm (~-2-3 and ~-4-7 mmHg, respectively), however, at 60 rpm, the pulse ranged from ~-10-45 mmHg. With the regulator valve set to deliver a maximum pressure of 50 mmHg, a similar pressure variation was seen across all three pump speeds, although at 20 and 60 rpm, a small period of negative pressure was generated at the end of each pulse (~-7 and ~-10 mmHg, respectively). Finally, when the regulator value was set to deliver a maximum pressure of 200 mmHg, the pressure pulse remained positive throughout. The pressure range covered in a single pulse increased with increasing rpm, from amplitudes of ~120 mmHg to ~140 mmHg at 6 and 60 rpm, respectively.

As the speed of the peristaltic pump increased, the time between each roller acting on the fluid decreased, resulting in shorter periods when the pump was not applying pressure. Therefore each pressure pulse was unable to subside and return to a near-zero pressure value before the following pulse began.

The results demonstrated that a pressure pulse ranging from 0-200 mmHg could not be generated in the bioreactor flow circuit at between 6 and 60 rpm. The maximum range possible was from ~60-200 mmHg at 60 rpm. A maximum flow pressure of 200 mmHg was specified as a design target for the bioreactor, based on similar designs in the literature. However, the pressure pulse amplitude was not considered. Engbers-Buijtenhuijs *et al*. did report using a pressure wave form ranging from 61 to 124 mmHg in the culture of TEVGs based on collagen and elastin scaffolds. This range had been selected based on the physiological blood pressure range in humans. Considering the biomimetic nature of the bioreactor herein, it was suggested that its performance would generate a suitable pressure range for applying mechanical

stimulation to TEVGs during culture. The maximum healthy blood pressure range within adult humans is 120 mmHg systolic to 60 mmHg diastolic and the average heart rate is 50-80 beats per minute. In adolescence, blood pressure is at its highest, ranging from 140 mmHg systolic to 60 mmHg diastolic at 60-105 beats per minute. In newborns, blood pressure is lower, at 100 mmHg systolic to 50 mmHg diastolic, but heart rate is at its fastest, at 100-160 beats per minute.[355] Considering these values and converting the pump rpm to beats per minute by multiplying by 3, due to the 3 rollers in the pump head, all of these pressure and frequency ranges could be produced by the bioreactor. The design, therefore, represented a suitable system for applying biomimetic mechanical stimulation to TEVGs.

It may be possible that TEVG development may actually be enhanced by mechanical stimulation operating outside of the normal human blood pressure and flow ranges. This may be examined to some degree using the current design of the bioreactor, as both the pressure and flowrate could be increased beyond the physiological values.

It was also noted that the pressure wave forms generated by the peristaltic pump appeared to be noisy. This was most apparent at 6 and 20 rpm, with smoother profiles generated at 60 rpm. This was likely a result of friction between the rollers of the peristaltic pump head and the flow circuit tubing. This friction was overcome as the rpm increased, resulting in a smoother application of pressure to the circulating fluid and a smoother pressure wave profile. Given the erratic pressure waveforms that natural blood vessels, in vivo, are subjected to as a result of the cardiac cycle, this was not considered to be potentially detrimental to the culture of the TEVGs.[355]

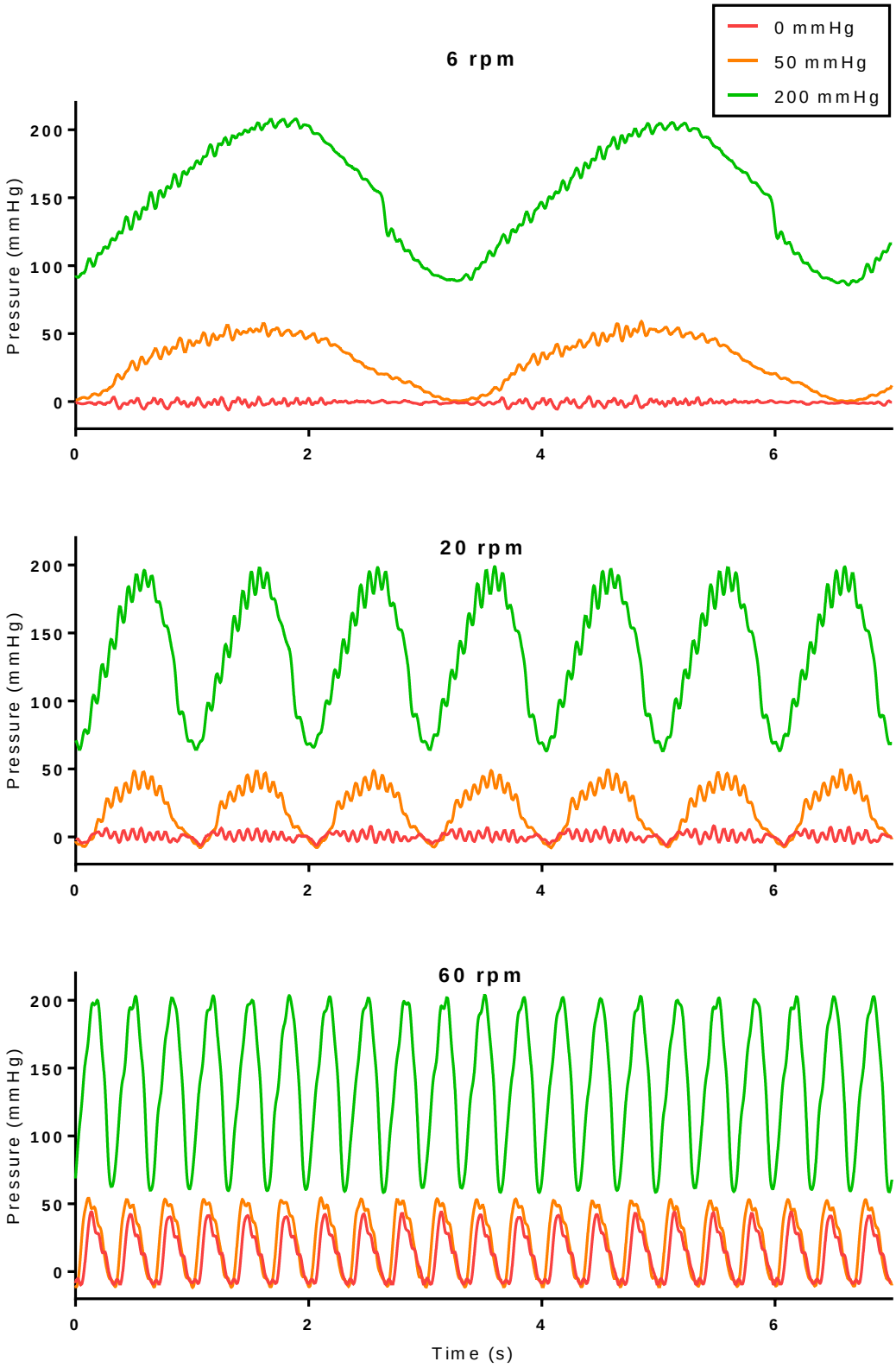

Figure 71. Bioreactor flow circuit relative pressure at pump speeds of 6, 20 and 60 rpm. The maximum relative pressure was modulated using the regulator valve and set to deliver 0 (fully open), 50 and 200 mmHg.

5.4 **Conclusions**

The design brief proposed at the beginning of this chapter was to produce a bioreactor cable of supporting the growth and development of TEVGs *in vitro*. The TEVGs would be composed of porous PGS-M scaffolds seeded with cells. The bioreactor culture environment would be regulated by an incubator and the bioreactor had to culture the TEVGs under dynamic conditions and apply mechanical stimulation.

The design process reported yielded a bioreactor that satisfied the design brief. It was demonstrated that bioreactor design 1.2 could be successfully sterilised and maintained a sterile environment throughout the simulated culture of a TEVG. The bioreactor was also capable of providing mechanical stimulation to the developing TEVGs, through a pulsatile flow. This flow could be modulated to produce pressures and flow rates within the range of physiological blood flow which were appropriate for the culture of TEVGs.

Chapter 6 - Bioreactor culture of TEVGs

6.1 Introduction

In the previous chapters, tubular scaffolds suitable for supporting the growth of TEVGs *in vitro* were fabricated from 30% Low M_w PGS-M. Additionally, a bioreactor capable of supporting the culture of TEVGs under dynamic conditions, through the application of mechanical stimulation, was designed and manufactured.

In this chapter, the technologies described previously are combined to produce TEVGs *in vitro*. Tubular PGS-M scaffolds were seeded with SMCs and cultured under dynamic and static conditions, for 7 days, as TEVGs. These grafts were then examined for cell proliferation, phenotype and ECM content to determine the effect of the different culture methods.

6.2 Materials and Methods

In the following methods, all chemical reagents were obtained from Sigma Aldrich, UK unless otherwise stated. These reagents were measured and utilised in inert vessels.

6.2.1 Sterilisation of tubular PGS-M scaffolds

Tubular scaffolds, 30 mm in length, were produced from 30% Low M_w PGS-M combined 1:3.8 with sucrose porogens (mixed size, 1:1 blend of 50-100 µm and 38-50 µm), using method v as described in (4.2.13).

Three different methods of sterilising the scaffolds were examined. In the first method, the PGS-M scaffolds were swelled by immersion in a 70% ethanol in dH_2O solution for 24 hours. The barbed ends of female luer x 1/8" hose barb nylon fittings (Cole-Parmer,

UK) were then inserted into each end of the swollen scaffolds. The scaffolds, with attached fittings, were then immersed in dH_2O. This caused them to contract and shrink around the fittings. This prevented the fittings from being pulled out of the scaffolds during handling. The scaffolds remained in dH_2O for 72 hours, with the dH_2O refreshed every 24 hours. After this time, the scaffolds were sealed in autoclave bags and sterilised by autoclave at 121°C for 30 minutes.

In the second sterilisation method, the PGS-M scaffolds were again placed in the ethanol solution; however, this was refreshed every 24 hours, three times, under sterile conditions inside a biological safety cabinet. After the third ethanol wash, female luer x 1/8" hose barb nylon fittings which had been sterilised by autoclave, at 121°C for 30 minutes, were inserted, using the barbed end, into each end of the scaffolds using forceps. The scaffolds were then soaked in sterile dH_2O for 24 hours, three times.

In the final sterilisation method, the scaffolds were prepared as described in the first method, except instead of autoclave bags, the scaffolds were placed in 50 ml of dH_2O inside borosilicate glass bottles and autoclaved, while submerged, at 121°C for 30 minutes. These scaffolds were subsequently incubated in SMC growth medium, prepared as described in (3.2.3) for 24 hours, with parallel samples of control medium also incubated.

6.2.2 **Sectioning of PGS-M scaffolds/TEVGs**

Fixed scaffolds/TEVGs were immersed in OCT compound (Tissue-Tek, Sakura, Japan) and frozen at -20°C. Frozen samples were mounted on stubs and cryosectioned (Lieca CM1860 UV), at -25°C, across their cross-sections, at a thickness of 5 µm. Sections were mounted on glass slides (Superfrost® Plus, Menzel-Gläser, Germany) and, after 24 hours, rinsed in dH_2O to remove the OCT compound.

6.2.3 **H&E staining of sections of PGS-M scaffolds/TEVGs**

Sections of PGS-M scaffolds/TEVGs, prepared and affixed to glass slides as described in (6.2.2), were immersed in Modified Harris haematoxylin solution for 90 seconds and then rinsed in H_2O for 4 minutes. They were then immersed in eosin Y solution for 5 minutes before being rinsed with H_2O, twice, followed by 70% IMS (Fisher Scientific, UK) solution in H_2O, then IMS and then Xylene. Samples were then coated with DPX mountant, covered with glass coverslips and allowed to dry for 12 hours. The sections were imaged using light microscopy (Zeiss Stemi 305 for low magnification, Motic B5 professional series for higher magnification). Staining was conducted on quadruplicate sections taken from each scaffold/TEVG sample.

Sections of human umbilical cord, prepared as described in (3.2.10), were also stained for use as positive controls.

6.2.4 **RR assay on used SMC growth medium**

Samples of used SMC growth medium, taken from the PGS-M scaffold sterilisation experiments or the bioreactor cultures, were examined for metabolic activity using the RR assay. Associated samples of control growth medium which had been incubated in parallel to the scaffold sterilisation experiments and bioreactor cultures were also examined. 0.0251 (w/v) resazurin sodium salt was dissolved in dH_2O and the solution filter sterilised using a 0.22 µm filter. The resazurin solution was mixed 10% (v/v) with triplicate samples of used SMC growth medium, and associated control medium, and placed in an incubator. Additionally, equivalent samples of resazurin-containing fresh SMC growth medium were also incubated, in parallel, for use as a blank. After 4 hours, all samples were removed from the incubator and 200 µl of solution was extracted from each, in triplicate, and placed in the wells of a 96-well plate. This plate was then read using a fluorescence plate reader (Bio-tek instruments FLX800) at 540 nm excitation and 635 nm emission, with the reading from the blank subtracted.

Results were analysed using two way ANOVA with Tukey multiple comparisons analysis. $P<0.05$ was considered significant (*), $P<0.01$ was considered very significant (**) and $P<0.001$ was considered extremely significant (***).

6.2.5 **Seeding of SMCs onto tubular PGS-M scaffolds**

Triplicate PGS-M scaffolds were sterilised by autoclave while immersed in dH_2O, as described in (6.2.1). They were then placed, individually, in petri dishes (100 x 25 mm, Fisher Scientific, UK) containing 60 ml of SMC growth medium and incubated at 37°C and 5% CO_2 for 24 hours, in preparation for cell seeding.

Human coronary artery SMCs (Promocell, Germany) were expanded on TCP in flasks, as described in (3.2.5). SMCs between passage 9 and 10 were harvested using trypsin (0.025%)/EDTA (0.01%) solution at 0.067 ml/cm^2 of culture area. This was quenched after 5 minutes with an equal volume of trypsin inhibitor (PromoCell, Germany) and the cell suspension centrifuged at 1200 rpm for 4 minutes (Hettich Zentrifugen Rotofix 32A with 131 mm rotor radius) before being resuspended in SMC growth medium at 13.6 x 10^6 cells/ml.

Using a pipette and forceps, the suspended SMCs were seeded intraluminally onto the PGS-M scaffolds in their petri dishes, following the removal of the growth medium. 110 µl of the cell suspension was applied to the lumen of each scaffold, this would result in a seeding density of 2 x 10^6 cells/cm^2 of lumen surface area.[70,88,93] The scaffolds in petri dishes were returned to the incubator for 6 hours, to allow for cell attachment. After this time, 60 ml of SMC growth medium was applied to each petri dish before being returned to the incubator again. After 12 hours, the growth medium was removed from the petri dishes and the scaffolds rotated axially 180°. Cell seeding was then repeated, as previously, and the scaffolds incubated for 6 hours again, before being immersed in 60 ml of growth medium, in their petri dishes, and incubated for a further 12 hours. Finally, all scaffolds were rinsed with PBS, three times, and then fixed with 3.7 % formaldehyde (methanol free) for 24 hours. After this, they were rinsed with PBS, three times, and stored in PBS until analysed.

Unseeded scaffolds acted as negative controls. These were incubated, rotated and fixed in an equivalent manner to the cell seeded scaffolds, except with cell-free SMC growth medium applied to their lumens. Experiments were performed in duplicate.

6.2.6 **Bioreactor culture of TEVGs under dynamic and static conditions.**

Bioreactor design 1.2, as described in (5.3.7), was assembled with triplicate, 30 mm long, tubular PGS-M scaffolds inserted into the TEVG channels of the flow circuit. The scaffolds were sterilised by autoclave while immersed in dH_2O, as described in (6.2.1), prior to insertion into the bioreactor. The bioreactor was then sterilised using 0.5% peracetic acid, as described in (5.2.9). Following this, the bioreactor was filled with 500 ml of SMC growth medium, using the growth medium exchange bottle, and placed in an incubator at 37°C and 5% CO_2 for 24 hours.

SMCs were then seeded onto the PGS-M scaffolds inside the bioreactor culture chamber. Working inside a biological safety cabinet, the growth medium was withdrawn from the bioreactor culture chamber into the exchange bottle and held there by closing the gate valve. The TEVG channels were isolated from the flow circuit, using the three-way stopcocks, and the cell seeding ports opened. SMCs, between passage 9 and 10, were cultured and suspended in SMC growth medium as described in (6.2.5). 110 µl of the cell suspension was then injected into each of the cell seeding ports, using a pipette. A sterile syringe was then attached to each port and depressed to move the 110 µl volume of growth medium down the TEVG channels and into the PGS-M scaffolds. The seeding ports were then closed and the TEVG channels reopened to the flow circuit. The bioreactor was then returned to the incubator with the culture chamber placed down on one of the sides that was parallel with the scaffolds axis of rotation. After 6 hours, the gate valve was opened and the SMC growth medium returned to the culture chamber. After a further 12 hours, the growth medium was once again withdrawn into the exchange bottle and the cell seeding process repeated. This time, the bioreactor culture chamber as placed down in the incubator on the opposite side to the previous occasion. Again, after 6 hours, the growth medium was

released back into the culture chamber. After a further 12 hours, the flow circuit outlet line was run through an access port in the incubator door and fitted to the peristaltic pump. For dynamic culture, where mechanical stimulation was applied to the TEVGs by a pulsatile flow, the peristaltic pump was then activated at 6 rpm with the pressure regulator valve set to deliver a relative pressure of 10 mmHg inside the TEVG channels, measured using the pressure transducer. Over the next 7 days, the pump and pressure were altered as described in Table 19. After 7 days, the pump was deactivated and the growth medium withdrawn from the culture chamber into the exchange bottle. Working inside a biological safety cabinet, the culture chamber was opened and the scaffolds, now considered TEVGs, were removed using forceps and rinsed with PBS, three times, before being fixed with 3.7 % formaldehyde (methanol free) for 24 hours. After this, they were rinsed with PBS, three times, and then cut into three equal lengths and stored in PBS until analysed.

TEVGs were also cultured under static conditions. In this case, the bioreactor was assembled and seeded with cells as described above, however the pump was only activated for 1 minute, to fill the flow circuit with growth medium. The pump remained off for the remaining 7 days of the culture.

Additionally, unseeded PGS-M scaffolds were also cultured to act as negative controls. These were cultured as described for the seeded scaffolds under dynamic conditions, however, without cells seeded onto them. Instead, 110 µl of fresh SMC growth medium was injected into each of the cell seeding ports.

TEVGs cultured under static conditions and unseeded negative controls were fixed and cut into three equal lengths as described for the TEVGs cultured under dynamic conditions.

Table 19. Pump speed and pressure regime for TEVGs under dynamic culture.

Day	Peristaltic pump speed (rpm)	Relative pressure in TEVG channels (mmHg)
1	6	10
2	6	12
3	7	15
4	7	18
5	8	21
6	9	24
7	10	27

6.2.7 **Staining of TEVGs for collagen**

Sections of TEVGs were prepared as described in (6.2.2). Staining was performed with Sirius red. Direct red 80 was dissolved at 1 mg/ml in saturated aqueous picric acid to produce the stain. The stain was applied to dry sections and left for 18 hours at room temperature. The sections were then rinsed with H_2O, twice, followed by 70% IMS (Fisher Scientific, UK) solution in H_2O, then IMS and then Xylene. Samples were then coated with DPX mountant, covered with glass coverslips and allowed to dry for 12 hours. The sections were imaged using light microscopy as described in (4.2.11). Staining was conducted on quadruplicate sections taken from each TEVG sample.
Sections of human umbilical cord, prepared as described in (3.2.10), were also stained for use as positive controls.

6.2.8 **Collagen visualisation and quantification using second harmonic generation**

Sections of TEVGs cultured under dynamic and static conditions for 7 days in the bioreactor were prepared as described in (6.2.2) and dried at room temperature. The sections were examined for the presence of collagen by examining second harmonic generation (SHG) using a laser-scanning confocal microscope (Zeiss LSM 510 Meta)

attached to a tuneable (700–1060 nm) Chameleon Ti:sapphire multiphoton laser (Coherent, USA). The multiphoton illumination wavelength was set at 50% 950 nm. SHG emissions were collected in a 10 nm bandpass filter centred around 474 nm. All imaging was performed using a 40x 1.3 NA oil immersion objective with the pinhole set to 1000 µm. SHG was collected in the backward direction after filtration through a primary dichroic (HFT KP650). Transmitted light DIC images were collected in tandem to assist subsequent image analysis. Imaging parameters were optimised and maintained for all samples.

Three images were taken from triplicate sections from each of the three lengths that the TEVGs were divided into following fixation, unless otherwise stated. Imaging was focused on areas of the TEVGs which showed the presence of cells. Additionally, the unseeded TEVGs cultured for 7 days in the bioreactor under dynamic conditions, as negative controls, were also examined to determine the SHG signal produced by the PGS-M scaffold alone.

Collagen content was quantified using image analysis software (ImageJ, version 1.45s) to determine the SHG signal strength. Firstly the background signal strength was determined by selecting 50 random sections from the background of the SHG images and averaging their signal intensities. Sections were selected using the transmitted light DIC counterpart images for guidance (Figure 72a). Next, the signal strength generated from the PGS-M scaffold was determined by selecting 50 random sections from the scaffold in the SHG images and averaging their signal intensities (Figure 72b). Finally, the signal strength generated from the regions of cells present in the TEVGs was determined by selecting 50 random sections from these regions in the SHG images and averaging their signal intensities (Figure 72c) The average background signal was then subtracted from the average signals calculated for the scaffold and the cellular regions.

The results were statistically analysed using two-way ANOVA with Tukey multiple comparisons analysis. $P<0.05$ was considered significant (*), $P<0.01$ was considered very significant (**) and $P<0.001$ was considered extremely significant (***).

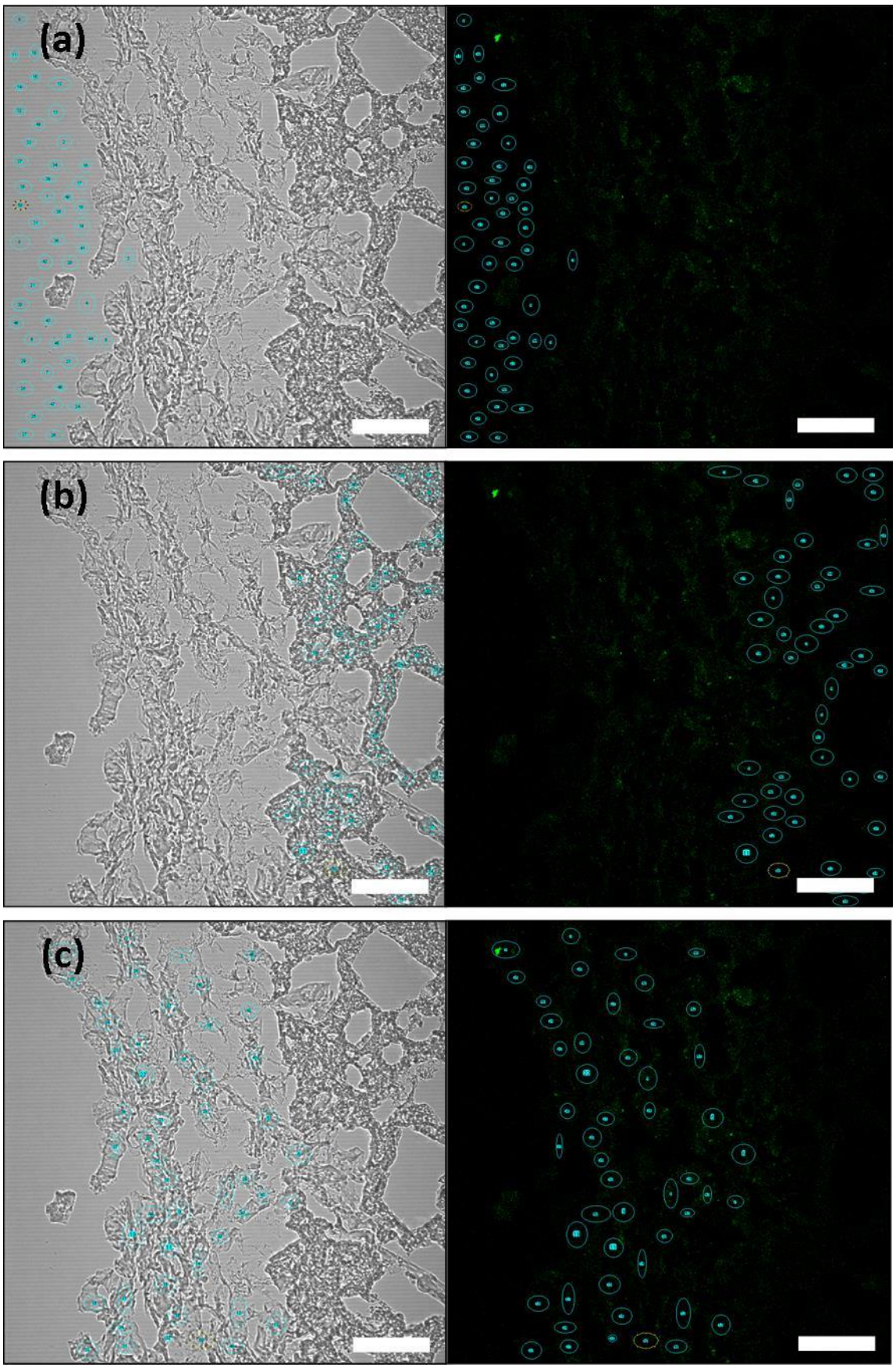

Figure 72. TEVG collagen quantification using transmitted light DIC (left) and SHG (right) images. (a) Background areas selected, (b) PGS-M scaffold selected, (c) Regions of cells selected. All images were processed using equal display settings. Scale bars are 50 µm.

6.2.9 **Staining of TEVGs for elastin**

Sections of TEVGs were prepared as described in (6.2.2). For staining, the sections were first rinsed in dH_2O, twice, followed by rinsing in a 95% solution of IMS in dH_2O, twice. The sections were then stained with Miller's Elastin stain (VWR, UK) for 1.5 hours, before being rinsed again in a 95% IMS solution, twice, followed by dH_2O, twice, to remove excess stain. The sections were then rinsed in 70% IMS (Fisher Scientific, UK) solution in H_2O, then IMS and then Xylene. Finally, the sections were coated with DPX mountant and coverslips applied over them. They were examined by light microscopy, as described in (4.2.11).

Sections of human umbilical cord, prepared as described in (3.2.10), were also stained for use as positive controls.

6.2.10 **Immunofluorescence staining of TEVGs for α-SMA**

Sections of TEVGs were prepared as described in (6.2.2) and dried at room temperature. The staining process then began by permeablising the samples with 100 µl of a 0.5% (v/v) solution of Triton X 100 (Fisher Scientific, UK) in PBS. After 1 hour of permeablisation, the Triton X 100 solution was removed and the samples washed with PBS, three times, before being blocked with 100 µl of a 5% (w/v) solution of BSA in PBS. After 1 hour, the BSA solution was removed and 100 µl of a 0.2% (v/v) anti α-SMA mouse monoclonal antibody conjugated with Cy3™ and 5% (w/v) BSA in PBS solution was added to each sample. After incubation at room temperature, in the absence of light, for 2 hours the antibody solution was removed and the sections again washed with PBS, three times, followed by once with dH_2O, to remove any remaining salts. The sections were then imaged, using a fluorescence microscope (Olympus IX73) with 550-570 nm excitation and 600-660 nm emission.

Various controls were also produced and imaged. TEVG sections, containing SMCs, that were fixed, permeablised and blocked, but not treated with antibody were used to establish the effect of any background fluorescence. Additionally, fixed unseeded

TEVGs were stained and left unstained to act as negative controls. Staining was conducted on quadruplicate sections taken from each of the three lengths that the TEVGs were divided into following fixation, unless otherwise stated.
Sections of human umbilical cord, prepared as described in (3.2.10), were also stained for use as positive controls.

6.2.11 **Immunofluorescence staining of TEVGs for calponin**

Sections of TEVGs were prepared, permeablised and blocked as described in (6.2.10). Following the removal of the BSA blocking solution, 100 µl of a 0.4% (v/v) anti calponin 1 rabbit polyclonal antibody conjugated with FITC (Insight Biotechnology, UK) and 5% (w/v) BSA in PBS solution was added to each sample. After incubation at room temperature, in the absence of light, for 2 hours the antibody solution was removed and the sections again washed with PBS, three times, followed by once with dH_2O, to remove any remaining salts. The sections were then imaged, using a fluorescence microscope (Olympus IX73) with 480-500 nm excitation and 510-550 nm emission.
Controls were also produced as described in (6.2.10). Staining was conducted on quadruplicate sections taken from each of the three lengths that the TEVGs were divided into following fixation, unless otherwise stated.
Sections of human umbilical cord, prepared as described in (3.2.10), were also stained for use as positive controls.

6.3 **Results**

6.3.1 **Sterilisation of tubular PGS-M scaffolds**

The PGS-M scaffolds required sterilisation prior to cell seeding. Initially, this was conducted using autoclaving, with the scaffolds in autoclave bags. Although this method had proven successful in the sterilisation of porous PGS-M disks, as described in (4.2.9), the tubular scaffolds suffered deformation as a result of the process. The scaffolds appeared to shrivel and were no longer able to retain a tubular shape (Figure 73). They had also become damaged and torn around the ends which were fitted over the nylon fittings.

As a result, an alternative sterilisation method was sought. Scaffolds were subsequently sterilised using triplicate washes in a 70% ethanol solution in dH_2O. This process did not appear to compromise the integrity of the scaffolds. However, after attempts at seeding cells onto them, an examination of the sectioned scaffolds suggested that they carried an infection. H&E staining revealed cellular bodies around the exterior of the scaffolds. These stained strongly purple and appeared to possess filamentous structures, possibly suggesting a fungal organism (Figure 74). This infection presented in two separate seeding experiments.

To avoid repeated infections, sterilisation by autoclave was reemployed; however, the scaffolds were now immersed in dH_2O throughout the process. This prevented them from deforming and becoming damaged as had been observed previously. Subsequent sectioning of the scaffolds sterilised in this manner did not show any signs of infection (Figure 75). Additionally, SMC growth medium incubated in the presence of these scaffolds for 24 hours did not show any significant difference compared to control growth medium, incubated in parallel without contact with the scaffolds, when examined using the RR assay. The results of the RR assay showed both medium samples generated negligible fluorescence values, suggesting that no metabolic activity was present in the medium (Figure 76).

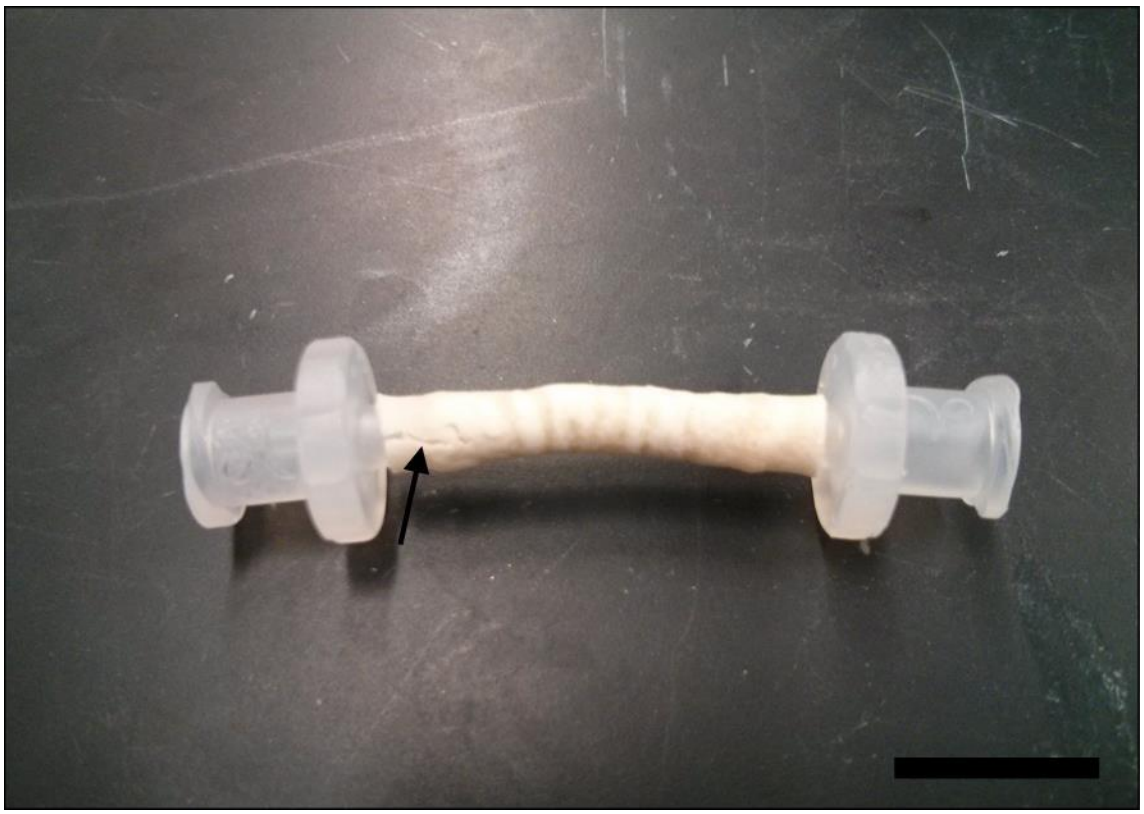

Figure 73. Representative image of a tubular PGS-M scaffold sterilised by autoclave in an autoclave bag. The scaffold deformed and shrivelled resulting in damage and tearing around the interface with the nylon fittings (arrowed). Scale bar is 1 cm.

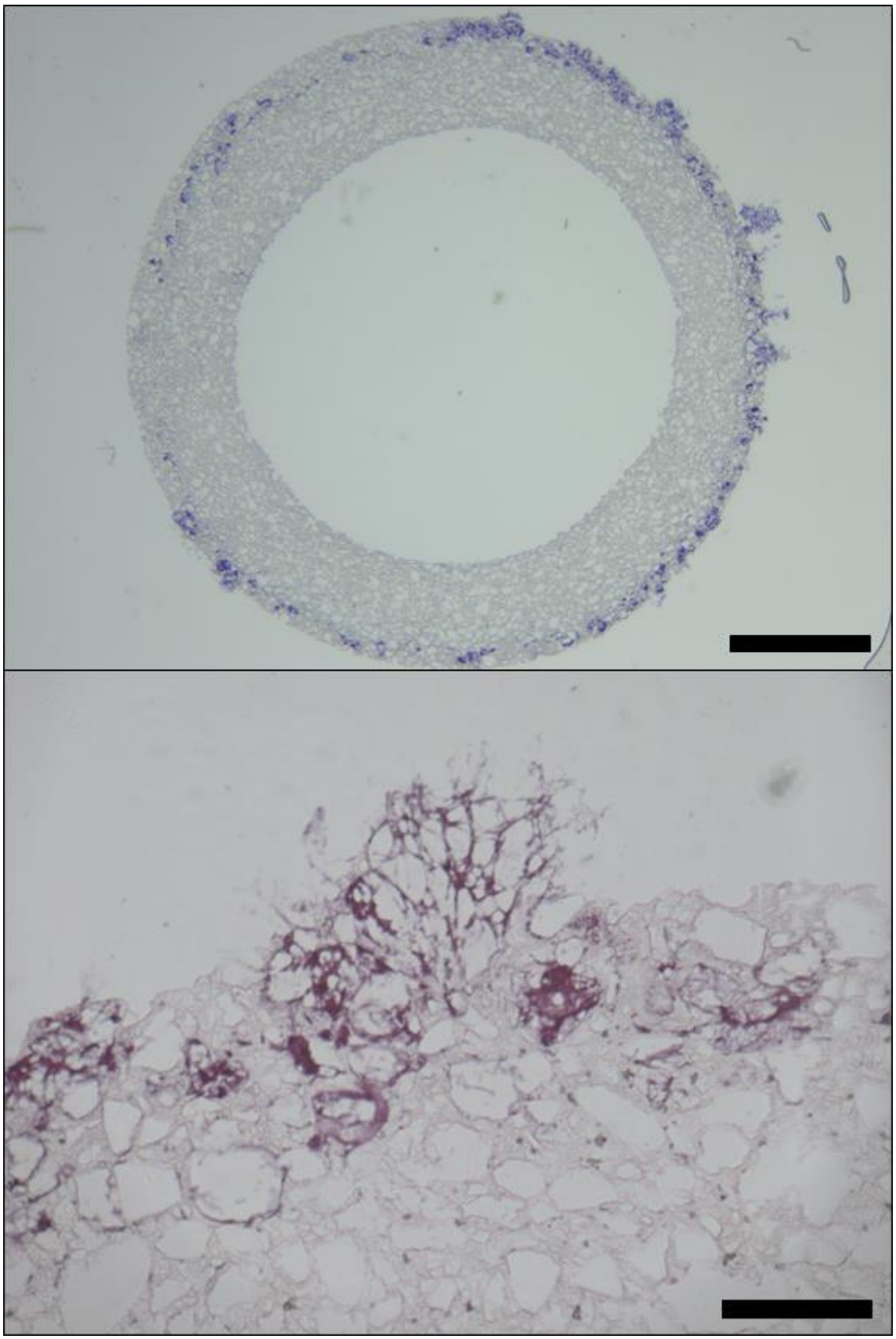

Figure 74. Representative H&E stained images of tubular PGS-M scaffolds sterilised by 70% ethanol treatment and seeded with SMCs (*n* = 2). (Above) Scaffold cross-sections showed cellular bodies present around the exterior of the scaffolds. No cells appeared to be present on the luminal surface. Scale bar is 1 mm. (Below) Cellular bodies appeared to possess filamentous structures. Scale bar is 250 µm.

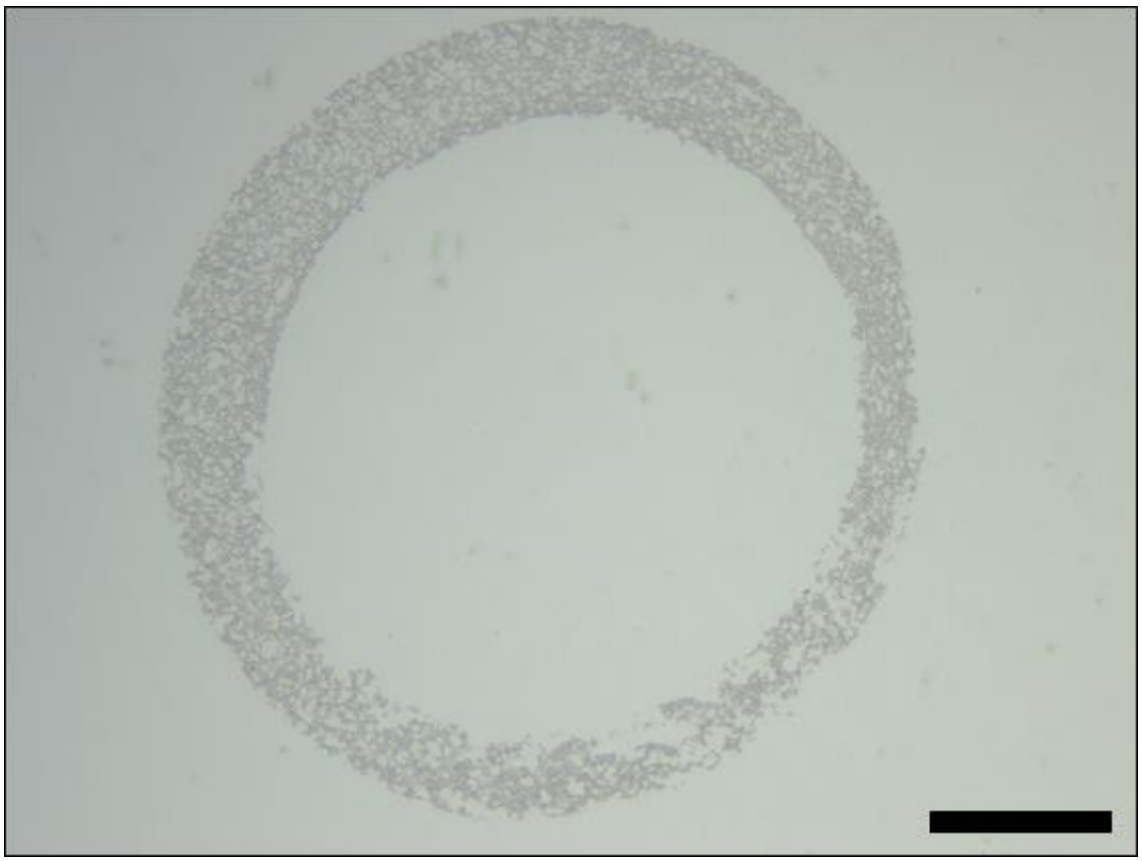

Figure 75. Representative H&E stained image of a tubular PGS-M scaffold sterilised by autoclave while immersed in dH_2O (n = 3). No evidence of infection was present throughout the scaffold after incubation in SMC growth medium for 24 hours. Scale bar is 1 mm.

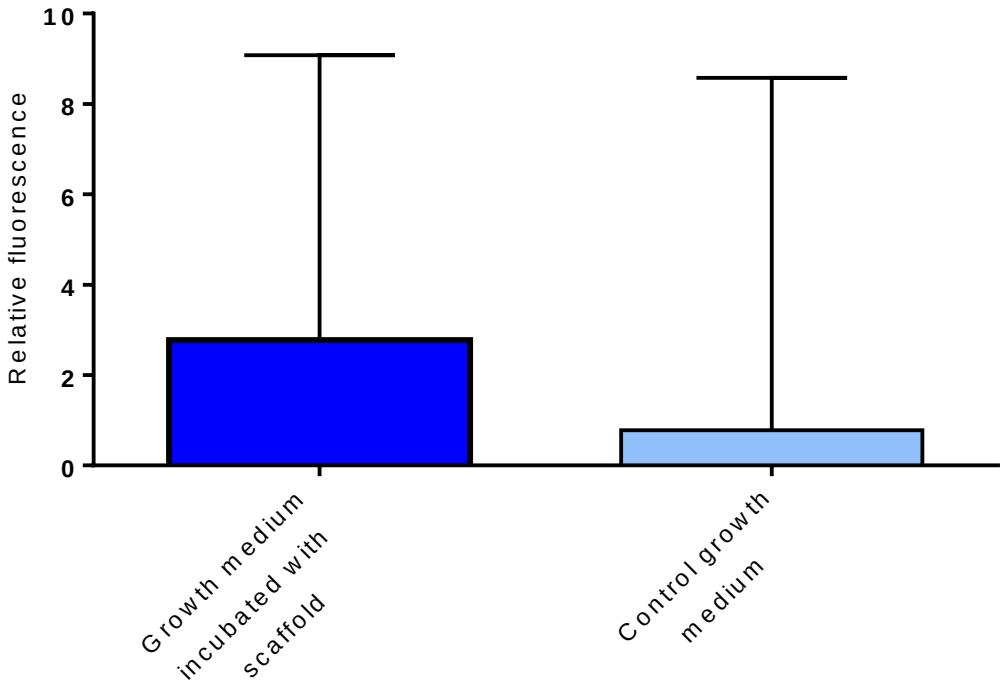

Figure 76. RR assay for metabolic activity in SMC growth medium incubated in the presence or absence (control) of tubular PGS-M scaffolds sterilised by autoclave while immersed in dH_2O. Error bars are SEM (n = 3).

6.3.2 **Seeding of SMCs onto tubular PGS-M scaffolds**

The seeding of SMCs onto the luminal surfaces of tubular PGS-M scaffolds was conducted in petri dishes, before it was attempted in the bioreactor (Figure 77). Scaffolds were seeded with SMCs, at a density of 2 x 10^6 cells/cm^2 of lumen. This was conducted twice with the scaffolds rotated 180° about their axis of rotation between seeding procedures.

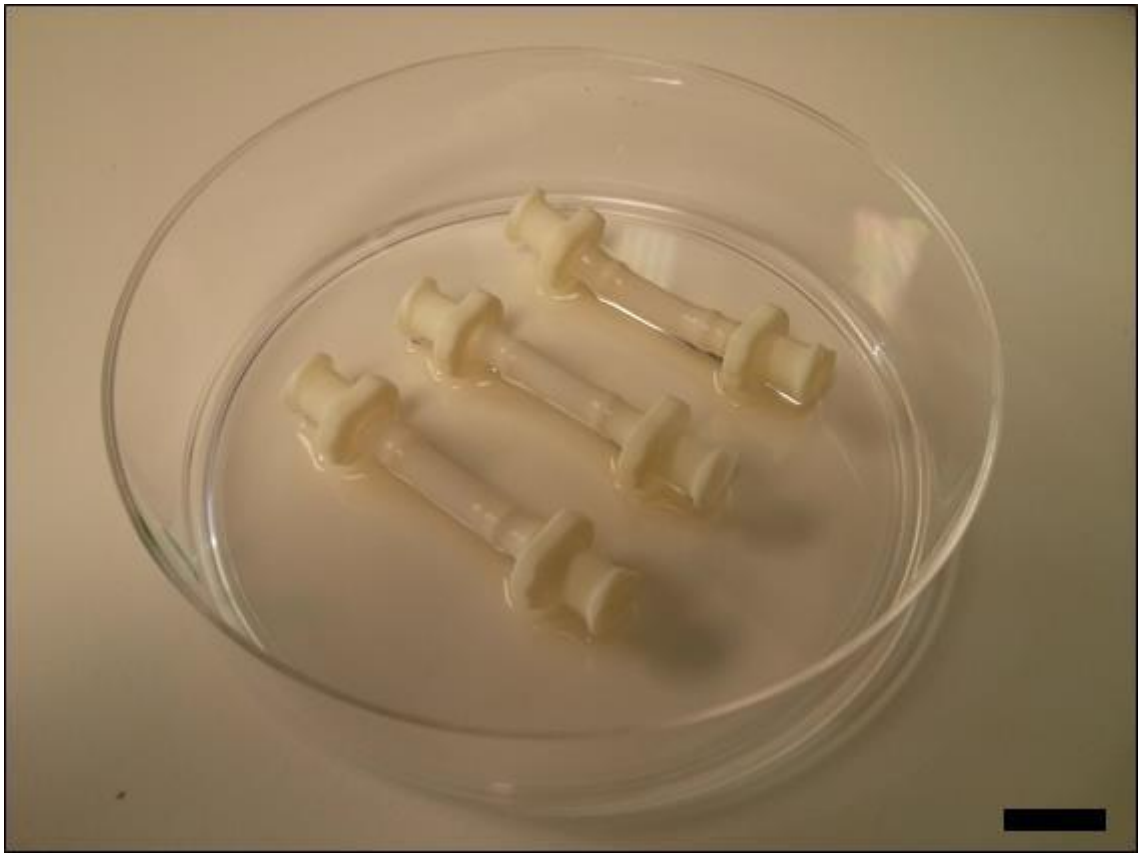

Figure 77. Tubular PGS-M scaffolds with attached nylon fittings seeded with SMCs and cultured in petri dishes. Scale bar is 1 cm.

The seeded scaffolds demonstrated the presence of attached SMCs. Sections stained with H&E showed cell masses clearly visible in all seeded scaffolds (Figure 78). Cells covered a large proportion of the luminal surface, but were concentrated at opposing sides. Cell invasion into the interior of the scaffold wall was also present in some areas. Unseeded negative control scaffolds, cultured in parallel in equivalent conditions, did not show any evidence of SMCs (Figure 79).

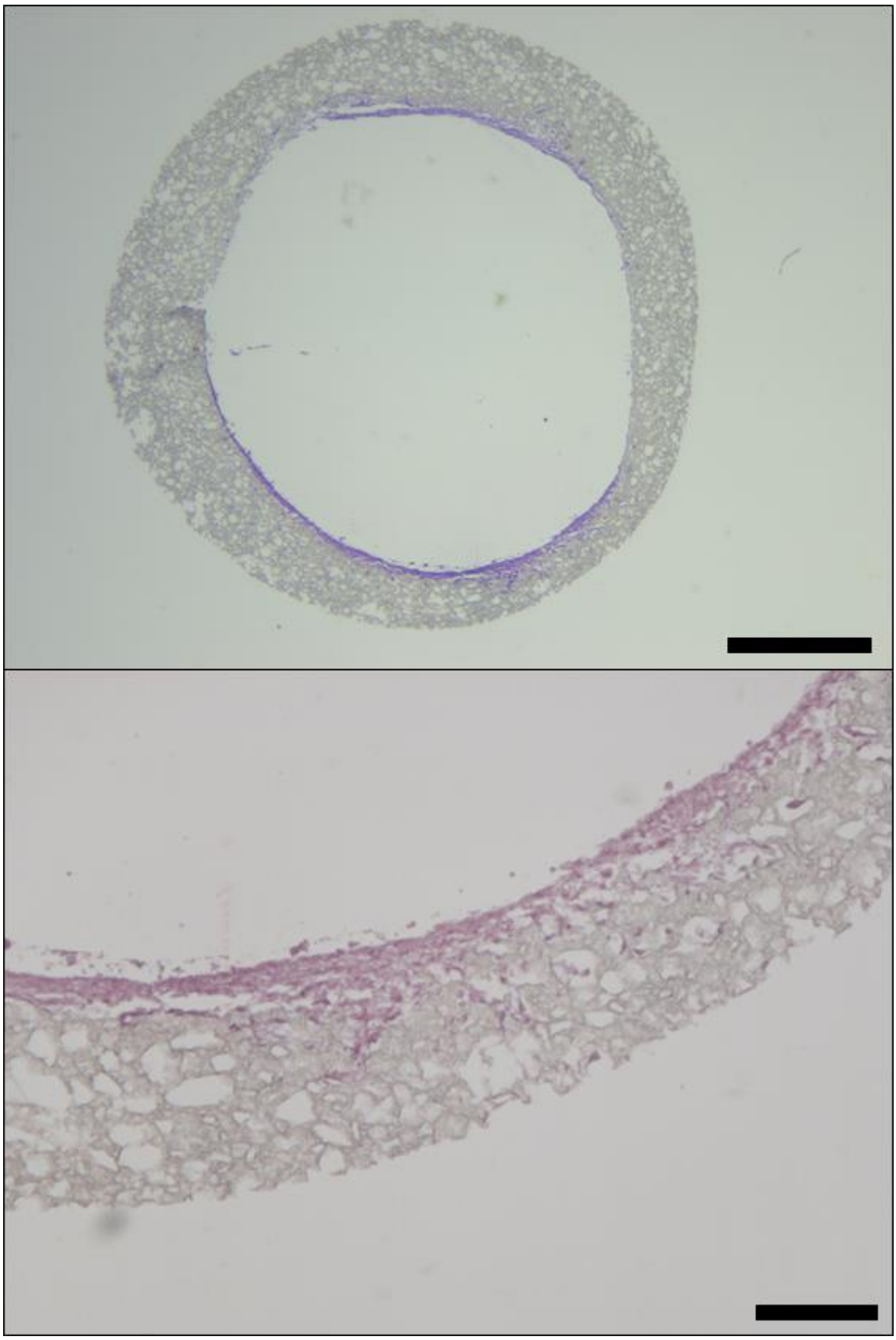

Figure 78. Representative images of sections of tubular PGS-M scaffolds seeded with SMCs (*n* = 2). (Above) SMCs attached around the luminal surface and were concentrated at opposing sides. Scale bar is 1 mm. (Below) SMCs invaded into the scaffold wall in some areas. Scale bar is 200 μm.

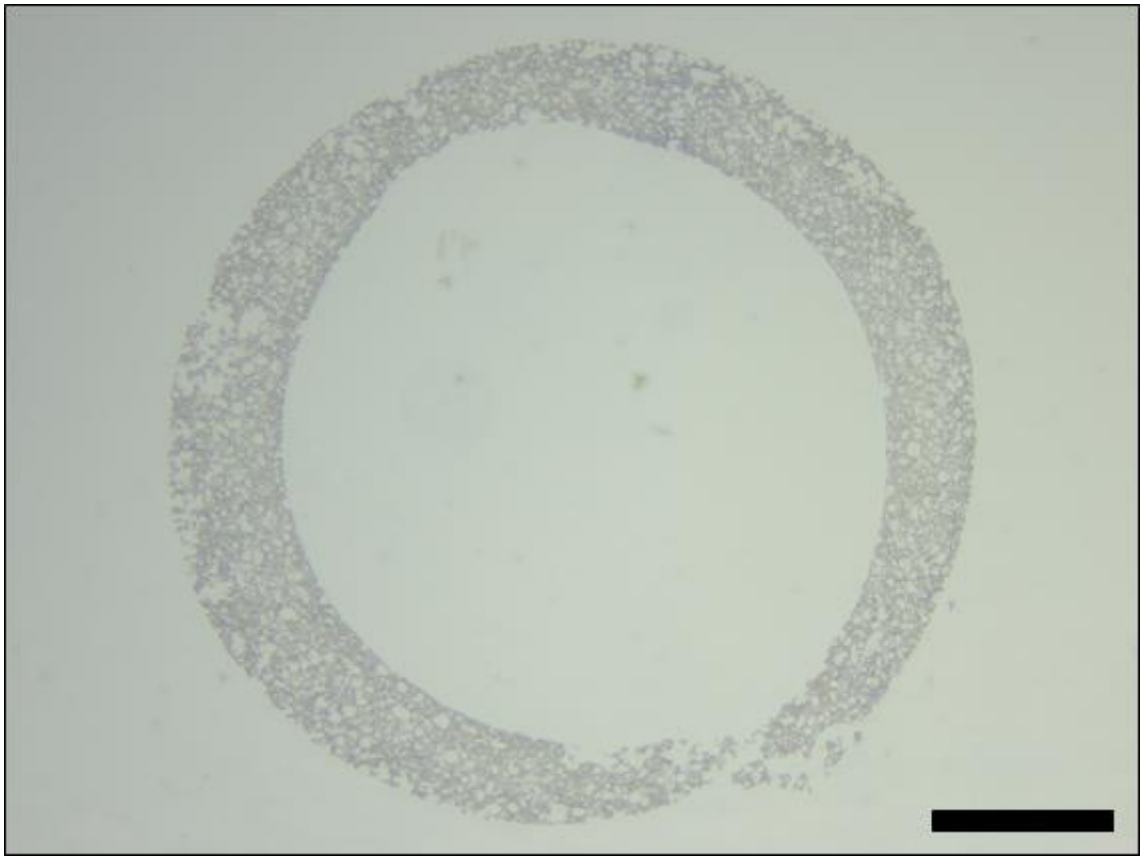

Figure 79. Representative image of unseeded tubular PGS-M scaffolds (negative controls) (*n* = 2). No evidence of SMCs was present. Scale bar is 1 mm.

6.3.3 **Bioreactor culture under dynamic and static conditions.**

Tubular PGS-M scaffolds were positioned inside bioreactor design 1.2 and seeded with SMCs, via the cell seeding ports. Seeding was conducted twice, at a cell density of 2×10^6 cells/cm^2 of lumen, with the bioreactor rotated 180° about the rotational axis of the scaffolds between seeding procedures. The seeded scaffolds, now referred to as TEVGs, were cultured for 7 days in the bioreactor under dynamic conditions with a pulsatile flow of incrementally increasing pressure and flow rate (Figure 80). The TEVGs maintained structural integrity throughout the culture. They could be seen to visibly deform and pulsate as a reaction to the flow moving through them. After 7 days the scaffolds were fixed and divided into three equal lengths for analysis. No evidence of infection was seen throughout the bioreactor culture, with the medium retaining its

clarity and colour. Additionally, a sample of the used SMC growth medium was taken from the bioreactor and tested for the presence of metabolic activity using the RR assay. This was compared to a sample of SMC growth medium cultured in parallel to the bioreactor. The results of the RR assay showed no significant difference between the two samples of medium. Both samples generated negligible fluorescence values, suggesting that no metabolic activity was present in the medium (Figure 81).

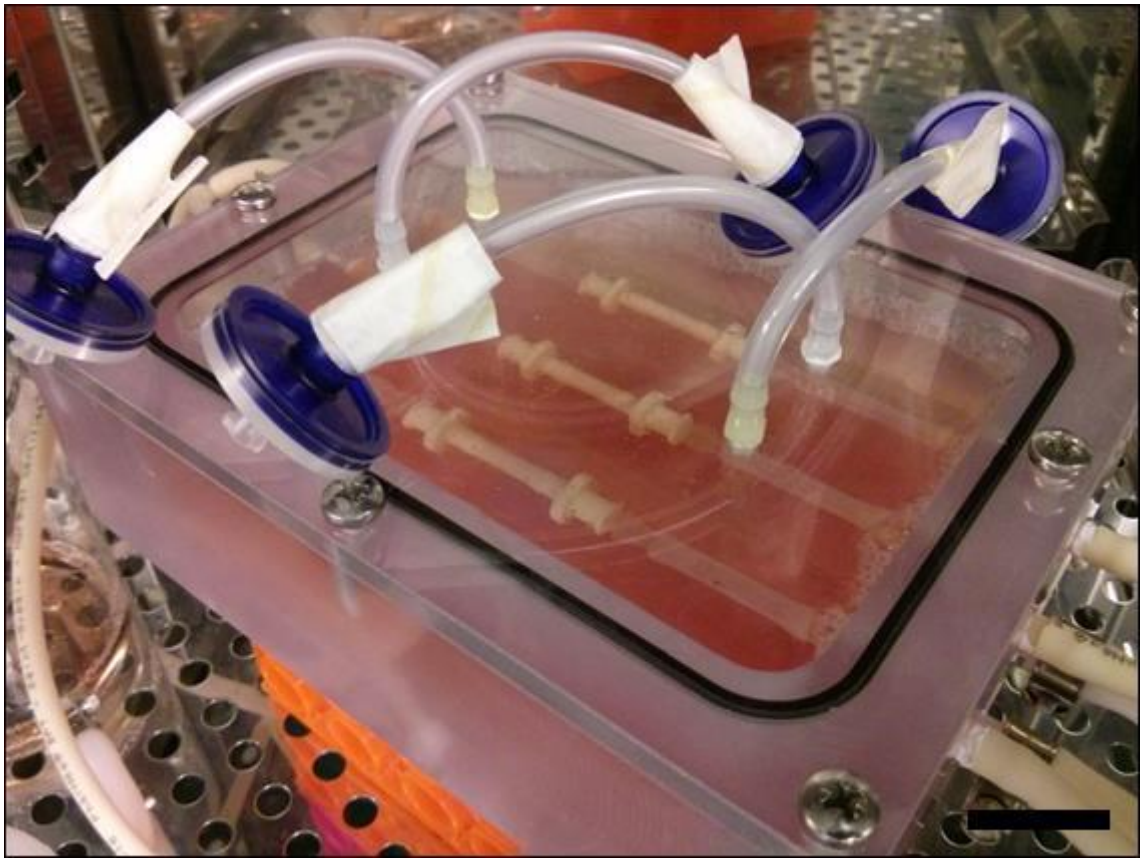

Figure 80. Bioreactor culture of TEVGs under pulsatile flow. Scale bar is 2 cm.

The three replicate TEVGs cultured under pulsatile flow in the bioreactor showed differing results (Figure 82). The TEVG attached to TEVG channel 1 of the bioreactor did not show any evidence of cells. 5 µm sections, stained for H&E, taken from each of the three lengths of the TEVG did not show any evidence of cells. The TEVG attached

to TEVG channel 2 of the bioreactor did not show any evidence of cells in the first two lengths, most proximal to the peristaltic pump. However, there were some small regions of cells attached to the scaffold lumen visible in H&E stained sections taken from the third length of the graft, most distal to the peristaltic pump. Finally, the TEVG attached to TEVG channel 3 of the bioreactor did not show any evidence of cells in first two lengths, most proximal to the peristaltic pump. However, there was considerable evidence of cells present in H&E stained sections taken from the third length of the graft (Figure 83). The cells appeared isolated to a single quadrant of the luminal surface and formed a densely packed cell sheet of ~200 µm thick. This thickness was constant across the sheet, tapering down smoothly to the luminal surface at the ends. The cells appeared confined to the lumen, with no evidence of invasion into the scaffold wall. Compared to sections of human umbilical artery, also stained with H&E, the cells attached to the luminal surface displayed a similar structure to the SMCs present in the tunica media of the artery (Figure 84).

TEVGs were also cultured in the bioreactor under static conditions. After 7 days, the TEVGs were removed and fixed and, as in the dynamic bioreactor culture, a sample of the used SMC growth medium was taken from the bioreactor and tested for the presence of metabolic activity using the RR assay. This was compared to a sample of SMC growth medium cultured in parallel to the bioreactor. The results of the RR assay showed no significant difference between the two samples of medium. Both samples generated negligible fluorescence values, suggesting that no metabolic activity was present in the medium (Figure 81).

Examination of all three TEVG replicates showed evidence of cells. H&E stained sections taken from all three lengths of all three replicate grafts showed the presence of cells attached to the luminal surface (Figure 85). Similar to the results from the cell seeding experiments, these cells appeared to be concentrated on opposing areas of the luminal surface. However, the cells appeared to be present over more of the lumen than in the cell seeding experiments, covering almost the entire surface. No significant differences were observed down the lengths of each TEVG, based on

comparisons of sections taken form the three lengths of each graft. All graft sections appeared to show some detachment of the cells from the scaffold lumen.

PGS-M scaffolds without seeded SMCs were also cultured in the bioreactor, under dynamic conditions, as negative controls. No evidence of cells was seen in any of the sections taken from the lengths of these scaffolds (Figure 85). Additionally, a sample of the used SMC growth medium, taken from the bioreactor, tested for the presence of metabolic activity using the RR assay showed no significant difference compared to a control sample of SMC growth medium cultured in parallel. Both medium samples generated negligible fluorescence values, suggesting that no metabolic activity was present in the medium (Figure 81).

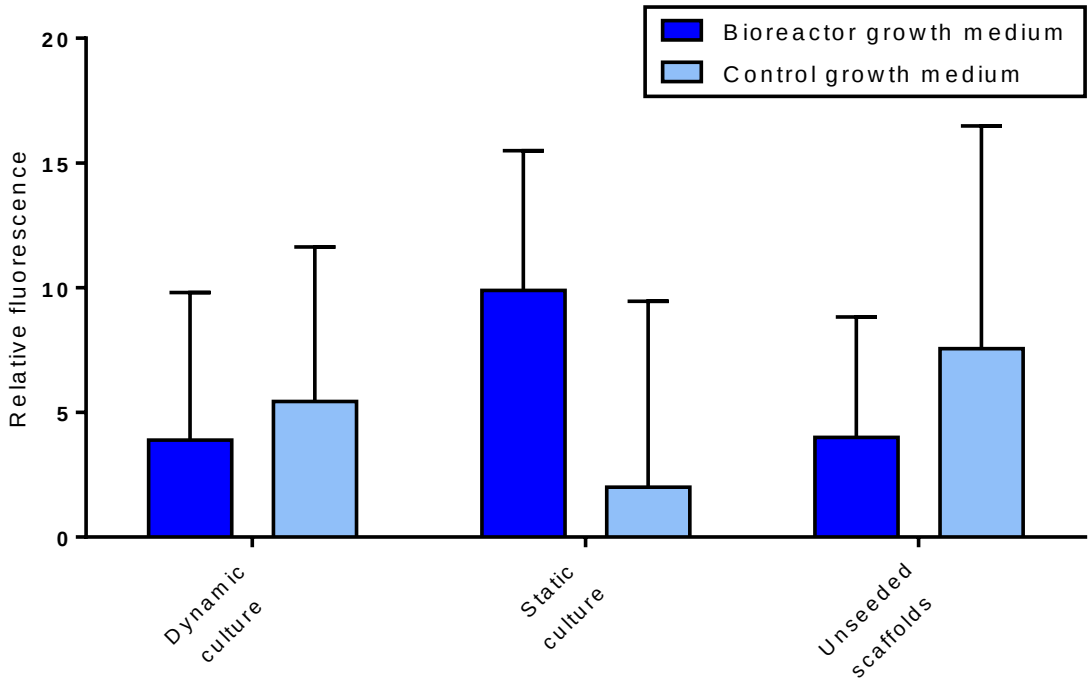

Figure 81. RR assay for metabolic activity in SMC growth medium used in the dynamic, static and unseeded bioreactor cultures for 7 days. Control medium was cultured in parallel to the bioreactor in equivalent conditions. Error bars are SEM (*n* = 1).

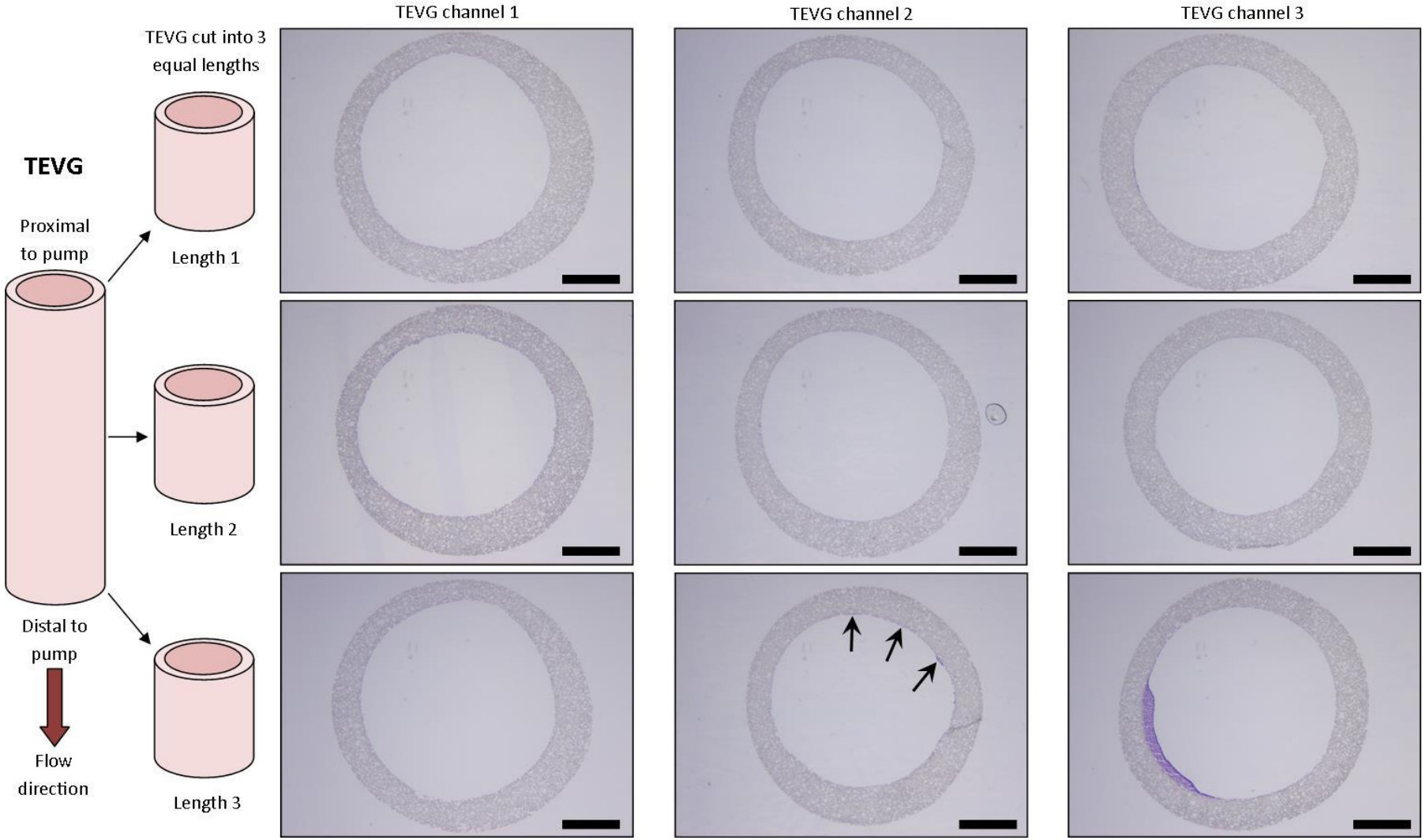

Figure 82. Representative H&E stained sections from TEVGs cultured under dynamic conditions (pulsatile flow) in the bioreactor for 7 days (*n* = 1). No cells were present in the TEVG connected to channel 1 in the bioreactor. Some small regions of cells were present in length 3 from the TEVG connected to channel 2 in the bioreactor (arrowed). A thick cell sheet was present around part of the lumen in length 3 from the TEVG connected to channel 3 in the bioreactor. Scale bars are 1 mm.

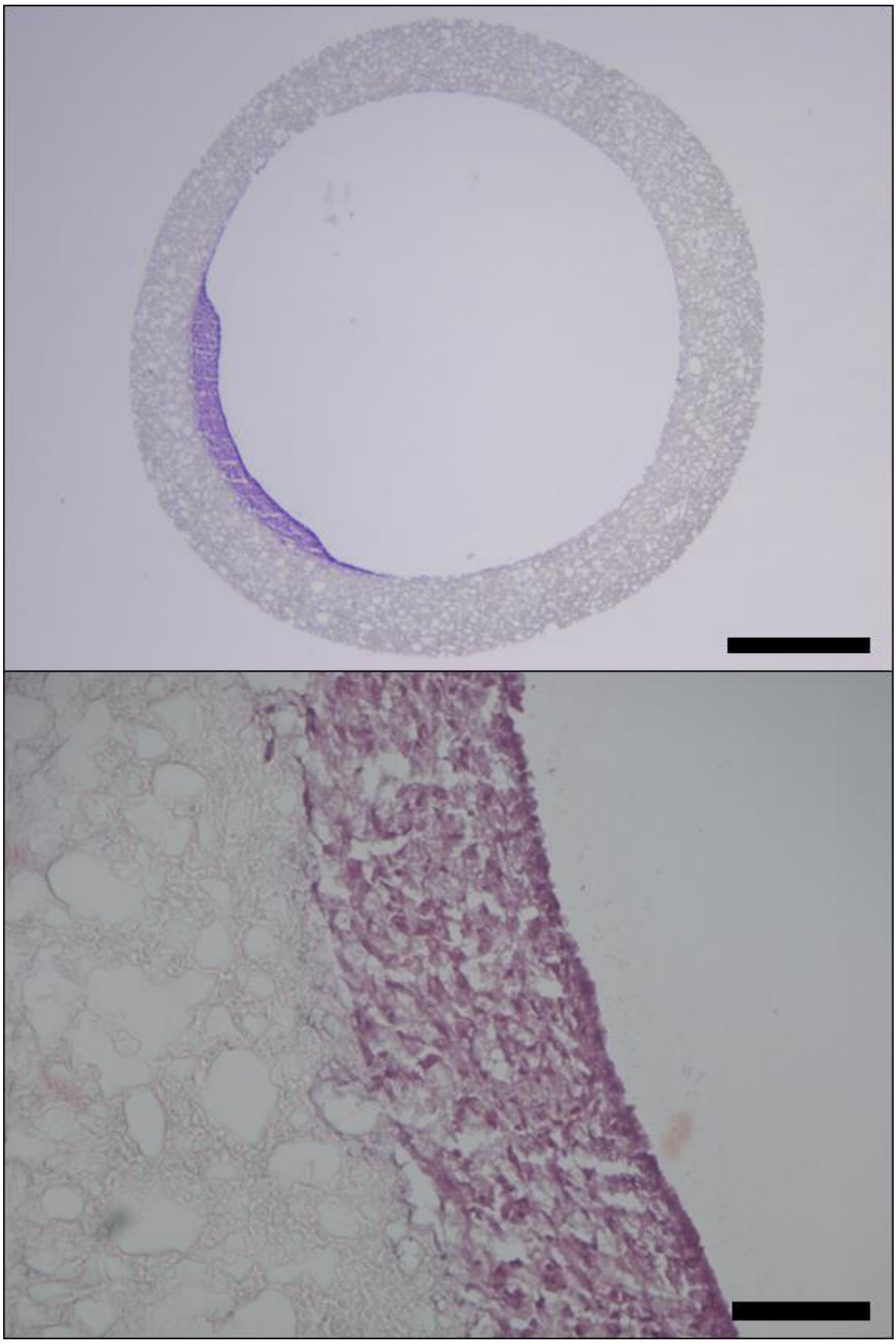

Figure 83. Representative H&E stained section from length 3 of the TEVG connected to channel 3 in the bioreactor and cultured under dynamic conditions (*n* = 1). (Above) The cell sheet was isolated to a single quadrant of the lumen. Scale bar is 1 mm. (Below) The cell sheet was ~200 µm thick. Scale bar is 100 µm.

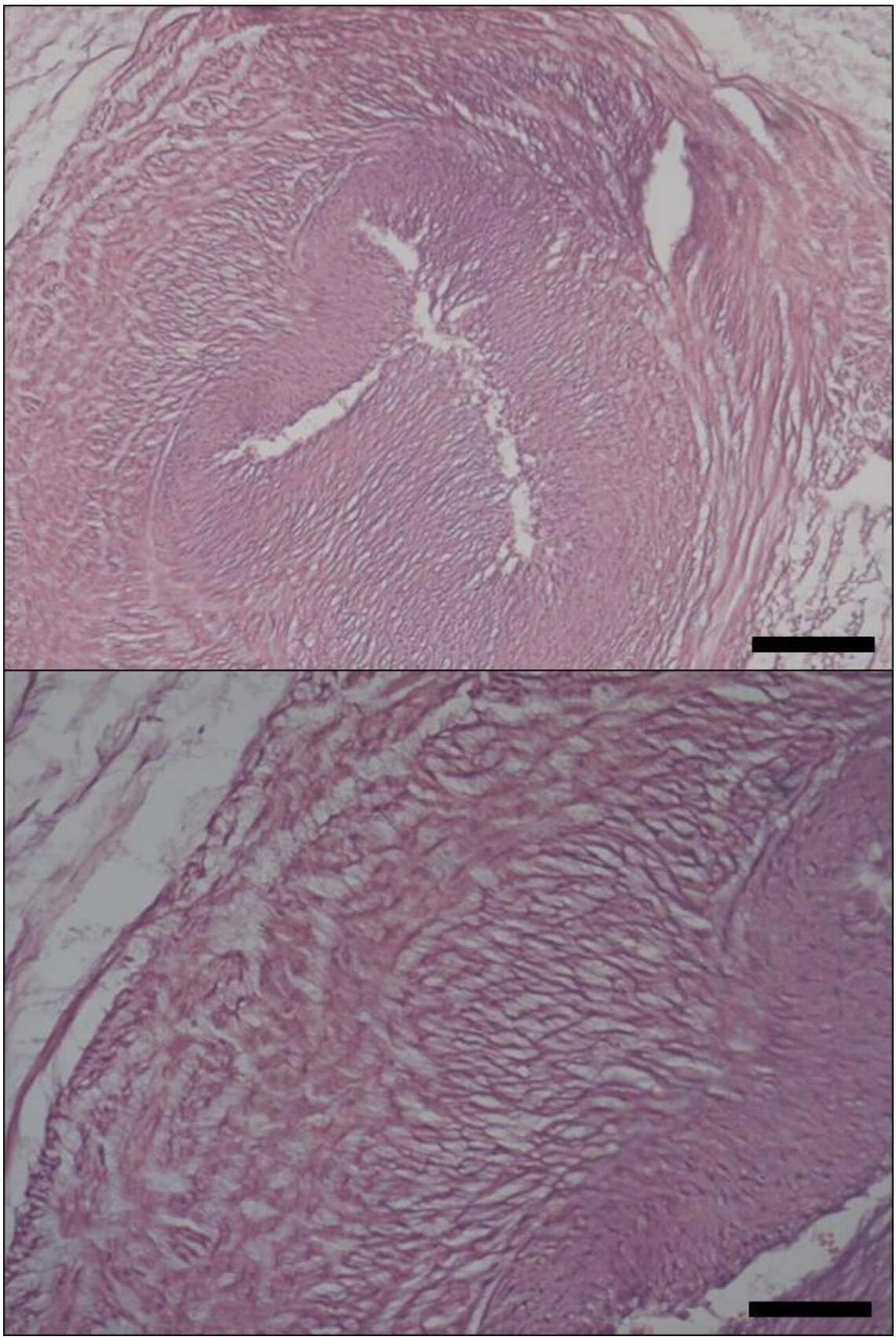

Figure 84. Representative H&E stained section of human umbilical artery (*n* = 1). (Above) Vessel cross-section. Scale bar is 200 µm. (Below) Enhanced view of the tunica media showing the arrangement of the SMCs. Scale bar is 100 µm.

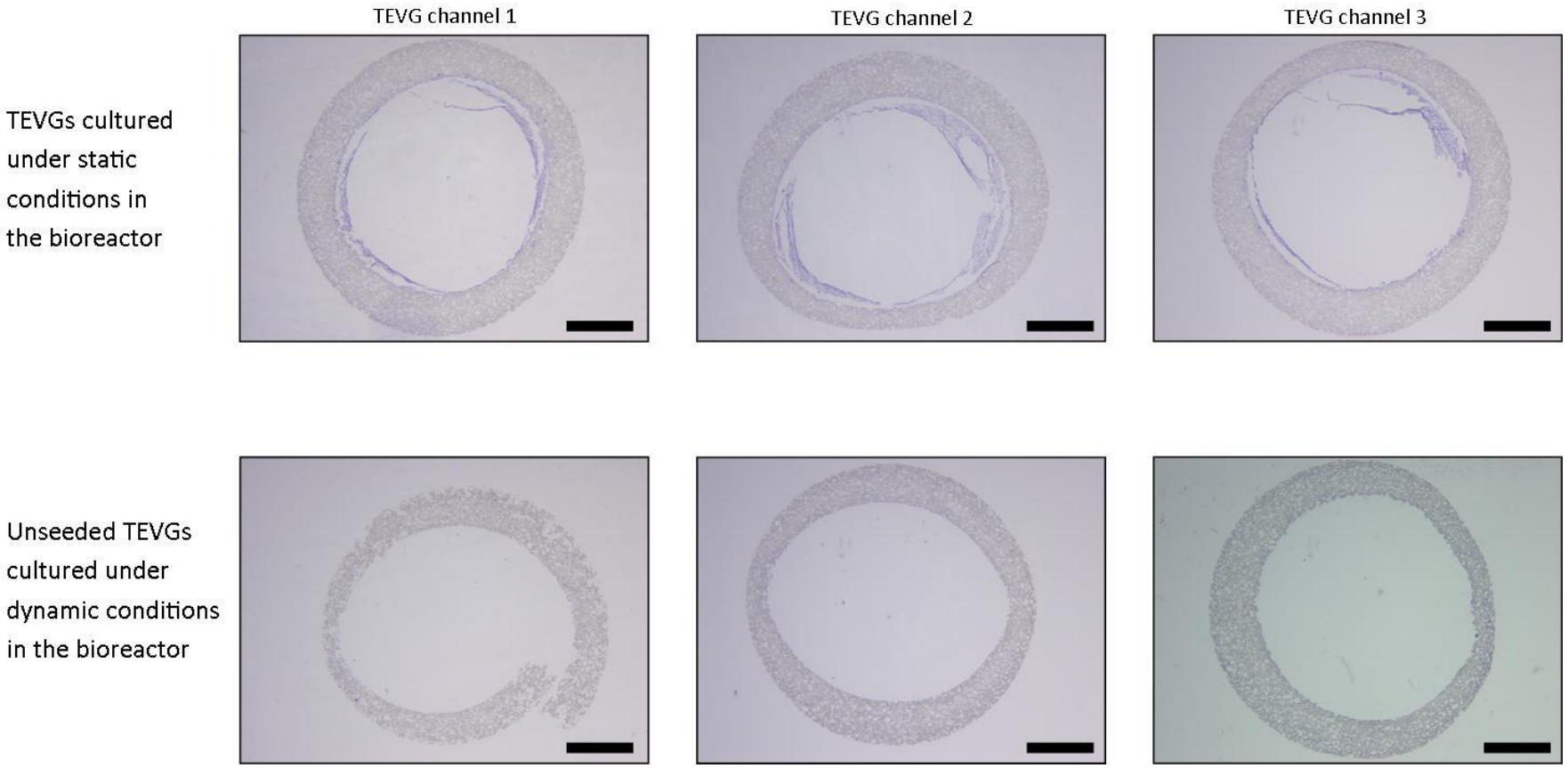

Figure 85. Representative H&E stained sections from TEVGs cultured under static conditions and unseeded control grafts cultured under dynamic conditions in the bioreactor for 7 days (*n* = 1). Cells were present throughout all sections of the TEVGs cultured under static conditions. The cells appeared concentrated on opposing regions of the luminal surface. Unseeded TEVGs cultured under dynamic conditions did not show any evidence of cells. Scale bars are 1 mm.

6.3.4 **Staining of TEVGs for collagen**

Sections from TEVGs cultured in the bioreactor were stained for the presence of collagen (Figure 86). In the TEVGs cultured under dynamic conditions, collagen only appeared present in the third length cut from the graft connected to TEVG channel 3 in the bioreactor. Collagen fibres stained orange/yellow. Collagen was located throughout the small cell sheet attached to the graft lumen in this area of the TEVG, although this only stained faintly, compared to the positive control (human umbilical artery) suggesting a lower quantity.

Collagen was also present in the TEVGs cultured under static conditions in the bioreactor. The collagen was present throughout the regions of cells attached to the graft lumens. Again, the staining strength was weaker than observed in the positive control, suggesting a smaller quantity of collagen was present. No significant difference could be determined, by observation, between the collagen present in the TEVGs cultured under dynamic conditions, compared to those cultured under static conditions.

No collagen was observed in the unseeded TEVGs cultured under dynamic conditions in the bioreactor.

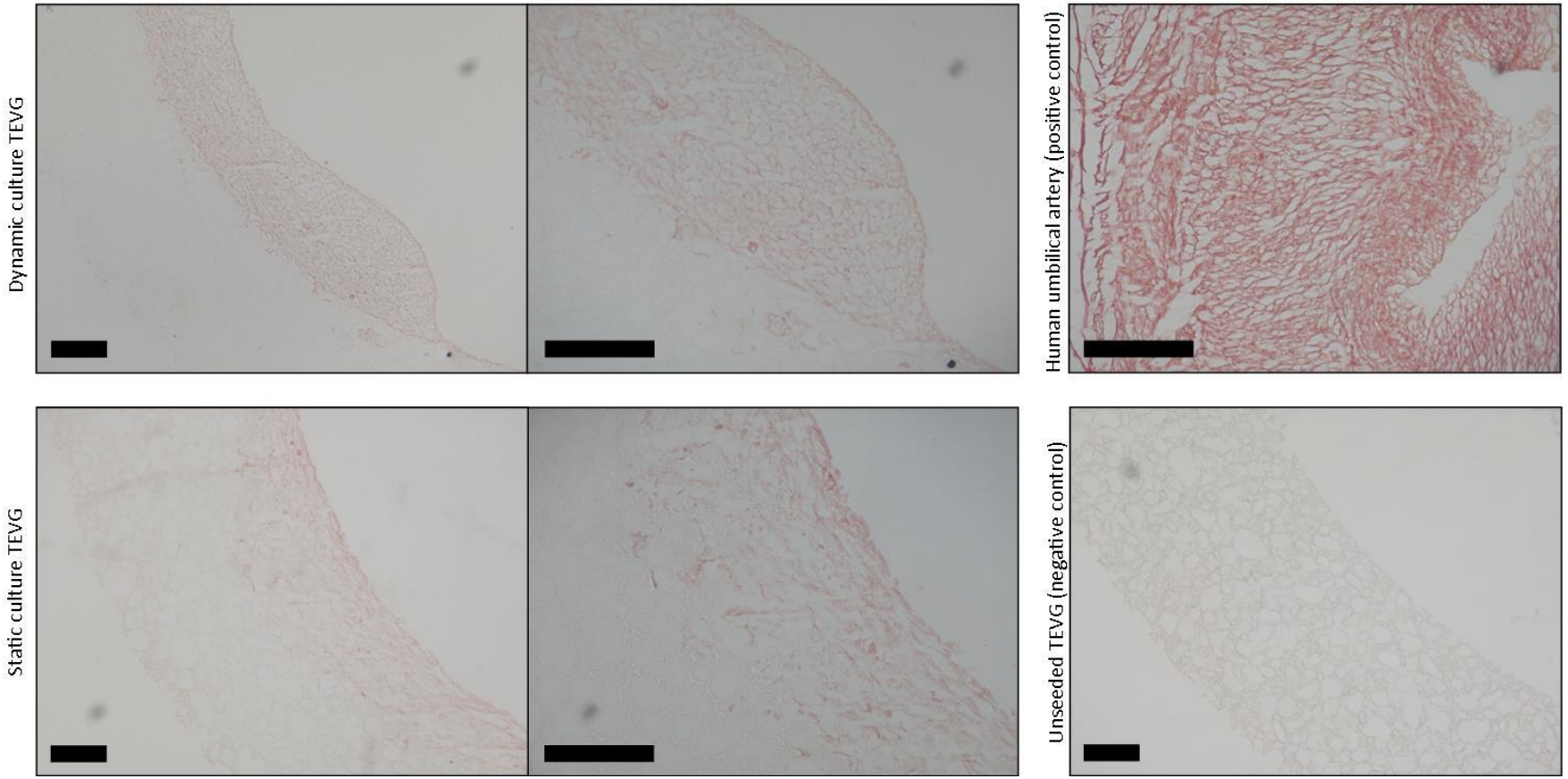

Figure 86. Representative collagen stained sections from TEVGs cultured under dynamic and static conditions in the bioreactor for 7 days (*n* = 1). Collagen was present throughout regions of attached cells on the grafts luminal surfaces. Human umbilical arteries (positive control) stained strongly for collagen. Unseeded TEVGs cultured under dynamic conditions in the bioreactor (negative controls) did not show any evidence of collagen. Scale bars are 200 µm.

6.3.5 **Collagen visualisation and quantification using second harmonic generation**

The collagen content of the TEVGs cultured in the bioreactor for 7 days under dynamic and static conditions was assessed using confocal microscopy to detect SHG (Figure 87). Images were then analysed to determine the signal intensities associated with the PGS-M scaffold and the regions of cells attached to the luminal surfaces of the TEVGs. In the examination of TEVGs cultured under dynamic conditions, only sections from the third length cut from the TEVG connected to channel 3 of the bioreactor were examined for SHG. All TEVGs cultured under static conditions in the bioreactor were examined.

The results are shown in Figure 88. The signal intensity generated by the regions of cells was significantly greater than the signal intensity generated by the PGS-M scaffold in TEVGs cultured under dynamic and static conditions ($P<0.001$ and 0.01, respectively). This suggested that collagen was present in the regions containing cells. There was no significant difference between the signal intensities generated by the regions of cells present in the TEVGs cultured under dynamic conditions and those cultured under static conditions. Additionally, the signal intensities generated by the PGS-M scaffolds in TEVGs cultured under dynamic and static conditions were not significantly different from the signal generated by unseeded TEVG scaffolds alone. This suggested that the presence of seeded cells during the bioreactor culture did not alter the scaffolds inherent fluorescence.

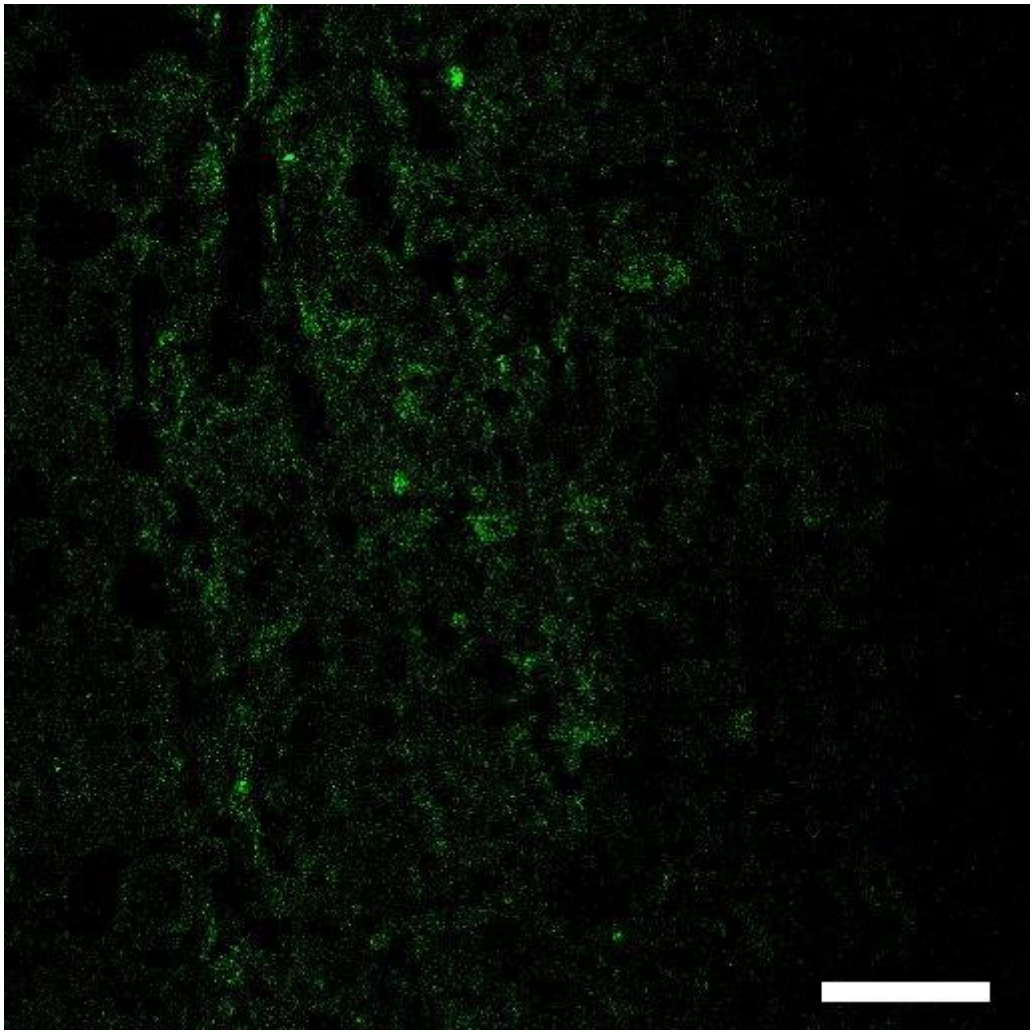

Figure 87. Example of a cell containing region of a TEVG imaged using SHG for collagen. Scale bar is 50 µm.

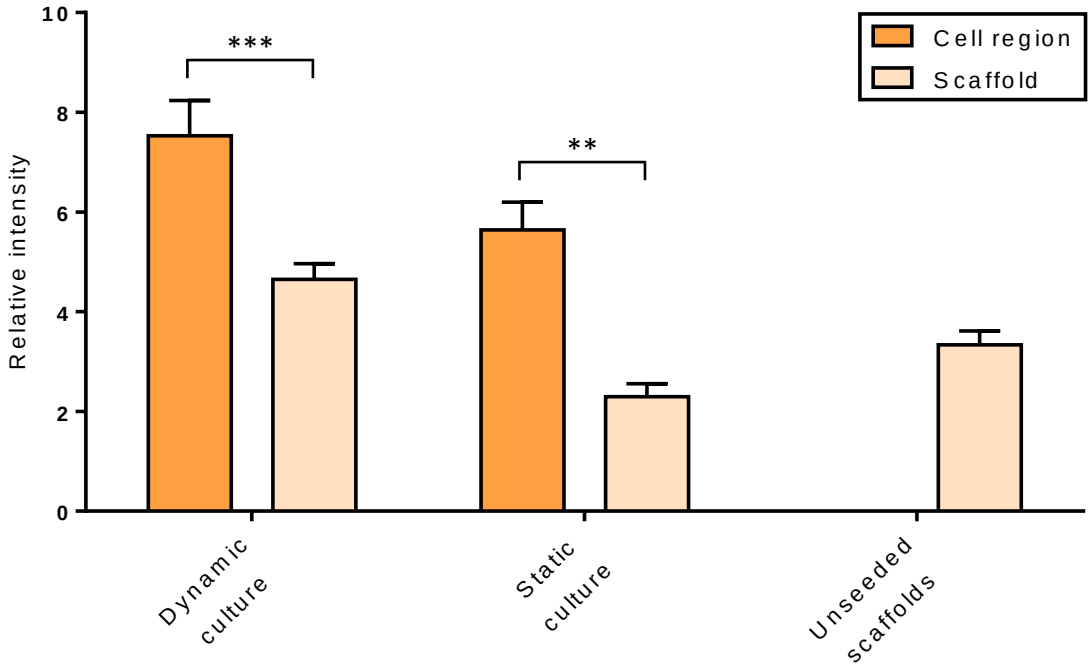

Figure 88. SHG signal intensities in images of TEVGs cultured under dynamic and static conditions for 7 days in the bioreactor (*n* = 1). Signals were analysed from regions of the TEVG images containing attached cells (Cell region) and regions only containing PGS-M scaffold (Scaffold). Signal intensities from images of unseeded TEVG scaffolds acted as controls.

6.3.6 **Staining of TEVGs for elastin**

Sections from TEVGs cultured in the bioreactor were stained for the presence of elastin (Figure 89). In the TEVGs cultured under dynamic conditions, elastin only appeared present in the third length cut from the graft connected to TEVG channel 3 in the bioreactor. Elastin fibres stained grey/black. The elastin was located throughout the small cell sheet attached to the graft lumen in this area of the TEVG, although this only stained faintly, compared to the positive control (human umbilical artery) suggesting a lower quantity.

Elastin was also present in the TEVGs cultured under static conditions in the bioreactor. The elastin was present throughout the regions of cells attached to the graft lumens. Again, the staining strength was weaker than observed in the positive control, suggesting a smaller quantity of elastin was present. No significant difference could be determined, by observation, between the elastin present in the TEVGs cultured under dynamic conditions, compared to those cultured under static conditions.

No elastin was observed in the unseeded TEVGs cultured under dynamic conditions in the bioreactor.

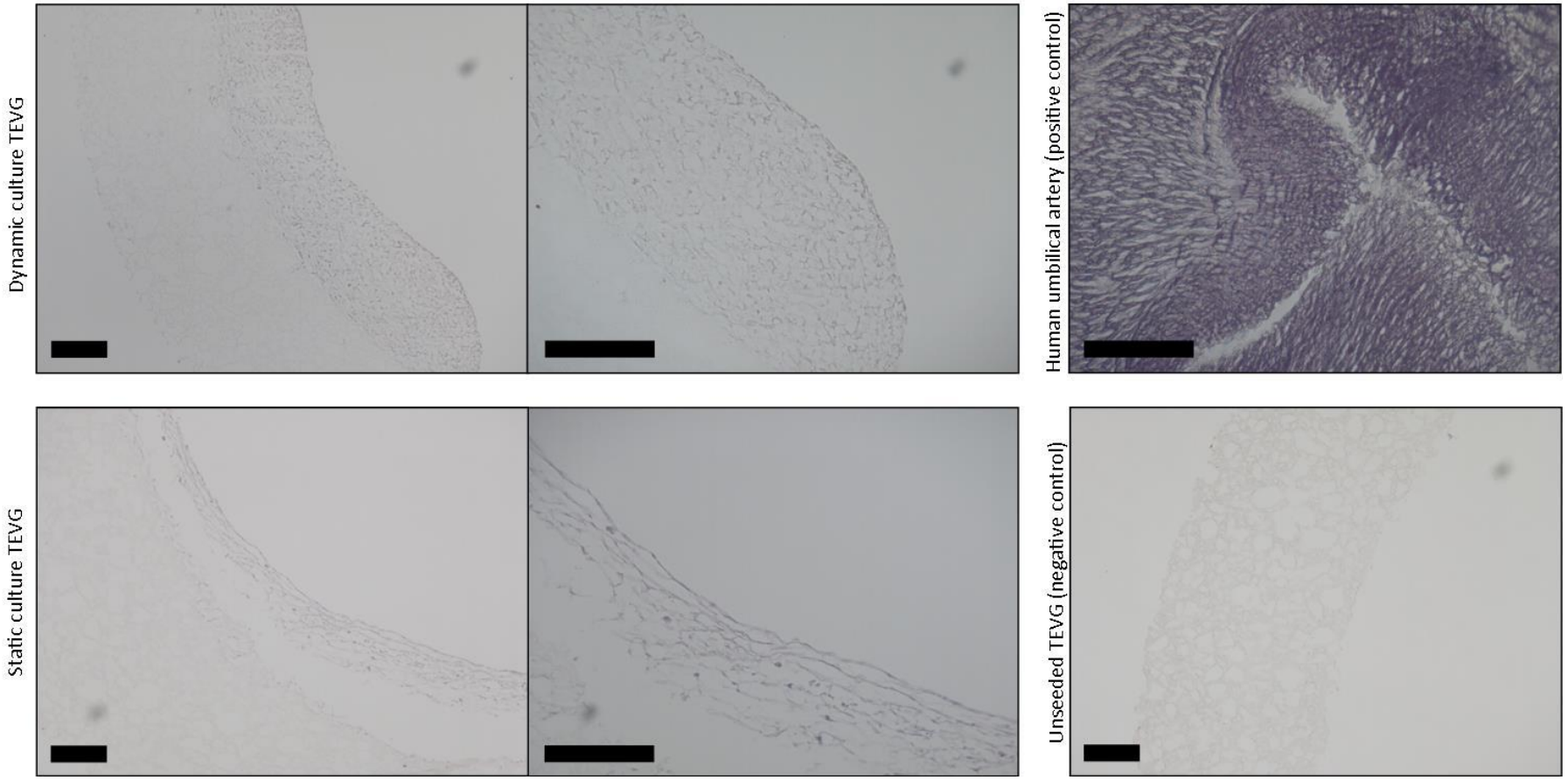

Figure 89. Representative elastin stained sections from TEVGs cultured under dynamic and static conditions in the bioreactor for 7 days (*n* = 1). Elastin was present throughout regions of attached cells on the grafts luminal surfaces. Human umbilical arteries (positive control) stained strongly for elastin. Unseeded TEVGs cultured under dynamic conditions in the bioreactor (negative controls) did not show any evidence of elastin. Scale bars are 200 µm.

6.3.7 **Immunofluorescence staining of TEVGs for α-SMA**

Sections from the TEVGs cultured under dynamic conditions were examined using immunohistochemistry to assess the expression of α-SMA in the SMCs seeded onto them in the bioreactor. α-SMA is a strong marker for contractile phenotype in SMCs. Only sections taken from the third length cut from the TEVG connected to channel 3 in the bioreactor were examined for α-SMA. This was the only region of the TEVGs cultured under dynamic conditions for 7 days which displayed significant cell attachment. The cells present in these sections did not appear to stain positive for α-SMA (Figure 90). No significant fluorescence signal could be detected above the background fluorescence.

Additionally, sections taken from the TEVGs cultured under static conditions for 7 days in the bioreactor were also examined. As in the TEVG cultured under dynamic conditions, the cells attached to these TEVGs did not stain positive for α-SMA, with no significant fluorescence signal above the background.

Sections of human umbilical artery were used as positive controls and did stain positive for the presence of α-SMA. Negative controls were blocked, but unstained, sections of TEVGs seeded with SMCs and cultured in the bioreactor; unseeded and stained TEVGs cultured in the bioreactor and unseeded and unstained TEVGs cultured in the bioreactor. All of the negative controls did not stain positive for α-SMA.

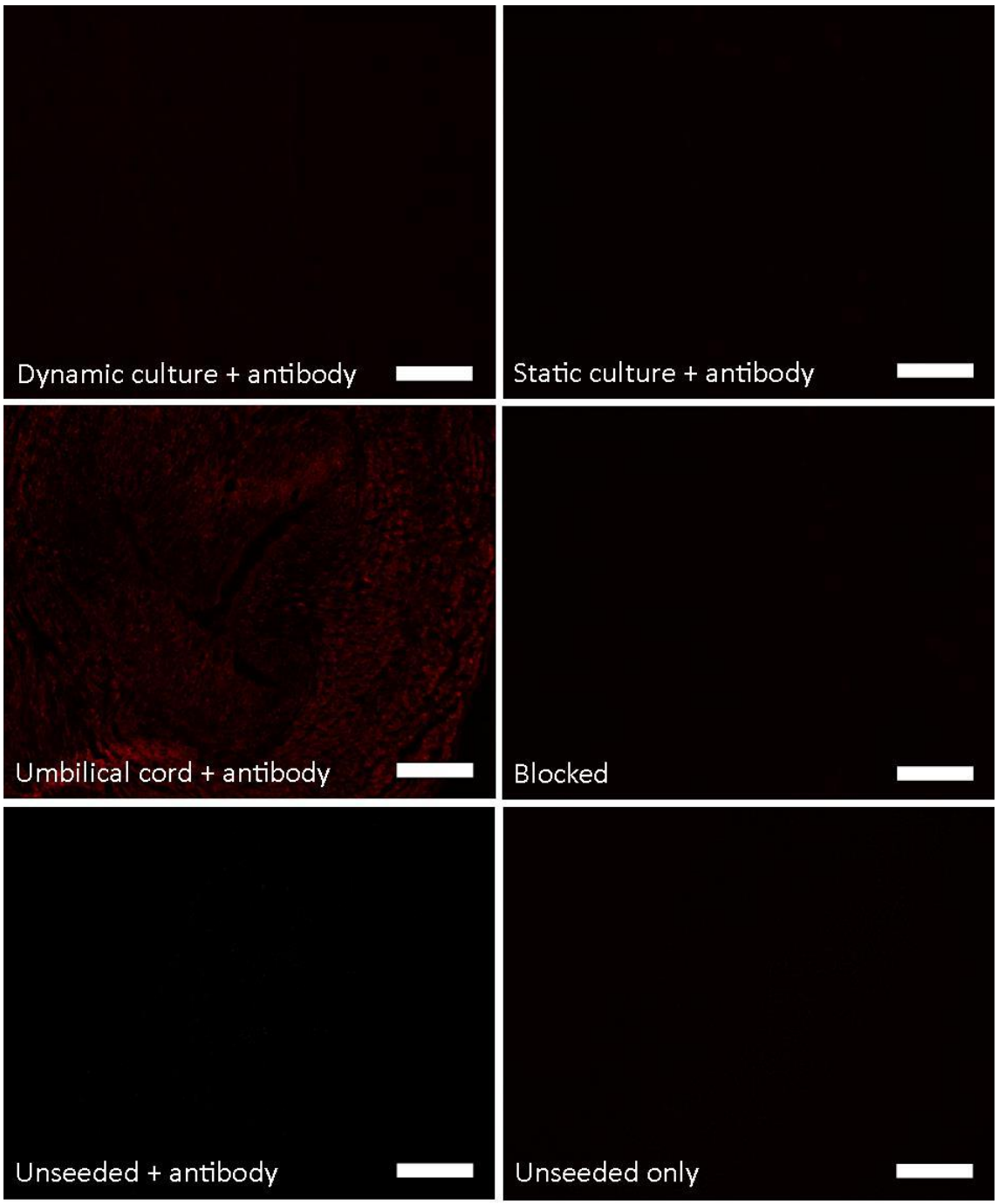

Figure 90. Representative sections from TEVGs cultured in the bioreactor, for 7 days, under dynamic and static conditions stained for α-SMA using immunohistochemistry (*n* = 1). TEVGs cultured under dynamic and static conditions did not stain positive for α-SMA (Dynamic culture + antibody and Static culture + antibody, respectively). Human umbilical cord arteries were used as positive controls and stained positive for α-SMA (Umbilical cord + antibody). Negative controls (Blocked, Unseeded + antibody and Unseeded only) did not stain positive for α-SMA. All images were captured and processed using equal exposure and display settings. Scale bars are 200 μm.

6.3.8 **Immunofluorescence staining of TEVGs for calponin**

Sections from the TEVGs cultured under dynamic conditions were also examined for the presence of calponin in the SMCs seeded onto them in the bioreactor, using immunohistochemistry. Similar to α-SMA, calponin is also a strong marker for contractile phenotype in SMCs. As in the examination of α-SMA, only sections taken from the third length cut from the TEVG connected to channel 3 in the bioreactor were examined for calponin. This was the only region of the TEVGs cultured under dynamic conditions for 7 days which displayed significant cell attachment. The results were similar to those observed for α-SMA. The cells present in these sections did not appear to stain positive for calponin (Figure 91). No significant fluorescence signal could be detected above that of the background.

Additionally, sections taken from the TEVGs cultured under static conditions for 7 days in the bioreactor were also examined for the presence of calponin. As in the TEVG cultured under dynamic conditions, the cells in these TEVGs did not stain positive for calponin, with no significant fluorescence signal detected.

Sections of human umbilical artery, used as positive controls, stained positive for the presence of Calponin. Negative controls were blocked, but unstained, sections of TEVGs seeded with SMCs and cultured in the bioreactor; unseeded and stained TEVGs cultured in the bioreactor and unseeded and unstained TEVGs cultured in the bioreactor. All of the negative controls did not stain positive for calponin.

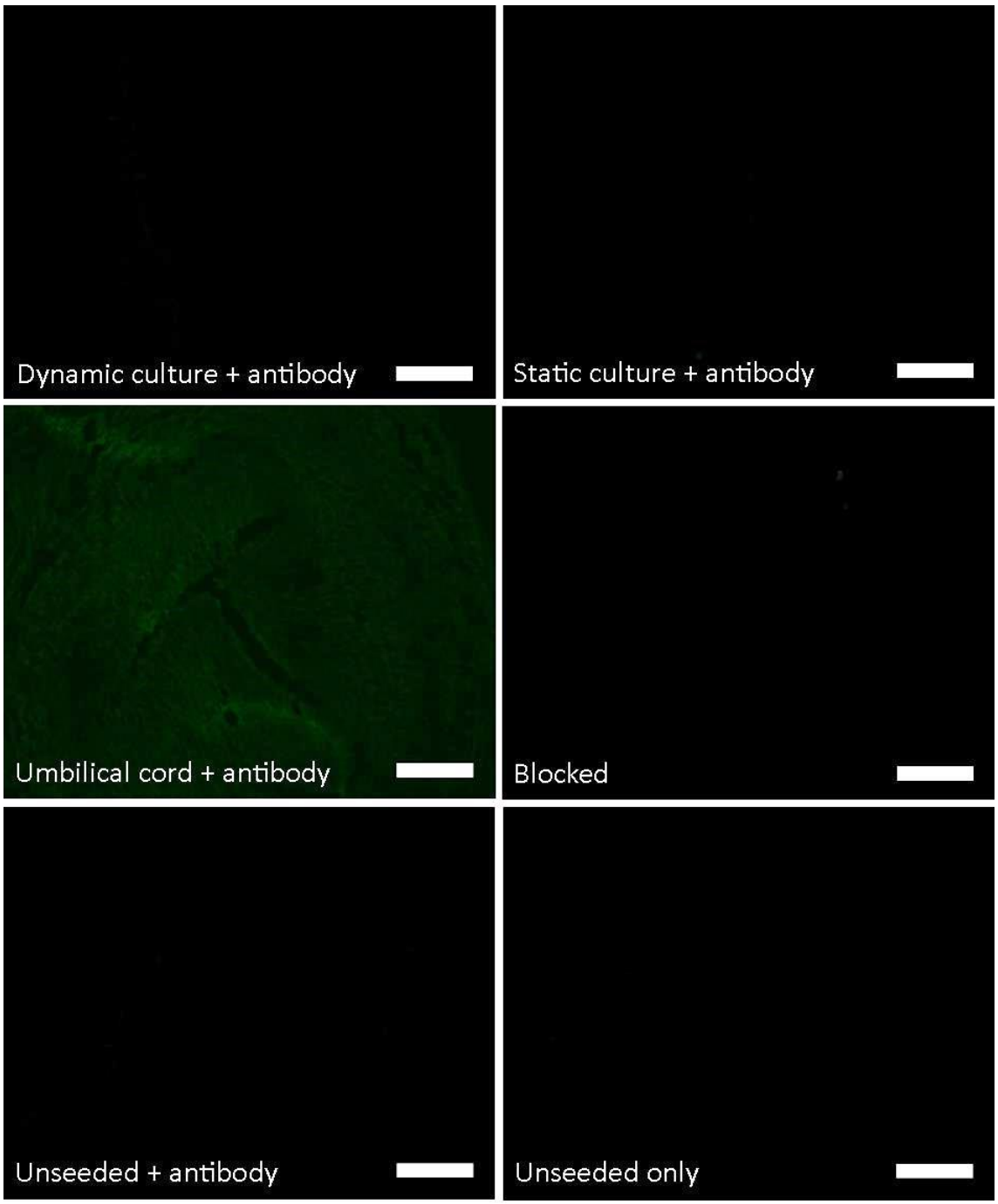

Figure 91. Representative sections from TEVGs cultured in the bioreactor, for 7 days, under dynamic and static conditions stained for calponin using immunohistochemistry (*n* = 1). TEVGs cultured under dynamic and static conditions did not stain positive for calponin (Dynamic culture + antibody and Static culture + antibody, respectively). Human umbilical cord arteries were used as positive controls and stained positive for calponin (Umbilical cord + antibody). Negative controls (Blocked, Unseeded + antibody and Unseeded only) did not stain positive for calponin. All images were captured and processed using equal exposure and display settings. Scale bars are 200 μm.

6.4 **Discussion**

Tubular PGS-M scaffolds seeded with SMCs were cultured for 7 days under dynamic and static conditions in bioreactor design 1.2 as TEVGs.

The PGS-M scaffolds required sterilisation prior to cell seeding. Sterilisation by autoclaving in autoclave bags resulted in severe deformation of the scaffolds. This may have been due to the pores in the scaffolds collapsing during the autoclave process. Subsequently, sterilisation using ethanol was employed. Although not appearing to damage the scaffolds structure, this resulted in infections appearing in the scaffolds during culture. Given that the sterilisation process had been undertaken using aseptic technique inside a biological safety cabinet and that the infection occurred on two separate occasions, it was possible that the infective agent was already present in the scaffolds. The infection appeared fungal, based on the appearance of filamentous structures in the scaffold sections examined using histology. It is possible that fungal spores were present in the sucrose porogens used to produce the scaffolds. Indeed, the dry environment required to store the porogens may have promoted fungal spore senescence. Fungal spores are highly resistant and may have survived the various solvent treatments involved in the scaffold manufacturing process along with the sterilisation with ethanol, which is not considered to be sporicidal.[361–363] Germination of the spores may then have been triggered during the incubation of the scaffolds in SMC growth medium.

Autoclaving the scaffolds while they were immersed in dH_2O ultimately rendered them sterile. The scaffolds retained their tubular shape. This may have been due to the surrounding fluid preventing the pores from collapsing during the autoclave process. Autoclaving is considered to have sporicidal action and therefore eliminated any infective spores that may have been present in the scaffolds. No evidence of infection was seen in the histological examination of the scaffolds sterilised by autoclaving while immersed in dH_2O. Additionally, the RR assay results for samples of the growth medium the scaffolds were incubated in were not significantly different from those of

the control growth medium. Both produced negligible fluorescence values suggesting that no metabolic activity, as a result of infection, was present in the medium.
Scaffold sterilisation by autoclaving while immersed in dH_2O was therefore employed prior to inserting the scaffolds into the bioreactor. The assembled bioreactor, containing the scaffolds was then sterilised by peracetic acid. This had previously been determined as a suitable method of sterilising the bioreactor. Although this treatment may also have been suitable to sterilise the scaffolds, the bioreactor represented a "high risk" environment for cell culture given the potential culture lengths that may ultimately be used (weeks/months). Using multiple sterilisation/disinfection processes is recommended as good practice in manufacturing and, therefore, both sterilisation methods were employed to treat the scaffolds. Autoclaving and peracetic acid treatment had been shown previously not to have a deleterious effect on the mechanical properties of the PGS-M scaffolds (2.3.7).

To validate the cell seeding process, the tubular PGS-M scaffolds were seeded in petri dishes, prior to any seeding attempts in the bioreactor. The scaffolds were seeded intraluminally with 2 x 10^6 cells/cm^2 of luminal surface area. This seeding density had been used in a number of previously published reports on producing TEVGs.[70,88,93] It was suggested that such a high seeding density is required to encourage the cells to quickly form a monolayer over the luminal surface, which is enlarged due to the presence of the pores. The cell-to-cell contact within the monolayer then promotes ECM formation.[93] Cell seeding was conducted twice with the scaffolds rotated about 180° in between. After 24 hours, histological examination of the seeded scaffolds showed the attachment of SMCs. These cells appeared be concentrated on the luminal surface on opposing sides. This likely reflected the seeding process with the areas of the lumen that were lowest during seeding receiving the greatest complement of cells due to them settling under gravity. Rotating the scaffold 180° between seeding processes thus resulted in the cells appearing to be concentrated on opposite sides of the lumen.

Proliferation of the cells attached to the luminal surface was likely limited by the short culture time (24 hours post seeding) prior to fixation and examination and therefore complete luminal coverage was not achieved.

A number of studies have demonstrated the positive effects of scaffold rotation during cell seeding. This process can be used to achieve greater and more uniform cell coverage of the scaffold and ultimately produce superior TEVGs. Seeding of scaffolds under rotation has be employed for both SMCs[88,93,116,122] and ECs[65,103,147] in vascular graft tissue engineering. Published methods appear to perform scaffold rotation about, 180°-360°, over a period of hours to allow for cell attachment across the luminal surface. A greater degree of rotation may be required to improve the luminal surface coverage the PGS-M scaffolds herein.

24 hours after cell seeding, limited cell invasion into the scaffold walls was observed. This was isolated to small regions and appeared sporadic. This suggested that the luminal surface porosity may be non-uniform and more limiting to cell invasion in some regions. This was similar to the observations of the PGS-M disks seeded with SMCs and cultured for 24 hours and 7 days (4.3.6). These results suggest that the surface of the porous PGS-M scaffolds may be a limiting factor to cell proliferation into the scaffold interiors.

Following validation of the cell seeding method, tubular PGS-M scaffolds were seeded with SMCs and cultured under dynamic conditions with pulsatile flow for 7 days in the bioreactor. Samples of the medium extracted from the bioreactor after completion of the culture did not show any significant metabolic activity when examined using the RR assay. The medium from the bioreactor culture produced fluorescence values that were not significantly different from a sample of control medium. This suggested that the bioreactor had remained free of infection throughout the dynamic culture. This result was replicated in the subsequent culture of TEVGs under static conditions and unseeded TEVGs under dynamic conditions, suggesting the bioreactor had also remained free of infection throughout these experiments.

Examination of the TEVGs seeded with SMCs and cultured under dynamic conditions showed high variability between the three replicates. SMCs were only present in the TEVGs connected to channels 2 and 3 of the bioreactor, and these were very limited in the former. In both cases, the cells were only present in the third length of the TEVGs, distal to the pump. These results suggested that the flow through the grafts may have had a detrimental effect on the seeded cells. When examining the TEVGs cultured under static conditions in the bioreactor, again for 7 days, SMCs were seen to be distributed throughout the graft lengths and appeared similar between replicates. This suggests that the seeding method was able to evenly distribute the cells across the lumen and adds further to the possibility of the flow being responsible for the variability observed between the TEVGs cultured under dynamic conditions. It is possible that the flow rate applied to the TEVGs was too high resulting in the removal of cells from the grafts or causing their movement down the luminal surfaces towards the distal end. The flow regime was selected based on a previously published successful method for culturing TEVGs in a bioreactor under pulsatile flow.[88,93] This work, by Wang and colleagues, utilised a similar scaffold design to that employed herein (a porous tubular PGS scaffold produced by porogen leaching with a 4 mm internal diameter, a 1 mm thick wall and ~70-80% porosity). Their scaffold was seeded with a different cell type to that used in this study, however (baboon carotid artery smooth muscle cells). Comparing the work by Wang and colleagues with the present study, it is possible that cell attachment and retention in the scaffolds may have varied due to subtle differences between the scaffold materials, porosity or surface topography, along with the cell type used. This could have produced the differences in the results observed.

Interestingly, flow rate measurements demonstrated that the flow rates across the three TEVG channels in the bioreactor were comparable between pump speeds of 6 and 60 rpm and relative pressures of 0 to 200 mmHg (5.3.8). In addition to this, the TEVGs cultured under static controls demonstrated that the cell seeding method used produced uniform cell coverage across the three TEVG replicates. The causes of the variability observed between the three TEVG replicates cultured under dynamic

conditions are therefore unclear. It must be noted, however, that the limited number of replicates makes drawing conclusions difficult. In the singular bioreactor culture conducted under dynamic conditions, it is possible that ineffective cell seeding may have affected the TEVG connected to channel 1 resulting in no cells being visible at day 7.

Although only small traces of SMCs could be seen in the TEVG connected to channel 2 in the bioreactor and cultured under dynamic conditions, in the TEVG connected to channel 3 the cell content was significant. Interestingly, the cells appeared to have formed a thick cell sheet across about one quarter of the luminal surface. This cell sheet appeared strongly attached to the scaffold, with no separation observed in any of the sections, as was common in sections from the TEVGs cultured under static conditions. The cell sheet appeared to be ~200 µm thick. It was unlikely that this was an artefact of the sectioning process or that a thinner layer of cells had become detached from the luminal surface and compacted to give the appearance of a thick sheet. This was because the structure of the cell sheet appeared conserved throughout the various sections cut and the ends of the sheet appeared to taper gradually down to reach the scaffold's luminal surface, suggesting some degree of order. Although cells were present throughout the TEVGs cultured under static conditions, none of these showed the formation of a cell sheet of equivalent structure or thickness to that seen in the TEVG cultured under dynamic conditions. This result suggests that the pulsatile flow applied during the dynamic culture may be the reason for the formation of this thick cell sheet. The flow may have improved the supply of nutrients to the cells attached to the scaffold or the mechanical stimulation resulting from the pressure pulses may have encouraged proliferation causing cell sheet thickening.

Wang and colleagues observed a similar behaviour in their TEVGs cultured under pulsatile flow. The group found that TEVG formation was improved by using scaffolds with smaller pore sizes.[93] They examined scaffolds produced from porogens of 75-90 µm, 45-53 µm and 25-35 µm. In the scaffolds with the smaller pores, cell infiltration was less than in those with larger pores; however, ECM deposition was

greater. The seeded SMCs formed a thick cell sheet of ~200 µm, similar to that observed in the present study (Figure 92). It was suggested that the limited infiltration of the SMCs into the scaffold, caused by the smaller pore sizes, produced greater cell-to-cell contact and aided self-assembly and organisation of the SMCs into a cell sheet. A similar effect may have occurred in the present study, with the luminal surface of the PGS-M scaffolds limiting cell penetration into the scaffold interior and promoting self-assembly and organisation into a cell sheet.

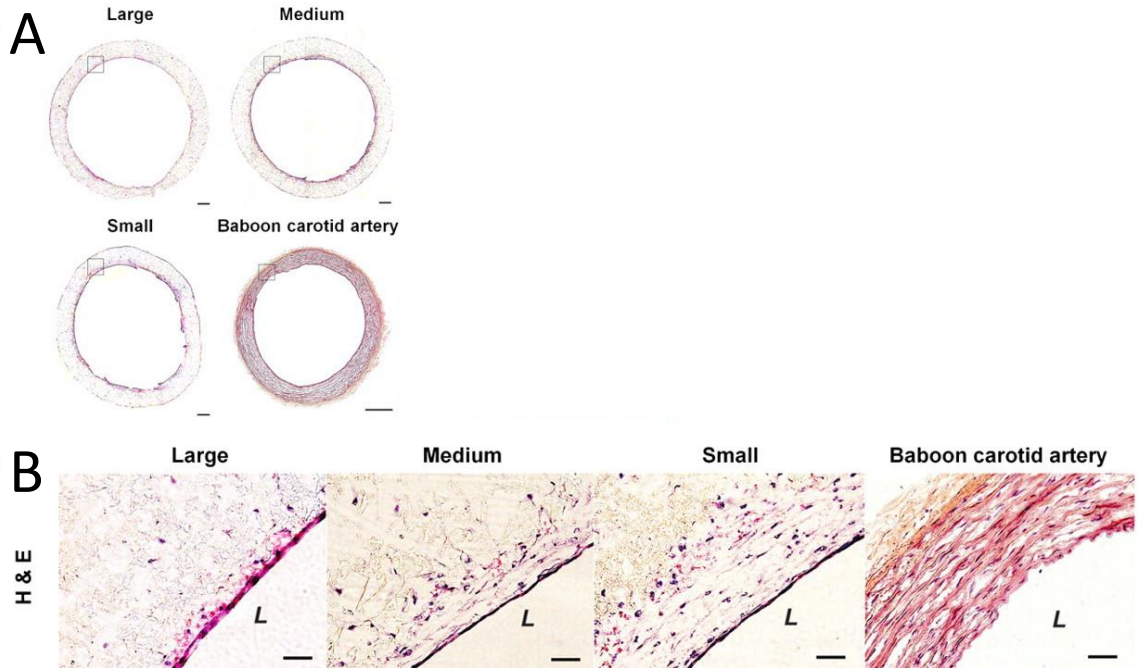

Figure 92. H&E stained sections from TEVGs produced by Wang and colleagues.[93] Porous PGS scaffolds were seeded with baboon carotid artery SMCs and cultured in a pulsatile flow bioreactor for 21 days. Scaffolds were produced from Large (75-90 µm), Medium (45-53 µm) and Small (25-35 µm) porogens to generate different pore size ranges. A baboon carotid artery was sectioned and stained to act as a control. (A) TEVG cross-sections, (B) boxed regions highlighted in A magnified. Cell sheets composed of SMCs were seen across the luminal surface of all of the seeded scaffolds. Limited cell invasion into the PGS scaffolds was observed with this being most pronounced in the Small pore scaffolds. Scale bars are 500 µm in A and 50 µm in B. *L* denotes the TEVG lumen. Figure reproduced with permission.

Comparing the structure of the cell sheet in the dynamic cultured TEVG with the human umbilical artery showed similar structures. H&E stained sections showed connective tissues with similar organisation. This suggests that the cell sheet was organised in a similar way to natural blood vessels. Comparing the sections taken from the TEVGs cultured under dynamic conditions with those cultured under static conditions suggested some difference in the organisation of the SMCs. All of the sections from TEVGs cultured under static conditions showed some detachment of the cells from the lumen. This was likely a result of the sectioning process; however, this also suggests that the attachment of the cells to the scaffold was weaker than in the TEVG cultured under dynamic conditions, where no detachment was observed. It may be possible that the relative pressure acting on the cells inside the lumen in the TEVGs in dynamic culture facilitated greater contact between the cells and the scaffold, resulting in greater adhesion between the two. Alternatively, the mechanical stimulation provided by the pulsatile flow may have resulted in gene expression changes which may have altered the cells binding to the PGS-M scaffold and improved cell attachment. Indeed, the expression of integrins, which are key proteins for the binding of cells to substrata, has been shown to be upregulated by mechanical stimulation in vascular cells.[364]

The SMCs present in the TEVGs cultured under dynamic and static conditions both appeared to generate collagen. Histological staining showed that collagen was present throughout the cellular regions of both types of TEVGs. No significant differences in quantity were suggested by the staining alone, although both appeared to stain weaker than in the positive control (human umbilical artery), suggesting a lesser quantity than in this. The organisation of the collagen appeared similar to that of the umbilical artery, also.

Subsequent analysis and quantification of the collagen content of the TEVGs using SHG supported the presence of collagen. The SHG signal intensity associated with collagen was higher than that generated by the PGS-M scaffold or background alone. No significant difference in collagen quantity could be found between the TEVGs cultured

under dynamic and static conditions. It should be noted, however, that the sample number used for this analysis was quite limited, as only the TEVG cultured under dynamic conditions connected to channel 3 of the bioreactor contained a significant area of cells for analysis. Although the effect of mechanical stimulation in dynamic culture on collagen deposition in TEVGs is well established, with dynamic cultures resulting in increased collagen deposition,[61,75,84,122,336] strong conclusions about the collagen contents of the TEVGs produced in dynamic and static cultures in this study cannot be drawn without a greater sample size.

Elastin also appeared to be present in the TEVGs cultured under dynamic and static conditions. Similar to the observations of collagen, no significant difference between the two culture regimes was observable from the staining alone. Both TEVGs stained less strongly than the umbilical artery, suggesting reduced elastin content compared to this. The organisation of the elastin also appeared similar to the umbilical artery.

No quantification of the elastin content was made. Given the very small sample size it was not possible to draw conclusions about the differences in elastin deposition based on dynamic and static cultures in this study. The presence of elastin in both types of TEVG is all that can be confirmed.

In the literature, generating elastin in TEVGs based on synthetic polymer scaffolds has proven challenging. Elastin deposition has been linked to a number of factors including scaffold stiffness, topography and degradation rate, along with application of mechanical stimulation and the cell source used.[82,84,86,88,93,101,103,235,240–243] In studies where dynamic and static cultures have been compared, it has been shown that dynamic culture appears to increases elastin deposition, although this may be as a result of a synergistic effect between mechanical stimulation and the scaffold material.

The organisation and maturity of the elastin deposited in TEVGs must also be considered. Although elastin may be detected in a TEVG, its assembly into microfibrils and mature fibres is required to achieve its native function.[230] Assessing elastin maturity is difficult using visual inspection alone and, therefore, it is not possible to meaningfully assess the maturity of the elastin fibres observed in the TEVGs produced

herein, in both dynamic and static cultures. Measuring the desmosine content of TEVGs allows a method of quantifying mature elastin content, as this is a cross-linker unique to mature elastin.[93,365] This could be employed to determine if any difference in the organisation and maturity of the elastin fibres is present between TEVGs produced using PGS-M scaffolds and dynamic and static cultures.

Examination using immunohistochemistry revealed that the SMCs present on the TEVGs cultured under dynamic and static conditions in the bioreactor did not appear to possess α-SMA or Calponin. α-SMA and calponin are considered as stronger markers for the mature contractile SMC phenotype, along with smooth muscle myosin heavy chains, SM22α and smoothelin.[328] These proteins may be expressed individually and transiently in other cell types and therefore it is considered that a multitude of them must be detected in order to confidently determine the SMC phenotype.

Mature SMCs are not terminally differentiated cells and possess considerable plasticity. This plasticity is required for blood vessel formation during embryogenesis and vascular remodelling and repair. SMC plasticity appears to be dependent on environmental and extracellular matrix signals sensed by the cells.[366–368] Control of the SMC phenotype appears to be highly complex and variable and is not fully understood. It has been demonstrated that switching from a mature contractile SMC phenotype to a synthetic proliferative SMC phenotype is associated with a marked decrease in SMC-selective marker gene expression and increased proliferation and migration.[328] Some studies have demonstrated that the use of mechanical stimulation through cyclic strain applied to SMCs allows retention of the mature SMC phenotypic markers while also encouraging proliferation,[369] although other works appear to contradict this.[94,370] SMCs have also been shown to change phenotype, from contractile to synthetic, in response to ECM interactions. Collagen I and fibronectin have both been shown to enhance SMC proliferation and ECM production while reducing the contractile phenotype markers.[371,372]

In the present study the cause of the reduction in α-SMA and calponin expression, to levels undetectable using immunohistochemistry, is unclear. Given that this result was

seen in TEVGs cultured using both dynamic and static conditions suggests that the cause may not be associated with the different culture regimes. Interaction between the SMCs and PGS-M scaffold may have been the cause, as this was a common element in the two different bioreactor cultures. Although SMCs of a similar age to those used in the bioreactor cultures had been previously shown to retain the expression of α-SMA and calponin when cultured on PGS-M (3.3.4 and 3.3.5), these experiments were performed using 2D PGS-M surfaces. It is possible that an interaction between the SMCs and the 3D porous PGS-M scaffold may have caused the change in phenotype marker expression. Interestingly, Niklason and colleagues suggested that the degradation products generated by the hydrolysis of a PGA scaffold were the cause of the dedifferentiation of SMCs in the bioreactor culture of a TEVG.[67] A similar effect had been previously observed in the interaction of SMCs with polyester based vascular prosthetics.[373] The mechanism behind this was unclear. A local decrease in pH due to glycolic acid components or effects of phagocytosed polymer particles, released by the degradation of the scaffold, were suggested as possible causes. A similar effect could have occurred in the present study. Indeed, the greater surface area of the PGS-M scaffolds compared to the 2D PGS-M surfaces would likely have enhanced degradation and this could explain the differences in α-SMA and calponin expression in the SMCs grown on these substrata.

Further investigation is required to understand the change in the expression of the contractile SMC phenotypic markers observed in the TEVGs cultured under dynamic and static conditions in the present study. This may benefit from employing a method of quantitative examination of the expression of the contractile SMC phenotypic markers.

Additionally, an interesting consideration is whether the apparent loss of the contractile SMC phenotype from the TEVGs cultured under dynamic and static conditions in the bioreactor is actually detrimental. The production of the TEVGs *in vitro*, using PGS-M scaffolds and the bioreactor requires the proliferation of SMCs, to populate the scaffold, and also requires the production of significant amounts of ECM,

to provide the graft with the required mechanical properties. SMC proliferation and ECM deposition are both typically associated with the dedifferentiated synthetic SMC phenotype and, therefore, this may be considered advantageous for TEVG generation. Historically, developers of TEVGs have attempted to avoid the synthetic SMC phenotype due to the issues this can cause *in vivo*. An underlying process in the formation of intimal hyperplasia and atherosclerosis is SMC phenotype switching, from contractile to proliferative.[328] Therefore, the retention of the contractile phenotype has been favoured in TEVGs designed for direct implantation into patients, following *in vitro* culture. However, new techniques in TEVG manufacturing, such as the decellularisation of *in vitro* derived vessels, decouple the cells used to produce the TEVGs in culture from the intended patient. If these methods were incorporated into the production of a TEVG, loss of the contractile SMC phenotype may not be problematic.

6.5 **Conclusions**

Human coronary artery SMCs were successfully seeded onto tubular PGS-M scaffolds and cultured for 7 days under dynamic and static conditions in a previously designed bioreactor. TEVGs cultured under dynamic conditions, with mechanical stimulation produced by a pulsatile flow, displayed highly variable results, but demonstrated the partial formation of blood vessel-like tissue in a small instance. TEVGs cultured under static conditions produced repeatable results, but demonstrated reduced vascular tissue formation compared to the grafts cultured under dynamic conditions. Both culture regimes produced TEVGs containing collagen and elastin and both also appeared to cause a change in the phenotype of the attached SMCs, from contractile to proliferative.

Further work is required to optimise the production of TEVGs using PGS-M scaffolds and bioreactor culture. A combination of static and dynamic culture regimes may be employed in achieving this. Greater repeatability between the grafts cultured under dynamic conditions and the generation of suitable cellularity and ECM deposition are required to produce TEVGs with the potential for clinical use.

Chapter 7 - Future work

In the previous chapters, the initial development of a TEVG based on a PGS-M polymer scaffold has been described. The original aim of this research was to produce a TEVG with mechanical properties more closely matching those of the gold standard autograft vessels (saphenous vein and internal thoracic artery) currently used in vascular surgery. To this end a synthetic polymer scaffold based approach to tissue engineering was employed. PGS-M was selected as the scaffold material because of its mechanical properties, degradation rate, biocompatibility and processing capabilities. Porous tubular scaffolds were fabricated from PGS-M, seeded with SMCs, and cultured inside a bespoke dynamic culture bioreactor. However, the bioreactor culture period was limited to only 7 days and only a small amount of vascular tissue was generated. Therefore, the original aim of this research has not yet been achieved. Future work may explore the further development of the PGS-M scaffold based TEVG, in an effort to achieve the originally defined aim.

Future work should begin with an optimisation of the bioreactor culture of the PGS-M scaffold based TEVGs. Bioreactor cultures were conducted under both static and dynamic conditions, with the former producing consistent results, across three TEVG replicates, and the latter producing the best tissue formation, although inconsistently and only in a very limited quantity. Since it was the application of pulsatile flow, and therefore mechanical stimulation, to the TEVGs that was the difference between the dynamic and static cultures, improving the consistency of the TEVGs cultured under dynamic conditions may begin with altering the flow parameters. A combination of the static and dynamic culture regimes may be explored. An initial period of bioreactor culture under static conditions, to permit initial cell attachment and proliferation, followed by the application of a dynamic culture regime, to enhance tissue formation and ECM deposition, may produce improved results.

Once the bioreactor is able to produce consistent results, for both static and dynamic culture conditions, the culture lengths may be extended to increase tissue formation. The resulting TEVGs may then be analysed on a cellular and structural level. Cellular analysis *in vitro* may be challenging due to the bioreactor environment, however, a number of assays compatible with fixed tissue may offer insight into the health and phenotype of the cells within the TEVGs. Calcein AM and TUNEL assays are both compatible with fixed tissues and can be used to determine cell health by measuring apoptosis.[374–376] Markers for mitosis; such as MPM-2, phospho-histone H3, proliferating cell nuclear antigen, topoisomerase II and Ki-67; can be detected using immunohistochemistry, offering information on the extent of cell proliferation within the TEVGs.[374,377–379] Immunohistochemistry may also be used to examine the SMC phenotype. The markers α-SMA and calponin may be examined, as previously, along with myosin heavy chains and smoothelin which are also associated with this phenotype.[328,329] Additionally, inflammation may be detected using assays for pro-inflammatory cytokines or markers such as RelA or C-reactive protein (Cuhlmann 2011, Amsen 2009 and Venugopal 2002).[380–382] The ECM composition of the TEVGs and their mechanical properties, including burst pressure, suture retention strength and compliance may also be examined. This would allow a comparison between the different culture regimes and also a comparison with the gold standard autograft vessels currently used in vascular grafting. These comparisons would then guide future developments of the TEVG culture protocol. Variation of the seeded cell type, flow parameters, culture length and medium supplementation may all be examined in an effort to generate a TEVG that demonstrates similar properties to the gold standard vessels.

It may also be interesting to explore the addition of vascular ECs to the TEVG culture. These cells line the luminal surfaces of natural blood vessels and have important anti-thrombogenic properties. Additionally, vascular ECs are able to sense shear stresses associated with blood flow and act as mechanotransducers. The detected shear stresses generate signals which are transduced to the SMCs beyond the ECs

basement membrane and result in blood vessel remodelling. High shear stresses have been shown to be detected by ECs and result in changes in the structure of arteries, including increasing vessel diameters and ECM deposition.[383,384]

Vascular ECs could be added to the TEVG culture without any modifications to the bioreactor. Following SMC seeding onto the PGS-M scaffolds, ECs could be seeded on top of the SMCs using the cell seeding ports. It is possible that adding ECs to the TEVG bioreactor culture may have a similar effect to that observed in the native vessels, with the mechanical stimulation provided by the bioreactor flow detected by the ECs and transduced to the underlying SMCs, resulting in improved ECM deposition. The bioreactor flow could be further modified to amplify this by generating higher flow rates. Utilising ECs in this way may offer a substitute to expensive media supplementation as a method of encouraging the SMCs to generate the required ECM proteins. The complexity added by the co-culture of the SMCs and ECs would have to be weighed against this gain, however.

In addition to modifications to the bioreactor culture protocol, the PGS-M scaffold may also be altered to improve vascular tissue formation. The results demonstrated in this research suggested that little cell invasion into the porous PGS-M scaffolds occurred during bioreactor culture. This may be improved be altering the scaffold porosity. It was demonstrated that utilising different sized sucrose particle porogens produced variations in scaffold porosity. Tubular scaffolds produced from different sized porogens may be explored to examine their effect on TEVG development.

With the exploration of longer bioreactor culture lengths, the degradation of the PGS-M scaffolds will become an important factor and warrant in depth investigation. PGS-M was selected for the scaffold material because of the rapid degradation rate the material exhibited during *in vitro* studies, although these results were not considered directly translatable to the TEVG culture environment. How the scaffold degrades and the effect that this has on the developing TEVGs must be explored. It may be interesting to explore the degradation of the scaffold using some of the spectroscopy

approaches used to characterise the PGS-M material. In particular, Raman spectroscopy may allow examination of the developing TEVG during culture, as Raman spectroscopy is compatible with live tissue samples.[385] This would represent an interesting study in the field of TEVGs.

Adding additional functionality to the bioreactor may also be considered. It may be valuable to add systems that allow for live monitoring of the developing TEVGs. Non-destructive methods such as optical coherence tomography and electrical impedance spectroscopy could be used. These techniques would be able to provide detail on the composition of the TEVGs, along with the migration and proliferation of the cells within them, without interfering with the culture process.[386–389]

During the development of the bioreactor, maintaining sterility was challenging. Various sterilisation methods and scaffold seeding procedures were explored in an effort to avoid infection of the developing TEVGs. Although a sterilisation protocol, using peracetic acid, and scaffold seeding method were developed that successfully maintained sterility, limited examination of the infections that were experienced previously was performed. As bioreactor culture lengths are increased and more advanced culture protocols are explored, using SMC and EC co-cultures for example, it may be wise to examine any future infections, should they occur, in more detail. Microbiological analysis could be used to identify the infective agents and this information then used to suggest the source of the infection and determine the best possible countermeasures.

It may also be useful to explore alternative sterilisation methods for the bioreactor. The peracetic acid sterilisation method employed previously is laborious and alternatives such as gamma irradiation or ethylene oxide treatment may be more efficient. It will be important to examine the effect that these methods have on the bioreactor and the porous PGS-M scaffolds, as different sterilisation methods have been shown to affect the mechanical properties of materials.[390–392]

Looking beyond the original aim of this research, should the PGS-M scaffold based TEVGs eventually display mechanical properties comparable to those of the current gold standards used in vascular grafting, research work should move towards potential clinical translation. To this end, it would be interesting to explore the possibility of decellularising the TEVGs following bioreactor culture. This process has proven successful in TEVGs currently undergoing the final stages of clinical trials and represents a potentially safer and more economical route to clinical application.[70,72] A decellularisation protocol would require developing specifically for the PGS-M based TEVGs. This protocol would need to achieve suitable removal of the antigenic components of the grafts, while retaining their mechanical properties.

Implantation *in vivo* should also be considered to assess the grafts under true physiological conditions. This should be performed for a short period in a small animal model first, with rabbit suggested as the most suitable, before examination in a larger host for a longer period.[352] Efficacy must be established in animal models before the first human implantations can be considered.

Additionally, it was also an aim of this research to produce a synthetic polymer scaffold for culturing TEVGs which could be made in any shape. This technology was demonstrated as a proof-of-concept and requires further development. The hybrid additive manufacturing and porogen leaching method may be further investigated. Producing scaffolds with varied porosities, by using different porogens, and in different geometries should be explored. This may be aided by some automation of the manufacturing process. Image projection may be used to selectively photocure the PGS-M prepolymer and sucrose layers and a mechanised deposition system added to apply these. Once different shaped porous PGS-M scaffolds have been produced they could then be seeded with cells and cultured in the bioreactor to produce TEVGs. This would likely require further investigations to develop culture protocols to produce the different shaped TEVGs. Ultimately, this technology may allow the production of

TEVGs with more complex geometries than simple tubes which has the potential to improve their performance and extend the possible clinical applications.

Finally, the PGS-M material has possible applications in other areas of tissue engineering. It was demonstrated that this material has a wide range of tuneable mechanical properties. This would make it a suitable candidate for use in both hard and soft tissue engineering applications.

References

1. Zoghbi, W. A. *et al.* Sustainable Development Goals and the Future of Cardiovascular Health: A Statement From the Global Cardiovascular Disease Taskforce. *Journal of the American College of Cardiology* **64,** 1385–1387 (2014).
2. Mathers, C. D. & Loncar, D. Projections of Global Mortality and Burden of Disease from 2002 to 2030. *PLoS Med* **3,** e442 (2006).
3. Abdulhannan, P., Russell, D. A. & Homer-Vanniasinkam, S. Peripheral arterial disease: a literature review. *British Medical Bulletin* **104,** 21–39 (2012).
4. Antoniou, G. A. *et al.* A meta-analysis of endovascular versus surgical reconstruction of femoropopliteal arterial disease. *Journal of Vascular Surgery* **57,** 242–253 (2013).
5. Conte, M. S. Critical appraisal of surgical revascularization for critical limb ischemia. *Journal of Vascular Surgery* **57,** 8S–13S (2013).
6. Mohr, F. W. *et al.* Coronary artery bypass graft surgery versus percutaneous coronary intervention in patients with three-vessel disease and left main coronary disease: 5-year follow-up of the randomised, clinical SYNTAX trial. *Lancet* **381,** 629–638 (2013).
7. Farkouh, M. E. *et al.* Strategies for Multivessel Revascularization in Patients with Diabetes. *New England Journal of Medicine* **367,** 2375–2384 (2012).
8. Weintraub, W. S. *et al.* Comparative Effectiveness of Revascularization Strategies. *New England Journal of Medicine* **366,** 1467–1476 (2012).
9. Go, A. S. *et al.* Heart Disease and Stroke Statistics—2013 Update A Report From the American Heart Association. *Circulation* **127,** e6–e245 (2013).
10. Masden, D. L., Seruya, M. & Higgins, J. P. A Systematic Review of the Outcomes of Distal Upper Extremity Bypass Surgery With Arterial and Venous Conduits. *The Journal of Hand Surgery* **37,** 2362–2367 (2012).

11. Athanasiou, T. *et al.* Radial artery versus saphenous vein conduits for coronary artery bypass surgery: forty years of competition — which conduit offers better patency? A systematic review and meta-analysis. *Eur J Cardiothorac Surg* **40,** 208–220 (2011).
12. Cho, K. R., Kim, J.-S., Jae-Sung, C. & Kim, K.-B. Serial angiographic follow-up of grafts one year and five years after coronary artery bypass surgery. *Eur J Cardiothorac Surg* **29,** 511–516 (2006).
13. Goldman, S. *et al.* Long-term patency of saphenous vein and left internal mammary artery grafts after coronary artery bypass surgeryResults from a Department of Veterans Affairs Cooperative Study. *J Am Coll Cardiol* **44,** 2149–2156 (2004).
14. Harskamp, R. E., Lopes, R. D., Baisden, C. E., de Winter, R. J. & Alexander, J. H. Saphenous Vein Graft Failure After Coronary Artery Bypass Surgery: Pathophysiology, Management, and Future Directions. *Annals of Surgery May 2013* **257,** 824–833 (2013).
15. Klinkert, P., Post, P. N., Breslau, P. J. & van Bockel, J. H. Saphenous Vein Versus PTFE for Above-Knee Femoropopliteal Bypass. A Review of the Literature. *European Journal of Vascular and Endovascular Surgery* **27,** 357–362 (2004).
16. Chew, D. K. W. *et al.* Bypass in the absence of ipsilateral greater saphenous vein: safety and superiority of the contralateral greater saphenous vein. *J. Vasc. Surg.* **35,** 1085–1092 (2002).
17. Taylor, L. M., Jr, Edwards, J. M., Brant, B., Phinney, E. S. & Porter, J. M. Autogenous reversed vein bypass for lower extremity ischemia in patients with absent or inadequate greater saphenous vein. *Am. J. Surg.* **153,** 505–510 (1987).
18. Junqueira, L. C. & Carneiro, J. in *Basic Histology* 205–222 (McGraw-Hill, 2003).
19. Brewster, D. C. Current controversies in the management of aortoiliac occlusive disease. *Journal of Vascular Surgery* **25,** 365–379 (1997).

20. Chlupác, J., Filova, E. & Ba\vcáková, L. Blood vessel replacement: 50 years of development and tissue engineering paradigms in vascular surgery. *Physiological Research* **58,** S119 (2009).

21. Hadinata, I. E. *et al.* Choice of Conduit for the Right Coronary System: 8-Year Analysis of Radial Artery Patency and Clinical Outcomes Trial. *The Annals of Thoracic Surgery* **88,** 1404–1409 (2009).

22. Shah, P. J. *et al.* Has the in situ right internal thoracic artery been overlooked? An angiographic study of the radial artery, internal thoracic arteries and saphenous vein graft patencies in symptomatic patients. *Eur J Cardiothorac Surg* **27,** 870–875 (2005).

23. Chard Rb, Johnson Dc, Nunn Gr & Cartmill Tb. Aorta-coronary bypass grafting with polytetrafluoroethylene conduits. Early and late outcome in eight patients. *J Thorac Cardiovasc Surg* **94,** 132–134 (1987).

24. Hehrlein, F., F, L., Hh, S., P, W. & J, M. The use of expanded polytetrafluoroethylene (PTFE) grafts for myocardial revascularization. *J Cardiovasc Surg (Torino)* **25,** 549–553 (1983).

25. Norgren, L. *et al.* Inter-Society Consensus for the Management of Peripheral Arterial Disease (TASC II). *Journal of Vascular Surgery* **45,** S5–S67 (2007).

26. Ballotta, E., Renon, L., Toffano, M. & Da Giau, G. Prospective randomized study on bilateral above-knee femoropopliteal revascularization: polytetrafluoroethylene graft versus reversed saphenous vein. *Journal of Vascular Surgery* **38,** 1051–1055 (2003).

27. Green, R. M. *et al.* Prosthetic above-knee femoropopliteal bypass grafting: Five-year results of a randomized trial. *Journal of Vascular Surgery* **31,** 417–425 (2000).

28. Johnson, W. C. & Lee, K. K. A comparative evaluation of polytetrafluoroethylene, umbilical vein, and saphenous vein bypass grafts for femoral-popliteal above-knee

revascularization: A prospective randomized Department of Veterans Affairs cooperative study. *Journal of Vascular Surgery* **32,** 268–277 (2000).

29. AbuRahma, A. F., Robinson, P. A. & Holt, S. M. Prospective controlled study of polytetrafluoroethylene versus saphenous vein in claudicant patients with bilateral above knee femoropopliteal bypasses. *Surgery* **126,** 594–602 (1999).
30. Deutsch, M. *et al.* Long-term experience in autologous in vitro endothelialization of infrainguinal ePTFE grafts. *Journal of Vascular Surgery* **49,** 352–362 (2009).
31. Eslami, M. H. *et al.* Monocyte adhesion to human vein grafts: A marker for occult intraoperative injury? *Journal of Vascular Surgery* **34,** 923–929 (2001).
32. Burkel, W. E. *et al.* Sequential studies of healing in endothelial seeded vascular prostheses: Histologic and ultrastructure characteristics of graft incorporation. *Journal of Surgical Research* **30,** 305–324 (1981).
33. Sarkar, S., Salacinski, H. J., Hamilton, G. & Seifalian, A. M. The Mechanical Properties of Infrainguinal Vascular Bypass Grafts: Their Role in Influencing Patency. *European Journal of Vascular and Endovascular Surgery* **31,** 627–636 (2006).
34. Haruguchi, H. & Teraoka, S. Intimal hyperplasia and hemodynamic factors in arterial bypass and arteriovenous grafts: a review. *J Artif Organs* **6,** 227–235 (2003).
35. Tiwari, A., Cheng, K.-S., Salacinski, H., Hamilton, G. & Seifalian, A. M. Improving the patency of vascular bypass grafts: The role of suture materials and surgical techniques on reducing anastomotic compliance mismatch. *European Journal of Vascular and Endovascular Surgery* **25,** 287–295 (2003).
36. Greenwald, S. E. & Berry, C. L. Improving vascular grafts: the importance of mechanical and haemodynamic properties. *The Journal of Pathology* **190,** 292–299 (2000).

37. Lemson, M. S., Tordoir, J. H. M., Daemen, M. J. A. P. & Kitslaar, P. J. E. H. M. Intimal Hyperplasia in Vascular Grafts. *European Journal of Vascular and Endovascular Surgery* **19,** 336–350 (2000).

38. Ballyk, P. D., Walsh, C., Butany, J. & Ojha, M. Compliance mismatch may promote graft–artery intimal hyperplasia by altering suture-line stresses. *Journal of Biomechanics* **31,** 229–237 (1997).

39. Davies, M. G. & Hagen, P.-O. Pathophysiology of vein graft failure: A review. *European Journal of Vascular and Endovascular Surgery* **9,** 7–18 (1995).

40. FitzGibbon, G. M., Leach, A. J., Kafka, H. P. & Keon, W. J. Coronary bypass graft fate: Long-term angiographic study. *Journal of the American College of Cardiology* **17,** 1075–1080 (1991).

41. van der Wal, A. C., Becker, A. E., Elbers, J. R. & Das, P. K. An immunocytochemical analysis of rapidly progressive atherosclerosis in human vein grafts. *Eur J Cardiothorac Surg* **6,** 469–473; discussion 474 (1992).

42. Cox, J. L., Chiasson, D. A. & Gotlieb, A. I. Stranger in a strange land: The pathogenesis of saphenous vein graft stenosis with emphasis on structural and functional differences between veins and arteries. *Progress in Cardiovascular Diseases* **34,** 45–68 (1991).

43. Padberg Jr, F. T., Calligaro, K. D. & Sidawy, A. N. Complications of arteriovenous hemodialysis access: Recognition and management. *Journal of Vascular Surgery* **48,** S55–S80 (2008).

44. Zetrenne, E. *et al.* Prosthetic Vascular Graft Infection: A Multi-Center Review of Surgical Management. *Yale J Biol Med* **80,** 113–121 (2007).

45. Chiesa, R. *et al.* Vascular prosthetic graft infection: epidemiology, bacteriology, pathogenesis and treatment. *Acta Chirurgica Belgica* 238–247 (2002).

46. Bunt, T. J. Vascular graft infections: an update. *Cardiovascular Surgery* **9,** 225–233 (2001).

47. Mertens, R. A., O'Hara, P. J., Hertzer, N. R., Krajewski, L. P. & Beven, E. G. Surgical management of infrainguinal arterial prosthetic graft infections: Review of a thirty-five-year experience. *Journal of Vascular Surgery* **21,** 782–791 (1995).

48. Ballotta, E. *et al.* Prospective randomized study on reversed saphenous vein infrapopliteal bypass to treat limb-threatening ischemia: Common femoral artery versus superficial femoral or popliteal and tibial arteries as inflow. *Journal of Vascular Surgery* **40,** 732–740 (2004).

49. Baguneid, M. S. *et al.* Tissue engineering of blood vessels. *British Journal of Surgery* **93,** 282–290 (2006).

50. Owida, A. A., Do, H. & Morsi, Y. S. Numerical analysis of coronary artery bypass grafts: An over view. *Computer Methods and Programs in Biomedicine* **108,** 689–705 (2012).

51. Scharn, D. M., Daamen, W. F., van Kuppevelt, T. H. & van der Vliet, J. A. Biological Mechanisms Influencing Prosthetic Bypass Graft Patency: Possible Targets for Modern Graft Design. *European Journal of Vascular and Endovascular Surgery* **43,** 66–72 (2012).

52. John, L. C. H. Biomechanics of Coronary Artery and Bypass Graft Disease: Potential New Approaches. *The Annals of Thoracic Surgery* **87,** 331–338 (2009).

53. Weinberg, C. B. & Bell, E. A blood vessel model constructed from collagen and cultured vascular cells. *Science* **231,** 397–400 (1986).

54. Shinoka, T. *et al.* Creation Of Viable Pulmonary Artery Autografts Through Tissue Engineering. *The Journal of Thoracic and Cardiovascular Surgery* **115,** 536–546 (1998).

55. Hibino, N. *et al.* Late-term results of tissue-engineered vascular grafts in humans. *The Journal of Thoracic and Cardiovascular Surgery* **139,** 431–436.e2 (2010).

56. Shin'oka, T. *et al.* Midterm clinical result of tissue-engineered vascular autografts seeded with autologous bone marrow cells. *The Journal of Thoracic and Cardiovascular Surgery* **129,** 1330–1338 (2005).

57. Kim, S.-J., Kim, W.-H., Lim, H.-G. & Lee, J.-Y. Outcome of 200 patients after an extracardiac Fontan procedure. *The Journal of Thoracic and Cardiovascular Surgery* **136,** 108–116 (2008).

58. Giannico, S. *et al.* Clinical Outcome of 193 Extracardiac Fontan PatientsThe First 15 Years. *J Am Coll Cardiol* **47,** 2065–2073 (2006).

59. Mirensky, T. L. *et al.* Tissue-engineered arterial grafts: long-term results after implantation in a small animal model. *Journal of Pediatric Surgery* **44,** 1127–1133 (2009).

60. Niklason, L. E. & Langer, R. Advances in tissue engineering of blood vessels and other tissues. *Transplant Immunology* **5,** 303–306 (1997).

61. Niklason, L. E. *et al.* Functional Arteries Grown in Vitro. *Science* **284,** 489–493 (1999).

62. Wise, S. G. *et al.* A multilayered synthetic human elastin/polycaprolactone hybrid vascular graft with tailored mechanical properties. *Acta Biomaterialia* **7,** 295–303 (2011).

63. Konig, G. *et al.* Mechanical properties of completely autologous human tissue engineered blood vessels compared to human saphenous vein and mammary artery. *Biomaterials* **30,** 1542–1550 (2009).

64. L'Heureux, N. *et al.* Human tissue-engineered blood vessels for adult arterial revascularization. *Nat Med* **12,** 361–365 (2006).

65. Lamm, P., Juchem, G., Milz, S., Schuffenhauer, M. & Reichart, B. Autologous Endothelialized Vein Allograft A Solution in the Search for Small-Caliber Grafts in Coronary Artery Bypass Graft Operations. *Circulation* **104,** I-108-I-114 (2001).

66. L'Heureux, N., Pâquet, S., Labbé, R., Germain, L. & Auger, F. A. A completely biological tissue-engineered human blood vessel. *FASEB J* **12,** 47–56 (1998).

67. Niklason, L. E. *et al.* Morphologic and mechanical characteristics of engineered bovine arteries. *Journal of Vascular Surgery* **33,** 628–638 (2001).

68. Quint, C., Arief, M., Muto, A., Dardik, A. & Niklason, L. E. Allogeneic human tissue-engineered blood vessel. *Journal of Vascular Surgery* **55,** 790–798 (2012).

69. Quint, C. *et al.* Decellularized tissue-engineered blood vessel as an arterial conduit. *PNAS* **108,** 9214–9219 (2011).

70. Dahl, S. L. M. *et al.* Readily Available Tissue-Engineered Vascular Grafts. *Science Translational Medicine* **3,** 68ra9-68ra9 (2011).

71. Tsutsumi, H., Miyawaki, F., Arakawa, H., Tsuji, T. & Tanigawa, M. Experience of Vein Grafting in Göttingen Minipigs. *Experimental Animals* **50,** 191–195 (2001).

72. Lawson, J. H. *et al.* Bioengineered human acellular vessels for dialysis access in patients with end-stage renal disease: two phase 2 single-arm trials. *The Lancet* **387,** 2026–2034 (2016).

73. Lok, C. E. *et al.* Cumulative Patency of Contemporary Fistulas versus Grafts (2000–2010). *CJASN* **8,** 810–818 (2013).

74. Huber, T. S., Carter, J. W., Carter, R. L. & Seeger, J. M. Patency of autogenous and polytetrafluoroethylene upper extremity arteriovenous hemodialysis accesses: a systematic review. *Journal of Vascular Surgery* **38,** 1005–1011 (2003).

75. Cummings, I. *et al.* Tissue-engineered vascular graft remodeling in a growing lamb model: expression of matrix metalloproteinases. *Eur J Cardiothorac Surg* **41,** 167–172 (2012).

76. Hoerstrup, S. P. *et al.* Functional Growth in Tissue-Engineered Living, Vascular Grafts Follow-Up at 100 Weeks in a Large Animal Model. *Circulation* **114,** I-159-I-166 (2006).

77. Nieponice, A. *et al. In Vivo* Assessment of a Tissue-Engineered Vascular Graft Combining a Biodegradable Elastomeric Scaffold and Muscle-Derived Stem Cells in a Rat Model. *Tissue Engineering Part A* **16,** 1215–1223 (2010).

78. He, W. *et al.* Pericyte-based human tissue engineered vascular grafts. *Biomaterials* **31,** 8235–8244 (2010).

79. Matsumura, G. *et al.* Long-term results of cell-free biodegradable scaffolds for in situ tissue engineering of pulmonary artery in a canine model. *Biomaterials* **34,** 6422–6428 (2013).

80. Lu, G. *et al.* Design and preparation of polyurethane-collagen/heparin-conjugated polycaprolactone double-layer bionic small-diameter vascular graft and its preliminary animal tests. *Chinese medical journal* **126,** 1310–1316 (2013).

81. Yokota, T. *et al.* In situ tissue regeneration using a novel tissue-engineered, small-caliber vascular graft without cell seeding. *The Journal of Thoracic and Cardiovascular Surgery* **136,** 900–907 (2008).

82. Wu, W., Allen, R. A. & Wang, Y. Fast-degrading elastomer enables rapid remodeling of a cell-free synthetic graft into a neoartery. *Nat Med* **18,** 1148–1153 (2012).

83. Kuwabara, F. *et al.* Long-term results of tissue-engineered small-caliber vascular grafts in a rat carotid arterial replacement model. *J Artif Organs* **15,** 399–405 (2012).

84. Thomas, L. V. & Nair, P. D. The Effect of Pulsatile Loading and Scaffold Structure for the Generation of a Medial Equivalent Tissue Engineered Vascular Graft. *BioResearch Open Access* **2,** 227–239 (2013).

85. de Valence, S. *et al.* Long term performance of polycaprolactone vascular grafts in a rat abdominal aorta replacement model. *Biomaterials* **33,** 38–47 (2012).

86. Lin, S., Sandig, M. & Mequanint, K. Three-Dimensional Topography of Synthetic Scaffolds Induces Elastin Synthesis by Human Coronary Artery Smooth Muscle Cells. *Tissue Engineering Part A* **17,** 1561–1571 (2011).

87. McMahon, R. E. *et al.* Hydrogel–Electrospun Mesh Composites for Coronary Artery Bypass Grafts. *Tissue Engineering Part C: Methods* **17,** 451–461 (2011).

88. Crapo, P. M. & Wang, Y. Physiologic compliance in engineered small-diameter arterial constructs based on an elastomeric substrate. *Biomaterials* **31,** 1626–1635 (2010).

89. Hu, J. *et al.* Porous nanofibrous PLLA scaffolds for vascular tissue engineering. *Biomaterials* **31,** 7971–7977 (2010).

90. Ju, Y. M., Choi, J. S., Atala, A., Yoo, J. J. & Lee, S. J. Bilayered scaffold for engineering cellularized blood vessels. *Biomaterials* **31,** 4313–4321 (2010).

91. Soletti, L. *et al.* A bilayered elastomeric scaffold for tissue engineering of small diameter vascular grafts. *Acta Biomaterialia* **6,** 110–122 (2010).

92. Dahl, S. *et al.* Abstracts From the Emerging Science Series, April 24, 2013. *Circulation* **127,** 2071–2072 (2013).

93. Lee, K.-W., Stolz, D. B. & Wang, Y. Substantial expression of mature elastin in arterial constructs. *PNAS* **108,** 2705–2710 (2011).

94. Sharifpoor, S., Simmons, C. A., Labow, R. S. & Paul Santerre, J. Functional characterization of human coronary artery smooth muscle cells under cyclic mechanical strain in a degradable polyurethane scaffold. *Biomaterials* **32,** 4816–4829 (2011).

95. Iwasaki, K. *et al.* Bioengineered Three-Layered Robust and Elastic Artery Using Hemodynamically-Equivalent Pulsatile Bioreactor. *Circulation* **118,** S52–S57 (2008).

96. Haisch, A. *et al.* Preparation of a pure autologous biodegradable fibrin matrix for tissue engineering. *Med. Biol. Eng. Comput.* **38,** 686–689 (2000).

97. Huynh, T. N. & Tranquillo, R. T. Fusion of Concentrically Layered Tubular Tissue Constructs Increases Burst Strength. *Ann Biomed Eng* **38,** 2226–2236 (2010).

98. Syedain, Z. H., Meier, L. A., Bjork, J. W., Lee, A. & Tranquillo, R. T. Implantable arterial grafts from human fibroblasts and fibrin using a multi-graft pulsed flow-stretch bioreactor with noninvasive strength monitoring. *Biomaterials* **32,** 714–722 (2011).

99. Syedain, Z. H., Meier, L. A., Lahti, M. T., Johnson, S. L. & Tranquillo, R. T. Implantation of Completely Biological Engineered Grafts Following Decellularization into the Sheep Femoral Artery. *Tissue Engineering Part A* **20,** 1726–1734 (2014).

100. Syedain, Z. *et al.* Tissue engineering of acellular vascular grafts capable of somatic growth in young lambs. *Nature Communications* **7,** 12951 (2016).

101. Swartz, D. D., Russell, J. A. & Andreadis, S. T. Engineering of fibrin-based functional and implantable small-diameter blood vessels. *American Journal of Physiology - Heart and Circulatory Physiology* **288,** H1451–H1460 (2005).

102. Yao, L., Liu, J. & Andreadis, S. T. Composite Fibrin Scaffolds Increase Mechanical Strength and Preserve Contractility of Tissue Engineered Blood Vessels. *Pharm Res* **25,** 1212–1221 (2008).

103. Liu, J. Y. *et al.* Functional tissue-engineered blood vessels from bone marrow progenitor cells. *Cardiovasc Res* **75,** 618–628 (2007).

104. Bjork, J. W., Meier, L. A., Johnson, S. L., Syedain, Z. H. & Tranquillo, R. T. Hypoxic Culture and Insulin Yield Improvements to Fibrin-Based Engineered Tissue. *Tissue Engineering Part A* **18,** 785–795 (2012).

105. Lovett, M. *et al.* Tubular silk scaffolds for small diameter vascular grafts. *Organogenesis* **6,** 217–224 (2010).

106. Enomoto, S. *et al.* Long-term patency of small-diameter vascular graft made from fibroin, a silk-based biodegradable material. *Journal of Vascular Surgery* **51,** 155–164 (2010).

107. Soffer, L. *et al.* Silk-based electrospun tubular scaffolds for tissue-engineered vascular grafts. *Journal of Biomaterials Science, Polymer Edition* **19,** 653–664 (2008).

108. Marelli, B. *et al.* Collagen-Reinforced Electrospun Silk Fibroin Tubular Construct as Small Calibre Vascular Graft. *Macromolecular Bioscience* **12,** 1566–1574 (2012).

109. Achilli, M., Lagueux, J. & Mantovani, D. On the Effects of UV-C and pH on the Mechanical Behavior, Molecular Conformation and Cell Viability of Collagen-Based Scaffold for Vascular Tissue Engineering. *Macromolecular Bioscience* **10,** 307–316 (2010).

110. Liang, W.-H. *et al.* Concentrated collagen-chondroitin sulfate scaffolds for tissue engineering applications. *Journal of Biomedical Materials Research Part A* **94A,** 1050–1060 (2010).

111. Girton, T. S., Oegema, T. R., Grassl, E. D., Isenberg, B. C. & Tranquillo, R. T. Mechanisms of Stiffening and Strengthening in Media-Equivalents Fabricated Using Glycation. *Journal of Biomechanical Engineering* **122,** 216 (2000).

112. Barocas, V. H., Girton, T. S. & Tranquillo, R. T. Engineered alignment in media equivalents : Magnetic prealignment and Mandrel compaction. *Journal of biomechanical engineering* **120,** 660–666 (1998).

113. L'Heureux, N., Germain, L., Labbé, R. & Auger, F. A. In vitro construction of a human blood vessel from cultured vascular cells: A morphologic study. *Journal of Vascular Surgery* **17,** 499–509 (1993).

114. Schutte, S. C., Chen, Z., Brockbank, K. G. M. & Nerem, R. M. Cyclic Strain Improves Strength and Function of a Collagen-Based Tissue-Engineered Vascular Media. *Tissue Engineering Part A* **16,** 3149–3157 (2010).

115. Seliktar, D., Black, R. A., Vito, R. P. & Nerem, R. M. Dynamic Mechanical Conditioning of Collagen-Gel Blood Vessel Constructs Induces Remodeling In Vitro. *Annals of Biomedical Engineering* **28,** 351–362 (2000).

116. Buttafoco, L. *et al.* Physical characterization of vascular grafts cultured in a bioreactor. *Biomaterials* **27,** 2380–2389 (2006).

117. Deng, C., Li, F., Griffith, M., Ruel, M. & Suuronen, E. J. Application of Chitosan-Based Biomaterials for Blood Vessel Regeneration. *Macromolecular Symposia* **297,** 138–146 (2010).

118. Zhang, L. *et al.* A sandwich tubular scaffold derived from chitosan for blood vessel tissue engineering. *Journal of Biomedical Materials Research Part A* **77A,** 277–284 (2006).

119. Zhu, C. *et al.* Initial investigation of novel human-like collagen/chitosan scaffold for vascular tissue engineering. *Journal of Biomedical Materials Research Part A* **89A,** 829–840 (2009).

120. Stegemann, J. P., Kaszuba, S. N. & Rowe, S. L. Review: Advances in Vascular Tissue Engineering Using Protein-Based Biomaterials. *Tissue Engineering* **13,** 2601–2613 (2007).

121. Boccafoschi, F., Rajan, N., Habermehl, J. & Mantovani, D. Preparation and Characterization of a Scaffold for Vascular Tissue Engineering by Direct-Assembling of Collagen and Cells in a Cylindrical Geometry. *Macromolecular Bioscience* **7,** 719–726 (2007).

122. Engbers-Buijtenhuijs, P. *et al.* Biological characterisation of vascular grafts cultured in a bioreactor. *Biomaterials* **27,** 2390–2397 (2006).

123. Dubey, G. & Mequanint, K. Conjugation of fibronectin onto three-dimensional porous scaffolds for vascular tissue engineering applications. *Acta Biomaterialia* **7,** 1114–1125 (2011).

124. Wang, S., Zhang, Y., Yin, G., Wang, H. & Dong, Z. Electrospun polylactide/silk fibroin–gelatin composite tubular scaffolds for small-diameter tissue engineering blood vessels. *Journal of Applied Polymer Science* **113,** 2675–2682 (2009).

125. Koch, S. *et al.* Fibrin-polylactide-based tissue-engineered vascular graft in the arterial circulation. *Biomaterials* **31,** 4731–4739 (2010).

126. Fukunishi, T. *et al.* Tissue-Engineered Small Diameter Arterial Vascular Grafts from Cell-Free Nanofiber PCL/Chitosan Scaffolds in a Sheep Model. *PLOS ONE* **11,** e0158555 (2016).

127. Zhao, J. *et al.* Development of nanofibrous scaffolds for vascular tissue engineering. *International Journal of Biological Macromolecules* **56,** 106–113 (2013).

128. Tillman, B. W. *et al.* The in vivo stability of electrospun polycaprolactone-collagen scaffolds in vascular reconstruction. *Biomaterials* **30,** 583–588 (2009).

129. Crapo, P. M., Gilbert, T. W. & Badylak, S. F. An overview of tissue and whole organ decellularization processes. *Biomaterials* **32,** 3233–3243 (2011).

130. Cho, S.-W. *et al.* Small-Diameter Blood Vessels Engineered With Bone Marrow-Derived Cells. *Ann Surg* **241,** 506–515 (2005).

131. Conklin, B. S., Richter, E. R., Kreutziger, K. L., Zhong, D.-S. & Chen, C. Development and evaluation of a novel decellularized vascular xenograft. *Medical Engineering & Physics* **24,** 173–183 (2002).

132. Rosenberg, N. *et al.* Tanned collagen arterial prosthesis of bovine carotid origin in man. Preliminary studies of enzyme-treated heterografts. *Ann Surg* **164,** 247–256 (1966).

133. Chemla, E. S. & Morsy, M. Randomized clinical trial comparing decellularized bovine ureter with expanded polytetrafluoroethylene for vascular access. *Br J Surg* **96,** 34–39 (2009).

134. Katzman, H. E., Glickman, M. H., Schild, A. F., Fujitani, R. M. & Lawson, J. H. Multicenter Evaluation of the Bovine Mesenteric Vein Bioprostheses for Hemodialysis Access in Patients with an Earlier Failed Prosthetic Graft. *Journal of the American College of Surgeons* **201,** 223–230 (2005).

135. Schmidli, J. *et al.* Bovine Mesenteric Vein Graft (ProCol) in Critical Limb Ischaemia with Tissue Loss and Infection. *European Journal of Vascular and Endovascular Surgery* **27,** 251–253 (2004).

136. Kovalic, A. J., Beattie, D. K. & Davies, A. H. Outcome of ProCol, a bovine mesenteric vein graft, in infrainguinal reconstruction. *European Journal of Vascular and Endovascular Surgery* **24,** 533–534 (2002).

137. Schröder, A., Imig, H., Peiper, U., Neidel, J. & Petereit, A. Results of a bovine collagen vascular graft (Solcograft-P) in infra-inguinal positions. *European Journal of Vascular Surgery* **2,** 315–321 (1988).

138. Hurt, A. V., Batello-Cruz, M., Skipper, B. J., Teaf, S. R. & Sterling Jr., W. A. Bovine carotid artery heterografts versus polytetrafluoroethylene grafts: A prospective, randomized study. *The American Journal of Surgery* **146,** 844–847 (1983).

139. Sabanayagam, P., Schwartz, A. B., Soricelli, R. R., Lyons, P. & Chinitz, J. A comparative study of 402 bovine heterografts and 225 reinforced expanded PTFE grafts as AVF in the ESRD patient. *Trans Am Soc Artif Intern Organs* **26,** 88–99 (1980).

140. Sawyer, P. N., Stanczewski, B., Sivakoff, S., Lucas, T. & Kirschenbaum, D. Search for the ideal collagen vascular prosthesis. *Trans Am Soc Artif Intern Organs* **23,** 288–295 (1977).

141. Dukkipati, R. *et al.* Biological Grafts for Hemodialysis Access: Historical Lessons, State-of-the-Art and Future Directions. *Seminars in Dialysis* **26,** 233–239 (2013).

142. Li, L., Terry, C. M., Shiu, Y.-T. E. & Cheung, A. K. Neointimal hyperplasia associated with synthetic hemodialysis grafts. *Kidney Int* **74,** 1247–1261 (2008).

143. Scott, E. C. & Glickman, M. H. Conduits for Hemodialysis Access. *Seminars in Vascular Surgery* **20,** 158–163 (2007).

144. Berardinelli, L. Grafts and Graft Materials as Vascular Substitutes for Haemodialysis Access Construction. *European Journal of Vascular and Endovascular Surgery* **32,** 203–211 (2006).

145. Madden, R. L., Lipkowitz, G. S., Browne, B. J. & Kurbanov, A. Experience with Cryopreserved Cadaveric Femoral Vein Allografts Used for Hemodialysis Access. *Annals of Vascular Surgery* **18,** 453–458 (2004).

146. Olausson, M. *et al.* Transplantation of an allogeneic vein bioengineered with autologous stem cells: a proof-of-concept study. *The Lancet* **380,** 230–237 (2012).

147. Tillman, B. W. *et al.* Bioengineered vascular access maintains structural integrity in response to arteriovenous flow and repeated needle puncture. *Journal of Vascular Surgery* **56,** 783–793 (2012).

148. Kaushal, S. *et al.* Functional small-diameter neovessels created using endothelial progenitor cells expanded ex vivo. *Nat Med* **7,** 1035–1040 (2001).

149. Piterina, A. V. *et al.* ECM-Based Materials in Cardiovascular Applications: Inherent Healing Potential and Augmentation of Native Regenerative Processes. *International Journal of Molecular Sciences* **10,** 4375–4417 (2009).

150. Sandusky, G. E., Lantz, G. C. & Badylak, S. F. Healing Comparison of Small Intestine Submucosa and ePTFE Grafts in the Canine Carotid Artery. *Journal of Surgical Research* **58,** 415–420 (1995).

151. Roeder, R., Lantz, G. C. & Geddes, L. A. Mechanical remodeling of small-intestine submucosa small-diameter vascular grafts-a preliminary report. *Biomed Instrum Technol* **35,** 110–120 (2000).

152. Hiles, M. C. *et al.* Mechanical properties of xenogeneic small-intestinal submucosa when used as an aortic graft in the dog. *Journal of Biomedical Materials Research* **29,** 883–891 (1995).

153. Peng, H.-F., Liu, J. Y., Andreadis, S. T. & Swartz, D. D. Hair Follicle-Derived Smooth Muscle Cells and Small Intestinal Submucosa for Engineering Mechanically Robust and Vasoreactive Vascular Media. *Tissue Eng. Part A* **17,** 981–990 (2011).

154. Koobatian, M. T. *et al.* Successful endothelialization and remodeling of a cell-free small-diameter arterial graft in a large animal model. *Biomaterials* **76,** 344–358 (2016).

155. Tosi, G. M., Massaro-Giordano, M., Caporossi, A. & Toti, P. Amniotic membrane transplantation in ocular surface disorders. *Journal of Cellular Physiology* **202,** 849–851 (2005).

156. Amensag, S. & McFetridge, P. S. Rolling the Human Amnion to Engineer Laminated Vascular Tissues. *Tissue Eng. Part C-Methods* **18,** 903–912 (2012).

157. Lee, P.-H. *et al.* A prototype tissue engineered blood vessel using amniotic membrane as scaffold. *Acta Biomaterialia* **8,** 3342–3348 (2012).

158. Peirovi, H., Rezvani, N., Hajinasrollah, M., Mohammadi, S. S. & Niknejad, H. Implantation of amniotic membrane as a vascular substitute in the external jugular vein of juvenile sheep. *Journal of Vascular Surgery* **56,** 1098–1104 (2012).

159. Badylak, S. F., Freytes, D. O. & Gilbert, T. W. Extracellular matrix as a biological scaffold material: Structure and function. *Acta Biomaterialia* **5,** 1–13 (2009).

160. Piterina, A. V. *et al.* Extracellular matrices as advanced scaffolds for vascular tissue engineering. *Bio-Medical Materials and Engineering* **19,** 333–348 (2009).

161. Woods, A. M., Rodenberg, E. J., Hiles, M. C. & Pavalko, F. M. Improved biocompatibility of small intestinal submucosa (SIS) following conditioning by human endothelial cells. *Biomaterials* **25,** 515–525 (2004).

162. Reing, J. E. *et al.* Degradation Products of Extracellular Matrix Affect Cell Migration and Proliferation. *Tissue Engineering Part A* **15,** 605–614 (2009).

163. Grauss, R. W. *et al.* Histological evaluation of decellularised porcine aortic valves: matrix changes due to different decellularisation methods. *Eur J Cardiothorac Surg* **27,** 566–571 (2005).

164. Schenke-Layland, K. *et al.* Impact of decellularization of xenogeneic tissue on extracellular matrix integrity for tissue engineering of heart valves. *Journal of Structural Biology* **143,** 201–208 (2003).

165. Keane, T. J., Londono, R., Turner, N. J. & Badylak, S. F. Consequences of ineffective decellularization of biologic scaffolds on the host response. *Biomaterials* **33,** 1771–1781 (2012).

166. Spark, J. I., Yeluri, S., Derham, C., Wong, Y. T. & Leitch, D. Incomplete cellular depopulation may explain the high failure rate of bovine ureteric grafts. *Br J Surg* **95,** 582–585 (2008).

167. Roy, S., Silacci, P. & Stergiopulos, N. Biomechanical proprieties of decellularized porcine common carotid arteries. *Am J Physiol Heart Circ Physiol* **289,** H1567–H1576 (2005).

168. Simon, P. *et al.* Early failure of the tissue engineered porcine heart valve SYNERGRAFT® in pediatric patients. *Eur J Cardiothorac Surg* **23,** 1002–1006 (2003).

169. Tosun, Z. & McFetridge, P. S. Improved recellularization of ex vivo vascular scaffolds using directed transport gradients to modulate ECM remodeling. *Biotechnology and Bioengineering* **110,** 2035–2045 (2013).

170. Gratzer, P. F., Harrison, R. D. & Woods, T. Matrix Alteration and Not Residual Sodium Dodecyl Sulfate Cytotoxicity Affects the Cellular Repopulation of a Decellularized Matrix. *Tissue Engineering* **12,** 2975–2983 (2006).

171. Ketchedjian, A. *et al.* Recellularization of Decellularized Allograft Scaffolds in Ovine Great Vessel Reconstructions. *The Annals of Thoracic Surgery* **79,** 888–896 (2005).

172. Butler III, H. G., Baker Jr, L. D. & Johnson, J. M. Vascular access for chronic hemodialysis: Polytetrafluoroethylene (PTFE) versus bovine heterograft. *The American Journal of Surgery* **134,** 791–793 (1977).

173. Peck, M., Gebhart, D., Dusserre, N., McAllister, T. N. & L'Heureux, N. The Evolution of Vascular Tissue Engineering and Current State of the Art. *Cells Tissues Organs* **195,** 144–158 (2012).

174. L'Heureux, N. *et al.* A human tissue-engineered vascular media: a new model for pharmacological studies of contractile responses. *FASEB J* **15,** 515–524 (2001).

175. McAllister, T. N. *et al.* Effectiveness of haemodialysis access with an autologous tissue-engineered vascular graft: a multicentre cohort study. *The Lancet* **373,** 1440–1446 (2009).

176. Rosas, S. E. *et al.* Determinants of successful synthetic hemodialysis vascular access graft placement. *Journal of Vascular Surgery* **37,** 1036–1042 (2003).

177. Wystrychowski, W. *et al.* First human use of an allogeneic tissue-engineered vascular graft for hemodialysis access. *Journal of Vascular Surgery* **60,** 1353–1357 (2014).

178. Wystrychowski, W. *et al.* Case study: first implantation of a frozen, devitalized tissue-engineered vascular graft for urgent hemodialysis access. *J Vasc Access* **12,** 67–70 (2011).

179. L'Heureux, N. *et al.* Abstracts From the Emerging Science Series, April 24, 2013. *Circulation* **127,** 2071–2072 (2013).

180. Peck, M., Dusserre, N., McAllister, T. N. & L'Heureux, N. Tissue engineering by self-assembly. *Materials Today* **14,** 218–224 (2011).

181. Zhao, J. *et al.* A Novel Strategy to Engineer Small-Diameter Vascular Grafts From Marrow-Derived Mesenchymal Stem Cells. *Artificial Organs* **36,** 93–101 (2012).

182. Bourget, J.-M. *et al.* Human fibroblast-derived ECM as a scaffold for vascular tissue engineering. *Biomaterials* **33,** 9205–9213 (2012).

183. Tondreau, M. Y. *et al.* In Vivo Remodeling of Fibroblast-Derived Vascular Scaffolds Implanted for 6 Months in Rats. *BioMed Research International* **2016,** e3762484 (2016).

184. Kelm, J. M. *et al.* A novel concept for scaffold-free vessel tissue engineering: Self-assembly of microtissue building blocks. *Journal of Biotechnology* **148,** 46–55 (2010).

185. Norotte, C., Marga, F. S., Niklason, L. E. & Forgacs, G. Scaffold-free vascular tissue engineering using bioprinting. *Biomaterials* **30,** 5910–5917 (2009).

186. Marga, F. *et al.* Toward engineering functional organ modules by additive manufacturing. *Biofabrication* **4,** 22001 (2012).

187. Poh, M. *et al.* Blood vessels engineered from human cells. *The Lancet* **365,** 2122–2124 (2005).

188. McKee, J. A. *et al.* Human arteries engineered in vitro. *EMBO reports* **4,** 633–638 (2003).

189. Gao, J., Ensley, A. E., Nerem, R. M. & Wang, Y. Poly(glycerol sebacate) supports the proliferation and phenotypic protein expression of primary baboon vascular cells. *Journal of Biomedical Materials Research Part A* **83A,** 1070–1075 (2007).

190. Shapira, O. M. *et al.* Enhanced Nitric Oxide–Mediated Vascular Relaxation in Radial Artery Compared With Internal Mammary Artery or Saphenous Vein. *Circulation* **100,** II-322-Ii-327 (1999).

191. Hill, J. M. *et al.* Circulating Endothelial Progenitor Cells, Vascular Function, and Cardiovascular Risk. *New England Journal of Medicine* **348,** 593–600 (2003).

192. Matsumura, G., Miyagawa-Tomita, S., Shin'oka, T., Ikada, Y. & Kurosawa, H. First Evidence That Bone Marrow Cells Contribute to the Construction of Tissue-Engineered Vascular Autografts In Vivo. *Circulation* **108,** 1729–1734 (2003).

193. Le Blanc, K., Tammik, C., Rosendahl, K., Zetterberg, E. & Ringdén, O. HLA expression and immunologic properties of differentiated and undifferentiated mesenchymal stem cells. *Experimental Hematology* **31,** 890–896 (2003).

194. Jiang, Y. *et al.* Multipotent progenitor cells can be isolated from postnatal murine bone marrow, muscle, and brain. *Experimental Hematology* **30,** 896–904 (2002).

195. Zuk, P. A. *et al.* Human Adipose Tissue Is a Source of Multipotent Stem Cells. *Mol. Biol. Cell* **13,** 4279–4295 (2002).

196. Campagnoli, C. *et al.* Identification of mesenchymal stem/progenitor cells in human first-trimester fetal blood, liver, and bone marrow. *Blood* **98,** 2396–2402 (2001).

197. Colter, D. C., Class, R., DiGirolamo, C. M. & Prockop, D. J. Rapid expansion of recycling stem cells in cultures of plastic-adherent cells from human bone marrow. *PNAS* **97,** 3213–3218 (2000).

198. Gong, Z. & Niklason, L. E. Small-diameter human vessel wall engineered from bone marrow-derived mesenchymal stem cells (hMSCs). *FASEB J* **22,** 1635–1648 (2008).

199. Melero-Martin, J. M. *et al.* Engineering Robust and Functional Vascular Networks In Vivo With Human Adult and Cord Blood–Derived Progenitor Cells. *Circulation Research* **103,** 194–202 (2008).

200. Mirza, A. *et al.* Undifferentiated mesenchymal stem cells seeded on a vascular prosthesis contribute to the restoration of a physiologic vascular wall. *Journal of Vascular Surgery* **47,** 1313–1321 (2008).

201. Hashi, C. K. *et al.* Antithrombogenic property of bone marrow mesenchymal stem cells in nanofibrous vascular grafts. *PNAS* **104,** 11915–11920 (2007).

202. Harris, L. J. *et al.* Differentiation of Adult Stem Cells into Smooth Muscle for Vascular Tissue Engineering. *Journal of Surgical Research* **168,** 306–314 (2011).

203. Heydarkhan-Hagvall, S. *et al.* Human Adipose Stem Cells: A Potential Cell Source for Cardiovascular Tissue Engineering. *Cells Tissues Organs* **187,** 263–274 (2008).

204. Planat-Benard, V. *et al.* Plasticity of Human Adipose Lineage Cells Toward Endothelial Cells Physiological and Therapeutic Perspectives. *Circulation* **109,** 656–663 (2004).

205. Zhang, P. *et al.* Endothelial Differentiation of Adipose-Derived Stem Cells from Elderly Patients with Cardiovascular Disease. *Stem Cells and Development* **20,** 977–988 (2011).

206. DiMuzio, P. & Tulenko, T. Tissue engineering applications to vascular bypass graft development: The use of adipose-derived stem cells. *Journal of Vascular Surgery* **45,** A99–A103 (2007).

207. Gao, Y. *et al.* Acellular Blood Vessels Combined Human Hair Follicle Mesenchymal Stem Cells for Engineering of Functional Arterial Grafts. *Ann Biomed Eng* **42,** 2177–2189 (2014).

208. Bajpai, V. K., Mistriotis, P. & Andreadis, S. T. Clonal multipotency and effect of long-term in vitro expansion on differentiation potential of human hair follicle derived mesenchymal stem cells. *Stem Cell Research* **8,** 74–84 (2012).

209. Hoogduijn, M. J., Gorjup, E. & Genever, P. G. Comparative Characterization of Hair Follicle Dermal Stem Cells and Bone Marrow Mesenchymal Stem Cells. *Stem Cells and Development* **15,** 49–60 (2006).

210. Reynolds, A. J., Lawrence, C., Cserhalmi-Friedman, P. B., Christiano, A. M. & Jahoda, C. A. B. Trans-gender induction of hair follicles. *Nature* **402,** 33–34 (1999).

211. Takahashi, K. & Yamanaka, S. Induction of Pluripotent Stem Cells from Mouse Embryonic and Adult Fibroblast Cultures by Defined Factors. *Cell* **126,** 663–676 (2006).

212. Hibino, N. *et al.* Evaluation of the use of an induced puripotent stem cell sheet for the construction of tissue-engineered vascular grafts. *The Journal of Thoracic and Cardiovascular Surgery* **143,** 696–703 (2012).

213. Gui, L. *et al.* Implantable tissue-engineered blood vessels from human induced pluripotent stem cells. *Biomaterials* **102,** 120–129 (2016).

214. Wang, Y. *et al.* Engineering vascular tissue with functional smooth muscle cells derived from human iPS cells and nanofibrous scaffolds. *Biomaterials* **35,** 8960–8969 (2014).

215. Li, Z., Hu, S., Ghosh, Z., Han, Z. & Wu, J. C. Functional Characterization and Expression Profiling of Human Induced Pluripotent Stem Cell- and Embryonic Stem Cell-Derived Endothelial Cells. *Stem Cells and Development* **20,** 1701–1710 (2011).

216. Okano, H. *et al.* Steps Toward Safe Cell Therapy Using Induced Pluripotent Stem Cells. *Circulation Research* **112,** 523–533 (2013).

217. Kim, S.-H. *et al.* Mechanical properties of compliant double layered poly(L-lactide-co-ε-caprolactone) vascular graft. *Macromol. Res.* **21,** 886–891 (2013).

218. Centola, M. *et al.* Combining electrospinning and fused deposition modeling for the fabrication of a hybrid vascular graft. *Biofabrication* **2,** 14102 (2010).

219. Song, Y. *et al.* Flexible and elastic porous poly(trimethylene carbonate) structures for use in vascular tissue engineering. *Acta Biomaterialia* **6,** 1269–1277 (2010).

220. Ozolanta, I., Tetere, G., Purinya, B. & Kasyanov, V. Changes in the mechanical properties, biochemical contents and wall structure of the human coronary arteries with age and sex. *Medical Engineering & Physics* **20,** 523–533 (1998).

221. Madhavan, K., Elliott, W. H., Bonani, W., Monnet, E. & Tan, W. Mechanical and biocompatible characterizations of a readily available multilayer vascular graft. *J. Biomed. Mater. Res.* **101B,** 506–519 (2013).

222. Rapoport, H. S. *et al.* Construction of a Tubular Scaffold that Mimics J-Shaped Stress/Strain Mechanics Using an Innovative Electrospinning Technique. *Tissue Engineering Part C: Methods* **18,** 567–574 (2012).

223. Rodriguez, M., Juran, C., McClendon, M., Eyadiel, C. & McFetridge, P. S. Development of a mechanically tuneable 3D scaffold for vascular reconstruction. *Journal of Biomedical Materials Research Part A* **100A,** 3480–3489 (2012).

224. Drilling, S., Gaumer, J. & Lannutti, J. Fabrication of burst pressure competent vascular grafts via electrospinning: Effects of microstructure. *Journal of Biomedical Materials Research Part A* **88A,** 923–934 (2009).

225. Stekelenburg, M., Rutten, M. C. M., Snoeckx, L. H. E. H. & Baaijens, F. P. T. Dynamic Straining Combined with Fibrin Gel Cell Seeding Improves Strength of Tissue-Engineered Small-Diameter Vascular Grafts. *Tissue Engineering Part A* **15,** 1081–1089 (2009).

226. Tschoeke, B. *et al.* Tissue-Engineered Small-Caliber Vascular Graft Based on a Novel Biodegradable Composite Fibrin-Polylactide Scaffold. *Tissue Engineering Part A* **15,** 1909–1918 (2009).

227. Roh, J. D. *et al.* Small-diameter biodegradable scaffolds for functional vascular tissue engineering in the mouse model. *Biomaterials* **29,** 1454–1463 (2008).

228. Stitzel, J. *et al.* Controlled fabrication of a biological vascular substitute. *Biomaterials* **27,** 1088–1094 (2006).

229. Torikai, K. *et al.* A self-renewing, tissue-engineered vascular graft for arterial reconstruction. *The Journal of Thoracic and Cardiovascular Surgery* **136,** 37–45.e1 (2008).

230. Patel, A., Fine, B., Sandig, M. & Mequanint, K. Elastin biosynthesis: The missing link in tissue-engineered blood vessels. *Cardiovasc Res* **71,** 40–49 (2006).

231. Cribb, A. M. & Scott, J. E. Tendon response to tensile stress: an ultrastructural investigation of collagen:proteoglycan interactions in stressed tendon. *J Anat* **187,** 423–428 (1995).

232. Diamant, J., Keller, A., Baer, E., Litt, M. & Arridge, R. G. C. Collagen; Ultrastructure and Its Relation to Mechanical Properties as a Function of Ageing. *Proc. R. Soc. Lond. B* **180,** 293–315 (1972).

233. Stankus, J. J. *et al.* Fabrication of cell microintegrated blood vessel constructs through electrohydrodynamic atomization. *Biomaterials* **28,** 2738–2746 (2007).

234. Higgins, S. P., Solan, A. K. & Niklason, L. E. Effects of polyglycolic acid on porcine smooth muscle cell growth and differentiation. *Journal of Biomedical Materials Research Part A* **67A,** 295–302 (2003).

235. Ramamurthi, A. & Vesely, I. Evaluation of the matrix-synthesis potential of crosslinked hyaluronan gels for tissue engineering of aortic heart valves. *Biomaterials* **26,** 999–1010 (2005).

236. Long, J. L. & Tranquillo, R. T. Elastic fiber production in cardiovascular tissue-equivalents. *Matrix Biology* **22,** 339–350 (2003).

237. Davidson, J. M., LuValle, P. A., Zoia, O., Quaglino, D. & Giro, M. Ascorbate Differentially Regulates Elastin and Collagen Biosynthesis in Vascular Smooth Muscle Cells and Skin Fibroblasts by Pretranslational Mechanisms. *J. Biol. Chem.* **272,** 345–352 (1997).

238. Hayashi, A., Suzuki, T. & Tajima, S. Modulations of Elastin Expression and Cell Proliferation by Retinoids in Cultured Vascular Smooth Muscle Cells. *J Biochem* **117,** 132–136 (1995).

239. Seliktar, D., Nerem, R. M. & Galis, Z. S. Mechanical Strain-Stimulated Remodeling of Tissue-Engineered Blood Vessel Constructs. *Tissue Engineering* **9,** 657–666 (2003).

240. Kim, B.-S., Nikolovski, J., Bonadio, J., Smiley, E. & Mooney, D. J. Engineered Smooth Muscle Tissues: Regulating Cell Phenotype with the Scaffold. *Experimental Cell Research* **251,** 318–328 (1999).

241. Kim, B.-S., Nikolovski, J., Bonadio, J. & Mooney, D. J. Cyclic mechanical strain regulates the development of engineered smooth muscle tissue. *Nat Biotech* **17,** 979–983 (1999).

242. Huang, A. H. *et al.* Biaxial Stretch Improves Elastic Fiber Maturation, Collagen Arrangement, and Mechanical Properties in Engineered Arteries. *Tissue Engineering Part C: Methods* **22,** 524–533 (2016).

243. Huang, A. H., Lee, Y., Humphrey, J. D. & Niklason, L. E. Biaxial stretch results in formation of mature functional elastic fibers in engineered vessels. *Angiogenesis* **17,** 275–322 (2014).

244. Davis, E. C. Elastic lamina growth in the developing mouse aorta. *J Histochem Cytochem* **43,** 1115–1123 (1995).

245. Bendeck, M. P. & Langille, B. L. Rapid accumulation of elastin and collagen in the aortas of sheep in the immediate perinatal period. *Circulation Research* **69,** 1165–1169 (1991).

246. Gerrity, R. G. & Cliff, W. J. The aortic tunica media of the developing rat. I. Quantitative stereologic and biochemical analysis. *Lab Invest* **32,** 585–600 (1975).

247. Looker, T. & Berry, C. L. The growth and development of the rat aorta. II. Changes in nucleic acid and scleroprotein content. *J Anat* **113,** 17–34 (1972).

248. Zhang, P. *et al.* Inhibition of MicroRNA-29 Enhances Elastin Levels in Cells Haploinsufficient for Elastin and in Bioengineered Vessels—Brief Report. *Arteriosclerosis, Thrombosis, and Vascular Biology* **32,** 756–759 (2012).

249. Loth, F., Fischer, P. F. & Bassiouny, H. S. Blood Flow in End-to-Side Anastomoses*. *Annual Review of Fluid Mechanics* **40,** 367–393 (2008).

250. Hughes, P. E. & How, T. V. Effects of geometry and flow division on flow structures in models of the distal end-to-side anastomosis. *Journal of Biomechanics* **29,** 855–872 (1996).

251. Bassiouny, H. S. *et al.* Anastomotic intimal hyperplasia: Mechanical injury or flow induced. *Journal of Vascular Surgery* **15,** 708–717 (1992).

252. Hofer, M., Rappitsch, G., Perktold, K., Trubel, W. & Schima, H. Numerical study of wall mechanics and fluid dynamics in end-to-side anastomoses and correlation to intimal hyperplasia. *Journal of Biomechanics* **29,** 1297–1308 (1996).

253. Steinman, D. A. & Ethier, C. R. The Effect of Wall Distensibility on Flow in a Two-Dimensional End-to-Side Anastomosis. *J Biomech Eng* **116,** 294–301 (1994).

254. O'Brien, T., Walsh, M. & McGloughlin, T. On Reducing Abnormal Hemodynamics in the Femoral End-to-Side Anastomosis: The Influence of Mechanical Factors. *Ann Biomed Eng* **33,** 310–322 (2005).

255. Longest, P. W., Kleinstreuer, C. & Archie Jr, J. P. Particle hemodynamics analysis of Miller cuff arterial anastomosis. *Journal of Vascular Surgery* **38,** 1353–1362 (2003).

256. Cole, J. S., Watterson, J. K. & O'Reilly, M. J. G. Numerical investigation of the haemodynamics at a patched arterial bypass anastomosis. *Medical Engineering & Physics* **24,** 393–401 (2002).

257. Khalil, A. A., Boyd, A. & Griffiths, G. in *Cochrane Database of Systematic Reviews* (John Wiley & Sons, Ltd, 2012).

258. Gough, M. J. Comments regarding 'PTFE Bypass to Below-knee Arteries: Distal Vein Collar or Not? A Prospective Randomised Multicentre Study'. *European Journal of Vascular and Endovascular Surgery* **39,** 755 (2010).

259. Griffiths, G. D., Nagy, J., Black, D. & Stonebridge, P. A. Randomized clinical trial of distal anastomotic interposition vein cuff in infrainguinal polytetrafluoroethylene bypass grafting. *Br J Surg* **91,** 560–562 (2004).

260. Yeung, K. K. *et al.* Improved patency of infrainguinal polytetrafluoroethylene bypass grafts using a distal Taylor vein patch. *The American Journal of Surgery* **182,** 578–583 (2001).

261. Donker, J. M. W. *et al.* Midterm Results of Autologous Saphenous Vein and ePTFE Pre-Cuffed Bypass Surgery in Peripheral Arterial Occlusive Disease. *VASC ENDOVASCULAR SURG* **45,** 598–603 (2011).

262. Panneton, J. M., Hollier, L. H. & Hofer, J. M. Multicenter Randomized Prospective Trial Comparing a Pre-cuffed Polytetrafluoroethylene Graft to a Vein Cuffed Polytetrafluoroethylene Graft for Infragenicular Arterial Bypass. *Annals of Vascular Surgery* **18,** 199–206 (2004).

263. Sorom, A. J. *et al.* Prospective, randomized evaluation of a cuffed expanded polytetrafluoroethylene graft for hemodialysis vascular access. *Surgery* **132,** 135–140 (2002).

264. Chua, L. P., Tong, J. H. & Zhou, T. Numerical simulation of steady flows in designed sleeve models at distal anastomoses. *International Communications in Heat and Mass Transfer* **32,** 707–714 (2005).

265. O'Brien, T. P., Grace, P., Walsh, M., Burke, P. & McGloughlin, T. Computational investigations of a new prosthetic femoral-popliteal bypass graft design. *Journal of Vascular Surgery* **42,** 1169–1175 (2005).

266. Longest PW, C. K. Computational haemodynamics analysis and comparison study of arterio-venous grafts. *J Med Eng Technol* **24,** 102–110 (2000).

267. Lei, M., Archie, J. P. & Kleinstreuer, C. Computational design of a bypass graft that minimizes wall shear stress gradients in the region of the distal anastomosis. *Journal of Vascular Surgery* **25,** 637–646 (1997).

268. Qiao, A. & Liu, Y. Influence of graft-host diameter ratio on the hemodynamics of CABG. *Bio-Medical Materials and Engineering* **16,** 189–201 (2006).

269. Papaharilaou, Y., Doorly, D. J. & Sherwin, S. J. The influence of out-of-plane geometry on pulsatile flow within a distal end-to-side anastomosis. *Journal of Biomechanics* **35,** 1225–1239 (2002).

270. Jackson, Z. S., Ishibashi, H., Gotlieb, A. I. & Langille, B. L. Effects of anastomotic angle on vascular tissue responses at end-to-side arterial grafts. *Journal of Vascular Surgery* **34,** 300–307 (2001).

271. Ojha, M., Cobbold, R. S. C. & Johnston, K. W. Influence of angle on wall shear stress distribution for an end-to-side anastomosis. *Journal of Vascular Surgery* **19,** 1067–1073 (1994).

272. Rickard, R. F., Meyer, C. & Hudson, D. A. Computational Modeling of Microarterial Anastomoses With Size Discrepancy (Small-to-Large). *Journal of Surgical Research* **153,** 1–11 (2009).

273. Migliavacca, F. & Dubini, G. Computational modeling of vascular anastomoses. *Biomech Model Mechanobiol* **3,** 235–250 (2005).

274. Mendelson, K. *et al.* Healing and remodeling of bioengineered pulmonary artery patches implanted in sheep. *Cardiovascular Pathology* **16,** 277–282 (2007).

275. Burn, T. C., Petrovick, M. S., Hohaus, S., Rollins, B. J. & Tenen, D. G. Monocyte chemoattractant protein-1 gene is expressed in activated neutrophils and retinoic acid-induced human myeloid cell lines. *Blood* **84,** 2776–2783 (1994).

276. Weber, B. *et al.* Tissue engineering on matrix: future of autologous tissue replacement. *Semin Immunopathol* **33,** 307–315 (2011).

277. Hibino, N. *et al.* A critical role for macrophages in neovessel formation and the development of stenosis in tissue-engineered vascular grafts. *FASEB J* **25,** 4253–4263 (2011).

278. Brown, B. N., Ratner, B. D., Goodman, S. B., Amar, S. & Badylak, S. F. Macrophage polarization: An opportunity for improved outcomes in biomaterials and regenerative medicine. *Biomaterials* **33,** 3792–3802 (2012).

279. Rehman, J., Li, J., Orschell, C. M. & March, K. L. Peripheral Blood 'Endothelial Progenitor Cells' Are Derived From Monocyte/Macrophages and Secrete Angiogenic Growth Factors. *Circulation* **107,** 1164–1169 (2003).

280. Roh, J. D. *et al.* Tissue-engineered vascular grafts transform into mature blood vessels via an inflammation-mediated process of vascular remodeling. *PNAS* **107,** 4669–4674 (2010).

281. Yang, S., Leong, K.-F., Du, Z. & Chua, C.-K. The Design of Scaffolds for Use in Tissue Engineering. Part I. Traditional Factors. *Tissue Engineering* **7,** 679–689 (2001).

282. Wang, Y., Ameer, G. A., Sheppard, B. J. & Langer, R. A tough biodegradable elastomer. *Nat Biotech* **20,** 602–606 (2002).

283. Bettinger, C. J. *et al.* Three-Dimensional Microfluidic Tissue-Engineering Scaffolds Using a Flexible Biodegradable Polymer. *Adv. Mater.* **18,** 165–169 (2006).

284. Gao, J., Crapo, P. M. & Wang, Y. Macroporous Elastomeric Scaffolds with Extensive Micropores for Soft Tissue Engineering. *Tissue Engineering* **12,** 917–925 (2006).

285. Fidkowski, C. *et al.* Endothelialized Microvasculature Based on a Biodegradable Elastomer. *Tissue Engineering* **11,** 302–309 (2005).

286. Crapo, P. M., Gao, J. & Wang, Y. Seamless tubular poly(glycerol sebacate) scaffolds: High-yield fabrication and potential applications. *J. Biomed. Mater. Res.* **86A,** 354–363 (2008).

287. Nijst, C. L. E. *et al.* Synthesis and Characterization of Photocurable Elastomers from Poly(glycerol-co-sebacate). *Biomacromolecules* **8,** 3067–3073 (2007).

288. Ifkovits, J. L., Padera, R. F. & Burdick, J. A. Biodegradable and radically polymerized elastomers with enhanced processing capabilities. *Biomed. Mater.* **3,** 34104 (2008).

289. International Organisation for Standardisation. *BS ISO 37:2011 - Rubber, vulcanized or thermoplastic. Determination of tensile stress-strain properties*. (International Organisation for Standardisation, 2011).

290. Li, Y., Cook, W. D., Moorhoff, C., Huang, W.-C. & Chen, Q.-Z. Synthesis, characterization and properties of biocompatible poly(glycerol sebacate) pre-polymer and gel. *Polym. Int* **62,** 534–547 (2013).

291. Jaafar, I. H., Ammar, M. M., Jedlicka, S. S., Pearson, R. A. & Coulter, J. P. Spectroscopic evaluation, thermal, and thermomechanical characterization of poly(glycerol-sebacate) with variations in curing temperatures and durations. *J Mater Sci* **45,** 2525–2529 (2010).

292. Cai, W. & Liu, L. Shape-memory effect of poly (glycerol–sebacate) elastomer. *Materials Letters* **62,** 2171–2173 (2008).

293. Rai, R., Tallawi, M., Grigore, A. & Boccaccini, A. R. Synthesis, properties and biomedical applications of poly(glycerol sebacate) (PGS): A review. *Progress in Polymer Science* **37,** 1051–1078 (2012).

294. Silverstein, R. M. & Bassler, G. C. Spectrometric identification of organic compounds. *J. Chem. Educ.* **39,** 546 (1962).

295. Smith, E. & Dent, G. in *Modern Raman Spectroscopy - A Practical Approach* 2–20 (J. Wiley, 2005).

296. Zhang, H. & Grinstaff, M. W. Recent Advances in Glycerol Polymers: Chemistry and Biomedical Applications. *Macromolecular Rapid Communications* **35,** 1906–1924 (2014).

297. Nagata, M., Machida, T., Sakai, W. & Tsutsumi, N. Synthesis, characterization, and enzymatic degradation of network aliphatic copolyesters. *J. Polym. Sci. A Polym. Chem.* **37,** 2005–2011 (1999).

298. Young, R. J. & Lovell, P. A. in *Introduction to Polymers* 21–60 (Taylor & Francis Group, LLC, 2011).

299. Young, R. J. & Lovell, P. A. in *Introduction to Polymers* 3–14 (Taylor & Francis Group, LLC, 2011).

300. Ifkovits, J. L. *et al.* Biodegradable Fibrous Scaffolds with Tunable Properties Formed from Photo-Cross-Linkable Poly(glycerol sebacate). *ACS Applied Materials & Interfaces* **1,** 1878–1886 (2009).

301. Frydrych, M., Román, S., MacNeil, S. & Chen, B. Biomimetic poly(glycerol sebacate)/poly(l-lactic acid) blend scaffolds for adipose tissue engineering. *Acta Biomaterialia* **18,** 40–49 (2015).

302. Castor Jr., C. A., Pontier, A., Durand, J., Pinto, J. C. & Prat, L. Real time monitoring of the quiescent suspension polymerization of methyl methacrylate in microreactors—Part 1. A kinetic study by Raman spectroscopy and evolution of droplet size. *Chemical Engineering Science* **131,** 340–352 (2015).

303. Kafouris, D. *et al.* Biosourced Amphiphilic Degradable Elastomers of Poly(glycerol sebacate): Synthesis and Network and Oligomer Characterization. *Macromolecules* **46,** 622–630 (2013).

304. Gaharwar, A. K. *et al.* Elastomeric nanocomposite scaffolds made from poly(glycerol sebacate) chemically crosslinked with carbon nanotubes. *ResearchGate* **3,** (2014).

305. Azevedo, H. S. & Reis, R. L. in *Biodegradable Systems in Tissue Engineering and Regenerative Medicine.* 178–197 (CRC Press, 2005).

306. Ifkovits, J. L. & Burdick, J. A. Review: Photopolymerizable and Degradable Biomaterials for Tissue Engineering Applications. *Tissue Engineering* **13,** 2369–2385 (2007).

307. Göpferich, A. Mechanisms of polymer degradation and erosion. *Biomaterials* **17,** 103–114 (1996).

308. Santerre, J. P., Woodhouse, K., Laroche, G. & Labow, R. S. Understanding the biodegradation of polyurethanes: From classical implants to tissue engineering materials. *Biomaterials* **26,** 7457–7470 (2005).

309. Tang, Y. W., Labow, R. S. & Santerre, J. P. Enzyme induced biodegradation of polycarbonate-polyurethanes: dose dependence effect of cholesterol esterase. *Biomaterials* **24,** 2003–2011 (2003).

310. Woo, G. L. Y., Mittelman, M. W. & Santerre, J. P. Synthesis and characterization of a novel biodegradable antimicrobial polymer. *Biomaterials* **21,** 1235–1246 (2000).

311. Labow, R. S., Meek, E. & Santerre, J. P. Differential synthesis of cholesterol esterase by monocyte-derived macrophages cultured on poly(ether or ester)-based poly(urethane)s. *J. Biomed. Mater. Res.* **39,** 469–477 (1998).

312. Frydrych, M. & Chen, B. Large three-dimensional poly(glycerol sebacate)-based scaffolds – a freeze-drying preparation approach. *Journal of Materials Chemistry B* **1,** 6650–6661 (2013).

313. Ashton, J. H. *et al.* Functional Endoluminal Paving (FELP): Thermoforming, Biodegradation, and Mechanical Properties of a Novel Polymer Graft for Abdominal Aortic Aneurysms. 905–906 (2010). doi:10.1115/SBC2010-19463

314. Wang, D., Williams, C. G., Li, Q., Sharma, B. & Elisseeff, J. H. Synthesis and characterization of a novel degradable phosphate-containing hydrogel. *Biomaterials* **24,** 3969–3980 (2003).

315. Nuttelman, C. R., Henry, S. M. & Anseth, K. S. Synthesis and characterization of photocrosslinkable, degradable poly(vinyl alcohol)-based tissue engineering scaffolds. *Biomaterials* **23,** 3617–3626 (2002).

316. Metters, A. T., Anseth, K. S. & Bowman, C. N. Fundamental studies of a novel, biodegradable PEG-b-PLA hydrogel. *Polymer* **41,** 3993–4004 (2000).

317. Young, R. J. & Lovell, P. A. in *Introduction to Polymers* 511–530 (Taylor & Francis Group, LLC, 2011).

318. Schmedlen, R. H., Masters, K. S. & West, J. L. Photocrosslinkable polyvinyl alcohol hydrogels that can be modified with cell adhesion peptides for use in tissue engineering. *Biomaterials* **23,** 4325–4332 (2002).

319. Mühlebach, A. *et al.* New water-soluble photo crosslinkable polymers based on modified poly(vinyl alcohol). *J. Polym. Sci. A Polym. Chem.* **35,** 3603–3611 (1997).

320. Ong, W. K. & Sugii, S. Adipose-derived stem cells: Fatty potentials for therapy. *The International Journal of Biochemistry & Cell Biology* **45,** 1083–1086 (2013).

321. Zuk, P. Adipose-Derived Stem Cells in Tissue Regeneration: A Review. *ISRN Stem Cells* **2013,** 1–35 (2013).

322. Alberts, B. *et al.* in *Molecular Biology of the Cell* 1–45 (Garland Science, 2002).

323. Moulin, V. *et al.* Modulated Response to Cytokines of Human Wound Healing Myofibroblasts Compared to Dermal Fibroblasts. *Experimental Cell Research* **238,** 283–293 (1998).

324. Zhu, Y. *et al.* Adipose-derived stem cell: a better stem cell than BMSC. *Cell Biochem. Funct.* **26,** 664–675 (2008).

325. Gimble, J. M., Katz, A. J. & Bunnell, B. A. Adipose-Derived Stem Cells for Regenerative Medicine. *Circulation Research* **100,** 1249–1260 (2007).

326. Kim, W.-S. *et al.* Wound healing effect of adipose-derived stem cells: A critical role of secretory factors on human dermal fibroblasts. *Journal of Dermatological Science* **48,** 15–24 (2007).

327. Chamley-Campbell, J., Campbell, G. R. & Ross, R. The smooth muscle cell in culture. *Physiological Reviews* **59,** 1–61 (1979).

328. Gomez, D. & Owens, G. K. Smooth muscle cell phenotypic switching in atherosclerosis. *Cardiovascular Research* cvs115 (2012). doi:10.1093/cvr/cvs115

329. Owens, G. K. Regulation of differentiation of vascular smooth muscle cells. *Physiological Reviews* **75,** 487–517 (1995).

330. Stevens, M. M. & George, J. H. Exploring and Engineering the Cell Surface Interface. *Science* **310,** 1135–1138 (2005).

331. Yeung, T. *et al.* Effects of substrate stiffness on cell morphology, cytoskeletal structure, and adhesion. *Cell Motil. Cytoskeleton* **60,** 24–34 (2005).

332. Curtis, A. & Wilkinson, C. New depths in cell behaviour: reactions of cells to nanotopography. *Biochem Soc Symp* **65,** 15–26 (1998).

333. Hambleton, J. *et al.* Culture surfaces coated with various implant materials affect chondrocyte growth and metabolism. *J. Orthop. Res.* **12,** 542–552 (1994).

334. Lydon, M. J., Minett, T. W. & Tighe, B. J. Cellular interactions with synthetic polymer surfaces in culture. *Biomaterials* **6,** 396–402 (1985).

335. Sachlos, E. & Czernuszka, J. Making Tissue Engineering Scaffolds Work. Review: The application of solid freeform fabrication technology to the production of tissue engineering scaffolds. *European Cells and Materials* **5,** 29–40 (2003).

336. Song, Y. *et al.* Dynamic Culturing of Smooth Muscle Cells in Tubular Poly(Trimethylene Carbonate) Scaffolds for Vascular Tissue Engineering. *Tissue Engineering Part A* **17,** 381–387 (2011).

337. Lumelsky, Y. & Silverstein, M. S. Biodegradable Porous Polymers through Emulsion Templating. *Macromolecules* **42,** 1627–1633 (2009).

338. Lee, M., Wu, B. M. & Dunn, J. C. Y. Effect of scaffold architecture and pore size on smooth muscle cell growth. *J. Biomed. Mater. Res.* **87A,** 1010–1016 (2008).

339. Karande, T. S., Ong, J. L. & Agrawal, C. M. Diffusion in Musculoskeletal Tissue Engineering Scaffolds: Design Issues Related to Porosity, Permeability, Architecture, and Nutrient Mixing. *Ann Biomed Eng* **32,** 1728–1743 (2004).

340. Zeltinger, J., Sherwood, J. K., Graham, D. A., Müeller, R. & Griffith, L. G. Effect of Pore Size and Void Fraction on Cellular Adhesion, Proliferation, and Matrix Deposition. *Tissue Engineering* **7,** 557–572 (2001).

341. Zhang, R. & Ma, P. X. Synthetic nano-fibrillar extracellular matrices with predesigned macroporous architectures. *J. Biomed. Mater. Res.* **52,** 430–438 (2000).

342. Matsiko, A., Gleeson, J. P. & O'Brien, F. J. Scaffold Mean Pore Size Influences Mesenchymal Stem Cell Chondrogenic Differentiation and Matrix Deposition. *Tissue Engineering Part A* **21,** 486–497 (2014).

343. Stansbury, J. W. Dimethacrylate network formation and polymer property evolution as determined by the selection of monomers and curing conditions. *Dental Materials* **28,** 13–22 (2012).

344. Sant, S., Hwang, C. M., Lee, S.-H. & Khademhosseini, A. Hybrid PGS–PCL microfibrous scaffolds with improved mechanical and biological properties. *J Tissue Eng Regen Med* **5,** 283–291 (2011).

345. Kemppainen, J. M. & Hollister, S. J. Tailoring the mechanical properties of 3D-designed poly(glycerol sebacate) scaffolds for cartilage applications. *J. Biomed. Mater. Res.* **94A,** 9–18 (2010).

346. Wilson, C. J., Clegg, R. E., Leavesley, D. I. & Pearcy, M. J. Mediation of Biomaterial–Cell Interactions by Adsorbed Proteins: A Review. *Tissue Engineering* **11,** 1–18 (2005).

347. Venkataraman, L., Bashur, C. A. & Ramamurthi, A. Impact of Cyclic Stretch on Induced Elastogenesis Within Collagenous Conduits. *Tissue Engineering Part A* **20,** 1403–1415 (2014).

348. Nieponice, A. *et al.* Development of a tissue-engineered vascular graft combining a biodegradable scaffold, muscle-derived stem cells and a rotational vacuum seeding technique. *Biomaterials* **29,** 825–833 (2008).

349. Pashneh-Tala, S., Malins, A., Lewis, R., Heppell, G. & Rodriguez-Falcon, E. in *The Little Book of Design* 1–11 (The University of Sheffield, 2011).

350. Pahl, G. & Beitz, W. *Engineering Design*. (Springer-Verlag, 1996).

351. Cross, N. *Engineering Design Methods*. (The Open University, 1994).

352. Byrom, M. J., Bannon, P. G., White, G. H. & Ng, M. K. C. Animal models for the assessment of novel vascular conduits. *Journal of Vascular Surgery* **52,** 176–195 (2010).

353. Gao, J., Crapo, P., Nerem, R. & Wang, Y. Co-expression of elastin and collagen leads to highly compliant engineered blood vessels. *J. Biomed. Mater. Res.* **85A,** 1120–1128 (2008).

354. Williams, C. & Wick, T. M. Endothelial Cell–Smooth Muscle Cell Co-Culture in a Perfusion Bioreactor System. *Ann Biomed Eng* **33,** 920–928 (2005).

355. Kumar, P. & Clark, M. in *Clinical Medicine* 681–810 (Elsevier, Spain, 2009).

356. Finkbeiner, S. R. *et al.* Generation of tissue-engineered small intestine using embryonic stem cell-derived human intestinal organoids. *Biology Open* **4,** 1462–1472 (2015).

357. Grant, D. N., Cozad, M. J., Grant, D. A., White, R. A. & Grant, S. A. In vitro electromagnetic stimulation to enhance cell proliferation in extracellular matrix constructs with and without metallic nanoparticles. *J. Biomed. Mater. Res.* **103,** 1532–1540 (2015).

358. Callanan, A., Davis, N. f., McGloughlin, T. M. & Walsh, M. T. Development of a rotational cell-seeding system for tubularized extracellular matrix (ECM) scaffolds in vascular surgery. *J. Biomed. Mater. Res.* **102,** 781–788 (2014).

359. Pithon, M. M. *et al.* Evaluation of the cytotoxicity of elastomeric ligatures after sterilization with 0.25% peracetic acid. *Aust Orthod J* **29,** 139–144 (2013).

360. Bye, F. J. *et al.* Development of bilayer and trilayer nanofibrous/microfibrous scaffolds for regenerative medicine. *Biomaterials Science* **1,** 942 (2013).

361. Crow, S. Peracetic Acid Sterilization: A Timely Development for a Busy Healthcare Industry. *Infection Control and Hospital Epidemiology* **13,** 111–113 (1992).

362. Eissa, M. E., Abd El Naby, M. & Beshir, M. M. Bacterial vs. fungal spore resistance to peroxygen biocide on inanimate surfaces. *Bulletin of Faculty of Pharmacy, Cairo University* **52,** 219–224 (2014).

363. Rutala, W. A. & Weber, D. J. Selection of the Ideal Disinfectant. *Infection Control and Hospital Epidemiology* **35,** 855–865 (2014).

364. Li, C. & Xu, Q. Mechanical stress-initiated signal transductions in vascular smooth muscle cells. *Cellular Signalling* **12,** 435–445 (2000).

365. Cantor, J. O. & Shteyngart, B. How a test for elastic fiber breakdown products in sputum could speed development of a treatment for pulmonary emphysema. *Med Sci Monit* **10,** RA1-RA4 (2004).

366. Carmeliet, P. Mechanisms of angiogenesis and arteriogenesis. *Nat Med* **6,** 389–395 (2000).

367. Hungerford, J. E. & Little, C. D. Developmental Biology of the Vascular Smooth Muscle Cell: Building a Multilayered Vessel Wall. *J Vasc Res* **36,** 2–27 (1999).

368. Hanahan, D. Signaling Vascular Morphogenesis and Maintenance. *Science* **277,** 48–50 (1997).

369. Birukov, K. G. *et al.* Stretch affects phenotype and proliferation of vascular smooth muscle cells. *Mol Cell Biochem* **144,** 131–139 (1995).

370. Chapman, G., Durante, W., Hellums, J. & Schafer, A. Physiological cyclic stretch causes cell cycle arrest in cultured vascular smooth muscle cells. *Am J Physiol Heart Circ Physiol* **278,** H748-54 (2000).

371. Pauly, R. *et al.* Experimental models that mimic the differentiation and dedifferentiation of vascular cells. *Circulation* **86,** III68-73 (1992).

372. Clyman, R. I., McDonald, K. A. & Kramer, R. H. Integrin receptors on aortic smooth muscle cells mediate adhesion to fibronectin, laminin, and collagen. *Circulation Research* **67,** 175–186 (1990).

373. Greisler, H. P. *et al.* Kinetics of cell proliferation as a function of vascular graft material. *J. Biomed. Mater. Res.* **27,** 955–961 (1993).

374. McMurtry, M. S. *et al.* Dichloroacetate Prevents and Reverses Pulmonary Hypertension by Inducing Pulmonary Artery Smooth Muscle Cell Apoptosis. *Circulation Research* **95,** 830–840 (2004).

375. Kingsley, K. *et al.* ERK1/2 mediates PDGF-BB stimulated vascular smooth muscle cell proliferation and migration on laminin-5. *Biochemical and Biophysical Research Communications* **293,** 1000–1006 (2002).

376. Green, P. S., Perez, E. J., Calloway, T. & Simpkins, J. W. Estradiol attenuation of β-amyloid-induced toxicity: A comparison of MTT and calcein AM assays. *J Neurocytol* **29,** 419–423 (2000).

377. Tapia, C. *et al.* Two mitosis-specific antibodies, Mpm-2 and phospho-histone H3 (ser28), allow rapid and precise determination of mitotic activity. *Am. J. Surg. Pathol.* **30,** 83–89 (2006).

378. Heck, M. M. S. & Earnshaw, W. C. Topoisomerase II: A specific marker for cell proliferation. *J Cell Biol* **103,** 2569–2581 (1986).

379. Gerdes, J. *et al.* Cell cycle analysis of a cell proliferation-associated human nuclear antigen defined by the monoclonal antibody Ki-67. *The Journal of Immunology* **133,** 1710–1715 (1984).

380. Cuhlmann, S. *et al.* Disturbed Blood Flow Induces RelA Expression via c-Jun N-Terminal Kinase 1Novelty and Significance. *Circulation Research* **108,** 950–959 (2011).

381. Amsen, D., de Visser, K. E. & Town, T. Approaches to Determine Expression of Inflammatory Cytokines. *Methods Mol Biol* **511,** 107–142 (2009).

382. Venugopal, S. K., Devaraj, S., Yuhanna, I., Shaul, P. & Jialal, I. Demonstration That C-Reactive Protein Decreases eNOS Expression and Bioactivity in Human Aortic Endothelial Cells. *Circulation* **106,** 1439–1441 (2002).

383. Hahn, C. & Schwartz, M. A. Mechanotransduction in vascular physiology and atherogenesis. *Nat Rev Mol Cell Biol* **10,** 53–62 (2009).

384. Stefano, I. D., Koopmans, D. R. & Langille, B. L. Modulation of Arterial Growth of the Rabbit Carotid Artery Associated with Experimental Elevation of Blood Flow. *JVR* **35,** 1–7 (1998).

385. Talari, A. C. S., Movasaghi, Z., Rehman, S. & Rehman, I. ur. Raman Spectroscopy of Biological Tissues. *Applied Spectroscopy Reviews* **50,** 46–111 (2015).

386. Jung, Y., Klein, O. J., Wang, H. & Evans, C. L. Longitudinal, label-free, quantitative tracking of cell death and viability in a 3D tumor model with OCT. *Sci Rep* **6,** (2016).

387. Dean, D. A., Ramanathan, T., Machado, D. & Sundararajan, R. Electrical impedance spectroscopy study of biological tissues. *Journal of Electrostatics* **66,** 165–177 (2008).

388. Tan, W., Oldenburg, A. L., Norman, J. J., Desai, T. A. & Boppart, S. A. Optical coherence tomography of cell dynamics in three-dimensional tissue models. *Opt. Express, OE* **14,** 7159–7171 (2006).

389. K'Owino, I. O. & Sadik, O. A. Impedance Spectroscopy: A Powerful Tool for Rapid Biomolecular Screening and Cell Culture Monitoring. *Electroanalysis* **17,** 2101–2113 (2005).

390. Freytes, D. O., Stoner, R. M. & Badylak, S. F. Uniaxial and biaxial properties of terminally sterilized porcine urinary bladder matrix scaffolds. *J. Biomed. Mater. Res.* **84B,** 408–414 (2008).

391. Mendes, G. C. C., Brandão, T. R. S. & Silva, C. L. M. Ethylene oxide sterilization of medical devices: A review. *American Journal of Infection Control* **35,** 574–581 (2007).

392. Marreco, P. R., Moreira, P. da L., Genari, S. C. & Moraes, Â. M. Effects of different sterilization methods on the morphology, mechanical properties, and cytotoxicity of chitosan membranes used as wound dressings. *J. Biomed. Mater. Res.* **71B,** 268–277 (2004).

Appendix

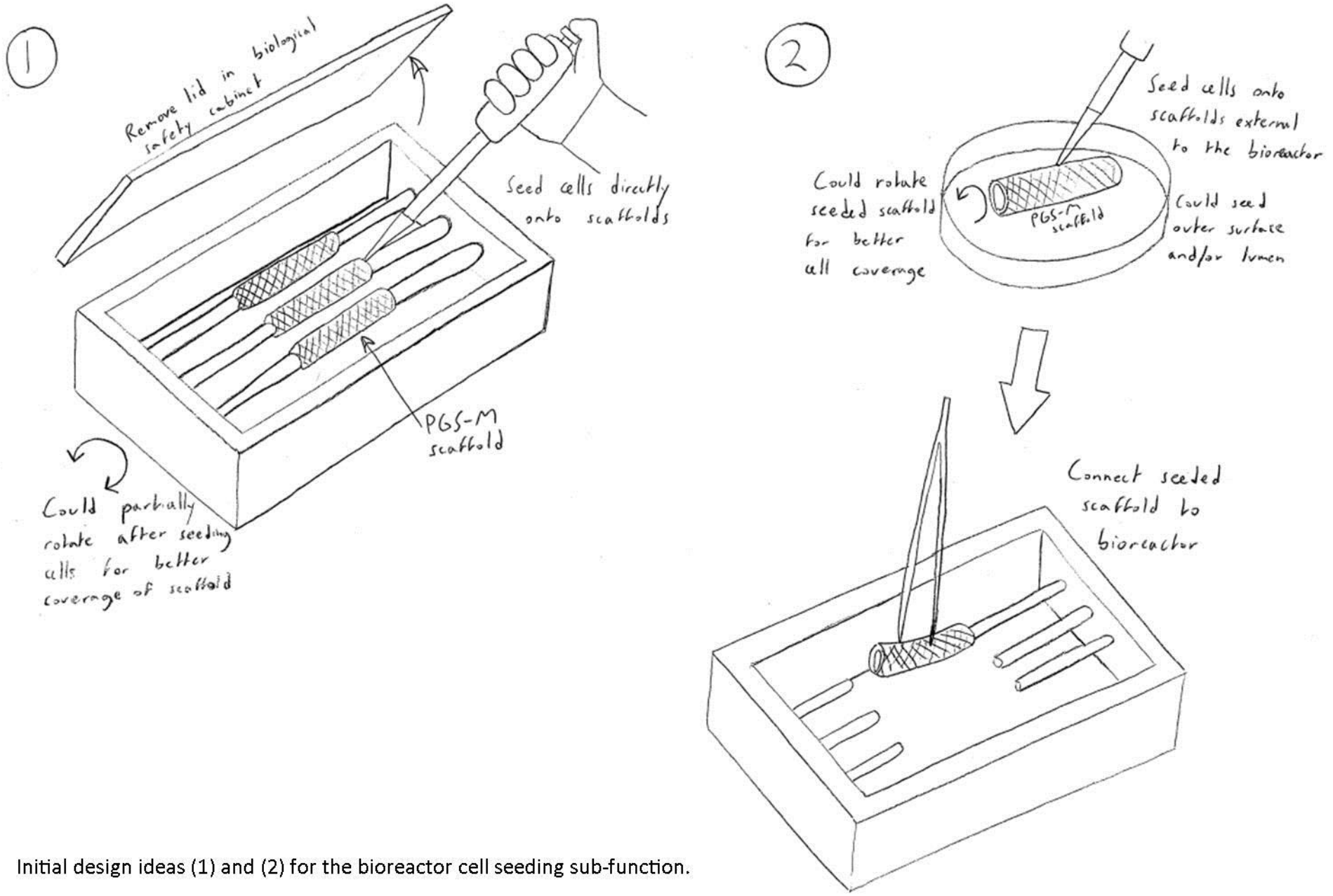

Initial design ideas (1) and (2) for the bioreactor cell seeding sub-function.

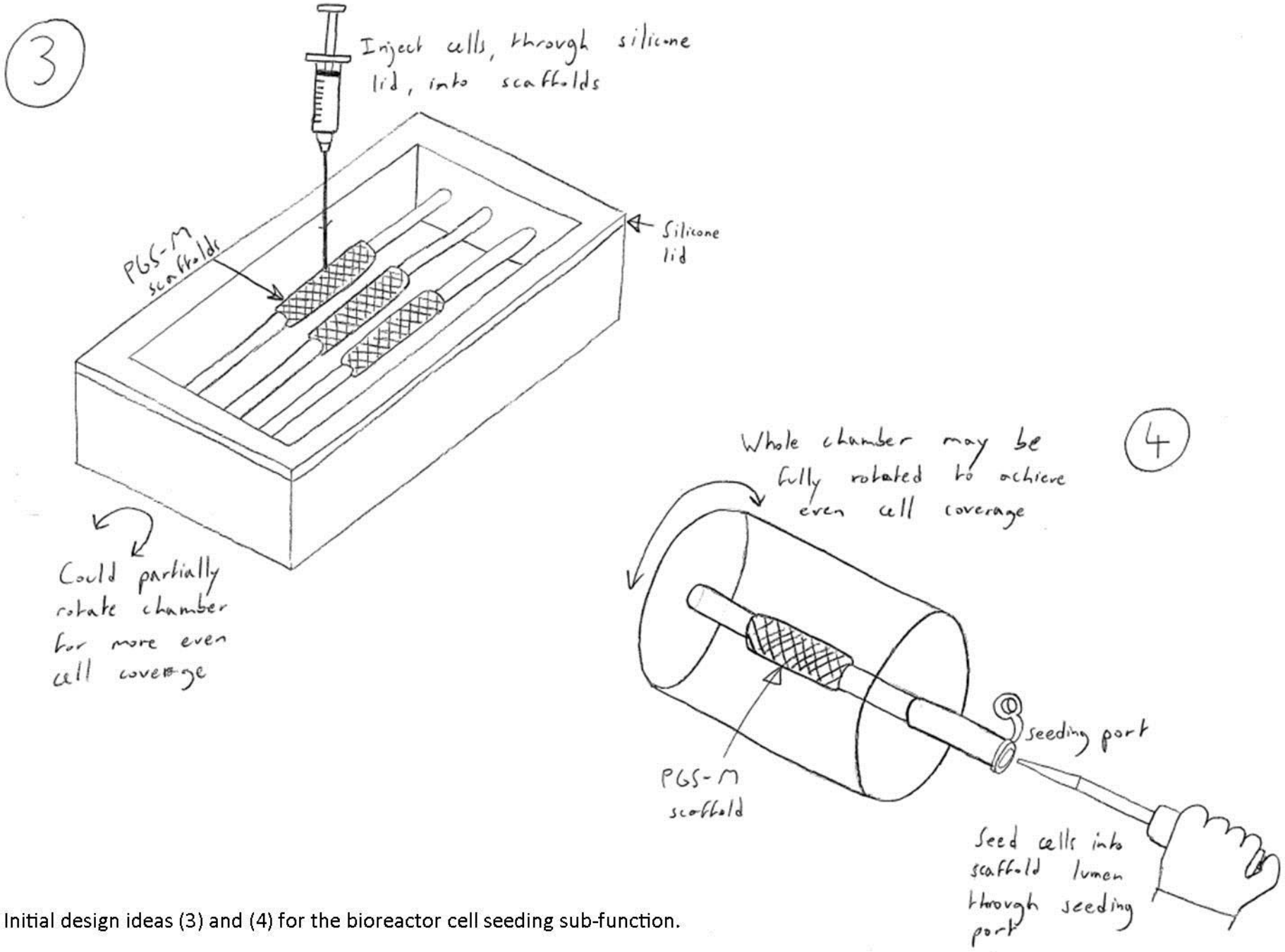

Initial design ideas (3) and (4) for the bioreactor cell seeding sub-function.

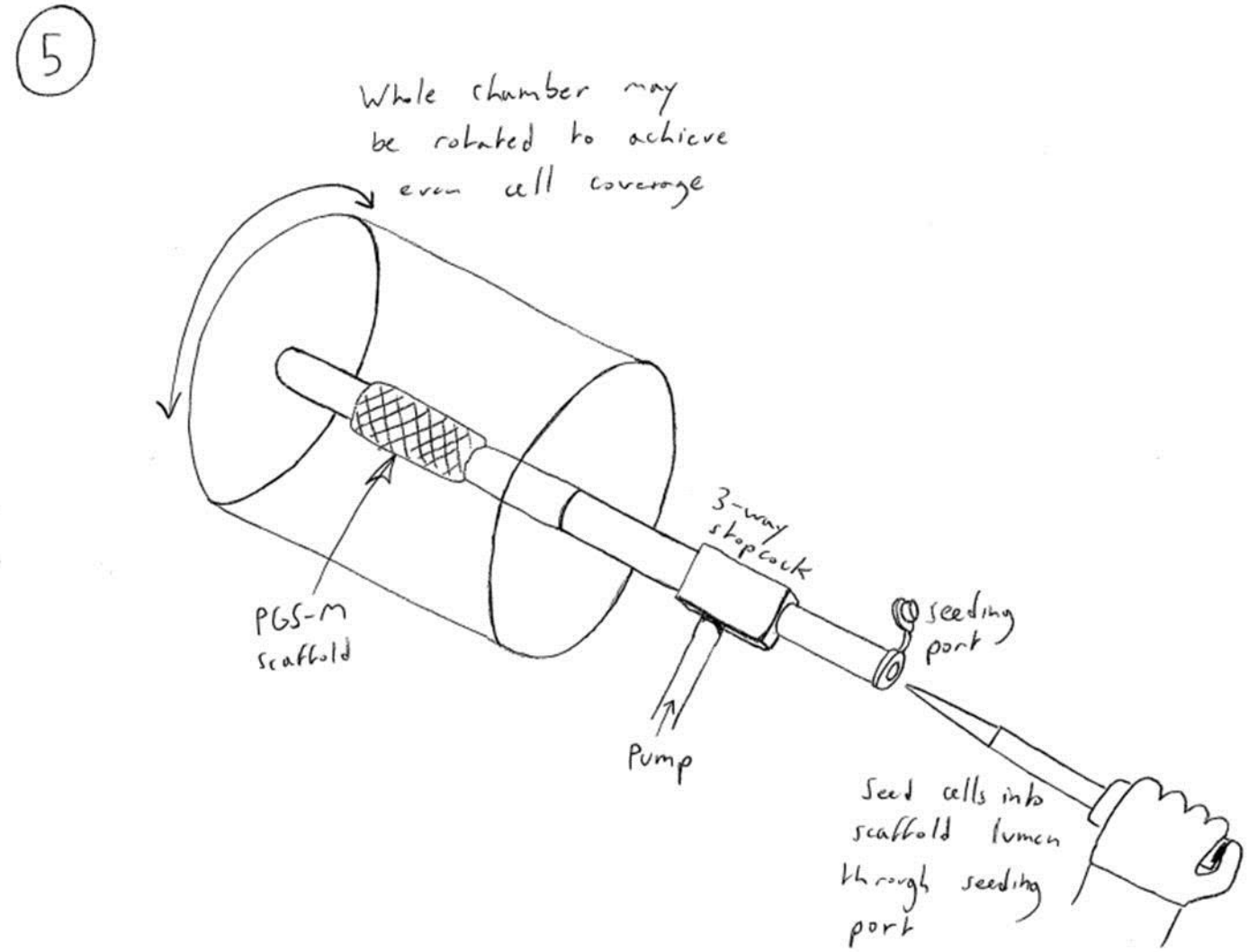

Initial design idea (5) for the bioreactor cell seeding sub-function.

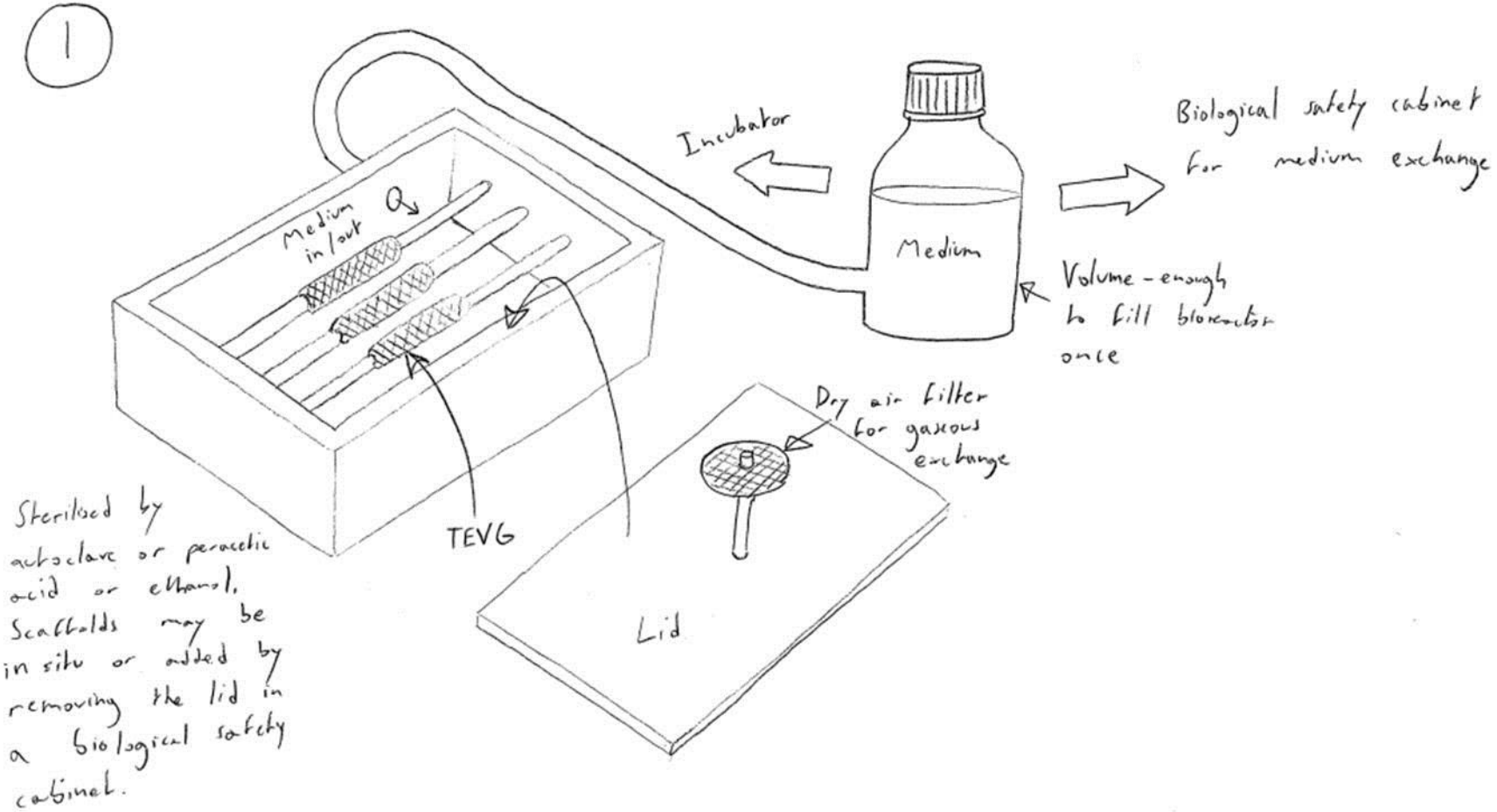

Initial design idea (1) for the bioreactor TEVG culture sub-function.

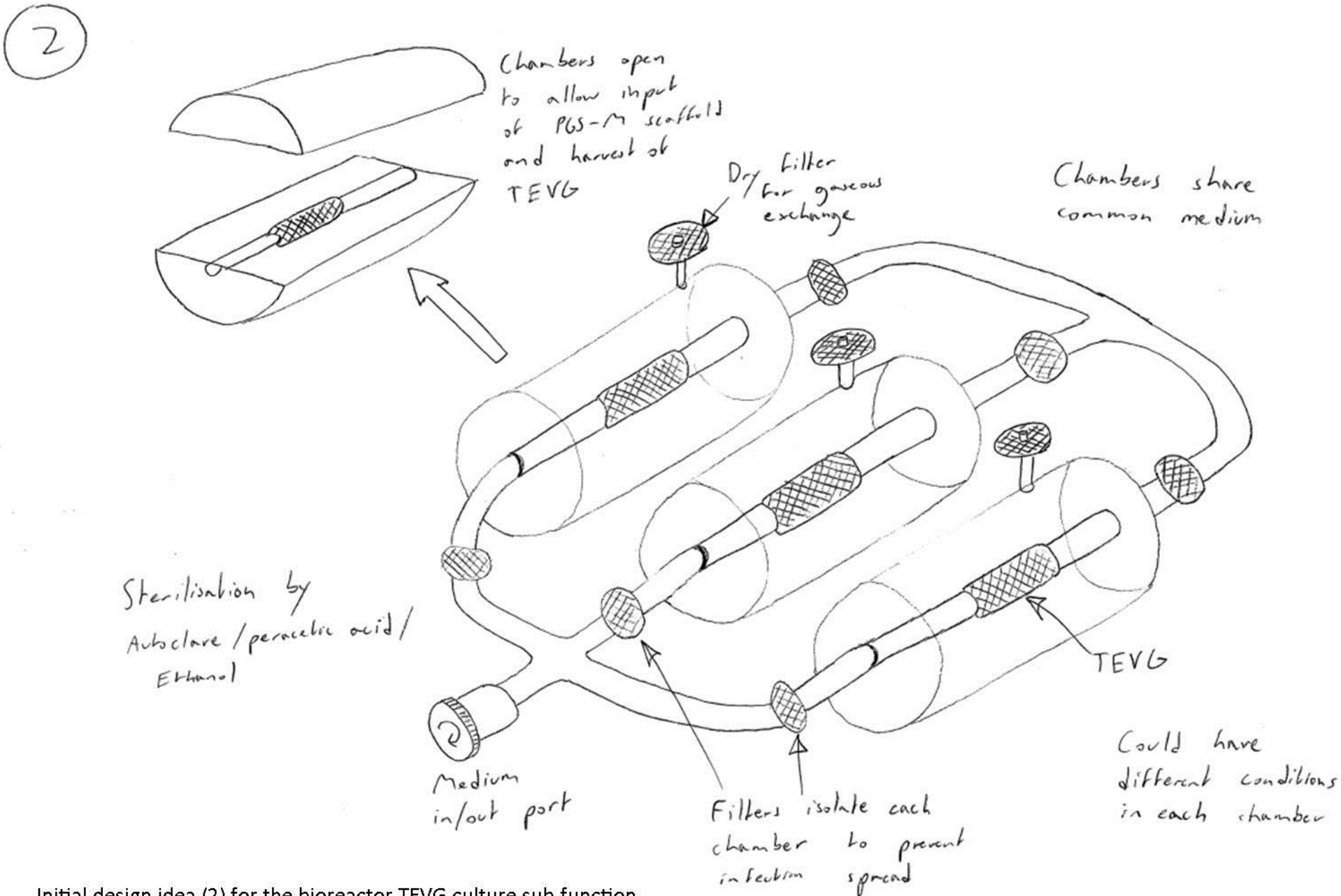

Initial design idea (2) for the bioreactor TEVG culture sub-function.

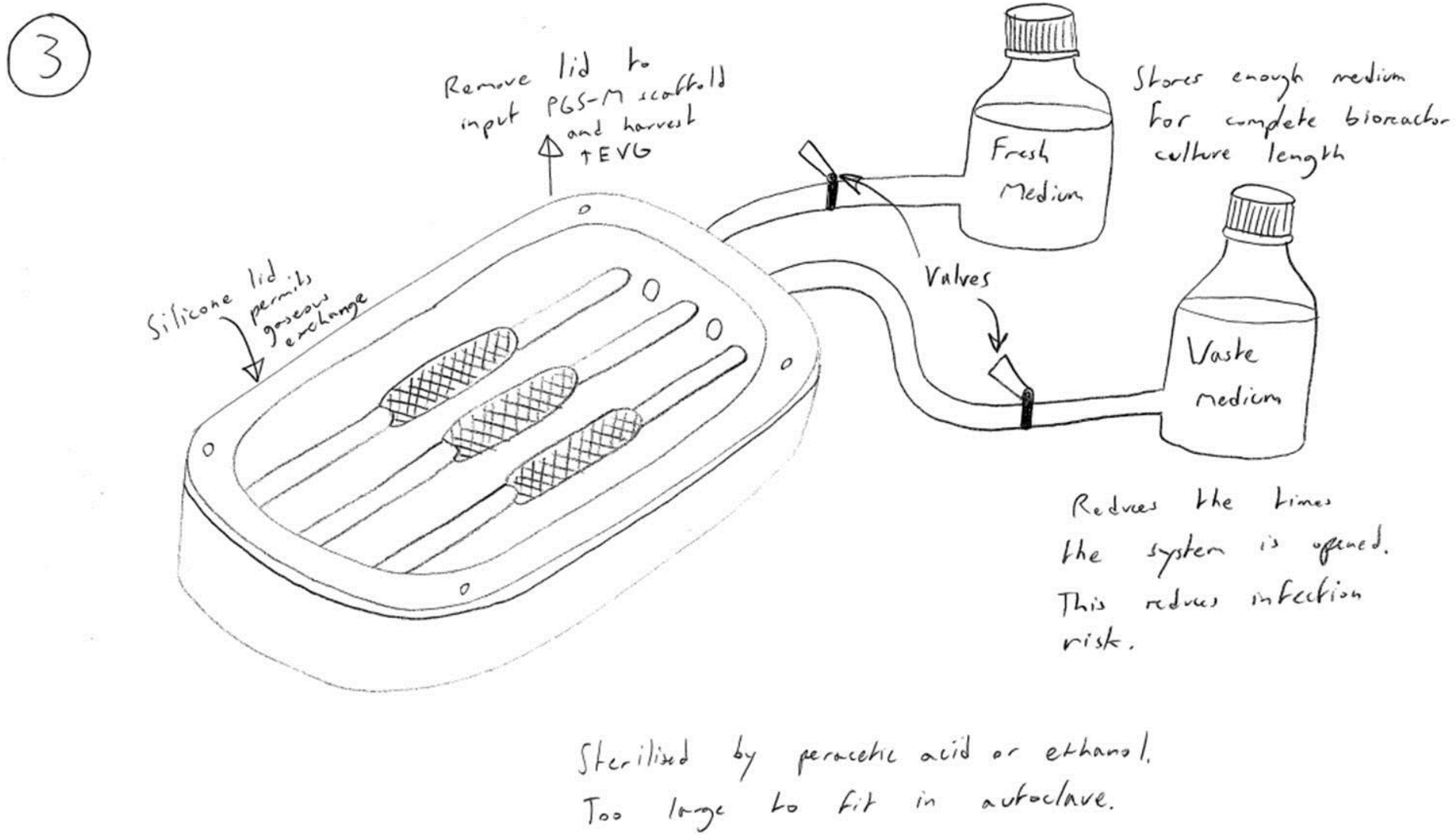

Initial design idea (3) for the bioreactor TEVG culture sub-function.

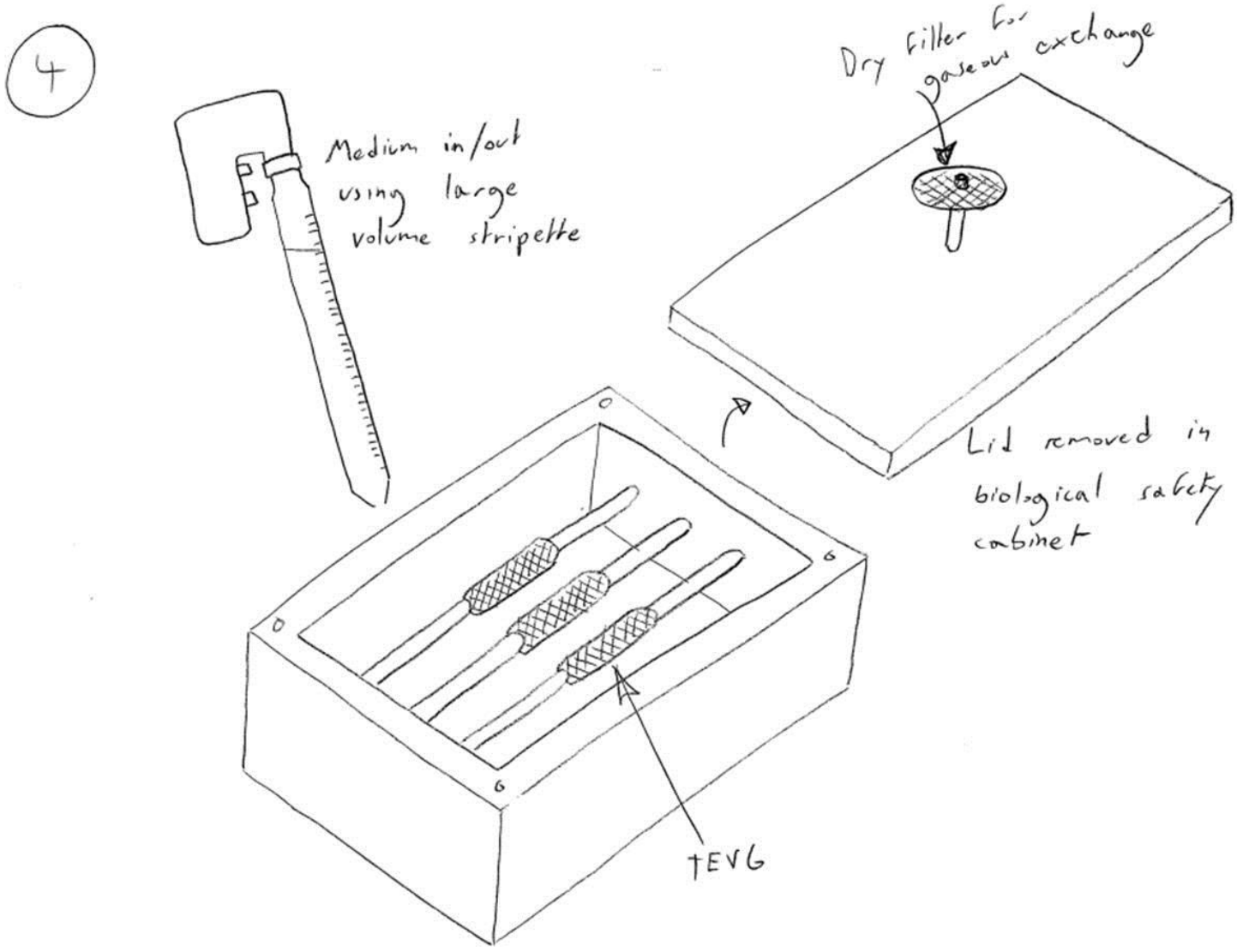

Initial design idea (4) for the bioreactor TEVG culture sub-function.

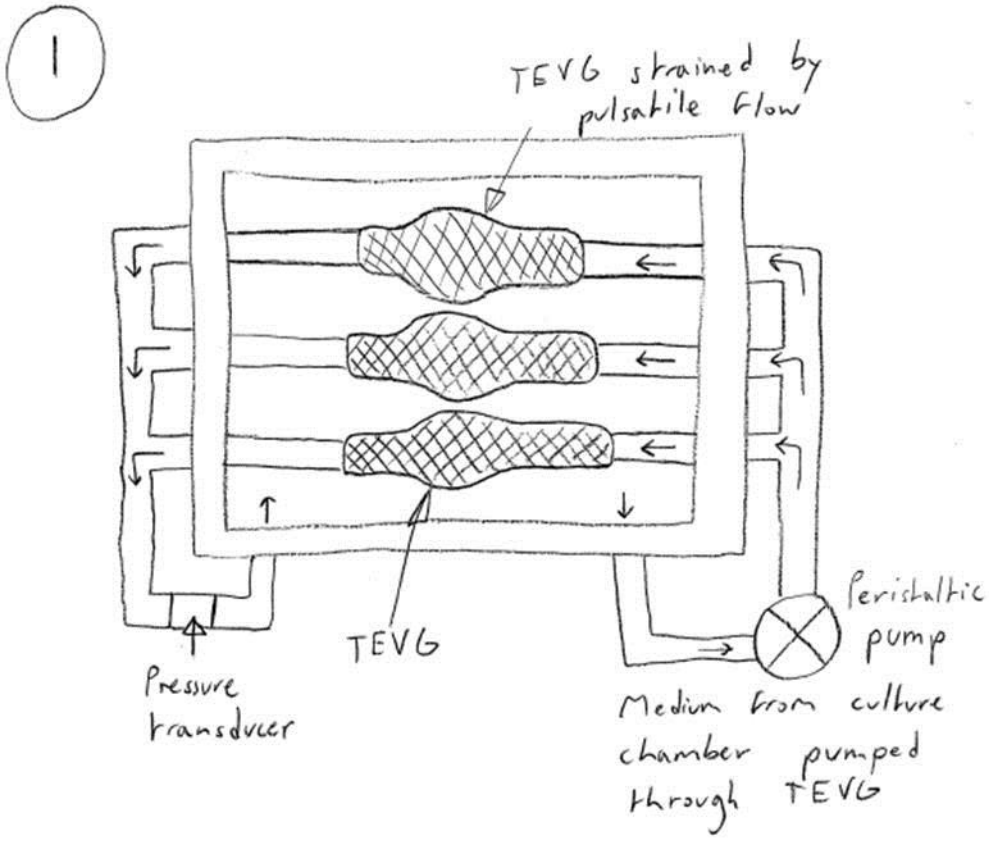

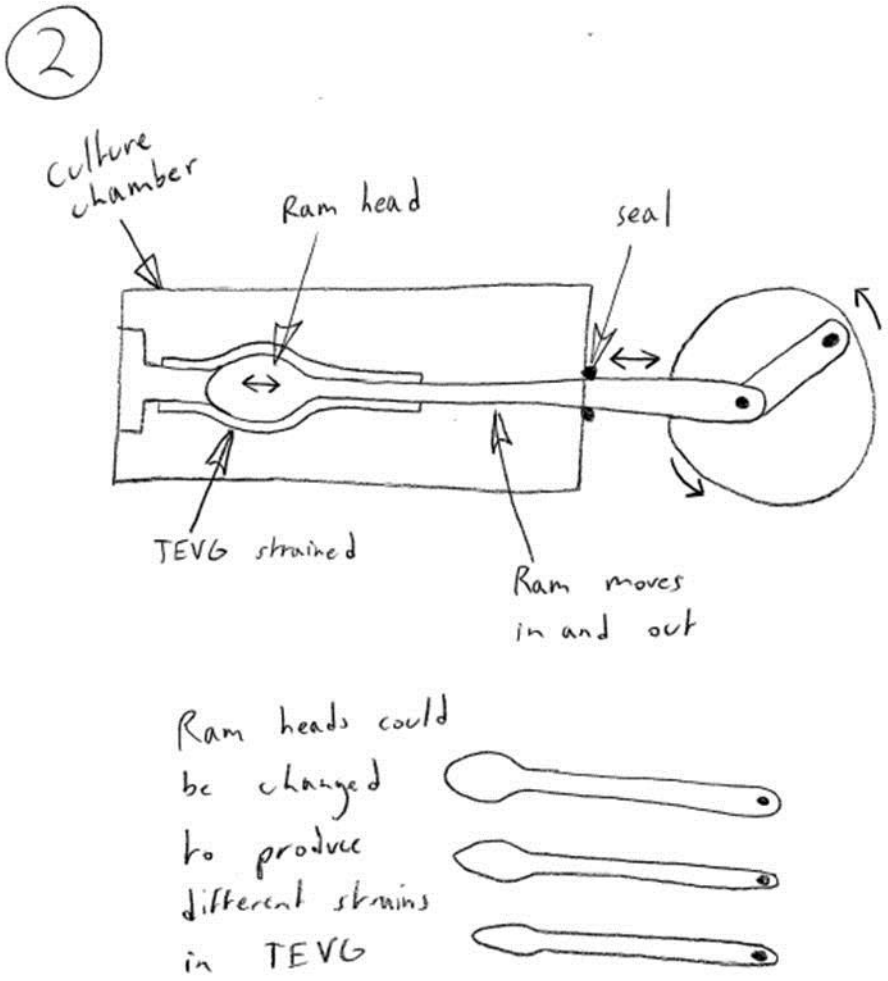

Initial design ideas (1) and (2) for the bioreactor mechanical stimulation sub-function.

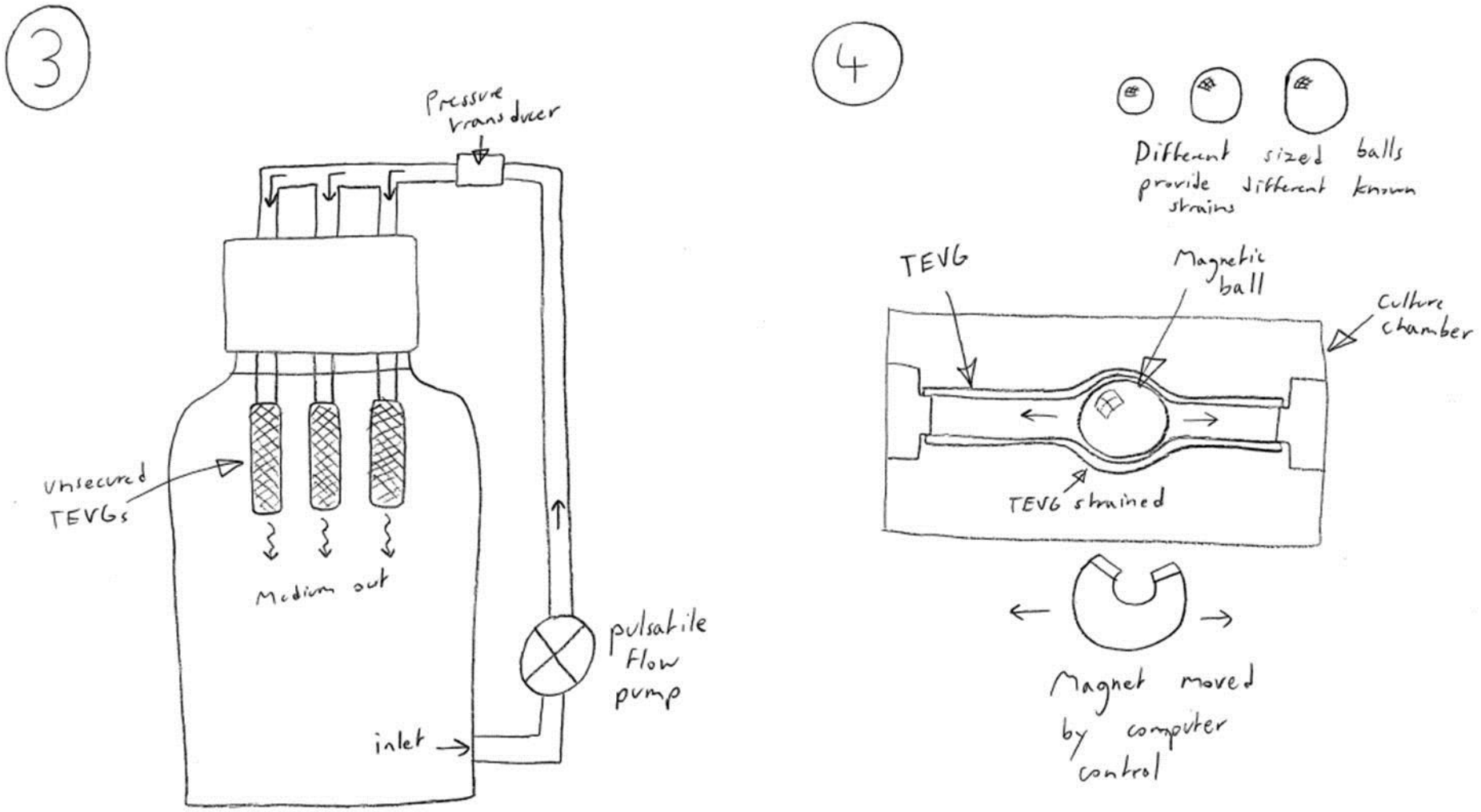

Initial design ideas (3) and (4) for the bioreactor mechanical stimulation sub-function.

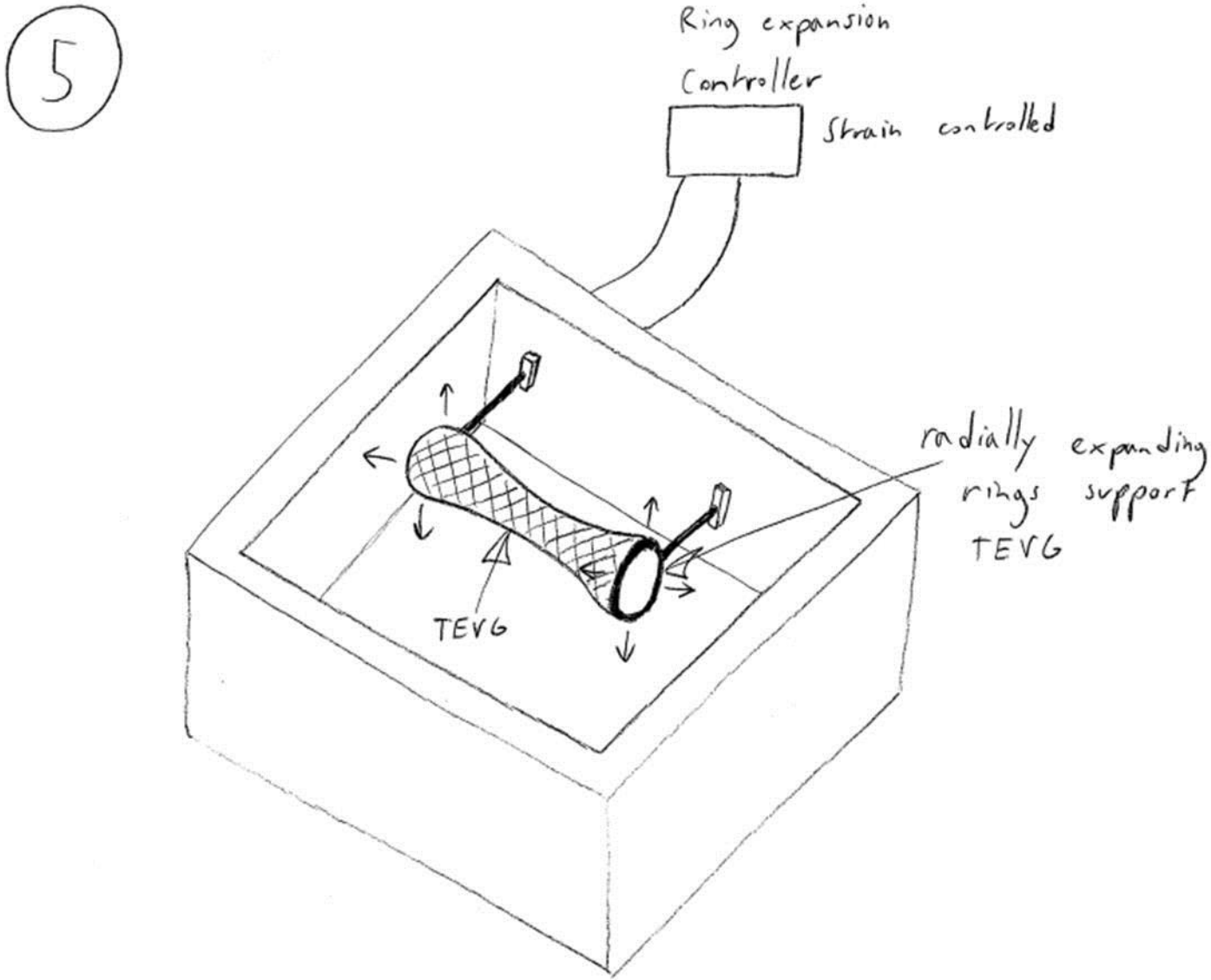

Initial design idea (5) for the bioreactor mechanical stimulation sub-function.